

**Structure activity relationships of glycosyl
transferases involved in protein O-
mannosylation in the actinobacteria**

Nathaniel Damien Malachi Holman

Doctor of Philosophy

University of York

Biology

September 2019

Abstract

Actinobacteria have a protein O-glycosylation system that resembles eukaryotic protein O-mannosylation. Both *M. tuberculosis* and *S. coelicolor* have growth retarded phenotypes when a membrane bound protein O-mannosyl transferase (Pmt), which transfers mannose from polyprenol phosphate mannose to a target protein, is absent. Moreover, *S. coelicolor pmt*⁻ mutants are resistant to infection by ϕ C31 phage and have increased susceptibility to vancomycin and several β -lactams. *S. coelicolor* strains that lack polyprenol phosphate mannose synthase (Ppm1), which transfers mannose from GDP-mannose to polyprenol phosphate, are even more susceptible to antibiotics and a *ppm1*⁻ mutant in *M. tuberculosis* is lethal. Pmt and Ppm1 are therefore possible new targets for the isolation of novel antimicrobials to be used against *M. tuberculosis*. The aim of this PhD thesis was to gain a deeper understanding of the structure and function of both *S. coelicolor* enzymes.

For Ppm1, ten mutant alleles (the majority being individual alanine substitutions) were tested and eight were essential for *S. coelicolor* DT3017, a *ppm1*⁻ strain, complementation, with four of the corresponding residues positioned close to the predicted catalytic DXD motif. Attempts were made to purify and develop an enzyme assay for Ppm1 but we were overtaken by the activities from another laboratory (Manuela Tosin, Warwick) with whom we then collaborated. Enzyme activity data of detergent solubilised Ppm1 from the Tosin laboratory was in general agreement with my work on the *in vivo* phenotypes. Roles for these critical residues have consequently been proposed with a great degree of confidence, with the majority likely being catalytic and/or involved in substrate binding.

Sequence alignments and structural bioinformatics were used with *S. coelicolor* Ppm1 and Pmt to identify targets for site-directed mutagenesis. Mutant alleles were introduced into *ppm1*⁻ (DT3017) or *pmt*⁻ (DT2008/DT1025) *S. coelicolor* strains using conjugative integrative plasmids and scored for their ability to complement phage sensitivity and antibiotic hyper-susceptible phenotypes. Twenty-three highly conserved Pmt residues were each changed to alanine and six mutant alleles failed to complement the *pmt*⁻ strains, indicating essentiality. Modelling the six corresponding residues indicated that five are positioned close to the predicted catalytic DE motif. Western blotting showed that none of the non-complementing *pmt*⁻ alleles expressed protein that could be localised to the membrane fractions and could not be detected in whole cell lysates. Conservative and semi-conservative substitutions were made to each of these six residues and with only a few exceptions, the alleles failed to complement DT1025 *pmt*⁻, indicating that strict conservation was necessary to preserve function. Moreover western blots continued to indicate that the non-complementing mutated Pmt proteins still failed to localise to the membrane. Evidently there is a relationship between the activity of Pmt and its localisation such that only functional Pmt could localise correctly to the membrane. Crucially, five of the six critical residues have not previously been proposed to have functional significance in the Pmt family and therefore could be important for the *M. tuberculosis* homologue. Whilst some of the mutations were predicted to impair catalytic activity, others may have affected localisation or substrate binding.

List of contents

Abstract.....	2
List of figures.....	8
List of tables.....	13
Acknowledgements.....	14
Declaration.....	15
Chapter 1 – Introduction.....	16
1.1 Antibiotics.....	16
1.2 <i>Streptomyces</i>.....	18
1.2.1 An introduction to <i>Streptomyces</i>	18
1.2.2 An introduction to the <i>Streptomyces</i> infecting phage: Φ C31.....	21
1.3 Glycosyltransferase structure and function	24
1.4 Eukaryotic protein O-mannosylation.....	27
1.4.1 Principles of protein O-mannosylation in the eukaryotes.....	27
1.4.2 Mannosyl donor synthesis in the eukaryotes.....	27
1.4.3 Protein O-mannosylation in the eukaryotes.....	28
1.5 Prokaryotic protein O-mannosylation.....	30
1.5.1 Principles of protein O-mannosylation in the prokaryotes.....	30
1.5.2 Mannosyl donor synthesis in the prokaryotes.....	30
1.5.3 Protein O-mannosylation in <i>Mycobacterium</i>	31
1.5.4 Protein O-mannosylation in <i>Streptomyces</i>	32
1.5.5 The current model for protein O-mannosylation in <i>S. coelicolor</i>	34
1.6 Aims.....	36
Chapter 2 – Materials and methods.....	37

2.1 Materials.....	37
2.1.1 Chemicals.....	37
2.1.2 Media and buffers.....	37
2.1.3 Software.....	38
2.1.4 Primers and plasmids.....	39
2.1.5 Strains.....	44
2.2 Molecular procedures.....	45
2.2.1 Growth of <i>E. coli</i>	45
2.2.2 Preparation of chemically competent cells.....	45
2.2.3 Transformation of <i>E. coli</i>	45
2.2.4 Plasmid DNA isolation.....	45
2.2.5 PCR/DNA digest clean up.....	45
2.2.6 Restriction digest.....	46
2.2.7 Agarose gel electrophoresis.....	46
2.2.8 In-Fusion Cloning.....	46
2.2.9 Ppm1 cloning into pIJ10257.....	46
2.2.10 Pmt mutagenesis and cloning into pIJ10257.....	46
2.3 <i>Streptomyces</i> work.....	47
2.3.1 Conjugation from <i>E. coli</i> and <i>S. coelicolor</i> spore harvesting.....	47
2.3.2 Antibiotic disc diffusion assay.....	48
2.3.3 Phage plaque assay.....	48
2.3.4 Phage streak assay.....	48
2.3.5 Isolation of genomic DNA from <i>S. coelicolor</i>	48
2.3.6 Ppm1 revertent analysis.....	49
2.4 Protein methods.....	49
2.4.1 SDS-PAGE.....	49

2.4.2 Harvesting membrane/soluble fractions for Western blotting.....	49
2.4.3 Ppm1 and Pmt Bioinformatics.....	50
2.4.5 Ppm1 expression and purification.....	51
2.4.6 Ni ²⁺ affinity chromatography.....	51
2.4.7 Dialysis.....	51
2.4.8 Gel filtration chromatography.....	51
2.4.9 Gel filtration (size exclusion) chromatography coupled with multi angle laser light scattering (SEC-MALLS).....	52
2.4.10 Buffers.....	52
Chapter 3 – Expression and purification of <i>S. coelicolor</i> Ppm1.....	53
3.1 Expression and purification of <i>S. coelicolor</i> Ppm1.....	54
3.1.1 Optimising small scale expression.....	54
3.1.2 Ni ²⁺ affinity and gel filtration purification of WT <i>S. coelicolor</i> Ppm1.....	56
3.2 Mitigating oligomerisation and aggregation.....	62
3.2.1 Troubleshooting expression and purification.....	66
3.2.2 Investigation of Ppm1 N-terminal truncation mutants.....	66
3.3 Discussion.....	71
Chapter 4 - Identification of essential residues for polyprenol phosphate mannose synthase function.....	75
4.1 Cloning mutant alleles into pIJ10257 and introduction of recombinant plasmids into <i>S. coelicolor</i> J1929 and DT3017 strains.....	77
4.2 Effect of <i>ppm1</i> alleles on the phenotype and growth of <i>Streptomyces</i>.....	80
4.2.1 <i>Streptomyces</i> spore growth and antibiotic hyper susceptibility.....	80

4.2.2 Identification of <i>ppm1</i> mutants unable to alleviate the antibiotic susceptibility phenotype of DT3017.....	83
4.2.3 Complemented DT3017 are vulnerable to ΦC31 Δ25 phage infection and exhibit increased growth rates.....	87
4.3 Ppm1 structural bioinformatics and mechanistic modelling.....	90
4.4 Discussion.....	95
Chapter 5 - Identification of essential residues for <i>S. coelicolor</i> protein O-mannosyl transferase function.....	100
5.1 Pmt site directed mutagenesis.....	102
5.1.1 Identification of site directed mutagenesis targets.....	102
5.1.2 Mutagenesis of targets.....	105
5.2 Pmt structural bioinformatics.....	107
5.2.1 Sequence analysis.....	107
5.2.2 Homology model analysis.....	110
5.3 <i>In vivo</i> pmt mutant characterisation.....	114
5.3.1 Identification of <i>pmt</i> mutants unable to alleviate the antibiotic susceptible phenotype of DT1025.....	114
5.3.2 Complemented DT1025 are vulnerable to Φ C31 Δ 25 phage infection and exhibit increased growth rates.....	121
5.3.3 Introduction of <i>pmt</i> mutants into DT2008.....	126
5.3.4 Complemented DT2008 are vulnerable to Φ C31 Δ 25 phage infection and exhibit increased growth rates.....	131
5.4 Pmt mechanistic model	134
5.5 Discussion.....	137
5.5.1 Overview of key findings.....	137
5.5.2 Defining the roles of the DE motif and the divalent metal.....	140
5.5.3 Defining the roles of H159, D233, K302 and R510.....	142

5.5.4 Building an improved homology model for <i>S. coelicolor</i> Pmt.....	143
Chapter 6 - Pmt localisation studies and mutant library expansion.....	148
6.1 Western blotting to probe enzyme localisation.....	149
6.2 Expansion of the <i>pmt</i> mutant library.....	157
6.3 Discussion.....	164
Chapter 7 - Overall conclusions and future perspectives.....	167
Chapter 8 - Appendix.....	168
8.2 Chapter 4 appendix.....	168
8.3 Chapter 5 appendix.....	171
8.4 Chapter 6 appendix.....	177
References.....	180
Abbreviations and acronyms.....	191

List of figures

Figure 1.1: Diagram showing the targets of clinically relevant antibiotic classes and individual antibiotics.....	17
Figure 1.2: Summary of the <i>Streptomyces</i> sporulation lifecycle.....	20
Figure 1.3: Summary of the phage lysogenic and lytic life cycles.....	23
Figure 1.4: Stereochemistry of glycosyltransferase catalysed reactions.....	25
Figure 1.5: Topology of GT-A, GT-B and GT-C enzymes.....	26
Figure 1.6: Current protein O-glycosylation model for <i>S. coelicolor</i>	35
Figure 3.1: <i>S. coelicolor</i> Ppm1 successfully expressed following IPTG induction.....	55
Figure 3.2: Ppm1 was successfully purified by Ni ²⁺ affinity chromatography.....	58
Figure 3.3: Ppm1 was successfully purified using gel filtration chromatography.....	59
Figure 3.4: Standards of known MW were eluted at expected elution volumes.....	60
Figure 3.5: Purified Ppm1 shows a wide distribution of aggregates and oligomers.....	61
Figure 3.6: Ppm1 was successfully purified using Ni ²⁺ affinity chromatography.....	63
Figure 3.7: Ppm1 was successfully purified using gel filtration chromatography.....	64
Figure 3.8: Fractions previously collected, pooled and reloaded onto the column were eluted with same volumes of buffer.....	65
Figure 3.9: <i>S. coelicolor</i> Ppm1 has a disordered N-terminus.....	67
Figure 3.10: <i>S. coelicolor</i> Ppm1WT, Ppm1Δ14 and Ppm1Δ20 were successfully expressed.....	68
Figure 3.11: <i>S. coelicolor</i> Ppm1WT, Ppm1Δ14 and Ppm1Δ21 were successfully expressed.....	69
Figure 3.12: Ppm1 gel filtration chromatogram for WT is comparable with Δ14 and Δ21 chromatograms.....	70
Figure 4.1: <i>S. coelicolor</i> Ppm1 has a GT-2 domain that is broadly conserved, in addition to a highly disordered C-terminus.....	78
Figure 4.2: <i>E. coli</i> purified plasmids are recombinant and non-methylated.....	79

Figure 4.3: DT3017 strains that are not complemented with an active <i>ppm1</i> allele exhibit increased susceptibility to antibiotic insult.....	82
Figure 4.4: Amplification of the native and integration site <i>ppm1</i> alleles.....	82
Figure 4.5: DT3017 strains that are not complemented with an active <i>ppm1</i> allele exhibit increased susceptibility to antibiotic insult.....	84
Figure 4.6: Complemented DT3017 strains do not show hypersensitivity to antibiotics targeting the bacterial cell wall and/or membrane.....	85
Figure 4.7: Complemented DT3017 strains do not show hypersensitivity to antibiotics targeting DNA replication, transcription and translation.....	86
Figure 4.8: Complemented DT3017 strains are vulnerable to Φ C31 phage infection.....	88
Figure 4.9: Complemented DT3017 strains show a large colony phenotype.....	89
Figure 4.10: <i>S. coelicolor</i> Ppm1 homology model exhibits typical facets of GT-A fold glycosyl transferase.....	91
Figure 4.11: G143 is within a loop.....	92
Figure 4.12: Strong conservation of the GT-2 domain in <i>S. coelicolor</i> Ppm1 and <i>P. furiosus</i> DPMS	93
Figure 4.13: Proposed mechanism for Ppm1, an inverting glycosyl transferase that utilises a single step SN2 mechanism.....	94
Figure 5.1: The catalytic GT-2 domain is broadly conserved across the prokaryotic and eukaryotic kingdoms.....	104
Figure 5.2: Introduction of the desired mutation by 2 separate PCR reactions gave high yields of correctly sized products.....	106
Figure 5.3: <i>S. coelicolor</i> Pmt has 11 predicted transmembrane helices and a disordered N-terminus.....	108
Figure 5.4: <i>S. coelicolor</i> Pmt and <i>C. metallidurans</i> ArnT share over 40 % sequence identity and similarity.....	109
Figure 5.5: Phyre2 homology model of <i>S. coelicolor</i> Pmt has typical facets of GT-C fold glycosyl transferases.....	112

Figure 5.6: Pmt Phyre2 homology model exhibits typical facets of a GT-C fold glycosyl transferase.....	113
Figure 5.7: DT1025 strains that are not complemented with an active <i>pmt</i> allele exhibit increased susceptibility to antibiotic insult.....	116
Figure 5.8: Non-complemented DT1025 strains show significant increases in sensitivity to cell wall/membrane targeting antibiotics, nitrofurantoin and rifampicin.....	117
Figure 5.9: Complemented DT1025 strains show no significant increases in sensitivity to cell wall/membrane targeting antibiotics, nitrofurantoin and rifampicin.....	118
Figure 5.10: Complemented and non-complemented DT1025 strains show no significant increases in sensitivity to DNA replication and translation inhibitors.....	119
Figure 5.11: Complemented DT1025 strains show no significant increases in sensitivity to DNA replication and translation inhibitors.....	120
Figure 5.12: Complemented DT1025 strains are vulnerable to Φ C31 c Δ 25 phage infection.....	122
Figure 5.13: Non-complemented DT1025 strains show a small colony phenotype.....	125
Figure 5.14: Non-complemented DT2008 strains show significant increases in sensitivity to cell wall/membrane targeting antibiotics, nitrofurantoin and rifampicin.....	127
Figure 5.15: Complemented DT2008 strains show no significant increases in sensitivity to DNA replication and translation inhibitors.....	128
Figure 5.16: Complemented and non-complemented DT2008 strains show no significant increases in sensitivity to DNA replication and translation inhibitors.....	129
Figure 5.17: Complemented DT2008 strains show no significant increases in sensitivity to DNA replication and translation inhibitors.....	130
Figure 5.18: Complemented DT2008 strains are vulnerable to Φ C31 c Δ 25 phage infection.....	132
Figure 5.19: <i>S. coelicolor</i> Pmt homology model exhibits typical facets of GT-A fold glycosyl transferase.....	135
Figure 5.20: Proposed mechanism for Pmt, an inverting glycosyl transferase that utilises a single step SN2 mechanism.....	136
Figure 5.21: Phyre2 homology models of <i>S. coelicolor</i> Pmt have typical facets of GT-C fold glycosyl transferases.....	145

Figure 5.22: <i>S. coelicolor</i> Pmt homology model exhibits typical facets of GT-C fold glycosyl transferase.....	146
Figure 5.23: Proposed mechanism of Pmt action, an inverting glycosyl transferase that utilises a single step SN2 mechanism.....	147
Figure 6.1: C-terminal Strep II tagged non-complementing Pmt mutants are absent in DT1025 membrane fractions.....	151
Figure 6.2: C-terminal Strep II tagged complementing Pmt mutants are present in DT1025 membrane fractions.....	155
Figure 6.3: C-terminal Strep II tagged complementing and non-complementing mutants were present and absent respectively in DT1025 membrane fractions.....	156
Figure 6.4: Successfully complemented DT1025 strains do not show hypersensitivity to antibiotics targeting the bacterial cell wall and/or membrane.....	160
Figure 6.5a: C-terminal Strep II tagged non-complementing Pmt mutants are absent in DT1025 membrane fractions.....	161
Figure 6.5b: C-terminal Strep II tagged non-complementing Pmt mutants are absent in DT1025 membrane fractions.....	162
Figure 6.5c: C-terminal Strep II tagged non-complementing Pmt mutants are absent in DT1025 membrane fractions.....	163
Figure A8.1: Introduced <i>ppm1</i> alleles have no effect on the antibiotic sensitivity profile of the J1929 parent strain.....	168
Figure A8.2: Introduced <i>ppm1</i> alleles have no effect on the antibiotic sensitivity profile of the J1929 parent strain.....	169
Figure A8.3: Introduced <i>pmt</i> alleles have no effect on the antibiotic sensitivity profile of the J1929 parent strain.....	171
Figure A8.4: Introduced <i>pmt</i> alleles have no effect on the antibiotic sensitivity profile of the J1929 parent strain.....	172
Figure A8.5: Introduced <i>pmt</i> alleles have no effect on the antibiotic sensitivity profile of the J1929 parent strain.....	173
Figure A8.6: Introduced <i>pmt</i> alleles have no effect on the antibiotic sensitivity profile of the J1929 parent strain.....	174

Figure A8.7: All J1929 strains are vulnerable to Φ C31 $c\Delta 25$ phage infection.....	175
Figure A8.8: C-terminal Strep II tagged non-complementing Pmt mutants are absent in DT2008 membrane fractions.....	178
Figure A8.9: C-terminal Strep II tagged complementing Pmt mutants are present in DT2008 membrane fractions.....	179

List of tables

Table 2.1: List of PCR primer sequences.....	39
Table 2.2: List of constructs.....	42
Table 2.3: List of bacterial strains.....	44
Table 4.1: Complemented DT3017 strains are vulnerable to Φ C31 c Δ 25 phage infection.....	89
Table 5.1: Complemented DT1025 strains are vulnerable to Φ C31 c Δ 25 phage infection.....	123
Table 5.2: Complemented DT2008 strains are vulnerable to Φ C31 c Δ 25 phage infection.....	133
Table 6.1: Presence of the Strep Tag II on either termini does not affect the ability of <i>pmt</i> alleles to complement DT1025.....	150
Table 6.2: Presence of the Strep Tag II on either termini does not affect the ability of <i>pmt</i> alleles to complement DT1025.....	154
Table 6.3: The majority of conservative and semi conservative substitutions yielded <i>pmt</i> alleles that were unable to complement DT1025.....	158
Table A8.1: Introduction of mutant alleles into J1929 had no effect on Φ C31 phage infection titres.....	170
Table A8.2: Introduced <i>pmt</i> alleles have no effect on the phage sensitivity J1929 parent strain.....	176
Table A8.3: Presence of the Strep Tag II on either termini does not affect the ability of <i>pmt</i> alleles to complement DT2008.....	177

Acknowledgments

Thank you very much to my supervisors Prof Maggie Smith and Prof Tony Wilkinson for your enthusiasm, patience, guidance and reassurance. I also want to thank my TAP panel members Dr Martin Fascione and Prof Jennifer Potts for their support during my PhD. My thanks can be extended further to everyone in the Smith group, with a special mention to Dr Nicholas Read and Dr Janina Hossbach for their great conversations and for listening to my work related complaints on the occasionally difficult day.

Thanks also to our collaborators from Warwick University Dr Manuela Tosin and Dr Pamela Dube for working with us to build a good story for the Ppm1 work. I want to say thanks to Prof Konstantin Severinov for allowing me to go to Moscow and work in his lab for 3 months, the Severinov group members and especially to Artem Isaev for being both a great co-worker and friend.

Thanks to my PhD buddies Alexandra, Matthew, Jack, Alex, Egle, Emma for your company, you all gave me a good excuse to leave the lab.

Finally, I want to thank my mum and dad for your enduring love and support.

Declaration

I hereby declare that this thesis is an original report of my research, has been written by me and has not been submitted for any previous degree at this or any other university. The experimental work described herein was performed by myself, except where otherwise stated. The collaborative contributions have been indicated clearly and acknowledged. Due references have been provided on all supporting literature and resources.

Introduction

1.1 Antibiotics

Antibiotics revolutionised modern medicine following their widespread use in the middle of the 20th century. Previously untreatable infections including tuberculosis, syphilis, pneumonia and cholera could now be tackled in the clinic. Since the introduction of antibiotics, they have saved millions of lives, it is estimated that at least 200 million lives across the globe have been saved by penicillin alone (Macfarlane 1984). Alexander Fleming is credited with the discovery of penicillin and in 1945 during his Nobel Lecture, he warned that 'man may easily under dose himself and by exposing his microbes to non-lethal quantities of the drug make them resistant', essentially predicting the evolutionary arms race between man and microbes before it had really begun (Fleming 1945). Antibiotics kill or inhibit the growth of bacteria by exploiting specific targets, the most common being cell wall biosynthesis, DNA replication, transcription and translation (Figure 1.1). Unfortunately, the over-prescription of antibiotics by clinicians, combined with patients failing to finish their prescribed course, has helped create an evolutionary selection pressure that has greatly favoured the survival of bacteria that have acquired resistance determinants (usually genes carried on a plasmid). Worryingly, a recent report estimated that antibiotic resistance would be responsible for around 300 million premature deaths by 2050, with a loss of up to \$100 trillion to the global economy (O'Neil 2014).

This increasingly dire situation is exacerbated by the lack of a robust antibiotic discovery pipeline. The pharmaceutical industry has reduced their focus on the discovery, development and testing of antimicrobials, instead favouring the development of medicines to treat cancer, in addition to respiratory, cardiovascular and neurodegenerative diseases. Consequently, despite modest improvements made to antibiotic prescribing practices and patient compliance, infections have emerged that are now almost untreatable. In extreme cases this has left clinicians with no reliable alternatives to treat patients infected with multi drug resistant bacteria. The growing resistance to the so-called antibiotics of last resort such as vancomycin is an especially worrying development.

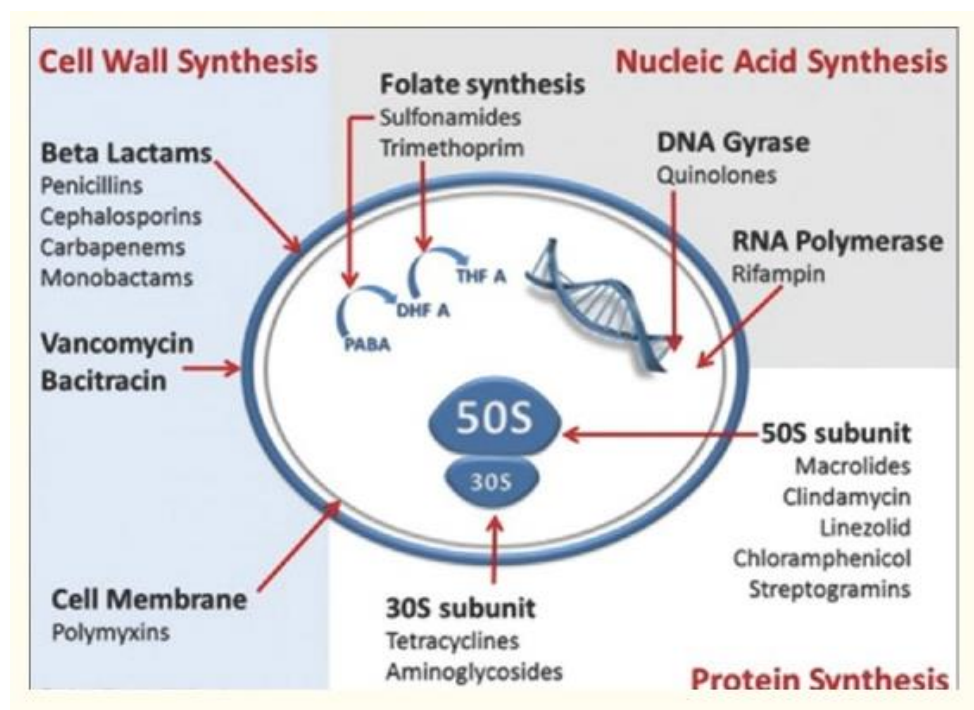


Figure 1.1: Diagram showing the targets of clinically relevant antibiotic classes and individual antibiotics

Image by Kendrick Johnson: Creative Commons Attribution-Share Alike 3.0 Unported license

1.2 *Streptomyces*

1.2.1 An introduction to *Streptomyces*

The majority of antibiotics used in medicine, veterinary practise and agriculture originate from bacteria of the *Streptomyces* genus. Remarkably, genome analysis of *Streptomyces* species reveal that only a fraction of the synthetic capacity of this genus has been tested for antibiotic activity (Charlop-Powers *et al.*, 2015). *Streptomyces* are a genus of high GC Gram-positive bacteria that belong to the Actinobacteria phylum, well known for a distinct “earthy odour” that results from the production of the volatile metabolite geosmin (Kieser *et al.*, 2000).

At the start of the *Streptomyces* lifecycle, semi-dormant spores capable of surviving in the soil for long periods germinate, with the emergence of distinct germ tubes. Streptomycetes then grow vegetatively as a network of branching hyphal filaments to form a mat of mycelium. The hyphae “dig” into the substrate to acquire nutrients and upon nutrient depletion, differentiation is triggered in which aerial hyphae emerge from the mycelium. Partition walls are more frequently formed and on the distal parts of the aerial hyphae, chains of spores are generated (Figure 1.2).

In the middle of the 20th century, Waksman and other pioneers of *Streptomyces* research could not decide whether they belonged to the prokaryotic or eukaryotic kingdoms. *Streptomyces* and other members of the actinomycete family were noted to have a cell wall structure and composition that was closer to bacteria than fungi, however their behaviours and appearance were very fungus-like. Consequently, a new taxonomic group was created whereby they were categorised as an intermediate life form that bridged the gap between fungi and bacteria. The development of *Streptomyces* genetics, pioneered by Hopwood at the John Innes Centre, ensured that *Streptomyces* and a whole host of other similar soil dwelling organisms would eventually be categorised as actinobacteria (Kieser *et al.*, 2000). The similarities between fungi and bacteria proved to be largely superficial.

Physiological studies have been conducted in the model organism *S. coelicolor* and studied on solid agar medium. *S. coelicolor* (and the majority of other streptomycetes) fail to undergo a full developmental cycle in liquid culture. Developmental asynchrony and heterogeneity were major recurring problems affecting surface grown cultures, these were recently circumvented through the development of the newer model organism *S. venezuelae*, which sporulates in liquid culture and is therefore able to undergo a full development cycle (Schlimpert *et al.*, 2016).

Streptomyces is the largest genus of the actinobacteria and to date, over 600 members of this genus have been identified. *S. coelicolor* was the first member of the *Streptomyces* genus to have

its genome fully sequenced. The genome is composed of a single ~8,670 kbp linear chromosome with 7,825 predicted genes (Bentley *et al.*, 2002). Remarkably, *S. coelicolor* was the first bacterium found to have a fully sequenced genome that harboured more genes than that of the eukaryotic model organism *Saccharomyces cerevisiae*, with 6203 genes (Bentley *et al.*, 2002). Indeed all *Streptomyces* chromosomes are large, with sizes typically ranging from 6,000-12,000 kbp. These chromosome sizes and configurations are however not representative of the entire family of actinobacteria. For example, the *S. coelicolor* genome is notably larger and configured differently to that of the first sequenced mycobacterial genome (*M. tuberculosis*), which has a single ~4,410 kbp circular chromosome (Cole *et al.*, 1998). It is also noteworthy that unlike the majority of bacterial genomes which exist as circular chromosomes, Actinobacteria have a relatively high number of genera with linear genomes including *Actinoplanes*, *Micromonospora*, *Nocardia* and of course *Streptomyces* (Ventura *et al.*, 2007).

In *S. coelicolor* over 20 gene clusters have been implicated in secondary metabolite biosynthesis and consequently, there is a lot of interest in the relationship between antibiotic production and physiology (Bibb 1996). These *S. coelicolor* studies have been made easier by the production of two pigmented antibiotics, the blue/red pigmented (depending on pH) polyketide actinorhodin (ACT) and the red pigmented tripyrrole prodiginines (REDs)(Liu *et al.*, 2013). The wide range of pigments, antibiotics and fungicides produced by *Streptomyces* sp. allow them to inhibit the growth of competing organisms. They are also well adapted to survive in nutrient scarce environments through the possession of multiple catabolic enzymes that facilitate the metabolism of abundant carbon sources such as cellulose, chitin, xylan and cellulose. Other notable *Streptomyces* genomes that have been sequenced include *S. ambofaciens*, which has remarkable genetic diversity (Choulet *et al.*, 2006), *S. avermitilis*, the producer of avermectin (Omura *et al.*, 2001) and *S. scabies*, the causative agent of potato scab disease (Loria *et al.*, 2006).

Streptomyces sp. are relatively benign, despite belonging to the Actinobacteria phylum that includes well known pathogens in the *Mycobacteria* family. Instances of pathogenicity have however been noted; examples include human mycetoma which is caused by *Streptomyces somaliensis* (Trujillo *et al.*, 2003) and potato scab disease caused by *Streptomyces scabies* (Loria *et al.*, 2006).

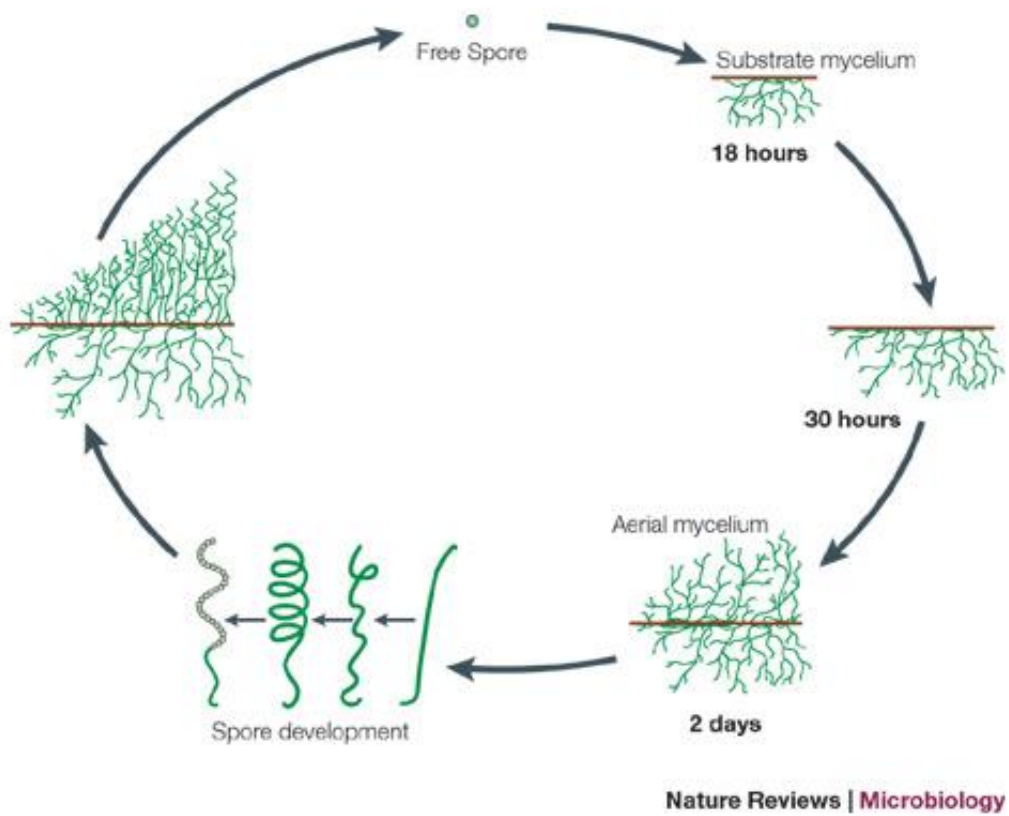


Figure 1.2: Summary of the *Streptomyces* lifecycle.

Taken from Angert *et al.*, 2005

1.2.2 An introduction to the *Streptomyces* infecting phage: Φ C31

Phages are viruses that infect and replicate in bacterial hosts. They are the most abundant biological agents on this planet, with the highest density in shallow sea water (Chen *et al.*, 2006). Their genetic diversity is largely unparalleled by any other life form. Upon infection of the bacterial host, temperate phages can embark on either lytic or lysogenic lifecycles (Figure 1.3). Prior to infection, the phage particle must first recognise and then bind to a host cell receptor, before injecting its DNA into the host. Lytic phage infection of a lawn of susceptible bacteria will lead to clear plaques on solid agar plates. Temperate phage can form lysogens, this happens where the viral DNA (genome) becomes stably integrated into the host genome. When this happens, the host bacterial cell carrying the integrated phage genome (prophage) is termed a lysogen. Induction of the lytic pathway through stress factors can subsequently result in the rapid assembly of infective phage particles and lysis of the host cell releasing phage particles that are now free to find and infect further hosts. The processes of integration and excision are highly regulated to ensure switching between the lytic and lysogenic pathways is efficient and yields favourable outcomes for the phage.

Streptomyces phage are of particular interest as they can provide useful tools such as integrases and phage vectors that have applications in genetic engineering (Smith 2006). *Streptomyces* sp. are susceptible to infection by multiple phages, with the temperate phage Φ C31 being the most extensively studied, in part, due to its ability to plaque and lysogenise roughly two thirds of *Streptomyces* sp. (Lomovskaya *et al.*, 1980; Kobler *et al.*, 1991; Smith *et al.*, 1999). Clear plaque mutants of Φ C31 were isolated that can only develop through the lytic cycle and were found to have undergone point mutation or deletions in the repressor gene *c*, which is required for both the establishment and maintenance of the lysogenic state. Φ C31 $c\Delta$ 25 is one of several common Φ C31 clear plaque mutants (Lomovskaya *et al.*, 1972). Electron microscopy analysis showed that Φ C31 is a typical tailed phage, roughly 150 nm in length. It is composed of an icosahedral capsid (57 x 54 nm) and a non-contractile tail (123 x 10 nm) with a basal plate and tail fibres (Lomovskaya *et al.*, 1980).

ϕ C31 was the first *Streptomyces* phage genome to be completely sequenced (Smith *et al.*, 1999). The double stranded DNA genome of Φ C31 is 41,495 bp in length and encodes 52 genes. The genes for phage assembly and DNA metabolism are clustered in accordance with their function in the genome. Late genes of Φ C31 principally include those encoding capsid head and tail assembly while early genes are mainly involved in regulation, DNA metabolism or recombination. This recombination region includes the integrase gene and the *attP* site, both of which have been exploited in vectors to facilitate the manipulation of *Streptomyces* sp (Kuhstoss *et al.*, 1991).

The integrase belongs to the serine recombinase family and catalyses site specific recombination between *attP* and *attB* attachment sites on the phage and bacterial genomes respectively. Phages use Recombination Directionality Factors (RDFs) to control the directionality of integrase. RDFs were historically difficult to study since for the serine integrase family, there is a general lack of sequence conservation. For Φ C31, the early protein gp3 was eventually identified as the RDF (Fogg *et al.*, 2018). Finally, in the virions there are cohesive ends derived from the *cos* sites these are required for both circularisation and DNA packaging of the capsid via *cos* site recognition.

Bacteria have evolved multiple mechanisms of resistance to phage infection. *S. coelicolor* has a variety of restriction-modification systems (González-Cerón *et al.*, 2009) and an unusual system called phage growth limitation or Pgl conferred by multiple genes (*pglW*, *pglX*, *pglY* and *pglZ*) (Chinenova *et al.*, 1982; Bedford *et al.*, 1995; Sumby *et al.*, 2003). Pgl⁺ strains support a phage burst upon initial infection but subsequent cycles are strongly attenuated. However mutations in any of the four *pgl* genes is sufficient to confer sensitivity to Φ C31.

A second mechanism of resistance to phage infection comes via blocking host recognition usually through phage adsorption. This mechanism depends on the interaction between the host's phage receptors and some component of the phage tail, usually the tail fibres. If the host receptor is changed or removed the stable interaction is removed and infection is severely compromised. The Φ C31 receptor in sensitive *Streptomyces* sp. remains unknown, although there has been progress on identification of a protein glycosylation pathway that is required for phage infection (Cowlshaw and Smith 2001; Cowlshaw and Smith 2002; Wehmeier *et al.*, 2009).

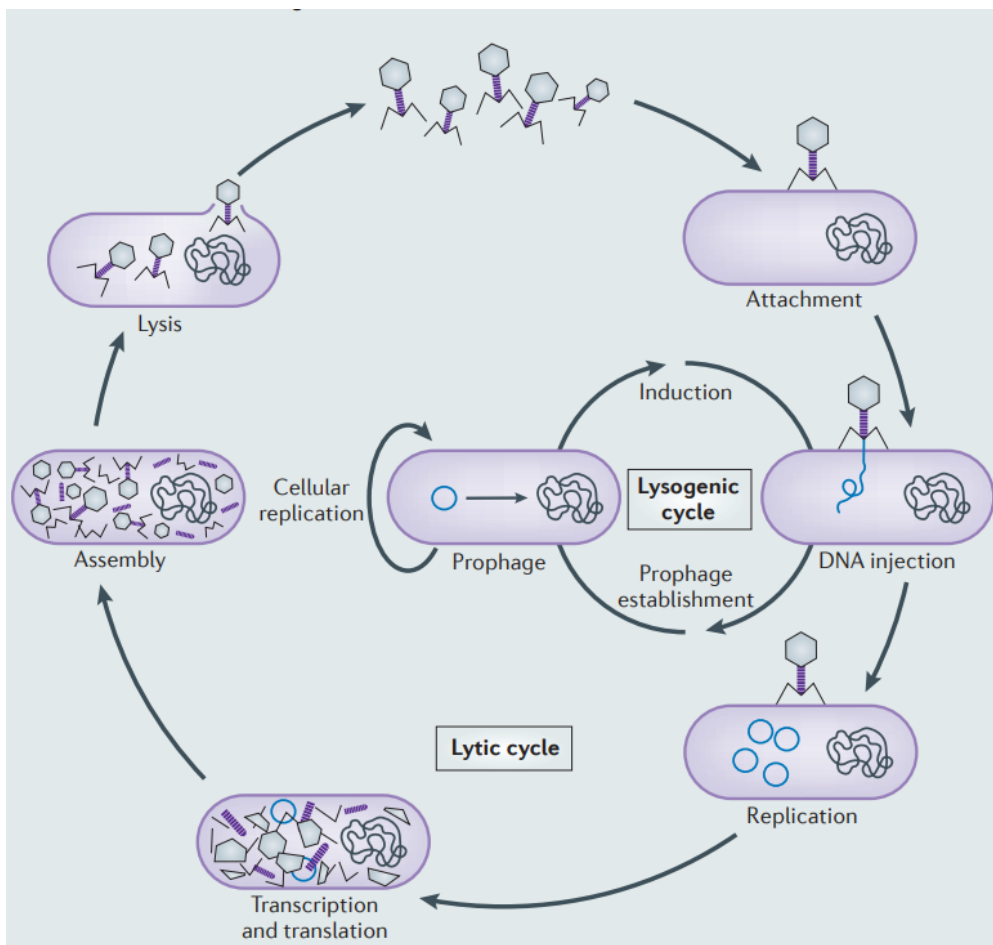


Figure 1.3: Summary of the phage lysogenic and lytic life cycles.

Taken from Seipke *et al.*, 2012

1.3 Glycosyltransferase structure and function

The glycosyltransferases are a diverse group of enzymes that transfer a sugar moiety from an activated donor substrate such as a nucleotide activated sugar to an acceptor substrate. Acceptor substrates include DNA, protein and lipid, in addition to sugar moieties of glycoproteins and glycolipids. (Lommel and Strahl, 2009). The names of many glycosyl transferases account for both the stereochemistry of the donor sugar and the created glycosidic linkage that connects the sugar with the acceptor substrate post catalysis (Figure 1.4). If the stereochemistry is changed from α to β or vice versa, the enzymes is characterised as an inverting glycosyl transferase, if the configuration remains unchanged, it is called a retaining glycosyl transferase.

Glycosyl transferases, exhibit a narrower range of folds, relative to the glycosyl hydrolases. The Carbohydrate Active Enzyme database (CAZy) classifies the glycosyltransferases into three distinct superfamilies GT-A, GT-B and GT-C, each with a distinct structural topology (Lombard *et al.*, 2014; Lommel and Strahl, 2009) (Figure 1.5). While the sequence diversity within the superfamilies can be considerable, the structural topologies and the chemical reaction mechanisms show little diversification.

Atomic resolution structures deposited in the Protein Data Bank show that the GT-A fold comprises an $\alpha/\beta/\alpha$ sandwich, whereby the β -sheet core has typically seven strands. In addition, the binding sites for the sugar nucleotide and acceptor substrate are in close proximity (within the same subdomain). Catalytic motifs are a hallmark of this family and while the DxD (where 'x' is any amino acid) motif is widespread, other variants including TDD, EDD and DxH have also been identified (Lommel and Strahl, 2009). GT-B domains consist of two Rossmann-like domains containing multiple parallel β -strands linked to α -helices. A linker region connects both N and C-terminal domains. One domain is involved in acceptor binding and the other in the donor nucleotide di-phosphate sugar binding, consequently, the active site resides in an interdomain cleft. In contrast to GT-A enzymes that are generally metal-ion dependent, the GT-B enzymes are generally metal-ion independent and consequently, lack the conserved motifs associated with divalent metal binding in the GT-A and GT-C enzymes. It is noteworthy that the GT-A and GT-B core structures can combine with other domains, such as regions that can anchor the protein to the membrane. Finally, the GT-C superfamily contains glycosyl transferases that have 8–13 predicted transmembrane (TM) helices, in addition to the first extracellular or luminal loop containing a DEx motif, other variants include DxD ExD, DxE, Dx. In many cases, multiple hydrophobic amino acids follow this acidic motif in the same loop (Lommel and Strahl, 2009).

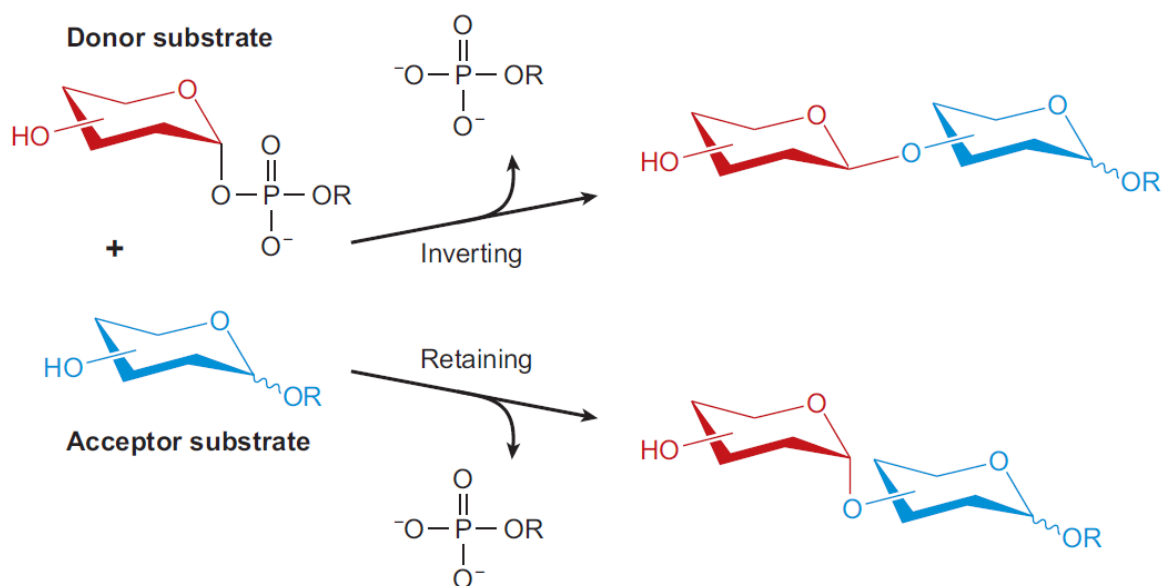


Figure 1.4: Stereochemistry of glycosyltransferase catalyzed reactions. Glycosyltransferases catalyse glycosyl group transfer with either inversion or retention of the anomeric stereochemistry with respect to the donor sugar.

Taken from Lommel and Strahl, 2009

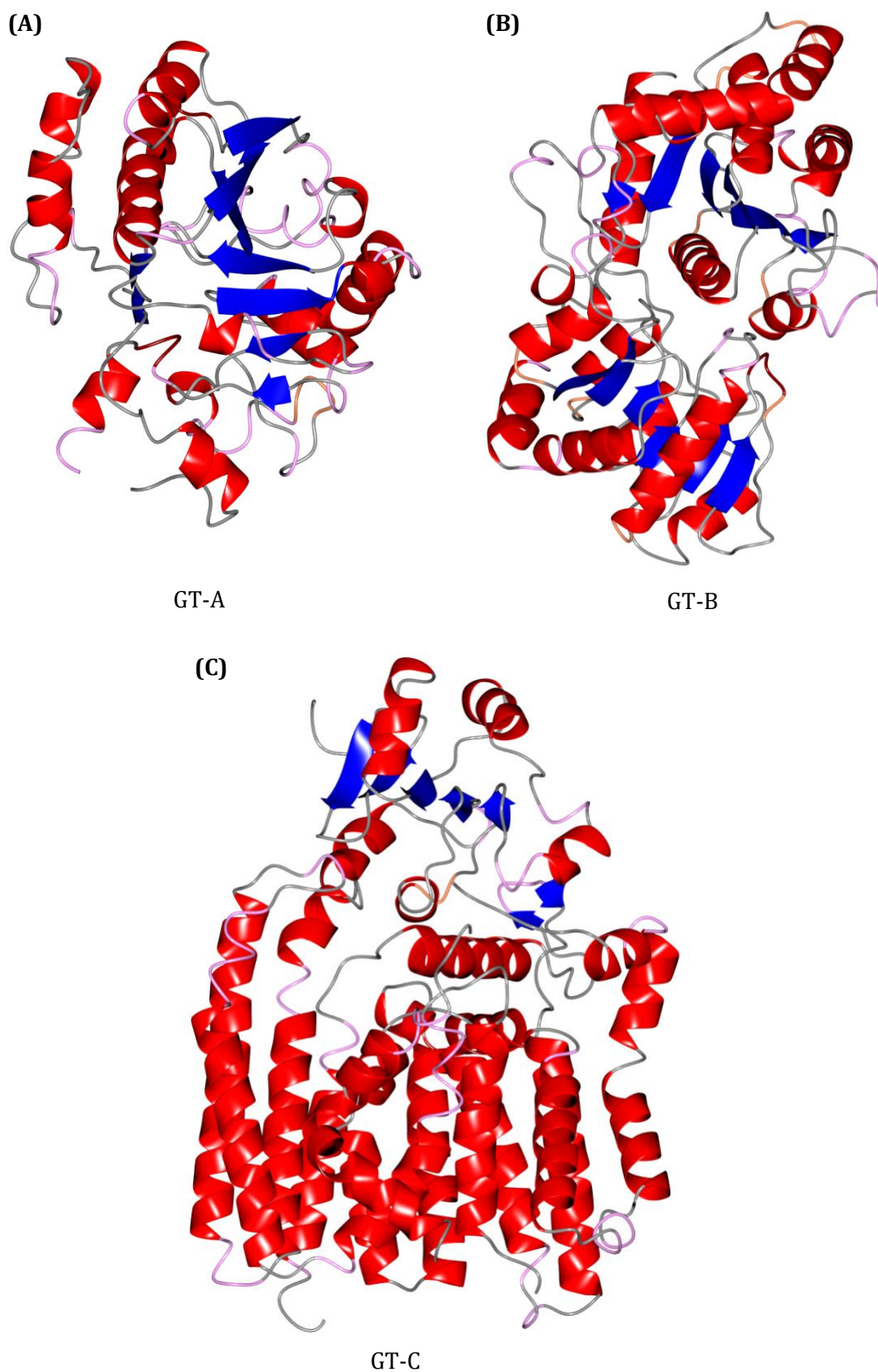


Figure 1.5: Topology of GT-A, GT-B and GT-C enzymes. (A) Lipopolysaccharyl-alpha-1,4-galactosyltransferase C (LgtC) from *Neisseria meningitides* (B) TDP-epi-Vancosaminyltransferase (GtfA) from *Amycolatopsis orientalis* (C) 4-amino-4-deoxy-L-arabinose transferase (ArnT) from *Cupriavidus metallidurans*.

1.4 Eukaryotic protein O-mannosylation

1.4.1 Principles of protein O-mannosylation in the eukaryotes

In *S. cerevisiae*, 20 % of cell dry weight is made up of cell wall, of which half is made up of mannosylated proteins (Strahl-Bolsinger *et al.*, 1999). Indeed, many of the fundamental features of protein O-mannosylation were first elucidated in yeast and later expanded, principally to humans and flies (Lommel and Strahl 2009). The O-linked sugar chains are unbranched and typically made up of four to five mannose sugars added to the serine or threonine side chain hydroxyl by a glycosidic linkage. These O-linked sugar chains are also notably shorter than N-linked sugar chains. Protein O-mannosylation is initiated in the endoplasmic reticulum in eukaryotes, with the initial steps between fungi, humans and animals being conserved (Haselbeck and Tanner 1983, Jurado *et al.*, 1999; Harty *et al.*, 2001; Ichimiya *et al.*, 2004; Manya *et al.*, 2004). Diversification is notable at the subsequent stage in the Golgi apparatus, where mannose chains are extended by the addition of mannose and/or other sugars such as N acetyl glucosamine, sialic acid and galactose (Romero *et al.*, 1999; Takahashi *et al.*, 2001). Protein O-mannosylation requires two glycosyl transferase catalysed steps: first the synthesis of the mannosyl donor and second, the transfer of mannose from the donor onto the acceptor polypeptide chains.

1.4.2 Mannosyl donor synthesis in the eukaryotes

The mannosyl donor in eukaryotes is dolichol phosphate β -D-mannose (Dol-P-Man). The donor is synthesised on the cytoplasmic face of the ER membrane and the mannose transfer to Dol-P is catalysed by GDP- α -D-Man:Dol-P β -D-mannosyltransferase (Lommel and Strahl 2009). Dpm1 was identified by Haselbeck (1989) with catalytic activity later demonstrated following *E. coli* heterologous expression (Orlean *et al.*, 1988). The same mannose donor is also used in N-glycosylation (whereby mannose is transferred to the amide of an asparagine side chain) and is required for LLO extension in the ER and GPI anchor biosynthesis (Kornfeld 1985; Stevens *et al.*, 1995) Knockout mutants of *dpm1* in the lower eukaryote *S. cerevisiae* are lethal (Orlean 1990), an unsurprising phenotype given the requirement of Dol-P-Man as a donor for yeast mannan synthesis. Similarly, in the higher eukaryote *Schizosaccharomyces pombe* disruption of the *dpm1* gene has also been shown to be lethal (Colussi *et al.*, 1997). In humans glycosylation defects related to human *dpm1* disruption have been linked to breast cancer, as well as congenital disorders of glycosylation (Lefeber *et al.*, 2009; Milde-Langosch *et al.*, 2014).

1.4.3 Protein O-mannosylation in the eukaryotes

Following Dol-P-Man synthesis by Dpm1, Dol-P-Man is flipped to the other side of the ER membrane by a currently unknown mechanism, though a flippase is believed to be involved (Lommel and Strahl 2009). A second glycosyl transferase Dol-P-Man:Protein O-mannosyltransferase (Pmt) then catalyses the transfer of mannose from Dol-P-Man to serine or threonine residues on the target protein. Considering the location of mannosylation, it was suggested that protein O-mannosylation was coupled to translocation into the ER (Shematek *et al.*, 1980). Since then, Pmt mediated protein O-mannosylation has been reported on misfolded proteins following their translocation to the ER. The modification served to both reduce the dependency on chaperones for protein folding, while increasing protein solubility through the addition of hydrophilic sugar moieties (Nakatsukasa *et al.*, 2004). Consequently, Pmt mediated protein O-mannosylation is not exclusively coupled to translocation into the ER, as previously thought.

In *S. cerevisiae*, there are at least six members of the PMT family (Pmt1p-Pmt6p) (Strahl-Bolsinger *et al.*, 1991; Strahl-Bolsinger *et al.*, 1993; Gentsch *et al.*, 1996). In *S. cerevisiae*, PMTs are known to form dimeric complexes; a complex readily observed is Pmt1p-Pmt2p (Lommel *et al.*, 2009). Functional studies showed the N-terminus of Pmt1p interacts with Pmt2p and that the central ER lumen facing loop 5 of Pmt1p is essential for the enzyme's mannosyl transferase activity (Girrbach *et al.*, 2000). The human equivalent to PMTs are the POMT family, Pomt1-Pomt2 complexes have been well studied and are essential for mannosyl transferase activity (Akasaka-Manyu *et al.*, 2006; Lommel and Strahl 2009). Complex formation therefore appears to be critical for PMT O-linked mannosylation activity in both yeast and humans.

Protein O-mannosylation and the impact of mannosylation defects have been more extensively probed in the eukaryotic kingdom. In *Candida albicans*, knockout mutations in Pmt isoforms affected growth, morphogenesis and antifungal resistance (Prill *et al.*, 2005) Protein O-mannosylation has a critical role in maintaining a stable cell wall in fungi, and it has been shown that knockout of Pmt family members in *S. cerevisiae*, *S. pombe*, *A. fumigatus* and *C. neoformans* is lethal (Gentsch and Tanner 1996; Willer *et al.*, 2005; Olson *et al.*, 2007; Mouyna *et al.*, 2010) Interestingly, in *S. cerevisiae*, ER stress can drive the expression of Pmt genes and the associated O-mannosylation helps to solubilise misfolded proteins in the ER. Solubilisation of misfolded proteins facilitates their degradation, preventing a potentially cytotoxic build-up of aggregates (Travers *et al.*, 2000; Nakatsukasa *et al.*, 2004; Hirayama *et al.*, 2008).

The best studied O-mannosylated protein in higher eukaryotes is α dystroglycan, an essential component of skeletal muscle. RNAi knockdown of *POMT1* or *POMT2* in *D. melanogaster*

reduced viability, notably, causing severe muscle development defects (Ichimiya *et al.*, 2004). Mutations in these genes during larval development yielded comparable phenotypes (Haines *et al.*, 2007). In mice embryos, *Pomt1* disruption is fatal (Willer *et al.*, 2004). In humans, mutations in either *POMT1* or *POMT2* contribute to Muscle-eye-brain disease (MEB) and Walker-Warburg syndrome (WWS). Both are autosomal recessively-inherited disorders characterised by muscular dystrophy and impaired neuronal migration. The visual impairment seen in both conditions is attributed to structural abnormalities and eye muscle paralysis in WWS and MBB respectively (Taniguchi *et al.*, 2003; Van Reeuwijk *et al.*, 2005; Van Reeuwijk *et al.*, 2006; Godfrey *et al.*, 2007).

While Pmt will add the first mannose to the protein in the ER membrane, extension of the growing chain is carried out by additional glycosyl transferases in the Golgi apparatus. In *S. cerevisiae* KTR and MNN-1 family mannosyl transferases further extend the glycan, creating $\alpha(1,2)$ and $\alpha(1,3)$ linkages (Lussier *et al.*, 1999). In *C. albicans* addition of the second mannose to the growing chain is catalysed by the mannosyl transferase, MNT1. The absence of this enzyme reduced the ability of the yeast cells to adhere to each other. These null mutants also showed greatly attenuated virulence in both mouse and guinea pig models of systemic candidosis (Buurman *et al.*, 1998).

1.5 Prokaryotic protein O-mannosylation

1.5.1 Principles of protein O-mannosylation in the prokaryotes

Before the mid-1970s protein glycosylation (and post translational modifications more generally) were thought to occur exclusively in the eukaryotic kingdom. This hypothesis was disproved upon the discovery of the first glycosylated prokaryotic glycoprotein in *Halobacterium salinarium* (Mescher *et al.*, 1976). It is now understood that prokaryotes can also decorate proteins with a variety of N- and O- linked glycans. Prokaryotic protein O-mannosylation is particularly well studied in *Mycobacteria* spp. with *Corynebacterium* spp. and *Streptomyces* spp. also attracting attention.

1.5.2 Mannosyl donor synthesis in the prokaryotes

The protein O-mannosylation pathway in prokaryotes is very similar to that seen in eukaryotes however there are several key differences. One notable difference is that the mannosyl donor is polyprenol phosphate, a functional analogue of dolichol phosphate (Strahl-Bolsinger *et al.*, 1999; Xing *et al.*, 2000; Cowlshaw *et al.*, 2002; Gurcha *et al.*, 2002; Gibson *et al.*, 2003). A polyprenol phosphate mannose synthase (homologous to the eukaryotic dolichol phosphate mannose synthases) transfers the mannose to the lipid phosphate. Prokaryotes however lack membrane bound organelles and consequently, mannosylation is initiated at the cytoplasmic membrane instead of the ER.

In *Corynebacterium glutamicum*, polyprenol phosphate mannose synthase possesses two domain architecture with separate catalytic and membrane domains (Gibson *et al.*, 2003). Inactivation of the catalytic domain led to a lipoglycan-less phenotype and a modest reduction in growth rate (Gibson *et al.*, 2003). The two domain architecture is also present in *M. tuberculosis*, but not in *M. smegmatis* and *M. leprae*, which instead produce two separate proteins (one catalytic and one membrane) encoded by adjacent genes (*ppm1* and *ppm2*) (Gurcha *et al.*, 2002). The *M. smegmatis* Ppm1 homologue of the *M. tuberculosis* catalytic domain has previously been shown to be essential for survival (Gurcha *et al.*, 2002). The introduction of a functional copy of the gene encoding *M. tuberculosis* PpmD2, the catalytic equivalent, was later shown to be sufficient to rescue the phenotype of *M. smegmatis* Ppm1 mutants (Rana *et al.*, 2012). Finally, in *M. smegmatis*, the membrane protein Ppm2 was shown to be an integral membrane protein that greatly enhanced the catalytic activity of Ppm1 (Baulard *et al.*, 2003). These studies indicate that the two domain architecture of *C. glutamicum* and *M. tuberculosis* Ppm1 likely also anchors the protein to the membrane.

1.5.3 Protein O-mannosylation in *Mycobacterium* species

As previously mentioned, protein O-mannosylation was first thought to be confined to the eukaryotes. The first understanding that mannosylation also took place in actinobacteria came with the isolation of culture filtrate proteins that were capable of binding the lectin concanavalin (Con A) (Espitia *et al.*, 1989). Direct evidence for glycosylated residues on a mycobacterial protein was shown a few years later, whereby a purified culture filtrate protein was shown to have mannobiose or mannotriose sugars linked to threonine residues, the glycans were composed of α 1,2 linkages (Dobos *et al.*, 1995). α 1,3 linkages were subsequently identified in a secreted glycoprotein from *Mycobacterium bovis* (Michell *et al.*, 2003). Analysis of *Mycobacterium tuberculosis* culture filtrate showed glycosylation occurring on both threonine and serine residues (Smith *et al.*, 2014).

The PMT homologue of *M. tuberculosis* was shown to catalyse the first step in the mannosylation of unfolded proteins translocated by the SEC pathway (VanderVen *et al.*, 2005). Inactivation of *M. tuberculosis* Pmt greatly impaired growth and reduced pathogenicity in immunocompromised mice (Liu *et al.*, 2013). Comparable mutants in *M. smegmatis* lacked the growth-retarded phenotype, however mutant hypersensitivity to SDS treatment indicates the loss of Pmt likely results in changes to overall cell wall composition.

A Ppm-dependent α 1,2 mannosyl transferase (PimE) was subsequently identified in *M. smegmatis* and implicated in elongation of the glycan chain, the identification of α 1,2- linked mannobiose and mannotriose glycans indicates a similar mechanism of glycan extension also exists in other mycobacteria (Morita *et al.*, 2006).

It is thought that protein O-mannosylation has a role in pathogenicity. Mannosylation of secreted proteins has specifically been shown to stimulate T lymphocyte responses (Horn *et al.*, 1999). Altered mannosylation patterns of the glycoprotein Apa in *M. smegmatis* had a limited ability to stimulate an *in vitro* T lymphocyte response, Apa that completely lacked mannosylation completely failed to stimulate a response (Horn *et al.*, 1999). This is supported by further studies showing that mannosylation is required for interactions with host immune system C-type lectins, again indicting the glycosylation status of Apa is important for immune system recognition (Ragas *et al.*, 2007). In *M. tuberculosis* and *M. leprae* similar studies have been conducted. A secreted protein SodC is recognised by antibodies (Sartain *et al.*, 2009). Furthermore, *M. leprae* SodC binds in a carbohydrate dependent manner to r-langerin on antigen presenting dendritic cells of the immune system (Kim *et al.*, 2015). These studies in mycobacteria indicates that antigenicity of secreted antigens is strongly linked to correct mannosylation.

1.5.4 Protein O-mannosylation in *Streptomyces*

Streptomyces protein O-mannosylation was first reported following Cowlshaw and Smith's investigation that aimed to probe the molecular basis of Φ C31 infection of *Streptomyces coelicolor*. UV-induced and spontaneous mutants were identified that were resistant to the lytic phage Φ C31 *c* Δ 25. While transfection of phage DNA into protoplasts of the resistant mutants that were regenerated in the presence of sensitive hosts was sufficient to cause a lytic burst, the phage could not form plaques on these mutants. The implication was that Φ C31 infection was blocked at the receptor binding stage. It was eventually deduced through genetic analysis and subsequent complementation studies that four of thirteen phage resistant mutants were deficient in *Pmt*. (Cowlshaw and Smith 2001). It was then thought that since PMT was a mannosyl transferase, another gene encoding an enzyme in the same pathway might complement the remaining nine mutants. A gene encoding a homologue of *S. cerevisiae* Dpm1 and mycobacterial Ppm1 was identified. The product was therefore predicted to be *S. coelicolor* Ppm1. Introduction of the *SCO1423* allele did complement three additional strains that had not been complemented by *SCO3145* (Cowlshaw and Smith 2002). The link with glycosylation was further shown with the identification of glycosylated proteins via western blot analysis of the *ppm1*⁺, *pmt*⁺ parent strain (J1929) using ConA as a probe. The proteins were not detected in the *pmt*⁻ strain DT1025 (Cowlshaw and Smith 2002).

The first characterised glycoprotein from *S. coelicolor* is PstS, a lipoprotein that is part of a high affinity phosphate uptake system. This protein was shown to be mannosylated with a trihexose in the J1929 parent strain, but not the *pmt* null mutant strain DT1025 (Wehmeier *et al.*, 2009). Two serine rich synthetic peptides, designed using the PstS sequence as a template, were shown to be glycosylated by membranes derived from J1929, these peptide studies indicated that O-mannosylation occurs only on specific serine or threonine residues, rather than being a random process. Further studies showed that Ppm1 was able to transfer mannose from a nucleotide activated sugar (GDP-mannose) onto the polyprenol phosphate in purified *S. coelicolor* membrane fractions. The lipid linked carrier polyprenol phosphate was therefore confirmed for the first time to be required for O-linked glycosylation, with the sugar itself being a mannose.

Since it was already understood that mycobacteria Ppm1 had a two-domain architecture (with either 1) one domain anchored to the membrane or 2) separate catalytic and membrane embedded proteins that formed a complex. One of these mechanisms was presumably involved in localisation of *S. coelicolor* Ppm1 to the membrane. The absence of continuous hydrophobic stretches that could constitute a transmembrane helix in the *S. coelicolor* Ppm1 primary structure meant that *S. coelicolor* Ppm1 presumably interacted with another protein that would ensure localisation to the membrane. The membrane protein Lnt1 (encoded by the *SCO1014*

gene) was identified as a homologue of the membrane associated domain of *M. tuberculosis* was identified in *S. coelicolor*. Lnt1 was suspected to be an interacting partner, however further investigation revealed that Lnt1 and Ppm1 did not interact (Anttonen 2010; Cordova Davalos *et al.*, 2014). Lnt1 mutants were sensitive to infection by Φ C31 and were also shown to glycosylate the *M. tuberculosis* glycoprotein Apa (Cordova Davalos *et al.*, 2014). There remains no evidence that Lnt1 is required for glycosylation in *S. coelicolor*.

In addition to being resistant to phage infections, the *ppm1* and *pmt* - strains identified by Cowlshaw and Smith (2001) had a growth-retarded phenotype. It was also noted that the *ppm1* - strains exhibited greatly increased susceptibility to multiple cell wall targeting antibiotics including vancomycin, daptomycin and multiple β -lactams (Howlett *et al.*, 2018a). The phenotype was less extreme in the *pmt* - strains, nevertheless notable increases in sensitivity were shown for vancomycin and the carbapenems imipenem and meropenem. Induction of the vancomycin resistance cluster failed to alleviate the high vancomycin sensitivity of the *ppm1* and *pmt* - mutants. The implication of these studies was that Pmt mediated glycosylation is required for the function of periplasmic and membrane enzymes required for cell wall biosynthesis. Furthermore, RNAseq analysis conducted by Howlett *et al.* (2018a) showed *S. coelicolor ppm1* - mutants had increased expression of fatty acid biosynthesis genes and a greater proportion of unsaturated fatty acids. Additional Raman spectroscopy analysis showed changes in membrane lipids in the *ppm1* deficient strain.

Enzymes in the GDP-mannose synthesis pathway were later probed, namely phosphomannomutase (ManB - encoded by *SCO3028*) which converts mannose-6-phosphate to mannose-1 phosphate, and the GDP mannose pyrophosphorylases (ManC - encoded by *SCO1388*, *SCO3039* and *SCO4238*) that use GTP and mannose-1-phosphate as substrates to synthesise GDP mannose. *SCO3039* and *SCO4238* were investigated further and their importance for growth was indicated by the failure to generate a strain in which *SCO3039* and *SCO4238* were completely knocked out (Howlett *et al.*, 2018b). *S. coelicolor* strains with knocked down ManC activity or with a mutation in *SCO3028* rendering ManB inactive acquire phenotypes that closely resemble those of the *ppm1* - mutants (ϕ C31 resistant and susceptible to cell wall inhibitor antibiotics). Interestingly, the *manB* - strains had an extremely small colony phenotype. These findings indicate that ManB and ManC are an essential part of the protein O-mannosylation pathway in *S. coelicolor*. Furthermore, GDP-mannose itself may lie at branch point in metabolism, whereby it could be subject to further modification to supply alternative nucleotide activated sugar donors.

The most recent published work on protein O-mannosylation in *S. coelicolor* describes a combination of biochemical and mass spectrometry approaches, resulting in the

characterisation of the *S. coelicolor* membrane glycoproteome for the first time (Keenan *et al.*, 2019). In this study, 37 novel *S. coelicolor* glycoproteins were identified, in addition to a more detailed understanding of PstS glycosylation sites. The glycoproteins identified have diverse roles including solute binding, ABC transporters, and cell wall biosynthesis. This is of particular interest considering the previously identified increased susceptibility of *pmt* - strains to cell wall targeting antibiotics. Two cell wall active glycoproteins identified in this study ((a putative D-Ala-D-Ala carboxypeptidase (SCO4847) and an L,D-transpeptidase (SCO4934)) were mutated and the resulting strains were found to be hypersensitive to cell wall targeting antibiotics. These findings indicate a crucial role for glycoproteins in the maintenance of cell wall stability in *S. coelicolor*.

1.5.5 The current model for protein O-mannosylation in *S. coelicolor*

Based on all the currently available literature, a model for *S. coelicolor* protein O-mannosylation can be proposed (Figure 1.6). GDP mannose biosynthesis is carried out by the phosphomannose isomerase, the phosphomannomutase Man B. and the GDP-Mannose pyrophosphorylases ManC. With the nucleotide activated sugar GDP-mannose synthesised, Ppm1 catalyses the transfer of mannose to polyprenol phosphate on the cytoplasmic face of the membrane. Presumably, Ppm1 is anchored to the membrane by an interacting membrane protein or an anchor of some kind, however the means by which Ppm1 is localised to the membrane remains unknown. The mannosylated polyprenol is then flipped onto the periplasmic face of the membrane, a flippase is thought to be responsible however the mechanism also remains unknown. Finally Pmt catalyses the first step in protein O-mannosylation by adding the first mannose from polyprenol phosphate mannose, to serine or threonine residues in target proteins.

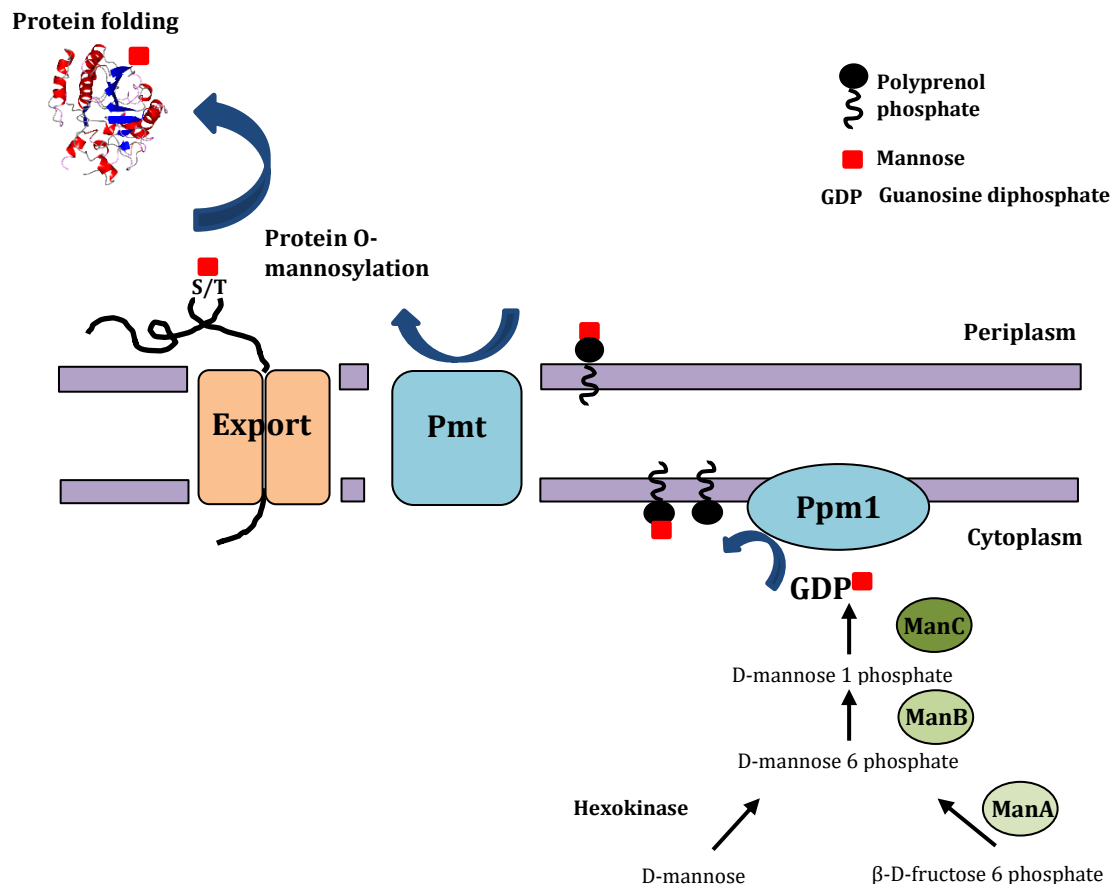


Figure 1.6: Current protein O-glycosylation model for *S. coelicolor*

1.6 Aims

The antibiotic hyper susceptibility phenotypes obtained in mannosylation deficient strains of *S. coelicolor* are of great interest, since homologues of Ppm1 and Pmt are found in pathogenic bacteria. Inhibitors of these enzymes could potentially be used in combination with our existing arsenal of antibiotics. Given the depleted antibiotic pipeline, and the ever-increasing emergence of resistance, resensitising pathogenic bacteria to our current arsenal of antibiotics could be a significant turning point in this evolutionary arms race. The long term goal of Ppm1 and Pmt inhibitor development, is contingent on first gaining a more intimate understanding of enzyme function through mutational analysis.

The aim of this project was therefore to develop and test a library of *S. coelicolor* Ppm1 and Pmt mutants in order to better understand the roles of residues critical for *in vivo* activity

Specifically the objectives were:

1. Express and purify pure, stable and homogenous polyprenol phosphate mannose synthase for structure and function studies.
2. Produce a library of *ppm1* mutant alleles and test their ability to complement a *ppm1*-strain using antibiotic/phage susceptibility assays, in addition to colony phenotype analysis.
3. Develop a model to define roles for any residues critical for Ppm1 activity using *in vivo* mutant characterisation, structural bioinformatics approaches and existing literature.
4. Produce a library of *pmt* mutant alleles and test their ability to complement a *pmt* - strain using antibiotic/phage susceptibility assays, in addition to colony phenotype analysis.
5. Develop a model to define roles for any residues critical for Pmt activity using *in vivo* mutant characterisation, structural bioinformatics approaches and existing literature.

Chapter 2 – Materials and methods

2.1 Materials

2.1.1 Chemicals

All chemicals were purchased from Sigma-Aldrich, Fisher Scientific, Thermo Fisher, Melford or VWR International unless otherwise stated. Difco nutrient broth (DNB) and Difco nutrient agar (DNA) (Beckton Dickinson and Company), both used for the growth of *S. coelicolor* were purchased from Appleton Woods Ltd. Soya flour, also used for *S. coelicolor* growth was purchased from Holland & Barratt. All restriction enzymes, DNA polymerases and deoxynucleotides were purchased from New England Biolabs. PCR primers were purchased from Integrated DNA Technologies. DNA sequencing was carried out by Eurofins Genomics.

2.1.2 Media and buffers

Difco nutrient broth (DNB) (Kieser *et al.*, 2000): 8 g of DNB powder was made up to 1000 ml with ddH₂O and autoclaved (115 °C, 15 min).

Difco nutrient agar (DNA) (Kieser *et al.*, 2000): 4.6 g of solid DNA was made up to 250 ml with ddH₂O and autoclaved (115 °C, 15 min).

Soft nutrient agar (SNA) (Kieser *et al.*, 2000): 8 g of DNB powder was made up to 1000 ml with ddH₂O and autoclaved (115 °C, 15 min).

Mannitol soya flour agar (MSA) (Kieser *et al.*, 2000): 4 g of mannitol, 4 g soya flour and 4 g agar was made up to 250 ml with ddH₂O and autoclaved twice (115 °C, 15 min).

2x YT medium (Sandbrook *et al.*, 1989): 16 g Bacto Tryptone, 10 g Bacto Yeast Extract and 5 g NaCl was made up to 1000 ml with ddH₂O and autoclaved (115 °C, 15 min).

Luria Burtani (LB) broth and agar (Sandbrook *et al.*, 1989): 10 g tryptone, 10 g NaCl and 5 g yeast extract were dissolved in ddH₂O and made up to 1000 ml. For LB agar, 1.5 g of agar per 100 ml of LB broth was added and autoclaved (115 °C, 15 min).

2.1.3 Software

Snappgene Viewer software (version 3.2) was used for plasmid map construction and analysis of sequencing data. BLAST was used to carry out gene and protein sequence homology searches <https://blast.ncbi.nlm.nih.gov/Blast.cgi>. Clustal omega was used to perform multiple sequence alignments <https://www.ebi.ac.uk/Tools/msa/clustalo/>. Agarose gels were analysed using Quantity one (version 4.6.2; Basic) software. Transmembrane helices were predicted using the TMHMM Server v. 2.0 algorithm <http://www.cbs.dtu.dk/services/TMHMM/>. Phyre2 was used to generate homology models <http://www.sbg.bio.ic.ac.uk/phyre2/html/page.cgi?id=index> . CCP4-MG was used to visualise protein structures (McNicholas *et al.*, 2011). ChemDraw was used to draw chemical structures and reaction mechanisms (PerkinElmer Informatics).

2.1.4 Primers and plasmids

Primers for PCR were supplied by IDT. Sequences are shown below:

Table 2.1: List of PCR primer sequences

Primer	Sequence	Use
<i>Ippm1F</i>	5'-ACAGGAGGCCCATATGAACGACGGCGACGGGAC	Amplify integration <i>ppm1</i>
<i>Ippm1R</i>	5'-TCACTCGAGATCTCATATGTCAGGCCTTGGCGT	Amplify integration <i>ppm1</i>
<i>Nppm1F</i>	5'-ATGCTAGTCGCGGTTGATCG	Amplify native <i>ppm1</i>
<i>Nppm1R</i>	5'-TCGTTAGTCGGAGGCCAAACG	Amplify native <i>ppm1</i>
<i>IpmtF</i>	5'-ACAGGAGGCCCATATGCACAGCGCGTTCCC	Amplify integration <i>pmt</i>
<i>IpmtR</i>	5'TCACTCGAGATCTCATATGCTAGACCCACGTGTCGAGCCAC	Amplify integration <i>pmt</i>
<i>IpmtNSF</i>	5'ACAGGAGGCCCATATGTGGAGCCACCCGAGTTCGAGAAGCACAGCGCGGTTCCC	Amplify integration <i>pmt</i> + N-terminal StrepII tag
<i>IpmtCSR</i>	5'TCACTCGAGATCTCATATGCTACTTCTCGAACTGCGGGTGGCTCCAGACCCACGTGT	Amplify integration <i>pmt</i> + C-terminal StrepII tag
R82AF	5'-GATGATC GCC TGGTCGGCGTGGGGCGGGC	<i>pmt</i> mutagenesis
R82AR	5'-GACCA GGC GATCATCCGGTCGGTGAGCGG	<i>pmt</i> mutagenesis
D113AF	5'-GATATTCG CG GAGACGTAACGCAAGGACGCG	<i>pmt</i> mutagenesis
D113AR	5'-CGTCTC CG GAATATCACCGCCTTCGGGC	<i>pmt</i> mutagenesis
E114AF	5'-ATTTCGACG CC ACGTAACGCAAGGACGCGT	<i>pmt</i> mutagenesis
E114AR	5'-GTACGT GGC GTGCAATATCACCGCCTTCGGGC	<i>pmt</i> mutagenesis
V158AF	5'-GTACGTCG CG CACCCGCGGTGCGCAAG	<i>pmt</i> mutagenesis
V158AR	5'-GGGTG CG CGACGTACGCCGCGTGGT	<i>pmt</i> mutagenesis
H159AF	5'-CGTCGTC GC CCCGCGGTGCGCAAGTAC	<i>pmt</i> mutagenesis
H159AR	5'-CCGGCGGG GC GACGACGTACGCCG	<i>pmt</i> mutagenesis
P160AF	5'-GTCCAC GCC CCGGTGGCAAGTACATCATCGG	<i>pmt</i> mutagenesis
P160AR	5'-CCGACCGG GGC GTGGACGACGTACGCCG	<i>pmt</i> mutagenesis
P161AF	5'-CCACCCG GCC GTGGCAAGTACATCATCGGC	<i>pmt</i> mutagenesis
P161AR	5'-CTTGCCGAC GGC CGGGTGGACGACGTAC	<i>pmt</i> mutagenesis
K164AF	5'-GGTCGGC GC GTACATCATCGGCCTCGGC	<i>pmt</i> mutagenesis
K164AR	5'-TGATGTAC GC GCCGACCGCGGGTGGAC	<i>pmt</i> mutagenesis
R182AF	5'-CGGCTGG GC CCTTCATGACGGCGCTGCTCG	<i>pmt</i> mutagenesis
R182AR	5'-ATGAAG GCC CAGCCGAACGGGTGCAAGCC	<i>pmt</i> mutagenesis
R201AF	5'-GATCGGC GC CCGCCTGTTCCGCTCCACGTTC	<i>pmt</i> mutagenesis
R201AR	5'-AGGCGG GC GCCGATCCGGCACAGCAGC	<i>pmt</i> mutagenesis
R228AF	5'-GATGAGC GC CACCGCGTGTGGACAGC	<i>pmt</i> mutagenesis
R228AR	5'-GCGGTG GC GCTCATCACGAAGTGCAGGCC	<i>pmt</i> mutagenesis
L231AF	5'-CACCGCG GC GCTGGACAGCGTGTGATGTTTC	<i>pmt</i> mutagenesis
L231AR	5'-TCCAGC GC CGGGTGGGCTCATCACG	<i>pmt</i> mutagenesis
L232AF	5'-CGCGCTG GC GGACAGCGTGTGATGTTCTTC	<i>pmt</i> mutagenesis
L232AR	5'-CTGTCC GC CAGCGCGGTGGGCTCATCACG	<i>pmt</i> mutagenesis
D220AF	5'-GGCGCTGG CG GGCCTGCACTTCGTGATGAGC	<i>pmt</i> mutagenesis
D220AR	5'-AGGCC CG CCAGCGCCATCAGGGCGC	<i>pmt</i> mutagenesis
D233AF	5'-GCTGCTGG CG AGCGTGTGATGTTCTTCGTGC	<i>pmt</i> mutagenesis

D233AR	5'-ACGCT CG CCAGCAGCGGGTGGGCTCATC	<i>pmt</i> mutagenesis
K332AF	5'-GGCCACC GCG TGGAACGGCCTCTACATCATGG	<i>pmt</i> mutagenesis
K332AR	5'-TTCCAC GCG GGTGGCCGCCAGGCCA	<i>pmt</i> mutagenesis
R338AF	5'-CGTACTC GCC CCAGACCTGGGCTGGGCTTCC	<i>pmt</i> mutagenesis
R338AR	5'-TCGTGG GCG GAGTACGGCGGGTAGGGGC	<i>pmt</i> mutagenesis
P393AF	5'-GCTCTTC GCG GACTGGTGGCGCAGCTGTG	<i>pmt</i> mutagenesis
P393AR	5'-CCAGTC GCG GAAGAGCCACGACCAGGAGCTG	<i>pmt</i> mutagenesis
W400AF	5'-GCAGCCTG GCC ACTACGAGACCAGGTCCTCG	<i>pmt</i> mutagenesis
W400AR	5'-GTAGTG GCC CAGGCTGCGCCACCAGTCGG	<i>pmt</i> mutagenesis
H410AF	5'-CGAATTC GCC CACCCACCTGACCTCGCCGCA	<i>pmt</i> mutagenesis
H410AR	5'-TGGGTG GCG GAATTCGAGGACCTGGGTCTCG	<i>pmt</i> mutagenesis
S421AF	5'-CTACCAG GCC AACCCCTGGAGCTGGATCG	<i>pmt</i> mutagenesis
S421AR	5'AGGGGTT GCC CTGGTAGGTGTGCGCGAGGTCAGG	<i>pmt</i> mutagenesis
W426AF	5'-CTGGAGC GCG GATCGTCTGGGCCGCCGGTCTC	<i>pmt</i> mutagenesis
W426AR	5'-ACGATC GCG GCTCCAGGGTTCGACTGGTAGG	<i>pmt</i> mutagenesis
R510AF	5'-CCAGGAG GCC CACGATCTTCTTCTACGCCG	<i>pmt</i> mutagenesis
R510AR	5'-ATCGTG GCC CTCCTGGTACATGAACCAGGGCAG	<i>pmt</i> mutagenesis
F564AF	5'-GTGGAAC GCC CATCTACTTCTGGCCCTGTACACGG	<i>pmt</i> mutagenesis
F564AR	5'-GTAGATG GCG TTCCACGCGATGAGGAGCACCAGG	<i>pmt</i> mutagenesis
R82KF	CGACCA CTT GATCATCCGGTCGGTGAGCGG	<i>pmt</i> mutagenesis
R82KR	ACCGGATGATC AAG TGGTCGGCGTGGGGC	<i>pmt</i> mutagenesis
R82HF	ATGATCC A CTGGTCGGCGTGGGGC	<i>pmt</i> mutagenesis
R82HR	GACCAG T GGATCATCCGGTCGGTGAG	<i>pmt</i> mutagenesis
D113PF	GATATTC CCC GAGACGTAACGCAAGGACGCG	<i>pmt</i> mutagenesis
D113PR	CGTCTCG GG GAATATCACCGCCTTCGGGC	<i>pmt</i> mutagenesis
D113LF	GATATTC CT CGAGACGTAACGCAAGGACGCG	<i>pmt</i> mutagenesis
D113LR	CGTCTCG AG GAATATCACCGCCTTCGGGC	<i>pmt</i> mutagenesis
D113YF	GATATTC T ACGAGACGTAACGCAAGGACGCG	<i>pmt</i> mutagenesis
D113YR	CGTCTCGT A GAATATCACCGCCTTCGGGC	<i>pmt</i> mutagenesis
D113SF	GATATTC AG CGAGACGTAACGCAAGGACGCG	<i>pmt</i> mutagenesis
D113SR	CGTCTCG CT GAATATCACCGCCTTCGGGC	<i>pmt</i> mutagenesis
D113RF	GATATTC CG CGAGACGTAACGCAAGGACGCG	<i>pmt</i> mutagenesis
D113RR	CGTCTCG CG GAATATCACCGCCTTCGGGC	<i>pmt</i> mutagenesis
D113NF	GATATTC A ACGAGACGTAACGCAAGGACGCG	<i>pmt</i> mutagenesis
D113NR	CGTCTCGT T GAATATCACCGCCTTCGGGC	<i>pmt</i> mutagenesis
D113EF	GATATTCG AG GAGACGTAACGCAAGGACGCG	<i>pmt</i> mutagenesis
D113ER	GTACGTCTC C TGAATATCACCGCCTTCGGGC	<i>pmt</i> mutagenesis
H159KF	GTCGTC AAG CCGCCGGTCGGCAAGTAC	<i>pmt</i> mutagenesis
H159KR	CCGGCGG CTT GACGACGTACGCCGCGTC	<i>pmt</i> mutagenesis
H159NF	TCGTC A ACCCGCCGGTCGGCAAG	<i>pmt</i> mutagenesis
H159NR	GGCGGGT T GACGACGTACGCCG	<i>pmt</i> mutagenesis
D233NF	GCTGCTG AAT AGCGTGCTGATGTTCTTCGTGC	<i>pmt</i> mutagenesis
D233NR	ACGCT ATT CAGCAGCGGGTGGGCTCATC	<i>pmt</i> mutagenesis
D233EF	CTGCTGG AG AGCGTGCTGATGTTCTTCGTGC	<i>pmt</i> mutagenesis
D233ER	ACGCT C TCCAGCAGCGGGTGGC	<i>pmt</i> mutagenesis
K332HF	CCACC CAC TGGAACGGCCTCTACATCATGG	<i>pmt</i> mutagenesis
K332HR	TTCCA GTG GGTGGCCGCCAGGCC	<i>pmt</i> mutagenesis
K332RF	CCACC CG GTGGAACGGCCTCTACATCATGG	<i>pmt</i> mutagenesis

K332RR	TTCCAC CG GGTGGCCGCGCCAGGCCA	<i>pmt</i> mutagenesis
R510HF	ACCAGGAGC A CACGATCTTCCTCTTCTACGCCGTC	<i>pmt</i> mutagenesis
R510HR	AGATCGTG T GCTCCTGGTACATGAACCAGGG	<i>pmt</i> mutagenesis
R510KF	ACCAGGAG AAG ACGATCTTCCTCTTCTACGCCGTC	<i>pmt</i> mutagenesis
R510KR	AGATCGT CTT CTCCTGGTACATGAACCAGGGCAGG	<i>pmt</i> mutagenesis

Table 2.2: List of constructs

Plasmid	Details	Reference
pIJ10257	Integrating vector conferring hygromycin resistance with constitutive ermEp* promoter	Gregory <i>et al.</i> , 2003
pNHC1	ScPpm1 (WT) in pIJ10257	This work
pNHC2	ScPpm1 (D57A) in pIJ10257	This work
pNHC3	ScPpm1 (R82A) in pIJ10257	This work
pNHC4	ScPpm1 (D111A) in pIJ10257	This work
pNHC5	ScPpm1 (D113A) in pIJ10257	This work
pNHC6	ScPpm1 (H116D) in pIJ10257	This work
pNHC7	ScPpm1 (R138A) in pIJ10257	This work
pNHC8	ScPpm1 (G143V) in pIJ10257	This work
pNHC9	ScPpm1 (S163L) in pIJ10257	This work
pNHC10	ScPpm1 (R226A) in pIJ10257	This work
pNHC18	ScPmt (WT) in pIJ10257	This work
pNHC19	ScPmt (R82) in pIJ10257	This work
pNHC20	ScPmt (D113A) in pIJ10257	This work
pNHC21	ScPmt (E114A) in pIJ10257	This work
pNHC22	ScPmt (V158A) in pIJ10257	This work
pNHC23	ScPmt (H159A) in pIJ10257	This work
pNHC24	ScPmt (P161A) in pIJ10257	This work
pNHC25	ScPmt (K164A) in pIJ10257	This work
pNHC26	ScPmt (R182A) in pIJ10257	This work
pNHC27	ScPmt (R201A) in pIJ10257	This work
pNHC28	ScPmt (R228A) in pIJ10257	This work
pNHC29	ScPmt (L231A) in pIJ10257	This work
pNHC30	ScPmt (L232A) in pIJ10257	This work
pNHC31	ScPmt (D233A) in pIJ10257	This work
pNHC32	ScPmt (K332A) in pIJ10257	This work
pNHC33	ScPmt (R335A) in pIJ10257	This work
pNHC34	ScPmt (P393A) in pIJ10257	This work
pNHC35	ScPmt (W400A) in pIJ10257	This work
pNHC36	ScPmt (H410A) in pIJ10257	This work
pNHC37	ScPmt (S421A) in pIJ10257	This work
pNHC38	ScPmt (W426A) in pIJ10257	This work
pNHC39	ScPmt (P503A) in pIJ10257	This work
pNHC40	ScPmt (R510A) in pIJ10257	This work
pNHC41	ScPmt (F564A) in pIJ10257	This work
pNHC42	ScPmt (N-StrepII R82A) in pIJ10257	This work
pNHC43	ScPmt (C-StrepII + R82A) in pIJ10257	This work
pNHC44	ScPmt (N-StrepII + D113A) in pIJ10257	This work
pNHC45	ScPmt (C-StrepII + D113A) in pIJ10257	This work
pNHC46	ScPmt (N-StrepII + H159A) in pIJ10257	This work
pNHC47	ScPmt (C-StrepII + H159A) in pIJ10257	This work
pNHC48	ScPmt (N-StrepII + D233A) in pIJ10257	This work

pNHC49	ScPmt (C-StrepII + D233A) in pIJ10257	This work
pNHC50	ScPmt (N-StrepII + K302A) in pIJ10257	This work
pNHC51	ScPmt (C-StrepII + K302A) in pIJ10257	This work
pNHC52	ScPmt (N-StrepII + R510A) in pIJ10257	This work
pNHC53	ScPmt (C-StrepII + R510A) in pIJ10257	This work
pNHC54	ScPmt (N-StrepII + P160A) in pIJ10257	This work
pNHC55	ScPmt (C-StrepII + P160A) in pIJ10257	This work
pNHC56	ScPmt (N-StrepII + K164A) in pIJ10257	This work
pNHC57	ScPmt (C-StrepII + K164A) in pIJ10257	This work
pNHC58	ScPmt (N-StrepII + R228A) in pIJ10257	This work
pNHC59	ScPmt (C-StrepII + R228A) in pIJ10257	This work
pNHC60	ScPmt (N-StrepII + L231A) in pIJ10257	This work
pNHC61	ScPmt (C-StrepII + L231A) in pIJ10257	This work
pNHC62	ScPmt (N-StrepII + R335A) in pIJ10257	This work
pNHC63	ScPmt (C-StrepII + R335A) in pIJ10257	This work
pNHC64	ScPmt (N-StrepII + S421A) in pIJ10257	This work
pNHC65	ScPmt (C-StrepII + S421A) in pIJ10257	This work
pNHC72	ScPmt (C-StrepII + R82K) in pIJ10257	This work
pNHC73	ScPmt (C-StrepII + R82H) in pIJ10257	This work
pNHC74	ScPmt (C-StrepII + D113P) in pIJ10257	This work
pNHC75	ScPmt (C-StrepII + D113L) in pIJ10257	This work
pNHC76	ScPmt (C-StrepII + D113Y) in pIJ10257	This work
pNHC77	ScPmt (C-StrepII + D113S) in pIJ10257	This work
pNHC78	ScPmt (C-StrepII + D113R) in pIJ10257	This work
pNHC79	ScPmt (C-StrepII + D113N) in pIJ10257	This work
pNHC80	ScPmt (C-StrepII + D113E) in pIJ10257	This work
pNHC81	ScPmt (C-StrepII + H159K) in pIJ10257	This work
pNHC82	ScPmt (C-StrepII + H159N) in pIJ10257	This work
pNHC83	ScPmt (C-StrepII + D233N) in pIJ10257	This work
pNHC84	ScPmt (C-StrepII + D233E) in pIJ10257	This work
pNHC85	ScPmt (C-StrepII + K332H) in pIJ10257	This work
pNHC86	ScPmt (C-StrepII + K332R) in pIJ10257	This work
pNHC87	ScPmt (C-StrepII + R510H) in pIJ10257	This work
pNHC88	ScPmt (C-StrepII + R510K) in pIJ10257	This work

2.1.5 Strains

S. coelicolor DT3017, DT1020, DT1029, DT1025, DT2008 (all derived from a J1929 parent strain) and J1929 were used as acceptor hosts for plasmid conjugation, these strains were obtained previously (Bedford *et al.*, 1995; Cowlshaw and Smith 2002). *E. coli* ET12567 (pUZ8002), a methylation deficient strain, was used as a donor host for plasmid conjugation with *Streptomyces* acceptor strains. *E. coli* DH5 α was used for pIJ10257 plasmid propagation and cloning to yield recombinant plasmids containing either a *pmt* or *ppm1* allele cloned into the NdeI site (Gregory *et al.*, 2003).

Table 2.3: List of bacterial strains

<i>Streptomyces</i> strain	Genotype	Reference
J1929	pglY mutant	Bedford <i>et al.</i> , 1995
DT1025	<i>pmt</i> W389STOP mutant	Cowlshaw and Smith 2002
DT2008	Not known	Cowlshaw and Smith 2002
DT1020	<i>ppm1</i> H116D mutant	Cowlshaw and Smith 2002
DT1029	<i>ppm1</i> S163L mutant	Cowlshaw and Smith 2002
DT3017	<i>ppm1</i> E218V mutant	Cowlshaw and Smith 2002
<i>E. coli</i> strain	Genotype	Reference
ET12567(pUZ8002)	dam- dcm- hsdS, RP4 transfer genes	MacNeil 1988
DH5 α	F- endA1 glnV44 thi-1 recA1 relA1 gyrA96 deoR nupG ϕ 80dlacZ Δ M15 l Δ (lacZYA-argF)U196, hsdR17(rk-mk+), λ -	Green <i>et al.</i> , 2012
Bl21 (DE3)	fhuA2 [lon] ompT gal (λ DE3) [dcm] Δ hsdS λ DE3 = λ sBamHIo Δ EcoRI-B int::(lacI::PlacUV5::T7 gene1) i21 Δ nin5	Hanahan 1983

2.2 Molecular procedures

2.2.1 Growth of *E. coli*

E. coli strains were cultivated on LB agar at 37 °C overnight. *E. coli* strains were cultured for 12 – 16 H at 37 °C (180 rpm). The LB broth growth medium was supplemented with antibiotics as required. To ensure plasmids were maintained in *E. coli*, glycerol stocks were prepared by storing the strains in (20 % v/v) glycerol at -80 °C

2.2.2 Preparation of chemically competent cells

A 5 ml 18 H overnight *E. coli* culture was grown and 500 µl added to 50 ml of LB. The culture was incubated at 37 °C with shaking until mid-log phase was reached ($OD_{600nm} = 0.4$). The cells were centrifuged (10 min, 4000 x g, 4 °C). The supernatant was discarded and the pellet resuspended in 15 ml TFB1 and incubated on ice for 90 min. Cells were harvested by centrifugation (10 min, 4000 x g, 4 °C) and the pellet resuspended in 2 ml TFB2. 250 µl aliquots of competent cells were snap frozen in liquid nitrogen. This method is based on that described in Sandbrook *et al.*, (1989).

TFB1: 100 mM RbCl, 50 mM MnCl₂, 30 mM KAc, 10 mM CaCl₂, 15 % glycerol (pH 5.8 with HCl)

TFB2: 10 mM MOPS, 10 mM RbCl, 75 mM CaCl₂, 15 % glycerol (pH 8.0 with NaOH)

2.2.3 Transformation of *E. coli*

100 ng DNA was added to 30 µl of competent *E. coli* DH5α and kept on ice for 30 min. The cells were heat shocked at 42 °C for 45 s and cooled on ice for 5 min. The cells were resuspended in 250 µl Luria-Bertani (LB) media and incubated at 37 °C for 45 min (200 rpm). 50 µl of transformation reaction was plated out on LB agar containing an appropriate selection antibiotic.

2.2.4 Plasmid DNA isolation

Plasmid DNA was isolated from overnight 5 ml LB cultures, centrifuged at 4000 x g 10 min. The cell pellet was processed and plasmid purified in accordance to the manufacturer's instructions using QIAprep Spin Miniprep Kit (QIAGEN). DNA was eluted in 50 µl 10 mM Tris-HCl pH 8.5.

2.2.5 PCR/DNA digest clean up

To remove enzymes and reaction components, samples were processed using QIA Quick PCR Purification Kit (QIAGEN) in accordance with the manufacturer's instructions. DNA was eluted in 30 µl 10 mM Tris-HCl pH 8.5.

2.2.6 Restriction digest

For analytical digests or to obtain digested DNA to be used for cloning, ~0.5 - 1.5 µg of DNA was digested with 20 units of restriction enzyme in a final volume of between 10 - 50 µl. Reactions were carried out in the NEB Cutsmart buffer for 4 H.

2.2.7 Agarose gel electrophoresis

Agarose 1 x gels were prepared in 1 x Tris-borate-EDTA (TBE = 90 mM Tris, 64.6 mM boric acid, 2.5 mM EDTA) buffer with 0.1 µg ml⁻¹ ethidium bromide. DNA samples were mixed with 6 X gel loading buffer (NEB) and run at 100 v, 400 mA for 45 min. A 1 KB ladder was used as a reference (NEB). DNA was visualised using a UV transilluminator system (BioRad).

2.2.8 In-Fusion Cloning

InFusion Cloning was carried out in accordance with the manufacturer's instructions. Assembly of the reaction required 50-100 ng of vector DNA and PCR insert(s), 2 µl of HD Infusion enzyme and ddH₂O to make the reaction up to 10 µl. Reactions were incubated for 15 min (50 °C), after which 5 µl of the product was used to transform into *E. coli* competent cells.

2.2.9 *ppm1* cloning into pIJ10257

In order to clone the mutated *S. coelicolor ppm1* alleles from pET28a into pIJ10257, they were first amplified by PCR with the *Ippm1F* and *Ippm1R* primers. Phusion Hi-Fidelity Polymerase (ThermoFisher) was used according to the manufacturer's instructions with the following reaction conditions: 98 °C/1 min, 25 cycles of 98 °C/10 s, 72 °C/30 s, 72 °C/1 min and 72 °C/ 10 min using a Biometra TProfessional Basic Thermocycler (Thistle Scientific). PCR products were digested with DpnI (NEB), purified using QIA Quick PCR Purification Kit (QIAGEN) and cloned into NdeI (NEB) digested pIJ10257 using the In-Fusion HD Cloning Kit (Clontech), all in accordance with the manufacturers' instructions. 5 µl of each reaction product was introduced into chemically competent DH5α *E. coli* by transformation.

2.2.10 *pmt* mutagenesis and cloning into pIJ10257

J1929 genomic DNA was used as the template to amplify *pmt* and introduce each mutation in tandem via two separate PCR reactions. The first reaction containing *IpmtF* to begin amplifying from the 5' end of the gene alongside a reverse mutagenic primer e.g. R82AR. The second reaction would use *IpmtR* to begin amplifying from the 3' end of the gene alongside a forward mutagenic primer e.g. R82AF. Consequently, there were two amplified products for each mutant allele. Phusion Hi-Fidelity Polymerase (ThermoFisher) was used according to the manufacturer's instructions with the following reaction conditions: 98 °C/1 min, 30 cycles of 98 °C/10 s, 60 °C/30 s, 72 °C/2 min and 72 °C/10 min using a Biometra TProfessional Basic Thermocycler (Thistle Scientific).

PCR products were digested with DpnI (NEB), purified using QIA Quick PCR Purification Kit (QIAGEN). The two amplified products corresponding to each mutant were joined together and then cloned into NdeI (NEB) digested pIJ10257 using the In-Fusion HD Cloning Kit (Clontech), all in accordance with the manufacturers' instructions. 5 µl of each reaction product was introduced into chemically competent DH5α *E. coli* by transformation.

2.3 Streptomyces work

2.3.1 Conjugation from *E. coli* and *S. coelicolor* spore harvesting

The method of intergeneric conjugation used in this work was previously described by Gust *et al.*, (2003). *E. coli* ET12567 (pUZ8002) competent cells were prepared after growing LB broth (37°C, 180 rpm) containing kanamycin (50 µg/ml) and chloramphenicol (25 µg/ml) to select for pUZ8002 and the *dam* mutation respectively. Following plasmid transformation, transformants were inoculated in 10 ml of LB both containing kanamycin (50 µg/ml), chloramphenicol (25 µg/ml) and 50 µg/ml hygromycin to select for the vector and grown overnight at 37 °C with shaking (180 rpm). The overnight culture was diluted 1/100 into 10 ml of fresh LB broth plus antibiotics and grown to an OD_{600nm} of ~0.4 at 37 °C. The cells were pelleted, washed twice with 10 ml LB both and then resuspended in 1 ml fresh LB broth. Approximately 10⁸ cfu ml⁻¹ *S. coelicolor* spores were added to 500 µL of the *E. coli* cells in LB broth. The mixture was centrifuged, the supernatant discarded and the pellet was resuspended in 100 µL LB broth. Using sterile MilliQ H₂O, a dilution series from 10⁻¹ to 10⁻⁴ was prepared, each step in a final volume of 100 µL. The 100 µL aliquots of each dilution were plated onto MSA + 10 mM MgCl₂ and incubated at 30 °C for 18 H. The plates were overlaid with 1 ml sterile MilliQ H₂O containing 0.5 mg Nalidixic acid and 0.5 mg hygromycin. The plates were further incubated for 7 days at 30 °C until antibiotic resistance *S. coelicolor* colonies were identified. Four exoconjugants corresponding (each representing a biological replicate) to each mutant allele were picked, resuspended in 100 µl water and streak plates made on soya mannitol (SM) agar (50 µg ml⁻¹ hygromycin). The plates were incubated for seven days at 30 °C. Single colonies were then picked, resuspended in 100 µl water and spread plates made on SM agar (50 µg ml⁻¹ hygromycin). The plates incubated for seven days at 30 °C. The spores were harvested by gentle resuspension in 20 % glycerol using cotton buds and stored at -30 °C. A revised protocol for Ppm1 mutant spore harvesting was also used. Following conjugations, antibiotic overlay and incubation for five days, four single colonies were picked (each representing a biological replicate). The picked colonies were crushed in water and corresponding spread plates prepared. After five days these spores were finally harvested.

2.3.2 Antibiotic disc diffusion assay

Approximately 1×10^7 *Streptomyces* spores were spread on a DN plate. Sterile filter discs were placed on the plate surface and 10 μ l of antibiotic stock solution absorbed to the disc. Plates were incubated at 30 °C for 36 H and the zone of clearance diameter measured in order to quantify antibiotic susceptibility. Four biological replicates were tested for each strain.

2.3.3 Phage plaque assay

The phage plaque assay was carried in accordance with the protocols described by Kieser and co-workers (Kieser *et al.*, 2000). A dilution series from the Φ C31 phage was prepared (10^{-1} - 10^{-6}) in DNB and 0.1 ml of each dilution was plated on a freshly poured 5 cm plate of DNA supplemented with 0.5 % glucose, 10 mM $MgSO_4$ and 8 mM $Ca(NO_3)_2$. Φ C31 phage was originally isolated by Lomovskaya and co-workers in Moscow (Lomovskaya *et al.*, 1972). 0.8 ml SN agar containing approximately 1×10^7 *Streptomyces* spores was added to each plate and swirled to ensure even coverage. The plates were incubated at 30 °C for 18 H and the plaques scored.

2.3.4 Phage streak assay

An undiluted stock of Φ C31 Δ 25 mutant was plated on half a freshly poured 10 cm square plate of DN agar supplemented with 0.5 % glucose, 10 mM $MgSO_4$ and 8 mM $Ca(NO_3)_2$. A streak of 1×10^7 of streptomyces spores was made starting from the phage free region and moving into the phage present region. The plates were incubated at 30 °C for 18 H.

2.3.5 Isolation of genomic DNA from *S. coelicolor*

S. coelicolor genomic DNA was isolated according to the salting out procedure described by Pospiech and Neumann (1995). The mycelium from a 30 ml culture grown in DNB was pelleted by centrifugation (4000 x g, 4 °C, 5 min) and resuspended in 5 ml SET buffer (75 mM NaCl, 25 mM EDTA pH 8, 20 mM Tris-HCl pH 7.5). 100 μ l of lysozyme solution (50 mg ml⁻¹ ddH₂O) was added and the suspension incubated for 60 min at 37°C. 140 μ l of proteinase K solution (50 mg ml⁻¹ in ddH₂O) was added and mixed by inversion. 600 μ l 10 % SDS was then added, the suspension was mixed by inversion and incubated at 55 °C for 60 min. 2 ml 5 M NaCl was added and the suspension mixed by inversion and then cooled to ~37 °C. 5 ml chloroform was added and the suspension mixed by inversion for 30 min at 20 °C. Samples were centrifuged (4500 x g, 20 °C, 15 min). The supernatant was transferred to a fresh tube and 0.6 volume isopropanol was added. Samples were mixed by inversion. After 3 min the DNA was spooled onto a sealed Pasteur pipette. The DNA was rinsed in 5 ml 70% ethanol, air dried and dissolved in ddH₂O at 55 °C for 5 min.

2.3.6 *ppm1* revertent analysis

Colonies present within the vancomycin zones of clearance on the disc diffusion assays plates were picked (one colony for each biological replicate), resuspended in 100 μ l of H₂O and streaked on SM agar plates supplemented with 40 μ g ml⁻¹ hygromycin and vancomycin. The plates were incubated at 30 °C for 7 days.

Phusion Hi-Fidelity Polymerase (ThermoFisher) was used to amplify the native locus *ppm1* and integration site *ppm1* alleles according to the manufacturer's instructions. Template DNA was provided by crushing a spore in 100 μ l of H₂O, 1 μ l was then added to the PCR tube.

To amplify the native locus *ppm1*, *Nppm1F* and *Nppm1R* primers were used with the following reaction conditions: 98 °C/3 min, 25 cycles of 98 °C/10 s, 60 °C/30 s, 72 °C/1.5 min and 72 °C/10 min. To amplify the integration site *ppm1*, *Ippm1F* and *Ippm1R* primers were used with the following reactions conditions: 98°C/3 min, 25 cycles of 98 °C/10 s, 60 °C/30 s, 72 °C/1 min and 72 °C/10 min. A Biometra TProfessional Basic thermocycler (Thistle Scientific) was used. PCR products were digested with DpnI and purified using QIA Quick PCR Purification Kit (QIAGEN). Presence or absence of reversion was confirmed by Sanger sequencing (GATC Biotech Ltd., London, UK).

2.4 Protein methods

2.4.1 SDS-PAGE

5 μ l of RunBlue 4 x LDS buffer (Expedeon) and 1 μ l of 100 % 2-Mercaptoethanol (Sigma) were added to the protein samples. The samples were boiled at 80 °C for 10 min. Samples were loaded onto RunBlue 4 - 12 % Bis Tris protein gels (Expedeon) and run at 160 V for 1 H using XCell SureLock Mini-Cell Electrophoresis System (Thermo Fisher Scientific). InstantBlue (Expediton) was used to simultaneously stain and destain the gels.

2.4.2 Harvesting membrane/soluble fractions for Western blotting

Mycelium from *streptomyces* cultures grown at 37°C for 48 H were centrifuged (2 min, 3500 x g), washed (20 mM Tris-HCl pH 8, 4°C) and stored at -80 °C. To prepare soluble and membrane fractions, mycelial pellets were resuspended in double the volume of lysis buffer (20 mM Tris-HCl pH 8, 4 mM MgCl₂, 4 mM DTT and protease inhibitors tablets by volume (Roche)). Mycelium was lysed by sonication using a Sonicator 3000 (Misonix) (10 cycles of 30 s pulse and 60 s cooling). Debris was removed by centrifugation (30 min, 5525 x g followed by 30 min at 13500 x g, 4 °C). Membranes were finally pelleted by ultracentrifugation (1 H at 100,000 x g, 4

°C) The membrane pellet was resuspended in 20 mM Tris-HCl pH 8 to yield the membrane fraction while the supernatant constituted the soluble fraction.

Protein concentrations were determined using the Nanodrop 2000 instrument (Thermo Scientific). Each membrane and soluble fraction was diluted to ~3 mg/ml and to 15 µl of each sample and SDS-PAGE performed, however instead of boiling, samples were incubated at 37 °C for 1 H.

Proteins were then transferred to 0.45 µM Amersham Hybond PVDF Blotting Membrane (GE healthcare) using the XCell II Blot Module (Invitrogen). Transfer was carried out at 30 V for 1 H. The preparation of the membrane for Western blotting was carried out according to the instructions for the Strep Tag II antibody HRP conjugate (Novagen). Membranes were washed with 1 x PBS twice and incubated in 20 ml blocking solution (3 % BSA, 0.5 % Tween-20 in 1 x PBS) overnight at 4 °C with gentle agitation. The membranes were washed 3 times with 20 ml PBST. 10 ml diluted Strep Tag II antibody (Novagen) in PBST (1:4000 dilution) was added to the membrane and incubated for 1 H at room temperature with gentle agitation. The membranes were washed twice, each for 10 min with 20ml PBST and finally washed twice for 10 min each with 20 ml PBS.

Chemiluminescent substrate for the Western blot was prepared as follows. Solution A: 13.3 µl of 90 mM *p*-coumaric in DMSO, 16.6 µl of 30 % H₂O₂ and 3 ml of 100 mM Tris (pH 8.5). Solution B: 30 µl of 250 mM luminol in DMSO and 3 ml of 100 mM Tris (pH 8.5). The combined volume of solutions A and B is enough to process a single blot. Under dark room conditions, membranes were incubated with chemiluminescent solutions A and B for 1 min. After exposure to the blot, X-ray film (GE healthcare) was incubated for 1 - 3 min in developer solution (Kodak) and 30 s in fixer solution (Kodak). The film was rinsed in water and allowed to dry.

2.4.3 Ppm1 and Pmt Bioinformatics

Primary structure pairwise and multiple sequence alignments were produced using EMBOSS Needle and Clustal Omega (Rice *et al.*, 2000; Sievers *et al.*, 2011).

S. coelicolor Pmt and Ppm1 homology models were produced using Phyre2 (Kelley *et al.*, 2015). The Pmt homology models was generated using *Cupriavidus metallidurans* ArnT (PDB ID: 5ezmA) as the template (Petrou *et al.*, 2016) and *S. cerevisiae* as the template Pmt1-Pmt2 (Bai *et al.*, 2019). Ppm1 model was generated using *P. furiosus* Dpm synthase (PDB ID: 5MM1) as the template (Gandini *et al.*, 2017).

Protein structures were visualised using CCP4mg (McNicholas *et al.*, 2011). Construct design and sequence trace analysis was carried out using SnapGene (GSL Biotech).

2.4.5 Ppm1 expression and purification

A single colony of *E. coli* BL21 (DE3) transformed with the construct plasmid was selected and used to inoculate a 5 ml volume of autoclaved LB containing 50 µg/ml of kanamycin. After 18 H, 1 ml of the culture was used to inoculate 1 L of LB media. Cultures were incubated at 37 °C until the OD_{600nm} was between 0.4 and 0.6. At this point IPTG was added (0.5 mM final concentration) and the flasks incubated at 20 °C for 18 H. Cells were harvested by centrifugation at 5000 x G at 4 °C for 10 min and the pellets were stored at -20 °C.

2.4.6 Ni²⁺ affinity chromatography

Prior to chromatography, cells were resuspended in freshly prepared lysis buffer containing protease inhibitor cocktail (Roche), one tablet was added for every 100 ml of buffer. Lysis buffer was added at 3 ml/g of pellet and supplemented with lysozyme added to a final concentration of 0.2 mg/ml.

The cell suspension was disrupted by sonication using a Sonicator 3000 (Misonix). The sonication protocol was 3 s on, 7 s off for a total of 7 min using a MicroTip horn with an initial output setting of 7.0. The lysed cells were pelleted at 5000 x g at 4 °C for 15 min.

The soluble protein was then loaded onto a HisTrap FF (5 ml) column and purification performed using an ÄKTA pure protein purification system. The flow rate was fixed at 5 ml/min and a 150 ml superloop was used for loading the protein onto the column. The column was washed 160 ml of binding buffer. Using elution buffer, the bound protein was eluted using an imidazole gradient (50 - 500 mM). Peak fractions were combined, concentrated to a final volume of 2 ml using Vivaspin 15R spin columns (Sartorius) by centrifugation (6000 x g, 4 °C).

2.4.7 Dialysis

SpectraPor molecular porous membrane tubing 3.5 kDa cut-off (Spectrum) was used for dialysis to remove the imidazole and exchange elution buffer for gel filtration buffer. Protein concentrations were determined using the Nanodrop 2000 spectrophotometer (Thermo).

2.4.8 Gel filtration chromatography

Overnight the Gel filtration column was equilibrated with 220 ml of gel filtration buffer and sample loaded onto a 16/60 Superdex 200 pg column and purification performed using an ÄKTA pure protein purification system. The flow rate was fixed at 1 ml/min and a 10 ml superloop was used for loading the protein onto the column and the column washed with 190 ml of elution buffer. Peak fractions were combined, concentrated to a final volume of 2 ml using Vivaspin 15R spin columns (Sartorius) by centrifugation (6000 x g, 4 °C).

2.4.9 Gel filtration (size exclusion) chromatography coupled with multi angle laser light scattering (SEC-MALLS)

Size exclusion chromatography was carried out on a Shimadzu HPLC system with a flow rate of 0.5 ml/min. The elution was monitored at 280 nm by a SPD20A UV/Vis detector. Light scattering data were recorded by a Dawn HELEOS-II 18 - angle and the concentration of the eluting protein was measured by an in-line Optilab rEX refractive index monitor (Wyatt Technology). Data was analysed using the ASTRA V software package.

2.4.10 Protein purification buffers

Lysis buffer: (50 mM sodium hydrogen phosphate, 300 mM sodium chloride, 0.3 mM magnesium chloride, 10 mM imidazole, 10 % glycerol, pH 7.5).

Binding buffer: 50 mM sodium hydrogen phosphate, 300 mM sodium chloride, 0.3 mM magnesium chloride, 20 mM imidazole, 10 % glycerol, pH 7.5

Elution buffer: (50 mM sodium hydrogen phosphate, 300 mM sodium chloride, 0.3 mM magnesium chloride, 250 mM imidazole, 10 % glycerol, pH 7.5)

Gel filtration buffer: 50 mM Tris-HCl, 100 mM sodium chloride, 10 % glycerol, pH 7.5.

Chapter 3 – Expression and purification of *S. coelicolor* Ppm1

S. coelicolor Ppm1 is a GT-A fold glycosyl transferase that catalyses mannose transfer from GDP-mannose to polyprenol phosphate and critically, *ppm1* null mutants of *S. coelicolor* are hyper susceptible to multiple antibiotics (Howlett *et al.*, 2018). Inhibitors of this enzyme could therefore be used in combination with existing antibiotics that, as a consequence of mannosylation perturbation, are more efficacious. In order to evaluate the potential of this enzyme as a target for novel antibiotics, its structure would first need to be determined. Currently no structure exists in the PDB for *S. coelicolor* Ppm1. The gene would therefore first need to be cloned into a plasmid for *E. coli* expression. With the development of optimised purification protocols, soluble, homogenous and pure protein could then be obtained for the requisite structure and function studies.

Characterisation of Ppm1, specifically an experimentally determined 3D structure, would then pave the way for fragment based screening to identify novel inhibitors of this enzyme, existing libraries could also be screened. There is notable sequence similarity and identity between *S. coelicolor* Ppm1 and their homologues in pathogens such as *M. tuberculosis* and *M. leprae*, it is therefore feasible that fragment inhibitors of *S. coelicolor* could be used to facilitate the identification or development of fragments active against mycobacterial Ppm1. During the course of the work described here, an experimentally determined 3D structure of the dolichol phosphate mannose synthase homologue (5MLZ) from *P. furiosus* was published (Gandini *et al.*, 2017). This represents the first published structure of a dolichol/polyprenol phosphate mannose synthase.

The aim of this chapter was to obtain soluble, pure, homogenous *S. coelicolor* Ppm1 protein for structure and function studies. Thus the following objectives were set:

1. Clone the *S. coelicolor ppm1* gene into suitable expression vectors
2. Optimise expression conditions for Ppm1
3. Purify Ppm1 that is suitable for structure and function studies
4. Investigate mutants of Ppm1 to determine if there could be more suitable candidates for expression and purification than the wild type (WT)

3.1 Expression and purification of *S. coelicolor* Ppm1

3.1.1 Optimising small scale expression

The *S. coelicolor ppm1* open reading frame had previously been cloned into pETFPP_49 (HIS-ORF) using InFusion cloning. Sequencing confirmed successful construction of the recombinant expression plasmid, with no mutations in the ORF or the flanking regions immediately upstream and downstream. The plasmid was introduced into the expression strain *E. coli* BL21 (DE3) by chemical transformation. The protocol used for expression is described in detail in the Material and Methods section. Overnight cultures of *E. coli* carrying the plasmid were added to 50 ml LB plus kanamycin (in 250 ml flasks). The flasks were incubated at 37 °C until the OD₆₀₀ was between 0.4 and 0.6. At this point IPTG was added (0.5 mM or 0.25 mM final concentration) and the flasks incubated for 18 H at either 20 °C, 27 °C or 37 °C. Samples were taken for SDS PAGE pre IPTG induction, 4 H post induction and 18 H post induction (Figure 3.1).

In each case, no notable protein band at roughly the expected molecular weight (MW) was obtained pre IPTG induction, indicating a lack of detectable leaky expression from the promoter. With the exception of 20 °C, 18 H, 0.25 mM IPTG, every sample post IPTG induction at either 4 or 18 H showed a clear protein band with intensity clearly higher than that of the background. The mobility of bands in each case were between the 46 kDa and 33 kDa reference bands, however the bands were positioned closer to the 46 kDa reference. Since Ppm1 with the 6xHis-tag and linker is ~37 kDa, the tagged Ppm1 had not migrated as far down the gel as expected. The migration pattern was reproducible in multiple gels and was also observed in the two similar BL21 (DE3) *E. coli* expression strains pLysS and ArcticExpress (DE3) (data not shown).

Small scale expression experiments showed that 1) there was no notable difference between the quantities of protein produced at the three temperatures, 2) 18 H expression consistently showed greater expression of protein 3) there was no notable difference in expression at the two IPTG concentrations tested. The decision was then made to proceed with large scale expression of Ppm1 (0.5 to 1 L culture volumes in 4-6 x 2000 ml baffled flasks). Ppm1 expression would be induced at 0.25 mM IPTG and would last for a duration of 18 H at 20 °C. Following this, the cell pellets would be harvested and then stored at -80 °C until required.

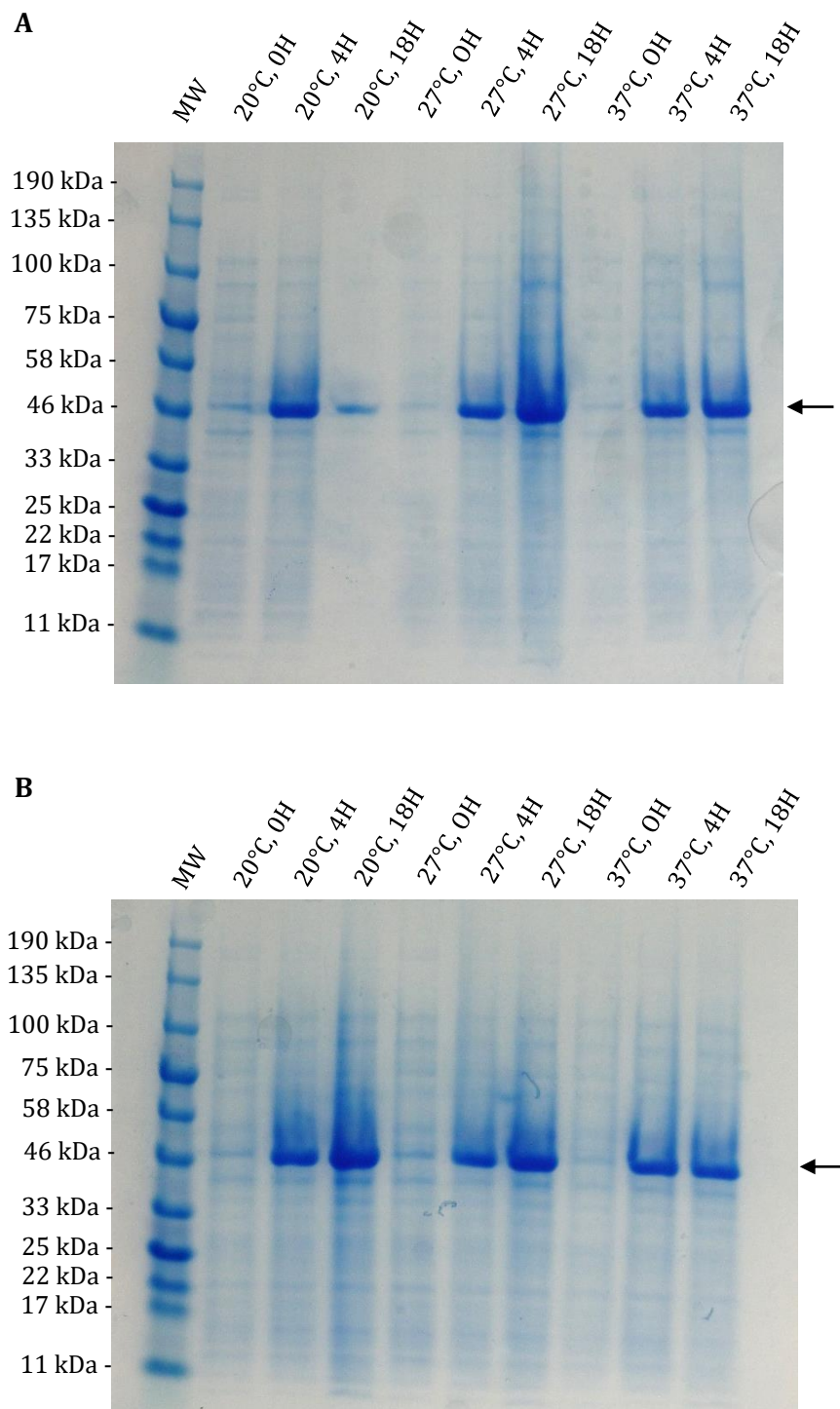


Figure 3.1: *S. coelicolor* Ppm1 successfully produced following IPTG induction. 0.5 (A) and 0.25 mM IPTG was used to induce expression at 20, 27 and 37 °C. Whole cell extract samples were taken for SDS-PAGE prior to induction, in addition to 4 and 18 h post induction. The MW ladder used was Blue Prestained Protein Standard, Broad Range (NEB).

3.1.2 Ni²⁺ affinity and gel filtration purification of WT *S. coelicolor* Ppm1

The overexpression and purification strategy for WT Pmt is explained in detail in the Materials and Methods section. WT Ppm1 was purified using a two-step purification process following overproduction in *E. coli* BL21 (DE3). After harvesting, cells were lysed by sonication and soluble protein was purified by Ni²⁺ affinity (Figure 3.2) and gel filtration chromatography (Figure 3.3), eluted protein was monitored using an absorbance trace at 280 nm. Using an imidazole gradient, His6-tagged Ppm1 was eluted as a single broad peak. Fractions were analysed by SDS PAGE, which confirmed the presence of protein with a mobility between 32 and 46 kDa reference marker bands. The tagged Ppm1 has a calculated MW of 37 kDa consistent with the mobility of the band seen on the gel. Other background (non-specifically bound) proteins were also observed in the fractions, necessitating an additional gel filtration purification step to obtain purer Ppm1 protein. Gel filtration was also used on the basis that it would give an indication of the oligomeric state of the expressed protein.

Following concentration and dialysis, the protein was purified by gel filtration chromatography (Figure 3.3). Three elution peaks were obtained and fractions analysed by SDS PAGE, the third peak was eluted with a volume of ~ 125 ml and contained no protein, this could represent a DTT impurity (data not shown). The first and most prominent peak with a height of 420 mAU yielded intense bands at the expected MW and fewer contaminants. At the right hand tail of this peak, an additional smaller peak at ~60 mAU was obtained. Fainter bands presumably corresponding to Ppm1 were again obtained but they were of comparable intensity to two possible contaminant proteins between 22 kDa and 25 kDa. Since bands corresponding to Ppm1 were obtained in multiple elution peaks, it was important to ascertain the oligomeric state of the enzyme.

Protein standards of known MW were therefore loaded onto the gel filtration column and the elution volume necessary to elute each protein was noted (Figure 3.4). Of greatest interest were peaks C (158 kDa bovine γ globulin) and D (44 kDa chicken ovalbumin) which were eluted at volumes of ~ 65 and 85 ml respectively. These peaks were comparable in position to the two peaks obtained for the Ppm1 purification. The implication was therefore that the tallest peak obtained corresponded to a combination of tetramers and higher MW aggregates of Ppm1, while the subsequent smaller peak was composed of monomer and/or dimer. Since *S. coelicolor* Ppm1 is unlikely to be present as a tetramer, this may signify unwanted aggregation.

The peak height distribution was however very clear and indicated that the majority of purified Ppm1 obtained by gel filtration might be unwanted larger oligomers (e.g. tetramers) or high MW aggregates, both would likely be of little physiological relevance. There was no

precipitation of the aggregates and they remained stable. As well as taking samples for gel filtration, samples were also taken for light scattering to more directly probe the MW, Gel filtration chromatography coupled to multi-angle light scattering (SEC-MALLS) was chosen for this (Figure 3.5). Similar to the gel filtration chromatogram, one major and one minor peak were obtained. The major peak showed a wide distribution of species with an estimated average MW range of roughly 165 kDa to 600 kDa, with the majority of material in this major peak estimated to be greater than 240 kDa. Interestingly, the minor peak average MW is roughly 45 kDa, which is quite close to that of monomeric Ppm1 (~36 kDa). Notably, there is an initial shoulder of the major peak with an average MW of 13 MDa, which will likely represent high MW aggregates (void).

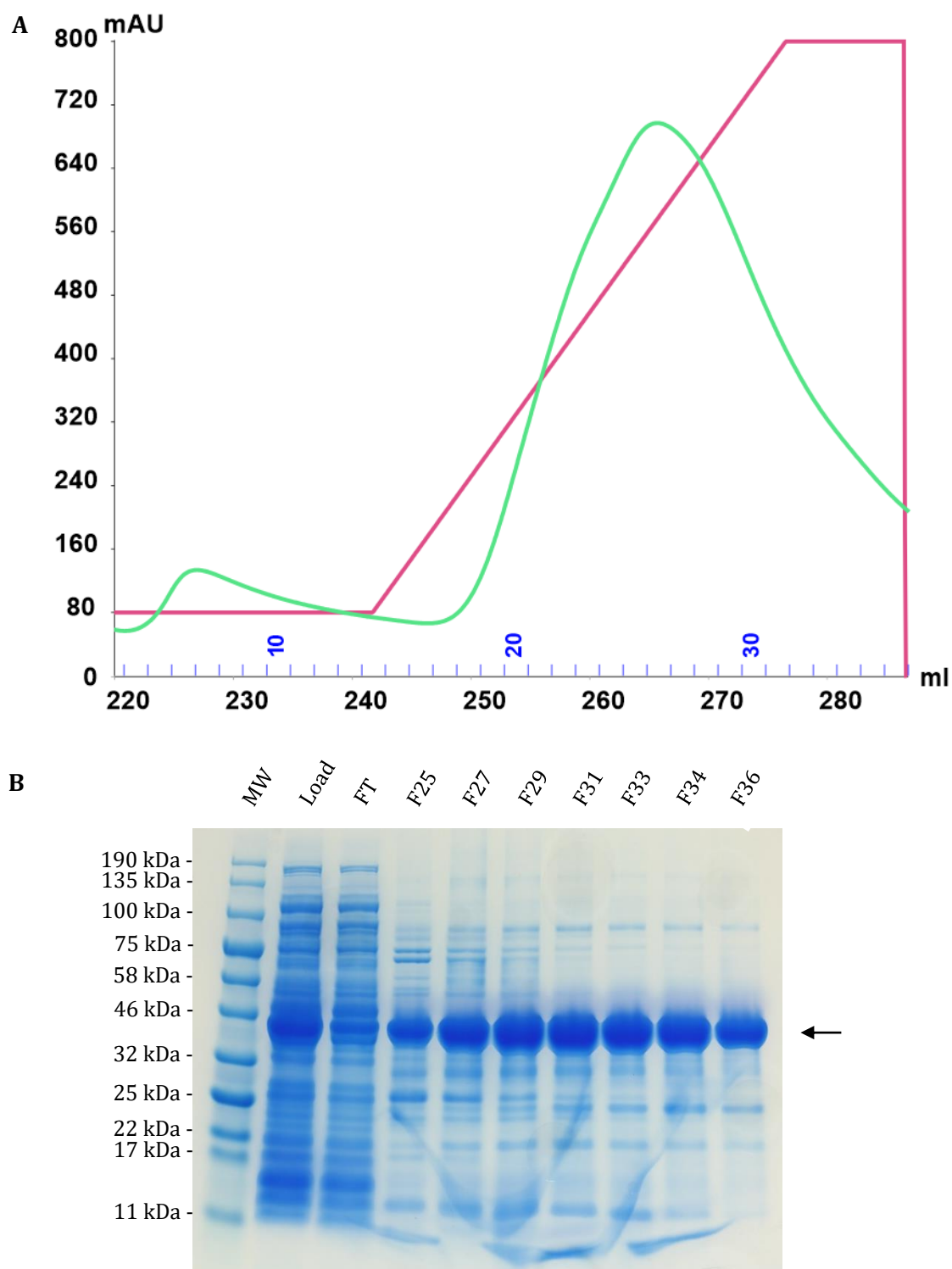


Figure 3.2: Ppm1 was successfully purified by Ni²⁺ affinity chromatography. (A) Ni²⁺ affinity chromatogram showing elution with an imidazole gradient. (B) Fractions collected from the elution peak were run on a 12 % SDS-PAGE gel. Load contained clarified lysate which was loaded onto the Ni²⁺ column. Flow through (FT) was collected upon washing the column with binding buffer. Remaining lanes contain fractions from the elution peaks. The MW ladder used was Blue Prestained Protein Standard, Broad Range (NEB). Purification was conducted on an AKTA Pure FPLC system using a HisTrap FF 5 ml column with a flow rate of 5 ml/min.

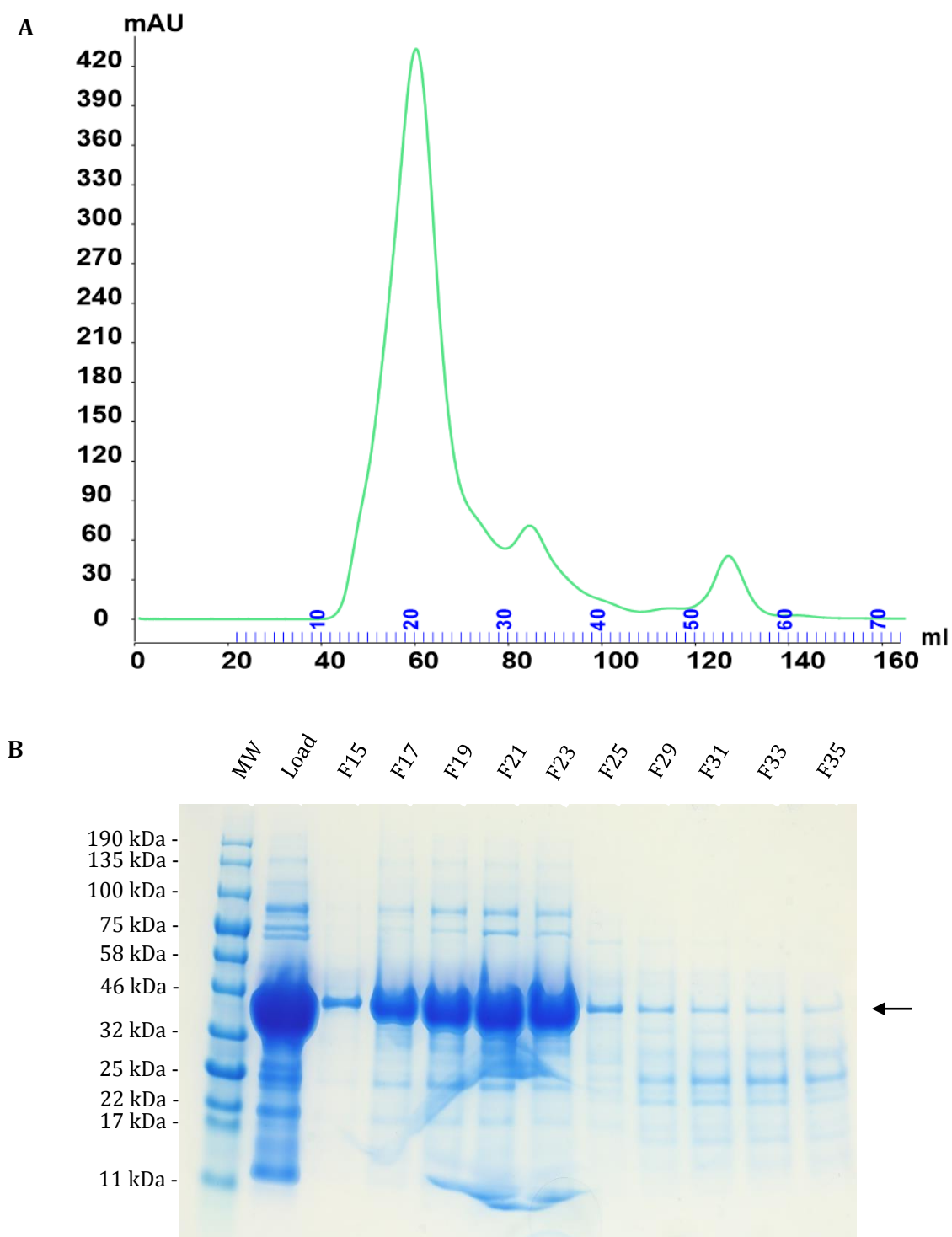


Figure 3.3: Ppm1 was successfully purified using gel filtration chromatography. (A) Gel filtration chromatogram of Ppm1, Experiments were conducted on an AKTA Pure FPLC system system using a HiLoad 16/60 superdex 200 pg column with a flow rate of 1 ml/min. (B) Fractions were collected and run on a 12 % SDS-PAGE gel. Load contained pooled Ni²⁺ affinity purified Ppm1 which was loaded onto the gel filtration column. Remaining lanes contained fractions from the first and second gel filtration elution peaks. The MW ladder used was Blue Prestained Protein Standard, Broad Range (NEB).

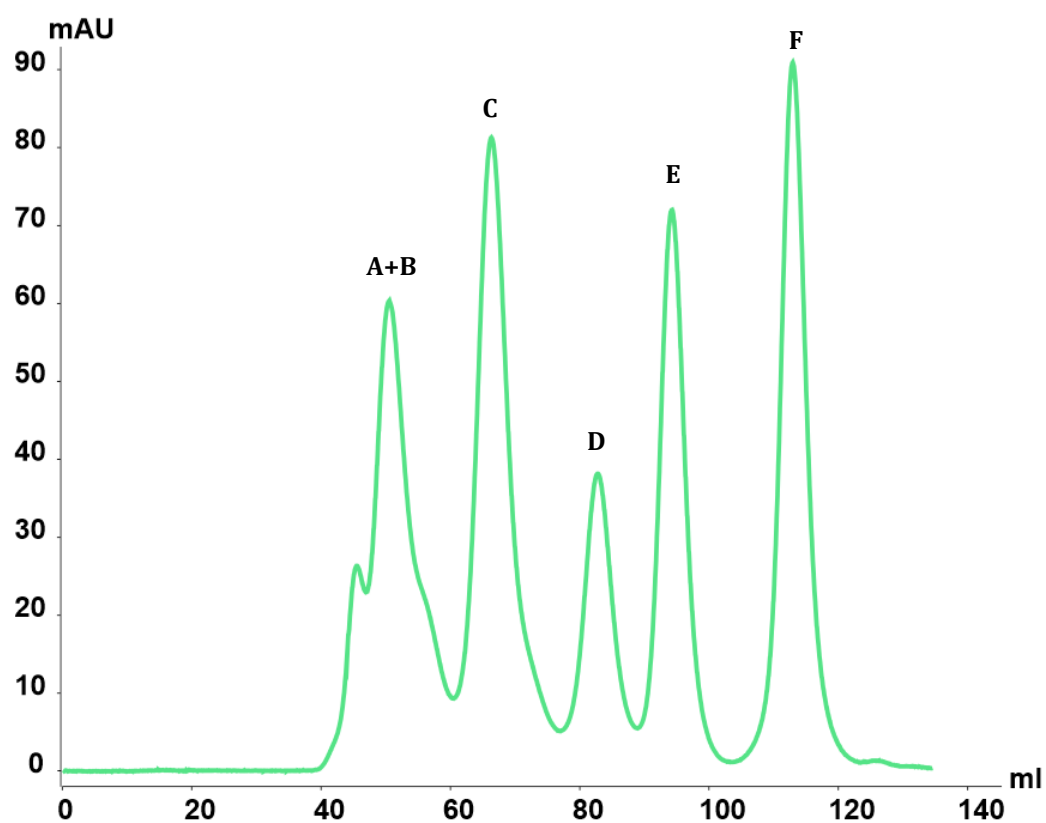


Figure 3.4: Standards of known MW were eluted at expected elution volumes. Gel filtration chromatogram for protein standards: (A) protein aggregates, (B) 670 kDa bovine thyroglobulin, (C) 158 kDa bovine γ globulin, (D) 44 kDa chicken ovalbumin, (E) 17 kDa horse myoglobin and (F) 1.3 kDa Vitamin B₁₂. Experiments were conducted on an AKTA Pure FPLC system using a HiLoad 16/60 superdex 200 pg column with a flow rate of 1 ml/min.

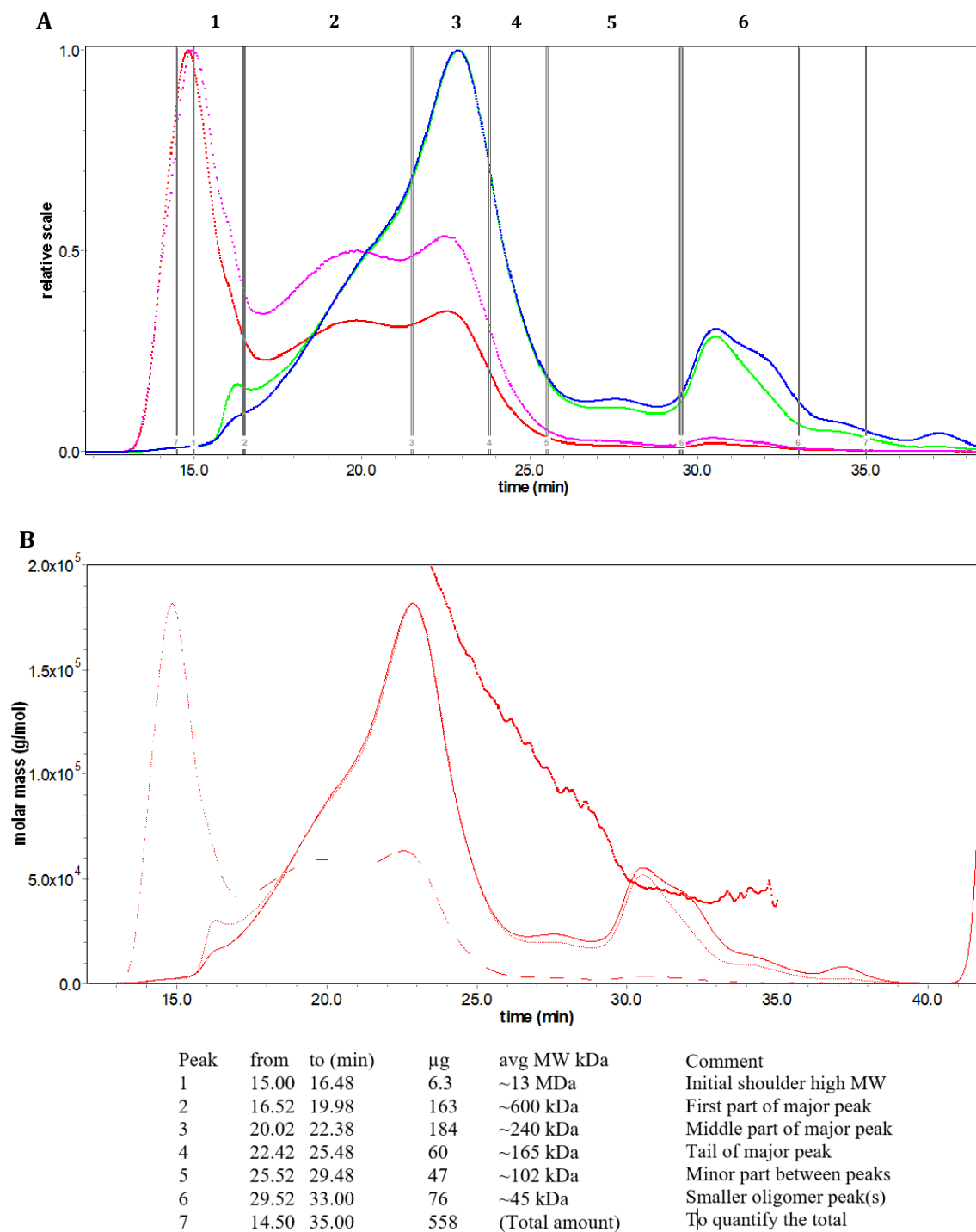


Figure 3.5: Purified Ppm1 shows a wide distribution of aggregates and oligomers.

Experiments were conducted on a system comprising a Wyatt HELEOS-II multi-angle light scattering detector and a Wyatt rEX refractive index detector linked to a Shimadzu HPLC system with a 10/300 Superdex 200 pg column and a flow rate of 0.5 ml/min. (A) The elution profile and peak positions plot shows UV (280 nm) in green, refractive index (RI) in blue, light scattering (LS) in red and QELS in magenta. (B) The Molar Mass plot shows the LS trace as a solid red line, the RI trace as a dashed red line, and the UV trace as a dotted red line. These are normalised to the largest peak.

3.2 Mitigating oligomerisation and aggregation

3.2.1 Troubleshooting expression and purification

In a subsequent experiment, the same expression and purification protocol was followed and comparable Ni²⁺ affinity (Figure 3.6) and gel filtration chromatograms (Figure 3.7) were obtained. On this occasion, fractions from each of these two peaks were obtained, pooled and run on the gel filtration column a second time on the same day (Figure 3.8), there were no changes to the positions of the elution peaks obtained, indicating that the oligomerisation state of the protein was stable. Comparable results were obtained when the gel filtration run was repeated on a second or third day (data not shown). The only notable change from the first to second gel filtration runs was that the mAU values were reduced, which can likely be attributed to sample loss.

Troubleshooting efforts to minimise oligomerisation and aggregation first focussed on experimenting with different protein storage conditions (data not shown) including (1) storage at 4 °C, (2) addition of 50 % glycerol/storage at -80 °C and (3) snap freezing 50 µL aliquots in liquid nitrogen/storage at -80 °C. None of these variations affected the peak distributions. Following this, buffer components were changed including varying the concentrations of sodium chloride, glycerol and DTT, these variations also had no notable effect. Finally, it was also thought that the use of spin concentrators might promote oligomerisation/ aggregation. Spin concentrators were therefore avoided in favour of dialysis or desalting columns to concentrate the protein, no deleterious effects were noted. In summary, multiple variations in the experimental protocol post lysis had no notable effect on the peak distributions obtained in gel filtration. SEC-MALLS confirmed that the amount of oligomers/high MW aggregates, greatly exceeded the amount of monomer in every case.

Conditions were however noted that increased the amount of high MW aggregates relative to monomer. In medium scale expression experiments, the peak height ratios were typically around 0.2:1 while for larger scale expressions (6 x 1 L cultures rather than 6 x 0.5 L) the difference in peak heights was as much as 0.1:1. The greater difference was also seen with the use of AI media. High concentrations of protein, in addition to rapid protein expression, appeared to favour aggregation.

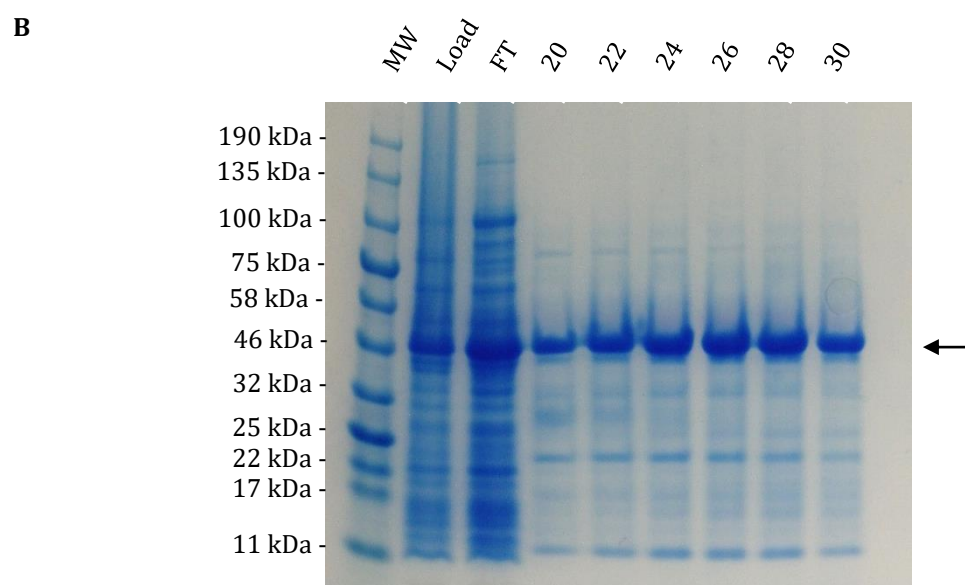
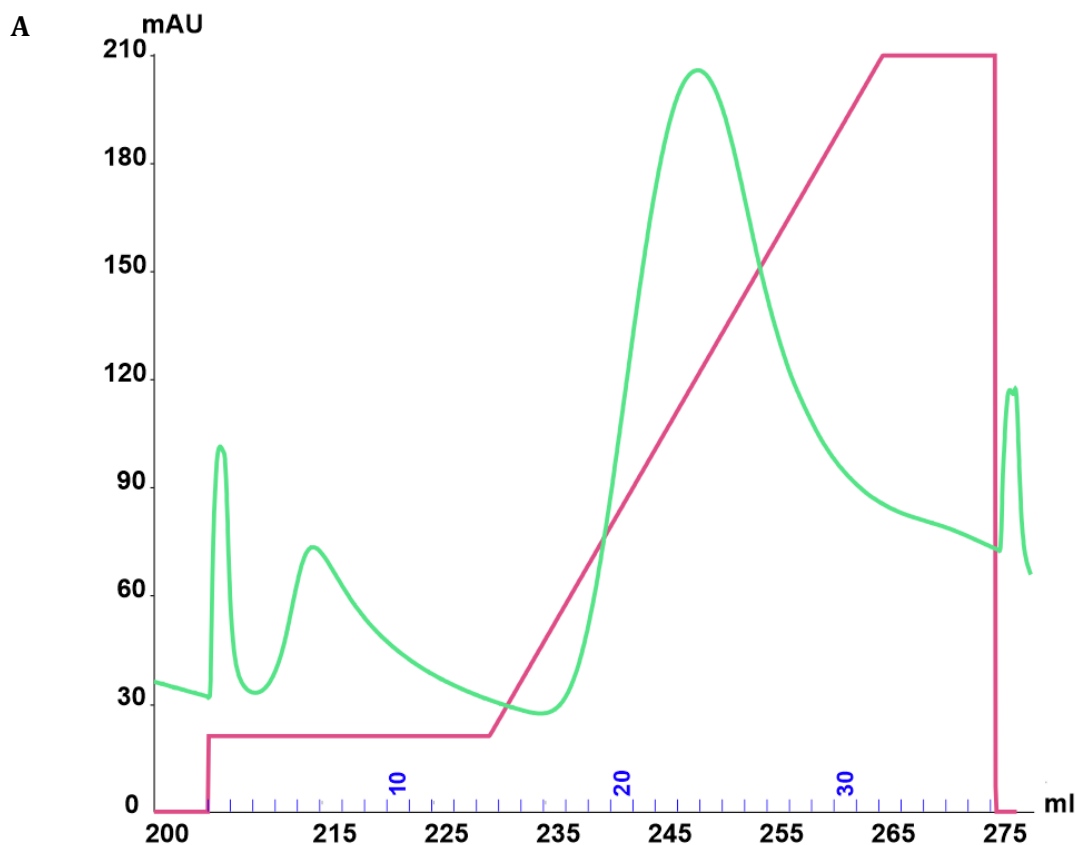


Figure 3.6: Ppm1 was successfully purified using Ni^{2+} affinity chromatography. (A) Ni^{2+} affinity chromatogram showing elution with an imidazole gradient. (B) Fractions collected from the elution peak were run on a 12 % SDS-PAGE gel. Load contained clarified lysate which was loaded onto the Ni^{2+} column. FT was collected upon washing the column with binding buffer. Remaining lanes contained fractions from the elution peaks. The MW ladder used was Blue Prestained Protein Standard, Broad Range (NEB). Experiments were conducted on an AKTA Pure FPLC system using a HisTrap FF 5 ml column with a flow rate of 5 ml/min.

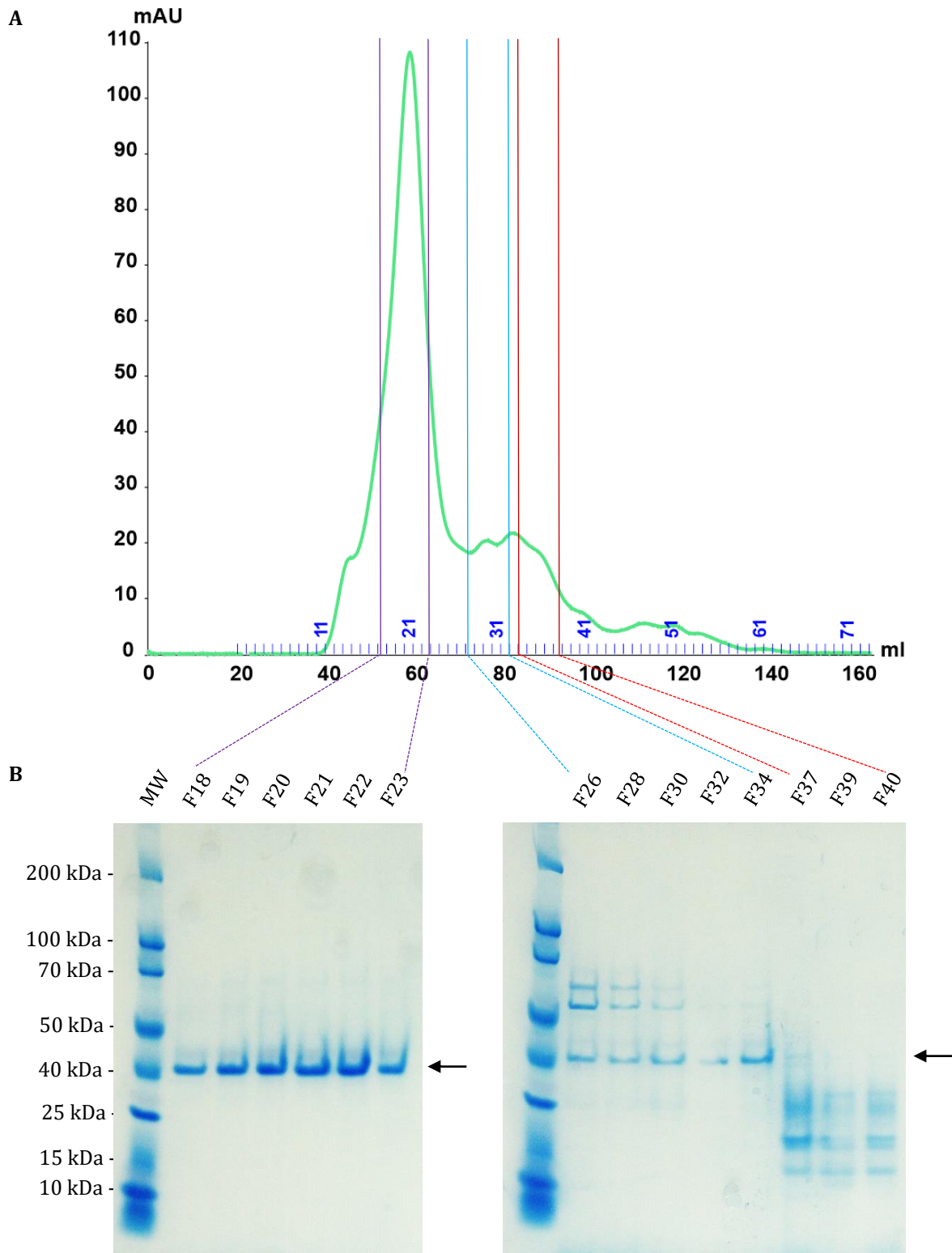


Figure 3.7: Ppm1 was successfully purified using gel filtration chromatography. (A) Gel filtration chromatogram of Ppm1. Experiments were conducted on an AKTA Pure FPLC system using a HiLoad 16/60 superdex 200 pg column with a flow rate of 1 ml/min. (B) Fractions were collected and run on a 12 % SDS-PAGE gel. The MW ladder used was Unstained Protein Marker, Broad Range (NEB). Fractions collected from the first and second gel filtration elution peaks were loaded on the remaining lanes.

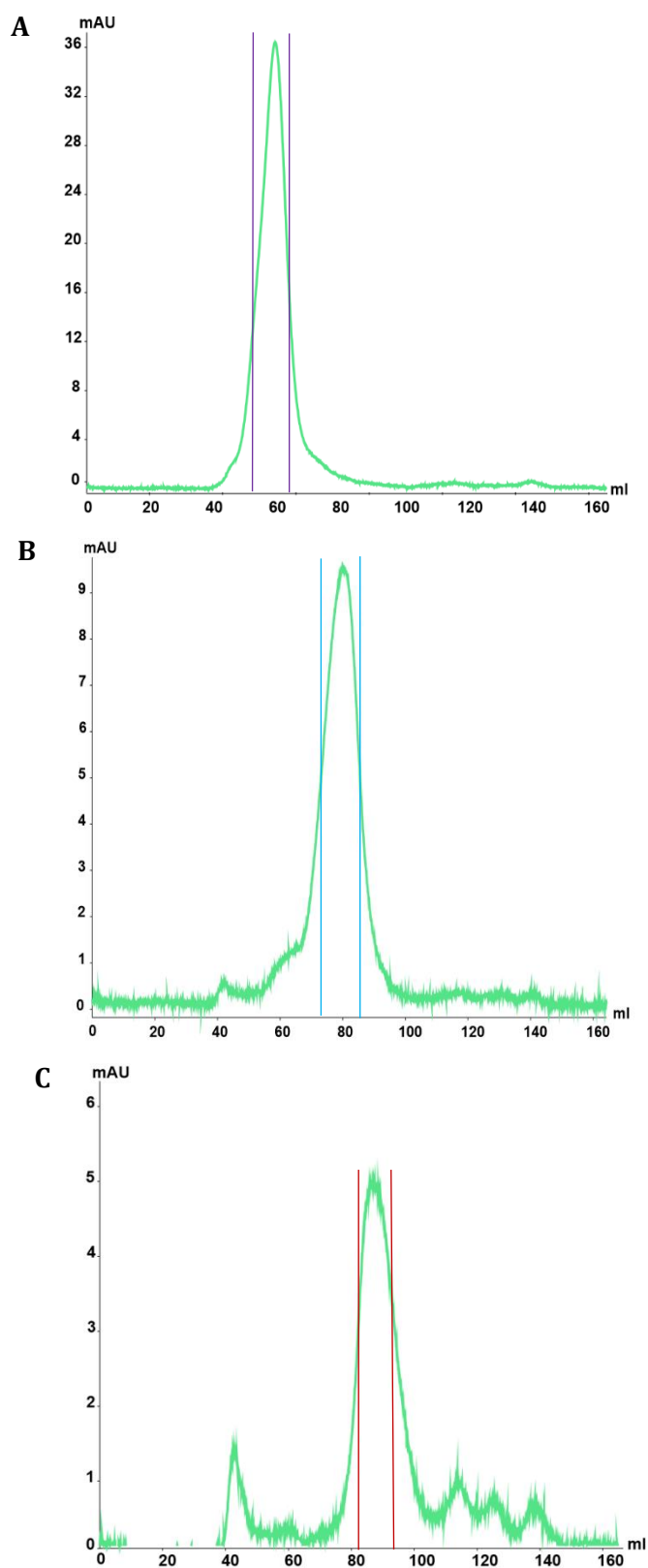


Figure 3.8: Fractions previously collected, pooled and reloaded onto the column were eluted with same volumes of buffer. Gel filtration chromatograms of Ppm1. Experiments were conducted on an AKTA Pure FPLC system using a HiLoad 16/60 superdex 200 pg column with a flow rate of 1 ml/min.

3.2.2 Investigation of Ppm1 N-terminal truncation mutants

Since troubleshooting with *S. coelicolor* WT Ppm1 had failed to yield any notable improvements to the amount of purified monomer, truncation mutants were made. A portion of the N-terminus is predicted to be disordered, the removal of this disordered region in addition to the adjacent upstream region could yield a Ppm1 protein with a reduced propensity to form the high MW soluble aggregates. The predicted disordered region comprises 14 amino acid residues (Figure 3.9). These residues were removed to yield a $\Delta 14$ truncation mutant. Additional residues were removed yielding $\Delta 21$ and $\Delta 30$ residue truncation mutants. Small scale expression experiments were first carried out under the same conditions previously described and the expression profile compared with that from the WT (Figures 3.10 and 3.11).

Expression of WT and 14/21 residue truncations all gave comparable results, whereby expression was typically highest at 27 °C, but was also obtained at 20 and 37 °C. Since there was no notable difference in the expression profile $\Delta 14$, $\Delta 20$ and WT proteins with the conditions tested, the same conditions for large scale expression could be used for the three proteins. A 20 °C overnight expression for large scale expression was chosen since overnight expression at lower temperatures would minimise over production of protein and unwanted aggregation. In each case there was no clear expression of protein with MW comparable to Ppm1 prior to IPTG induction, again confirming the lack of leaky expression from the promoter.

The $\Delta 30$ truncation mutant failed to express at 0.5 mM IPTG with all temperatures tested, the same was also true with 0.25 and 0.125 mM IPTG (data not shown). The failure of the $\Delta 30$ residue truncation to properly express indicates that between residues 22 and 30, there is presumably at least one amino acid residue critical for stability and/or correct protein folding. Failure to express is indicative of either poor stability of the folded protein, or incorrect protein folding to yield a toxic product which is cleared by the cell.

The same expression and purification protocols previously used were followed for Ppm1WT Ppm1 $\Delta 14$ and Ppm1 $\Delta 21$. Following Ni²⁺ purification, gel filtration purification was carried out (Figure 3.12). The chromatograms for the WT and two truncations mutants were largely identical, indicating that removal of the disordered region (Ppm1 $\Delta 14$), in addition to six further residues (Ppm1 $\Delta 21$) did not alleviate the oligomerisation/aggregation previously obtained. SEC-MALLS analysis showed comparable peak profiles (major followed by a smaller minor peak) and MW distributions within said peaks that were comparable to the values previously noted in Figure 3.5 (data not shown).

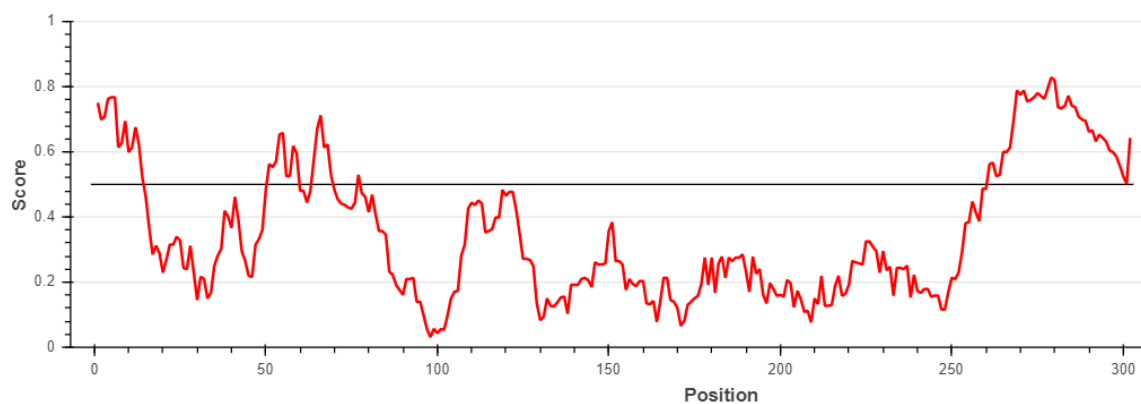


Figure 3.9: *S. coelicolor* Ppm1 has a disordered N-terminus. (A) IUPred2A plot shows the score of each residue in the protein from 0 to 1 (low to high predicted disorder respectively). A residue with a score of ≥ 0.5 is considered to have more disordered character.

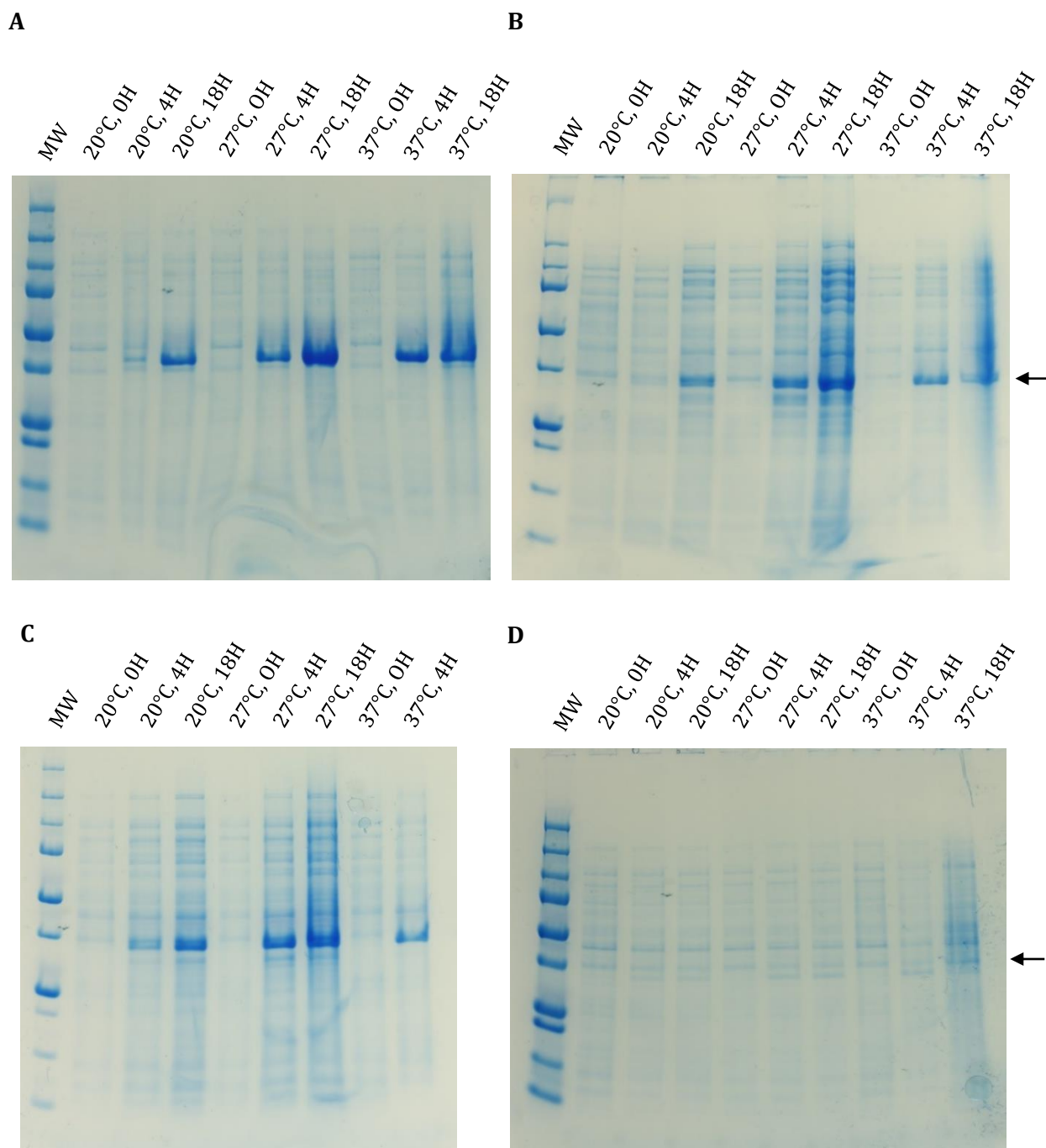


Figure 3.10: *S. coelicolor* Ppm1WT, Ppm1Δ14 and Ppm1Δ20 were successfully produced. 0.5 mM IPTG was used to induce expression Ppm1WT (A) Ppm1Δ14 (B), Ppm1Δ21 (C) and Ppm1Δ30 (D) 20, 27 and 37 °C. Whole cell extract samples were taken for SDS-PAGE prior to IPTG induction, in addition to 4 and 18 H post induction. The MW ladder used was Blue Prestained Protein Standard, Broad Range (NEB).

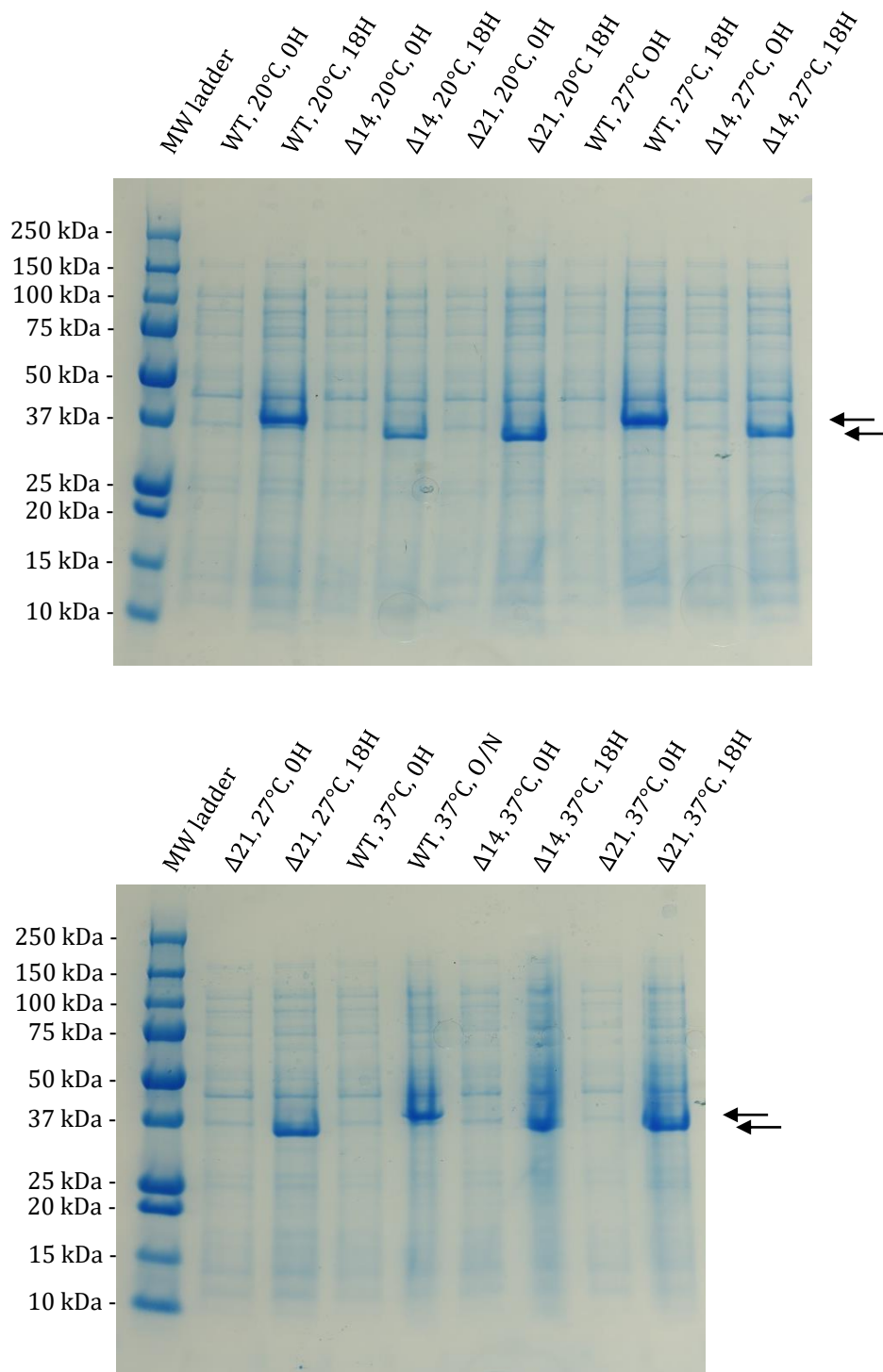


Figure 3.11: *S. coelicolor* Ppm1WT, Ppm1 $\Delta 14$ and Ppm1 $\Delta 21$ were successfully produced. 0.5 mM IPTG was used to induce expression Ppm1WT (A) Ppm1 $\Delta 14$ (B), Ppm1 $\Delta 21$ (C) and Ppm1 $\Delta 30$ (D) 20, 27 and 37 °C. Whole cell extract samples were taken for SDS-PAGE prior to IPTG induction and 18 h post induction. The MW ladder used was Blue Prestained Protein Standard, Broad Range (NEB).

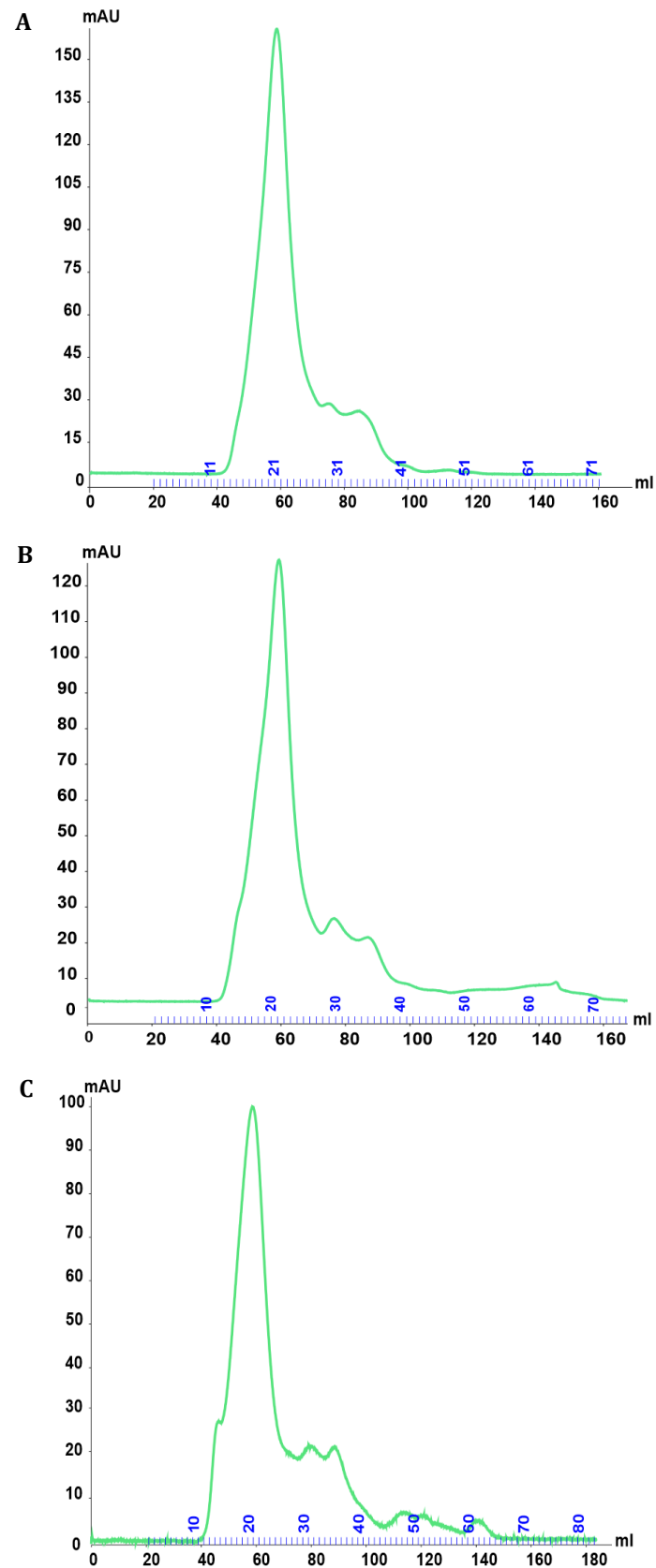


Figure 3.12: Ppm1 gel filtration chromatogram for WT (A) is comparable with $\Delta 14$ (B) and $\Delta 21$ chromatograms (C). Experiments were conducted on an AKTA Pure FPLC system using a HiLoad 16/60 superdex 200 pg column with a flow rate of 1 ml/min.

3.3 Discussion

S. coelicolor ppm1 - strains DT1020, DT1029 and DT3017 were previously shown to have antibiotic hyper susceptibility phenotypes (Howlett *et al.*, 2018; Wehmeier *et al.*, 2009). In addition, these strains have growth retarded phenotypes and resistance to Φ C31 Δ 25 infection (Howlett *et al.*, 2018; Cowlshaw and Smith 2001; Cowlshaw and Smith 2002). These antibiotic hyper susceptibility phenotype observations suggested that Ppm1, could be a good target for antimicrobials to be used in combination therapy with our existing arsenal of antibiotics. No structure of *S. coelicolor* Ppm1 or homologues in mycobacterial pathogens currently exists in the PDB. In order to identify inhibitors of *S. coelicolor* Ppm1 with therapeutic potential, structure and function studies are necessary.

Initially, the *S. coelicolor ppm1* gene was cloned into the expression plasmid pETFPP_49 (HIS-ORF). Following expression, Ppm1 was purified by Ni²⁺ affinity chromatography eluting as a single broad peak. However, gel filtration chromatography indicated that the purified Ppm1 was present as a mixture of oligomeric species and aggregates. This was confirmed using SEC-MALLS.

SEC-MALLS showed a wide distribution of MWs in the sample, with the major peak being particularly heterogeneous. The extended tail on the right of the minor peak indicated heterogeneity and based on the MW estimation (~45 kDa), can likely be attributed to monomeric (~36 kDa) and dimeric (~72 kDa) Ppm1, assuming they are present in roughly the same proportions with no other impurities present. Ppm1 functions as a dimer in *M. smegmatis* and *M. leprae* (Gurcha *et al.*, 2002). In *C. glutamicum* and *M. tuberculosis* the protein possesses a two-domain architecture with separate catalytic and membrane domains (Gibson *et al.*, 2003; Gurcha *et al.*, 2002). The possibility cannot be excluded that *S. coelicolor* Ppm1 also functions as a dimer, but further investigation is required here. It should be stressed that even if *S. coelicolor* Ppm1 has been purified as a dimer, it may not be physiologically relevant. The presence of the dimer could instead be indicative of a poorly optimised expression and purification protocol that has driven oligomerisation. Unfortunately, the protein concentration loaded was less than 1 mg/ml, which has likely contributed to noise in the RI trace, consequently making the MW estimates more erratic.

Multiple attempts were made to increase the yield of purified protein collected from the gel filtration column at roughly 80 ml, corresponding to the tailed minor peak. This region was of interest due to conventional calibration and SEC-MALLS indicating that purified Ppm1 constituting this peak is a possible combination of dimer and monomer. Fractions

corresponding to this peak could then be purified away from the larger oligomers and higher-order aggregates and the dimer and monomer resolved using a more suitable column (Superdex 75 10/300GL column). This step would be necessary to obtain homogenous protein necessary for structure and function studies. In order to take this approach, the yield of protein in this peak had to be increased and optimisation efforts were made to obtain greater yields of Ppm1 in monomeric and/or dimeric form.

Glycerol was added to the buffers up to 30 % in an effort to stabilise Ppm1 and therefore prevent its aggregation. The use of glycerol as an additive has been widely reported in the literature (Vagenende *et al.*, 2009). It induces protein compaction (Priev *et al.*, 1996), reduces flexibility (Gregory *et al.*, 1988) and stabilises partially unfolded intermediates (Mishra *et al.*, 2007). When glycerol was not added, the height of the major peak (corresponding to large oligomers and higher-order aggregates) increased on some occasions but this was not particularly reproducible. Glycerol was not added above 30 % due to concerns about FPLC overpressure.

NaCl is another useful additive conventionally added to buffers to help reduce non-specific binding of proteins to chromatographic resins, however at high concentrations it has been known to enhance aggregation and consequently precipitate protein (salting out). Based on the Ppm1 homology model (described in Chapter 4), there are only a limited number of solvent exposed aspartates and glutamates. It is therefore not too surprising that varying the NaCl concentration between 0.1 and 0.5 M did not change the chromatographic profiles significantly. Furthermore, low concentrations of NaCl (<0.1 M) increased the amount of non-specific column binding, showed by greater background in SDS-PAGE. At concentrations >0.5 M precipitation was noted in some cases. Aggregation can be driven by electrostatic and hydrophobic interactions acting in tandem or individually, increasing ionic strength would help prevent aggregation driven by electrostatics but conversely promote aggregation if it was primarily driven by hydrophobic interactions.

It is well known that even a single freeze thaw cycle can destabilise a protein by changing the buffer environment, this includes the formation of ice-water interfaces, adsorption to container surfaces, pH changes and other factors (Xiang *et al.*, 2015). Ppm1 was snap frozen in 20 μ l aliquots in liquid nitrogen and stored at -80°C. Snap freezing proteins has been shown to reduce protein aggregation, which can be attributed mainly to the reduced length of the solid-liquid phase transition (Xiang *et al.*, 2015). However, this protocol failed to change the chromatographic profiles of Ppm1. Attempts to bypass a freeze thaw cycle completely by progressing immediately from Ni²⁺ affinity chromatography to buffer exchange and gel filtration chromatography in the same day similarly had no impact. This indicates that a single freeze

thaw cycle was not the primary reason for the observed oligomerisation and aggregation. It should be stressed that freeze thaw cycles can reduce and even completely eliminate activities of enzymes without inducing a change in the oligomeric state of the protein (Bartolin *et al.*, 2017).

Efforts were also made to avoid the use of spin concentrators, since it is known that concentrated protein can build up near the membranes and will need to be regularly recirculated to both maintain an adequate flow rate, and minimise any potential concentration dependent aggregation. Efforts to recirculate protein in the upper chamber were made to minimise the time spent concentrating and prevent proteins building up on the membrane, however it failed to change the chromatographic profiles. Dialysis, admittedly a less harsh technique for simultaneous buffer exchange and concentrating, also failed to have any notable impact.

The impact of concentration on aggregation has been extensively probed in amyloid proteins and it was thought that the presence of large oligomers and higher-order aggregates could themselves promote oligomerisation and/or aggregation (Zhang *et al.*, 2013). Fractions taken corresponding to the 1) major peak 2) left shoulder of the minor peak) and 3) right shoulder of the minor peak were re-run on the same gel filtration column and the positions of the eluted peaks did not change. This indicates that the oligomers and higher-order aggregates once formed, are stable and maintain their form.

Troubleshooting with *S. coelicolor* WT Ppm1 ultimately failed to yield improvements in the amount of purified monomer and dimer obtained. The next step was to produce several N-terminal truncation variants. The basis for targeting the N-terminus was the IUPRED identification of disorder in the first 14 residues of the Ppm1 N-terminus. The contribution of intrinsically disordered regions to protein aggregation has for example been studied extensively in S100 Proteins (Carvalho *et al.*, 2013). If these disordered regions are (under certain conditions) prone to local unfolding or adopting a conformation that exposes the hydrophobic core of the globular protein to the solvent, aggregation would likely result. Given the documented role of intrinsically disordered regions in promoting aggregation, the removal of the entire disordered region (14 residues), in addition to the adjacent upstream region (21 and 30 residues) was undertaken in a search for a Ppm1 variant with a reduced propensity to form larger oligomers and higher-order aggregates. The 14 and 21 residue truncations variants expressed at comparable levels to the WT, protein whereas no evidence of expression was obtained for the 30 residue truncation variant. Failure to express is usually indicative of either poor stability of the folded protein, or incorrect protein folding to yield a toxic product which is cleared by the cell. At any rate, at least one residue in this region (residue 22-30) is likely critical

for correct protein form and function. Unfortunately, gel filtration chromatography showed that neither the 14 nor the 21 residue truncation variants behaved differently to the WT; the distribution of peaks and MW were consistent to that which was previously obtained.

Preliminary work then started with the screening of a number of detergents. While lacking transmembrane helices, Ppm1 is expected to be membrane associated. It was therefore expected that detergents might stabilise Ppm1. The detergent screening analysis was terminated when a collaboration was launched with Dr Tosin's research group at Warwick University. This group were able to develop a purification protocol similar to the one discussed here, the main difference being the use of the detergent DDM. DDM is a commonly used detergent for protein purification and crystallisation – it is non-ionic and has a low critical micellar concentration (CMC). Non-ionic detergents are less likely to denature the protein while low CMCs correspond to more stable detergent micelles (Stetsenko *et al.*, 2017). Using DDM, Dube *et al.*, were able to purify the WT and several variants of Ppm1 in monomeric (and occasionally dimeric) form in sufficient quantities for structure and function studies. While the structure of Ppm1 remains elusive, Ppm1 WT and variants have been biochemically characterised (Dube *et al.*, 2019) as will be discussed in Chapter 4.

Chapter 4 - Identification of essential residues for polyprenol phosphate mannosyl transferase function

The *ppm1* - strains: DT1020, DT1029 and DT3017 were previously isolated by Smith and co-workers, and sequencing confirmed the presence of point mutations: H116D S163L and E218V in *ppm1*, respectively (Wehmeier *et al.*, 2009). The efficiency of Φ C31 phage formation is severely reduced on the three aforementioned *ppm1* - strains, compared to the phage susceptible parent strain, J1929 (Cowlshaw and Smith 2001; Cowlshaw and Smith 2002). These *ppm1* - strains also exhibit growth retarded phenotypes and hyper-susceptibility to multiple antibiotics, notably β -lactams and vancomycin (Howlett *et al.*, 2018a). A detailed rational mutagenesis study of *S. coelicolor* Ppm1 has yet to be carried out and the functional significance of the three residues that confer the null mutant phenotype is not understood.

In addition to *S. coelicolor*, actinobacterial homologues of Ppm1 have been experimentally probed in corynebacteria and mycobacteria. In *Corynebacterium glutamicum* the protein possesses a two-domain architecture with separate catalytic and membrane domains (Gibson *et al.*, 2003). Inactivation of the catalytic domain leads to a lipoglycan-less phenotype and a reduction in growth rate (Gibson *et al.*, 2003). The two-domain architecture is also present in Ppm1 from *M. tuberculosis*, but not those in *M. smegmatis* or *M. leprae*, which instead produce two separate proteins encoded by adjacent genes (Gurcha *et al.*, 2002). Furthermore, the *M. smegmatis* Ppm1 homologue of the *M. tuberculosis* catalytic domain is essential for survival (Gurcha *et al.*, 2002). Further experiments have shown that the introduction of a functional copy of the gene encoding *M. tuberculosis* PpmD2, the catalytic domain, is also sufficient to rescue the phenotype of *M. smegmatis* Ppm1 mutants (Rana *et al.*, 2012). Current evidence indicates that *S. coelicolor* Ppm1 lacks a membrane associated domain and that there is only one protein involved in polyprenol mannosylation, contrasting with *M. tuberculosis* and *M. smegmatis*/*M. leprae* respectively. *S. coelicolor* does have a homologue to the membrane domain of *M. tuberculosis* PpmD1, *SCO1014*. However, this gene is not required for protein glycosylation in *S. coelicolor* (Cordova-Davalos *et al.*, 2013). The mechanism of membrane association of Ppm1 in *S. coelicolor* consequently remains unknown.

The aim of this chapter was to develop a biochemical mechanistic model for Ppm1, with the following objectives:

1. Introduction of *S. coelicolor* mutant *ppm1* alleles into *S. coelicolor* DT3017 and J1929 strains, followed by spore preparation/harvesting

2. *In vivo* characterisation to probe essentiality of the targeted residues
3. Utilisation of structural bioinformatics approaches combined with biochemical data from our collaborators (Manuela Tosin and Pamela Dube, University of Warwick), to develop a robust mechanistic model for Ppm1

4.1 Cloning mutant alleles into pIJ10257 and introduction of recombinant plasmids into *S. coelicolor* J1929 and DT3017 strains

To probe residues essential for Ppm1 function, our collaborators at Warwick University had previously used site-directed mutagenesis to direct residue substitutions into Ppm1 (Dube *et al.*, 2019). In total nine residue substitutions were made (D57A, R82A, D111, D113, H116D, R138, G143V, S163L, R228). The residue equivalent to D57 contributes to GDP mannose binding in the *P. furiosus* homologue, while residues equivalent to R138 and R226 are known to bind the lipid phosphate, orientating the nucleophilic phosphate head group (Gandini *et al.*, 2017). In the human homologue of Ppm1, substitutions of residues equivalent to R82 and G143 are associated with congenital disorders of glycosylation (CDG) (Garcia-Silva *et al.*, 2004, Yang *et al.*, 2013). D111 and D113 constitute the DXD motif, which is highly conserved in the GT-A family of glycosyl transferases (Lairson *et al.*, 2008). H116 and S163 substitutions were already known to eliminate Ppm1 function in *S. coelicolor* (Wehmeier *et al.*, 2009). In addition to the nine substitutions, a single truncation mutant was also made resulting in the removal of 42 residues from the C-terminus of Ppm1 that is predicted to be highly disordered in *S. coelicolor* (Figure 4.1).

Homologues of Ppm1 are found across both the prokaryotic and eukaryotic kingdoms. Using Clustal Omega the GT-2 catalytic domain of *S. coelicolor* was aligned with those of *M. smegmatis*, *M. tuberculosis*, *P. furiosus*, *S. cerevisiae* and *H. sapiens*. With the exception of S163, all of the *S. coelicolor* Ppm1 residues targeted for mutation in this study are tightly conserved across the prokaryotic and eukaryotic kingdoms (Figure 4.1).

The 10 mutant alleles had previously been made by Pamela Dube and cloned into pETFPP_1 for protein production. To facilitate introduction of these mutant alleles into *S. coelicolor* strains, they were cloned into the integration plasmid pIJ10257. The inserts were sequenced to verify the absence of frame shifts and other unwanted mutations. The plasmids were then introduced firstly into the methylation-deficient *E. coli* strain ET12567 (pUZ8002) to generate the donor strains. Plasmids from the transformants were purified and digested with the restriction endonucleases Nde1 and Dpn1 to confirm presence of the insert and the absence of methylation respectively (Figure 4.2). The *ppm1* open reading frame is flanked by a pair of Nde1 sites; there are no other Nde1 sites present in the plasmid. Thus the Nde1 digestion products precisely correspond to the insert (~906 bp) and the plasmid backbone (6430 bp). All plasmids were confirmed to be recombinant. Furthermore, the absence of Dpn1 digestion products confirmed the plasmids were not methylated, and therefore would not be subject to *S. coelicolor*'s methyl sensing restriction system. The *E. coli* donor strains were subsequently used in conjugation reactions with the *ppm1* - strain DT3017 and the J1929 parent strain.

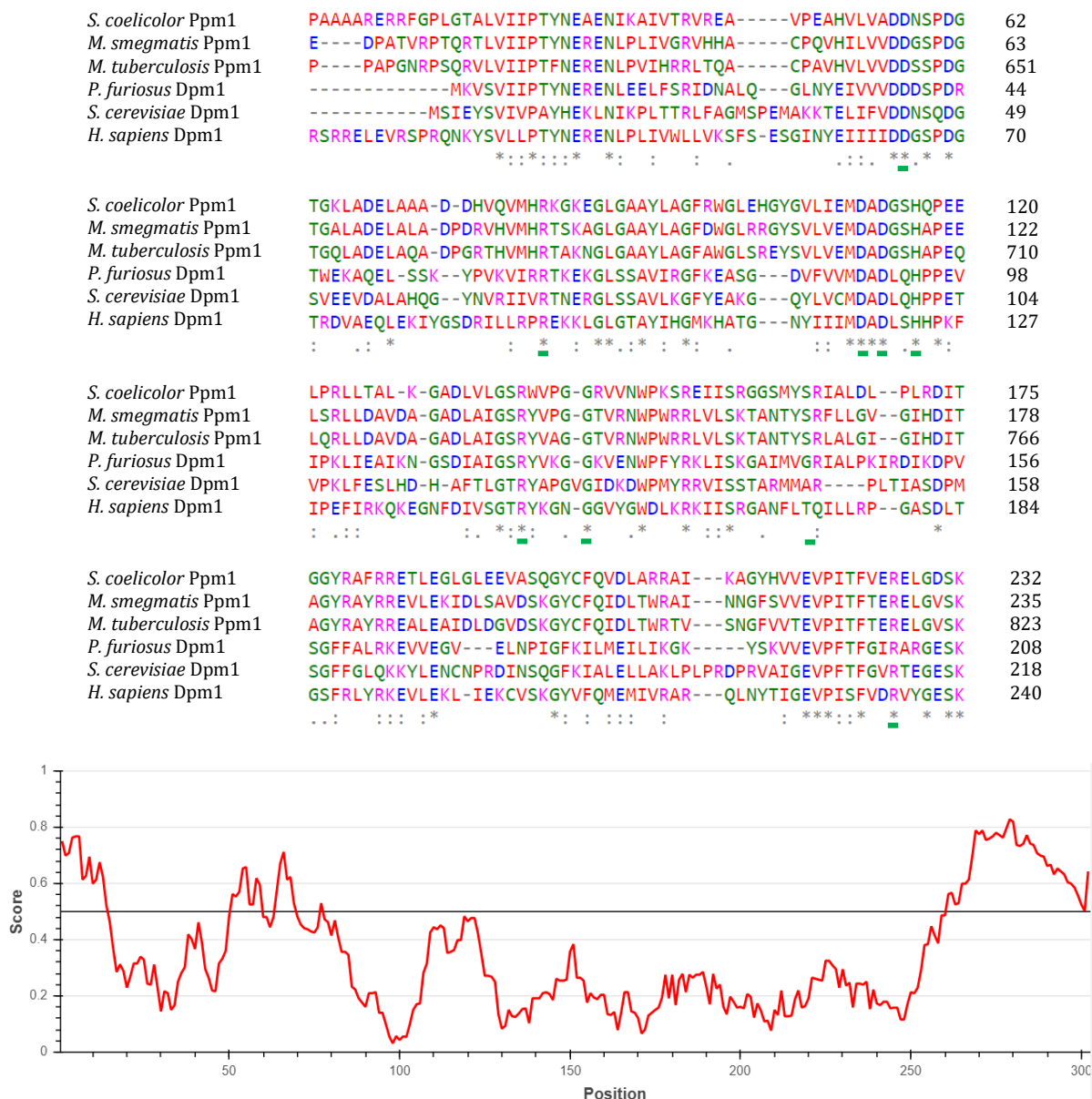


Figure 4.1: *S. coelicolor* Ppm1 has a GT-2 domain that is broadly conserved, in addition to a highly disordered C-terminus. (A) Clustal Omega alignment of the *S. coelicolor* GT-2 domain (Uniprot entry: Q9RKY2_STRCO) with *M. smegmatis* (PPM1_MYCS2), *M. tuberculosis* (PPMNT_MYCTU), *P. furiosus* (Q8U4M3_PYRFU), *S. cerevisiae* (DPM1_YEAST) and *H. sapiens* (DPM_HUMAN). The *S. coelicolor* residues targeted for substitution are underlined in green. (B) IUPred2A plot shows the score of each residue in the protein from 0 to 1 (low to high disorder respectively). A residue with a score of ≥ 0.5 is considered to have more disordered character.

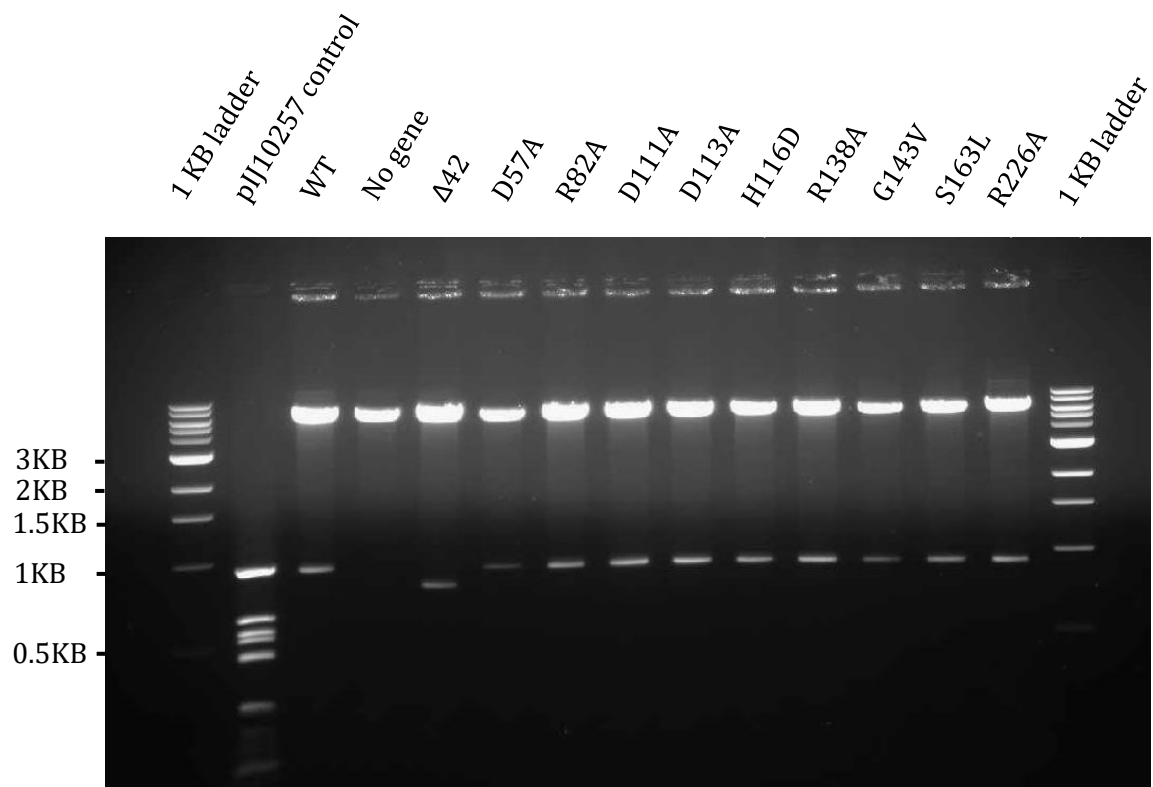


Figure 4.2: *E. coli* purified plasmids are recombinant and non-methylated. pIJ10257 plasmid containing no *ppm1* allele, WT allele and mutant alleles derived from the non-methylating *E. coli* donor strain ET12567 (pUZ8002). The pIJ10257 control was derived from the methylating BL21 (DE3) *E. coli* strain. All plasmids were digested with both Nde1 and Dpn1 to confirm insert presence and methylation status respectively. The NEB 1 KB ladder is used for reference.

4.2 Effect of *ppm1* alleles on the phenotype and growth of *Streptomyces*

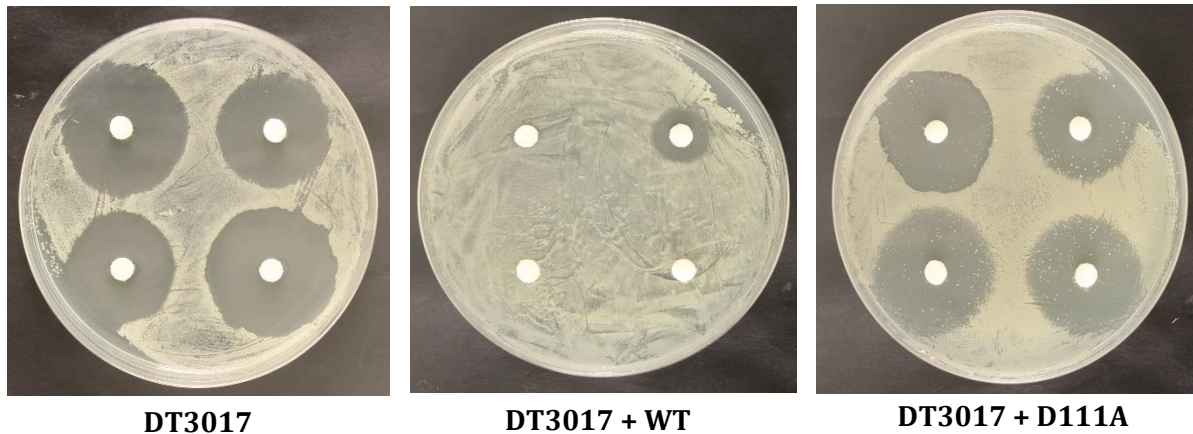
4.2.1 *Streptomyces* spore growth and antibiotic hyper susceptibility

Following introduction of the recombinant plasmids into the DT3017 and J1929 strains, the conjugation plates were overlaid with nalidixic acid and hygromycin to eliminate the *E. coli* plasmid donors and select for *Streptomyces* plasmid recipients respectively. Four independent exconjugant *Streptomyces* lines were isolated from each conjugation and stock spore preparations were generated.

Disc diffusion assays were performed with each spore preparation. Within the antibiotic zones of inhibition for DT3017 mutant strains, colonies could be identified that were suspected to be revertents and/or antibiotic suppressors (Figure 4.3). While identifiable for all antibiotics used in this study, the number of colonies was notably greater for antibiotics that showed the greatest difference in sensitivity between J1929 and DT3017, for example vancomycin and ampicillin. The zones of clearance for all the antibiotics tested were completely clear in the empty plasmid negative control, indicating that the presence of two *ppm1* alleles in the same cell could be responsible for this unexpected phenotype. In extreme cases, the proportion of putative revertents was so high that it was very difficult to accurately measure the diameter of the zones of clearance. To confirm that reversion of one of the *ppm1* alleles was cause of these phenomena, colonies growing within the vancomycin zones of clearance for the DT3017 strains harbouring the D111A and D113A alleles were picked and further analysed. One colony for each of the four biological replicates was analysed using two PCR primer pairs to amplify both the native and integration locus *ppm1* alleles separately (Figure 4.4). Sequencing showed that the *ppm1* at the native locus was unchanged, (encoding Ppm1E218V). However, the *ppm1* mutant at the integration site (introduced by pIJ10257) had undergone reversion, the wild type (WT) GAC codon was therefore present rather than the mutant GCC codon. The frequency of this phenomenon suggests that the gene introduced at the integration site may be subject to a DNA repair mechanism that does not affect the native locus *ppm1*. The native locus *ppm1* might therefore be used as a template to repair the mutation in the integration locus *ppm1*, but not *vice versa*. To test this hypothesis, an identical *ppm1* allele to that present in DT3017 (encoding Ppm1E218V) was introduced into DT3017. Now both the integration locus and native locus *ppm1* genes would harbour the same mutation. DT3017exoconjugants containing an additional copy of the *ppm1* allele encoding Ppm1E218V at the integration site showed no evidence of reversion in the disc diffusion assays.

Since, the revertents (encoding WT Ppm1) were already known to grow faster than the *ppm1*-mutants, *Streptomyces* spore preparation procedure was modified to allow less time for fitter

revertants to outgrow the less fit *ppm1*- alleles. The seven day incubations after conjugation and during amplification of spore preparations were reduced to five days and exconjugant colonies were squashed and plated directly to generate the stock spore preparation (eliminating one round of sporulation; see revised protocol in the Materials and Methods).



DT3017

DT3017 + WT

DT3017 + D111A

Figure 4.3: DT3017 strains that are not complemented with an active *ppm1* allele exhibit increased susceptibility to antibiotic insult. Revertent colonies can be identified clearly in the ampicillin and vancomycin zones of clearance. *S. coelicolor* DT3017 spores were plated out on DN agar and 40 μ g of bacitracin (top right), hygromycin (top left), ampicillin (bottom right) and vancomycin (bottom left) were added to each disc. The plates were then incubated at 30 $^{\circ}$ C for 48 hours. Images are representative of 4 biological replicates.

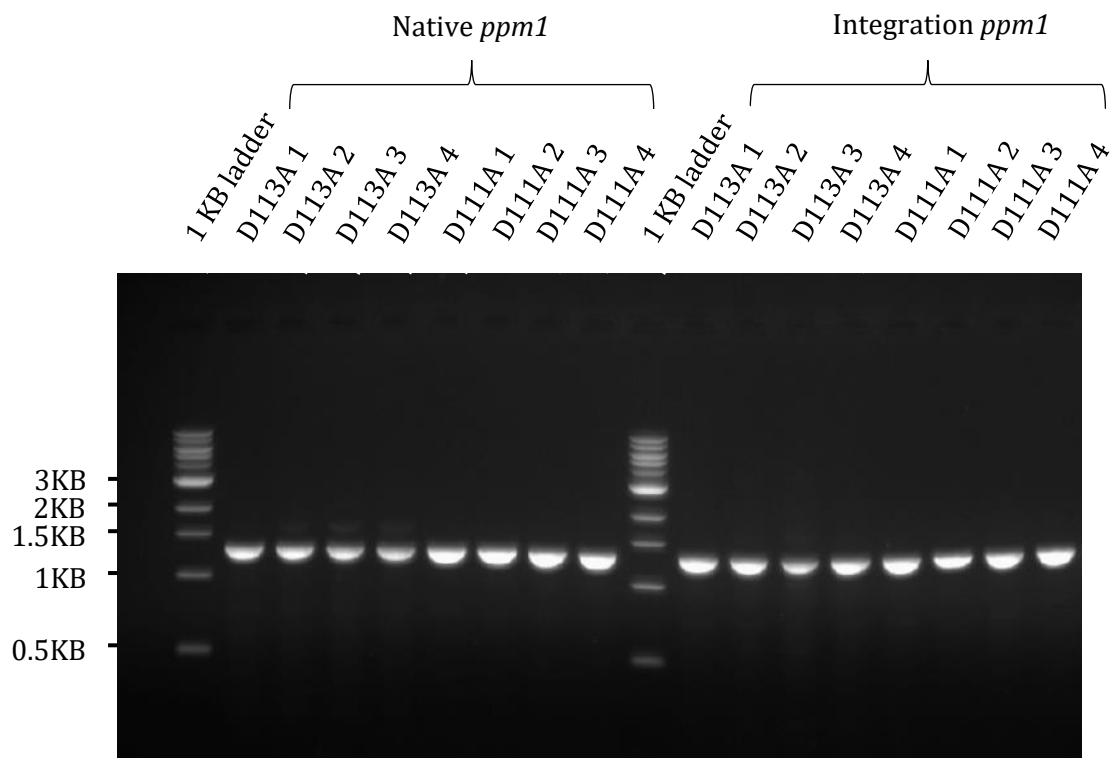


Figure 4.4: Amplification of the native and integration site *ppm1* alleles. Alleles were amplified from four revertent DT3017 colonies containing the integrated D113A *ppm1* allele and four containing the D111A *ppm1* alleles. The NEB 1 KB ladder is used for reference.

4.2.2 Identification of *ppm1* mutants unable to alleviate the antibiotic susceptibility phenotype of DT3017

Six of the *ppm1* mutants tested failed to complement DT3017: D111A, D113A, H116D, R138A, S163L, R226A in disc diffusion assays (Figures 4.5 and 4.6). These strains showed significantly increased susceptibility to all cell wall and/or membrane targeting antibiotics tested when compared to the J1929 parent strain, and therefore resembled the *ppm1* - mutant ($p < 0.05$).

Ppm1 defective strains of *S. coelicolor* are highly susceptible to vancomycin, with zone of inhibition diameters >25 mm. In comparison bacitracin yielded the smallest increase at ~ 10 mm. Alleles encoding the WT, or *Ppm1* $\Delta 42$ and *Ppm1*R82A were able to complement DT3017, alleviating the antibiotic susceptibility phenotype. The antibiotic susceptibility for the complemented stains was consequently not significantly different to J1929 for any of the antibiotics tested ($p < 0.05$). The alleles encoding *Ppm1*D57A and *Ppm1*G143V partially complemented DT3017 exhibiting mildly less susceptible phenotypes than DT3017.

Out of curiosity, I tested the susceptibility of the *ppm1* - strains to a wider range of antibiotics. The *ppm1* - strains exhibited significantly increased susceptibility to antibiotics inhibiting DNA replication, transcription and translation when compared to the J1929 parent strain ($p < 0.05$) (Figure 4.7). The zones of inhibition typically ranged from 10-15 mm and while significant, the differences in susceptibility for these antibiotics are not as drastic when compared to ampicillin, carbenicillin, vancomycin, imipenem, meropenem and daptomycin, which all gave susceptibility differences of >20 mm. The *ppm1* alleles encoding the WT, *Ppm1* $\Delta 42$ and *Ppm1*R82A complemented DT3017 *ppm1* and with the exception doxycycline and ciprofloxacin for $\Delta 42$ and R82A respectively, the strains showed no significant increase in antibiotic susceptibility compared to J1929. The partially complementing alleles encoding D57A and G143V showed significantly increased susceptibility to all antibiotics with the exception of ciprofloxacin and mitomycin C respectively ($p < 0.05$). As observed for the cell wall and/or membrane targeting antibiotics, the increase in susceptibility is again lower than the non-complementing strains for multiple antibiotics, the most notable examples being mitomycin C for G143V and doxycycline and minocycline for D57A.

All mutant *ppm1* alleles were additionally introduced into the J1929 parent strain and there was no difference in susceptibility to any antibiotic tested (Figures A4.1 and 4.2). This demonstrates that the expression of the non-complementing and complementing *ppm1* mutants in the parent strain, failed to reduce or enhance the function of the WT enzyme respectively.

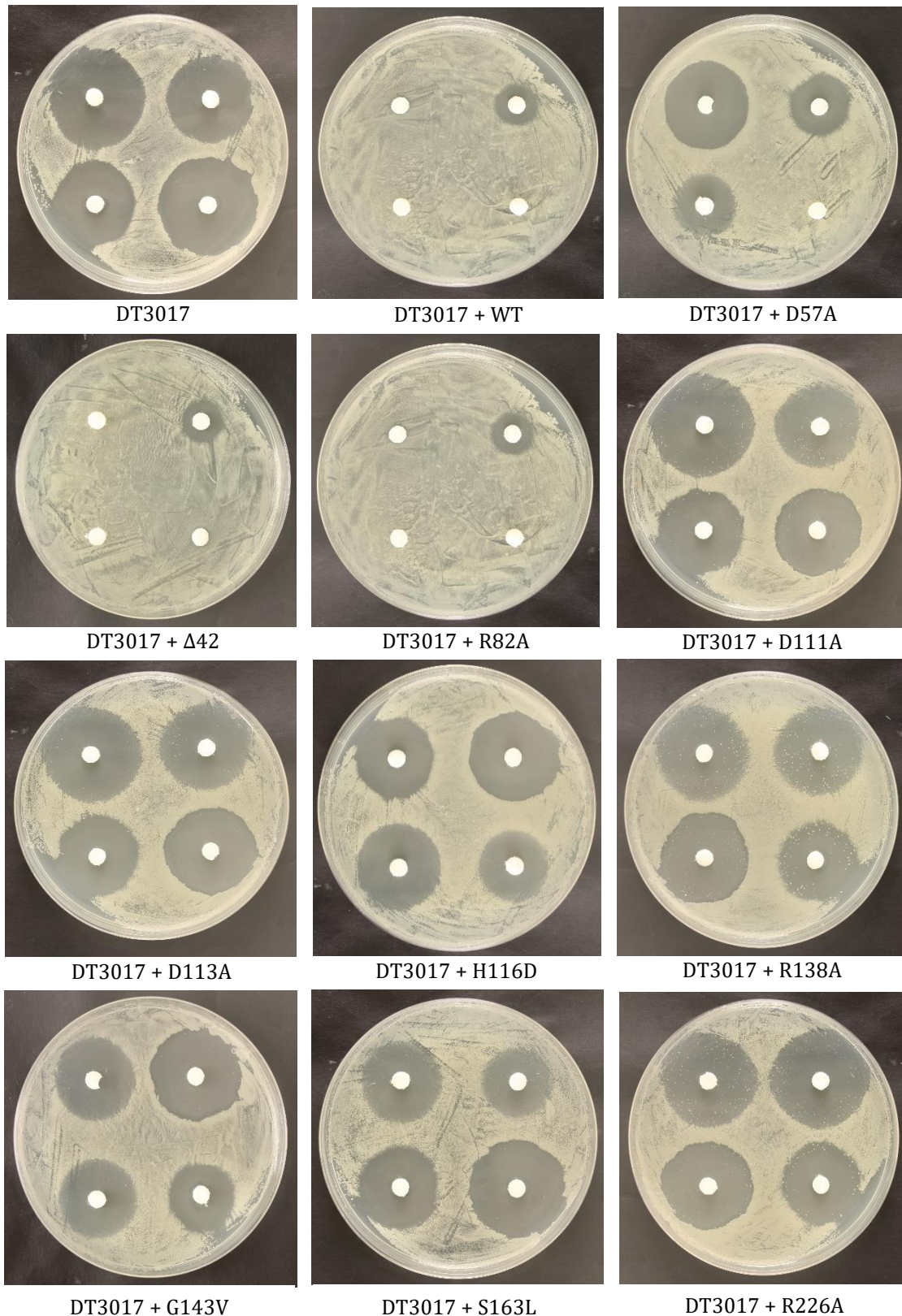


Figure 4.5: DT3017 strains that are not complemented with an active *ppm1* allele exhibit increased susceptibility to antibiotic insult. *S. coelicolor* DT3017 spores were plated out on DN agar and 40 μ g of vancomycin (top left), 80 μ g ampicillin (top right), 4 μ g meropenem (bottom left) and 40 μ g daptomycin (bottom right) were added to each disc. The plates were then incubated at 30 $^{\circ}$ C for 48 hours. Images are representative of 4 biological replicates.

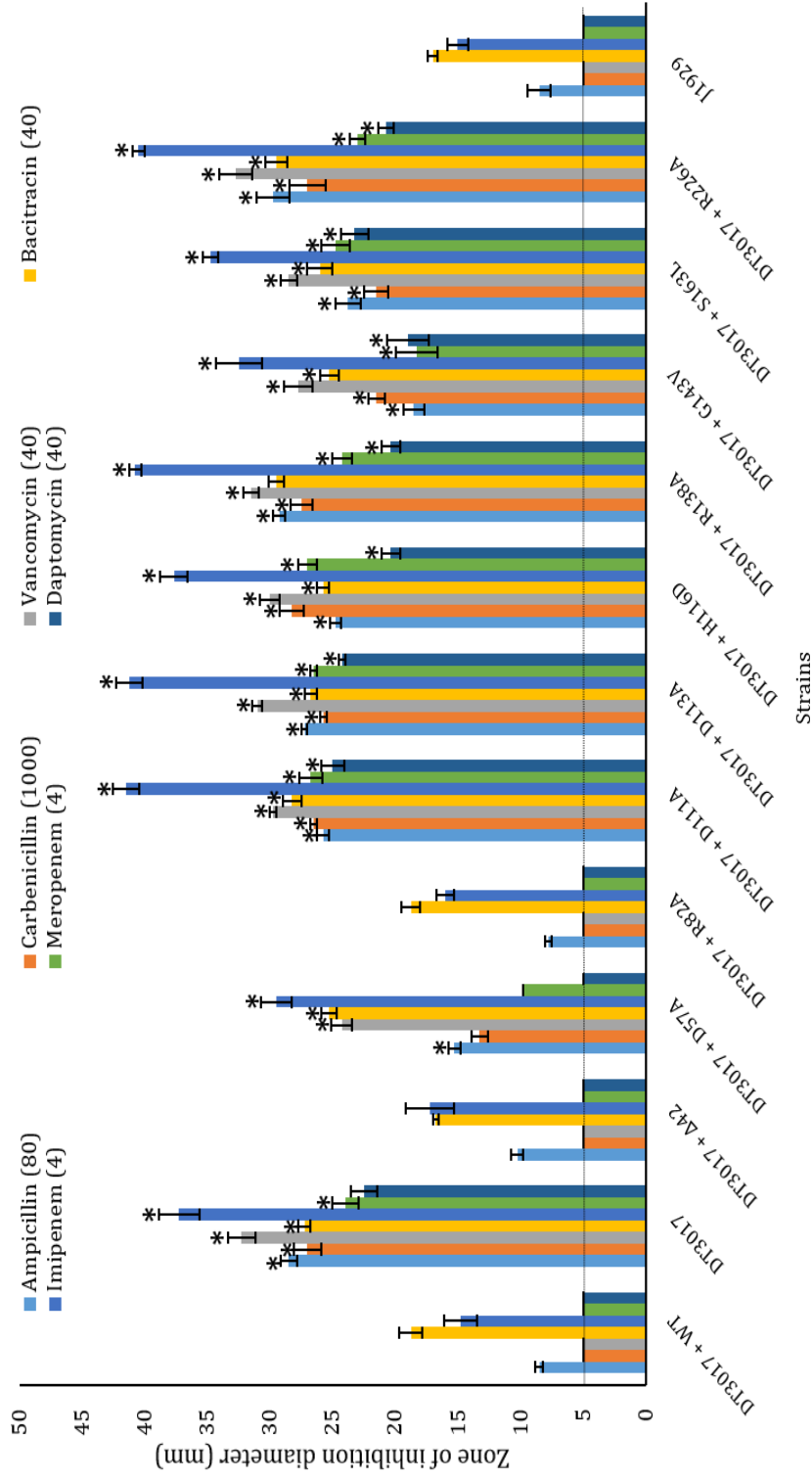


Figure 4.6: Complemented DT3017 strains do not show hypersensitivity to antibiotics targeting the bacterial cell wall and/or membrane. Antibiotic hypersensitivity was quantified by measuring the zone of inhibition diameter for the DT3017 WT *ppm1* control, no *ppm1* control and the *ppm1* mutants. J1929 refers to the parent strain. Strains were plated on DN agar and incubated at 30 °C for 48 hours. Shown are the averages of 4 biological replicates with SEM. The paper used to administer each antibiotic has a diameter of 5 mm and is shown as the dotted line threshold. The amount of antibiotic used in μg is shown in brackets in the legend.

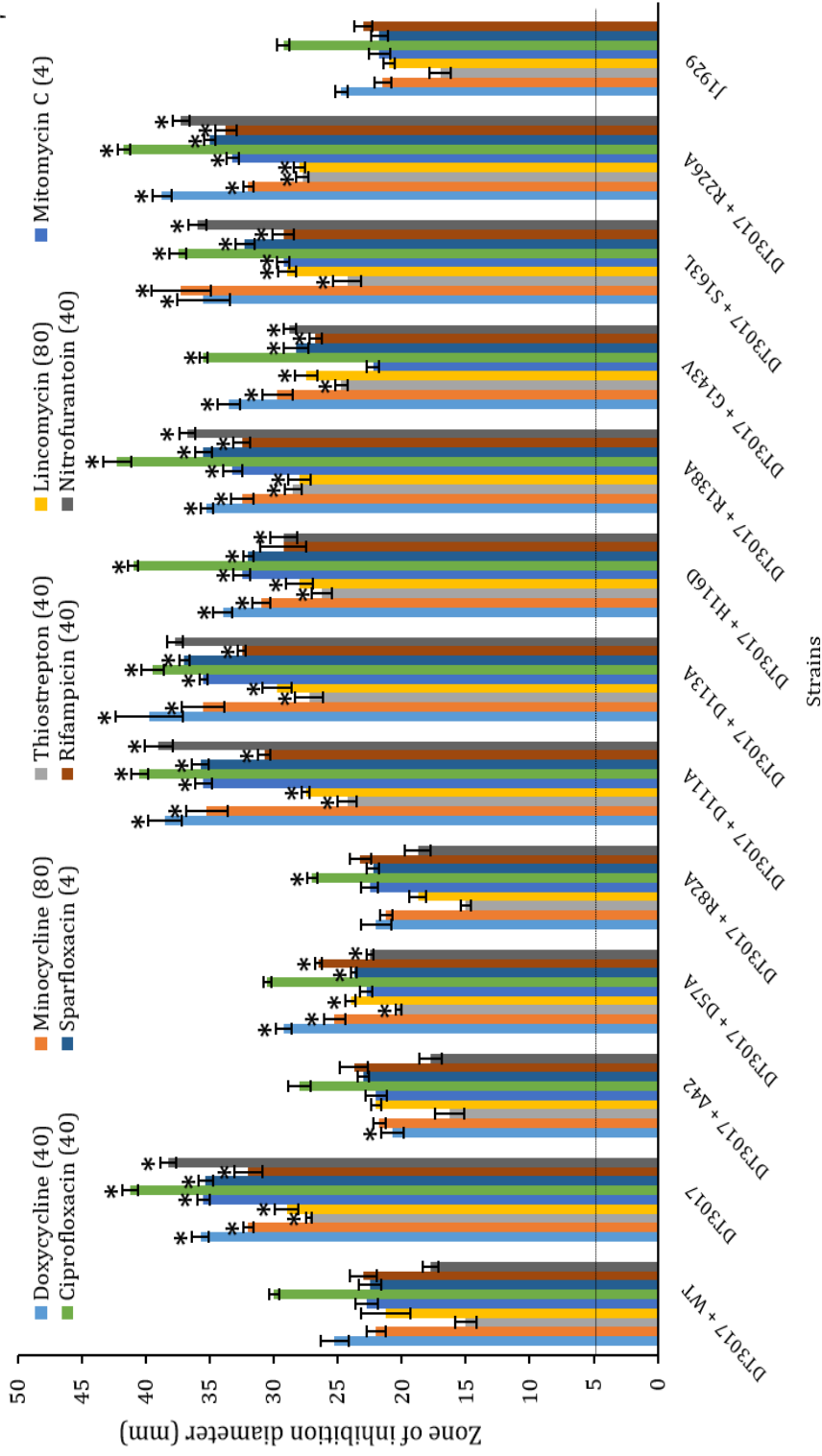


Figure 4.7: Complemented DT3017 strains do not show hypersensitivity to antibiotics targeting DNA replication, transcription and translation. Antibiotic hypersensitivity was quantified by measuring the zone of inhibition diameter for the DT3017 WT *ppm1* control, no *ppm1* control and the *ppm1* mutants. J1929 refers to the parent strain. Strains were plated on DN agar and incubated at 30 °C for 48 hours. Shown are the averages of 4 biological replicates with SEM. The paper used to administer each antibiotic has a diameter of 5 mm and is shown as the dotted line threshold. The amount of antibiotic used in µg is shown in brackets in the legend.

4.2.3 Complemented DT3017 are vulnerable to Φ C31 Δ 25 phage infection and exhibit increased growth rates

To further test the aforementioned strains, Φ C31 phage infection assays were performed (Figure 4.8 and Table 4.1). If the integrity of the glycosylation cascade has been restored, the complemented strains should be vulnerable to infection by this phage. As expected, the no gene negative control and the mutants that failed to alleviate the DT3017 antibiotic susceptibility phenotype: encoding Ppm1D111A, Ppm1D113A, Ppm1H116D, Ppm1R138A, Ppm1S163L and Ppm1R226A showed no evidence of infection within the phage dilution range tested. The WT positive control and the *ppm1* alleles (encoding Ppm1 Δ 42 and Ppm1R82A) that restored the antibiotic susceptibility to that of the J1929 parent strain were vulnerable to phage infection, with countable plaques obtained at a 10^{-6} phage stock dilution. Interestingly, plaques at this dilution were also obtained for strains containing Ppm1D57A and Ppm1G143V. The plaques obtained for the complemented strains were comparable in their size and clarity to the J1929 parent strain. Clear plaques are a hallmark of infection by a lytic phage such as Φ C31 Δ 25 (Lomovskaya *et al.*, 1972). Introduction of the alleles in the J1929 parent strain had no effect on phage susceptibility (Table A4.1).

DT3017 possesses a small colony phenotype when grown on DN agar (Figure 4.9), the strains containing WT, Ppm1 Δ 42, Ppm1D57A, Ppm1R82A and Ppm1G143V alleles grew faster yielding large colonies similar to those produced by J1929. Ppm1D111A, Ppm1D113A, Ppm1H116D, Ppm1R138, Ppm1S163L and Ppm1R226A failed to complement in DT3017, as indicated by the small colony phenotype.

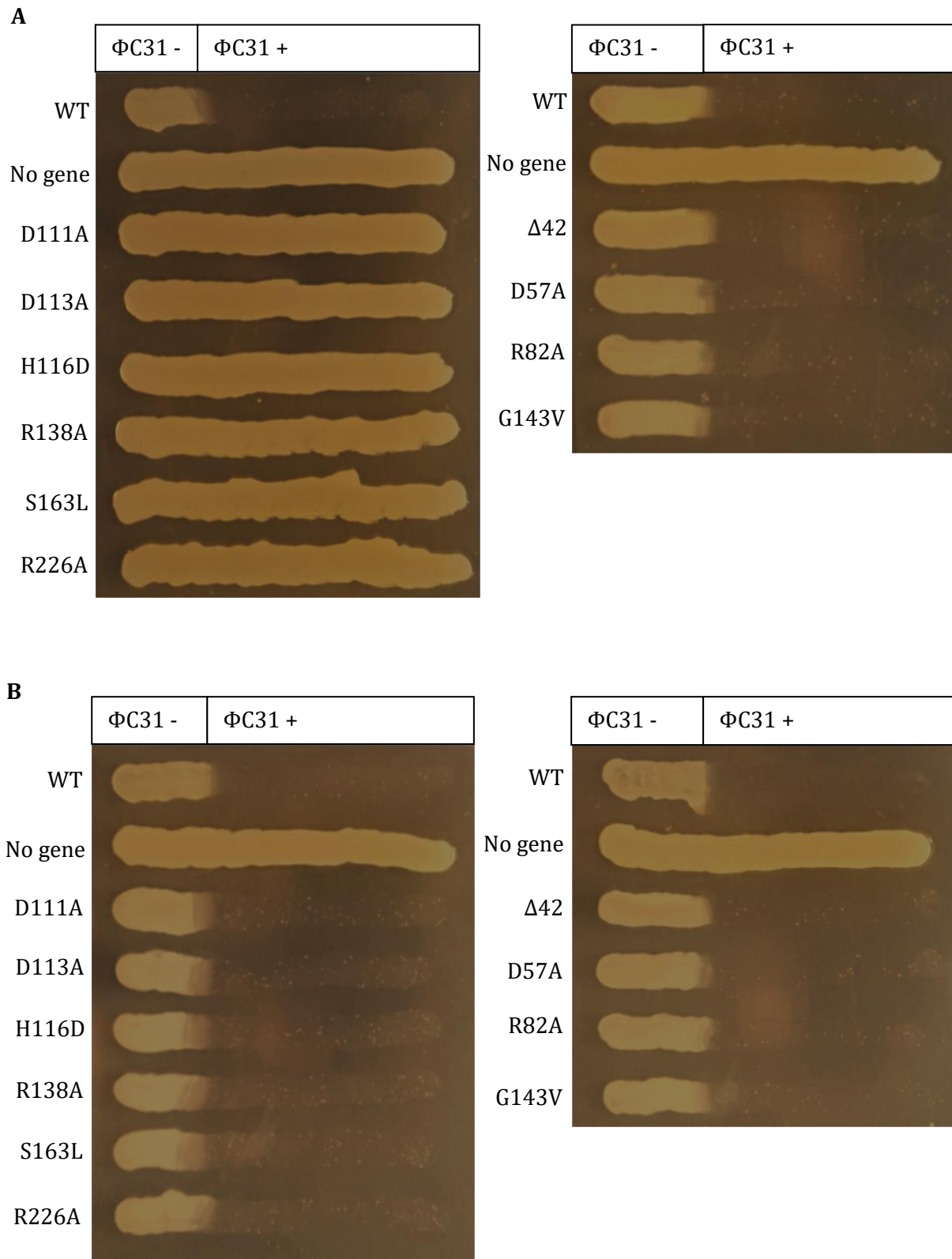


Figure 4.8: Complemented DT3017 strains are vulnerable to Φ C31 phage infection. Phage were plated out on a portion of DN agar and then DT3017 (A) or J1929 (B) spores containing the alleles were streaked from the phage absent region to the phage present region. Plates were incubated at 30 °C for 48 hours. Images are representative of 4 biological replicates.

Table 4.1: Complemented DT3017 strains are vulnerable to Φ C31 Δ 25 phage infection.

Phage were plated out on DN agar and then SN agar containing spores was added to the top with the plates incubated at 30 °C for 18 hours. The average titre is shown \pm SEM from 4 biological replicates. 0.1 ml of a 10^{-6} phage stock dilution was used to obtain countable plaques for phage sensitive strains. Strains that showed no plaques at the lowest phage stock dilution tested (10^{-1}) are represented as having a PFU/ml $< 1 \times 10^2$.

Strain	Titre (PFU/ml)
DT3017 + WT	$(1.05 \pm 0.06) \times 10^8$
DT3017	$< 1 \times 10^2$
DT3017 + Δ 42	$(1.25 \pm 0.08) \times 10^8$
DT3017 + D57A	$(1.38 \pm 0.08) \times 10^8$
DT3017 + R82A	$(1.43 \pm 0.11) \times 10^8$
DT3017 + D111A	$< 1 \times 10^2$
DT3017 + D113A	$< 1 \times 10^2$
DT3017 + H116D	$< 1 \times 10^2$
DT3017 + R138A	$< 1 \times 10^2$
DT3017 + G143V	$(1.30 \pm 0.04) \times 10^8$
DT3017 + S163L	$< 1 \times 10^2$
DT3017 + R226A	$< 1 \times 10^2$

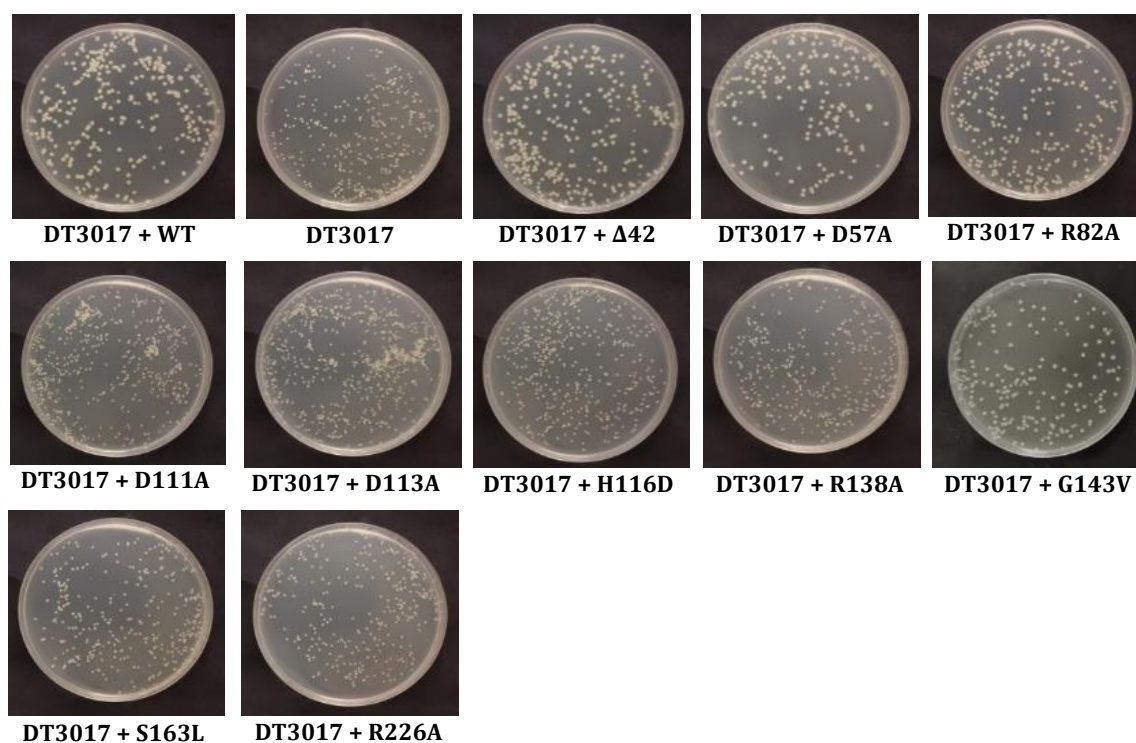


Figure 4.9: Complemented DT3017 strains show a large colony phenotype. Strains were grown on DN agar and incubated at 30 °C for 48 hours. Images are representative of 4 biological replicates.

4.3 Ppm1 structural bioinformatics and mechanistic modelling

Recently crystal structures were obtained of the dolichol phosphate mannose synthase (DPMS) from *P. furiosus* (PDB 5MLZ, 5MM0, 5MM1) (Gandini *et al.*, 2017). As expected, sequence conservation with *S. coelicolor* Ppm1 is high with sequence identity and similarity being 39.9 and 59.3% respectively (Figure 4.12). Using Phyre2, the PDB structure of the archaeal Dpm synthase in its post catalytic state (5MLZ) was used as a template to generate a homology model for *S. coelicolor* Ppm1 (Figure 4.10). The C-terminal portion is predicted to be disordered according to IUPred2A (Figure 4.1) and both termini are weakly conserved; consequently in this 302 residue protein, only residues 25-256 were modelled.

The model clearly shows the catalytic DXD motif and a Rossmann fold encompassing it, with parallel β stands in the characteristic secondary structure topology β - α - β - α - β (Lairson *et al.*, 2008). This model (including GDP and dolichyl phosphate mannose substrates) was then aligned with the template. In addition to the strongly conserved catalytic domain, the model and template both possess parallel helices at the base of the Rossmann fold, in the latter they are orientated towards the membrane. Towards the C-terminus of the *P. furiosus* DPMS there are four transmembrane domains, over a stretch of 100 residues, that serve to anchor the protein to the membrane. *S. coelicolor* Ppm1 lacks transmembrane helices and the mechanism of membrane association remains unknown. With the exception of G143, all residues targeted for mutation are closely located to the superimposed GDP donor or Und-P acceptor substrate. The template is in the post catalysis state of the reaction, whereby mannose has been transferred to Und-P and GDP has been released.

The *P. furiosus* DPMS structure and Ppm1 *S. coelicolor* model, in combination with the *in vivo* and *in vitro* data for all 10 mutants (Dube *et al.*, 2019), can be used as a framework for assigning roles to individual residues in a mechanistic model (figure 4.13). Six point mutants completely failed to complement DT3017 and of these, biochemical roles can be assigned to five (D111, D113, H116, R226 and R138). For the two mutants with intermediate phenotypes, a biochemical role can be assigned to D57 and a structural role to G143. It still remains mechanistically unclear why Ppm1S163L in DT1029 is inactive and consequently, no biochemical or structural role was proposed for this residue in the model.

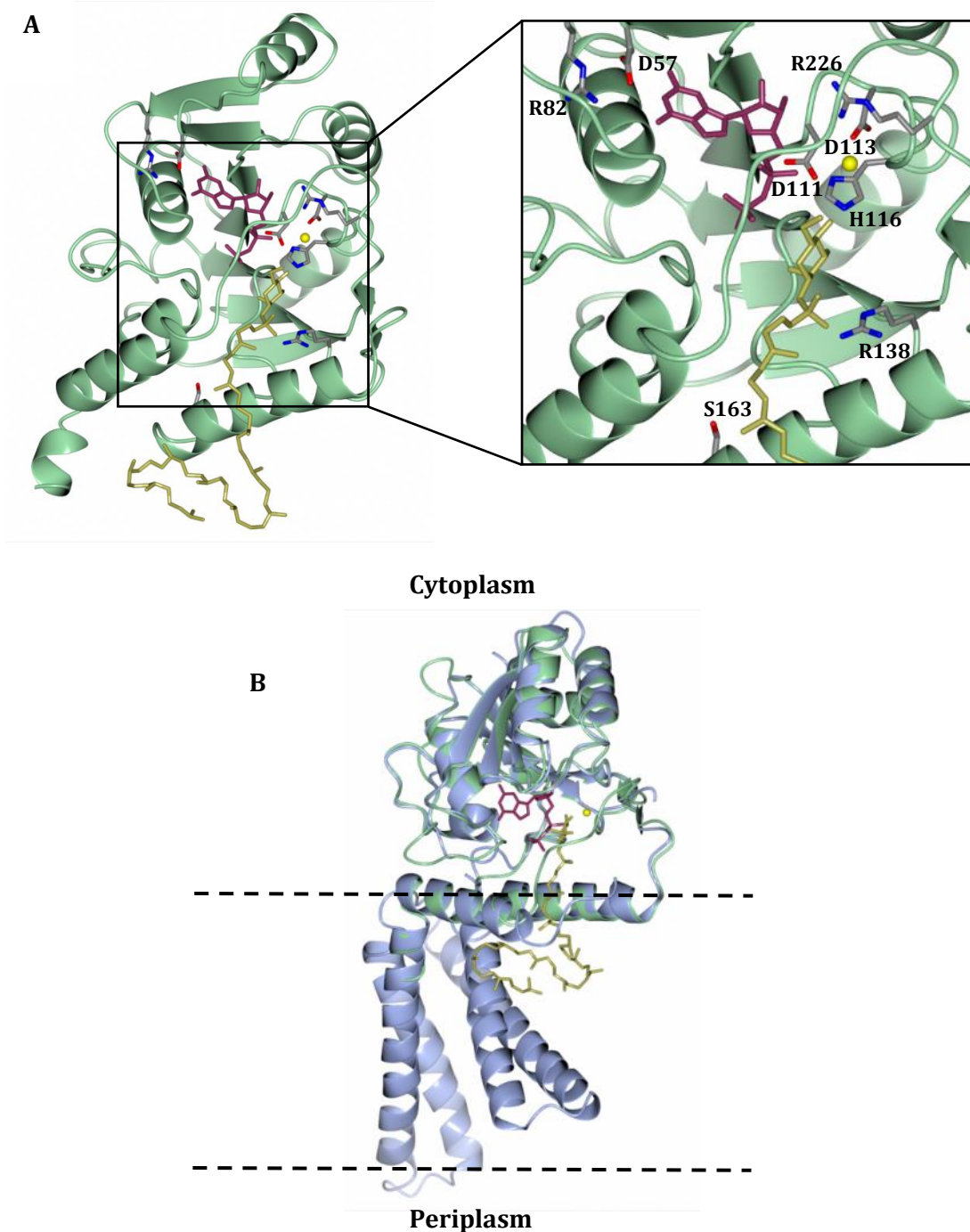


Figure 4.10: *S. coelicolor* Ppm1 homology model exhibits typical facets of GT-A fold glycosyl transferase. Using Phyre2, the PDB structure of the archaeal *P. furiosus* DPMS (5MLZ) was used as a template to generate a homology model for *S. coelicolor* Ppm1 (residues 25-256 modelled). Residues targeted for mutation are highlighted as cylinders. The model and template are coloured green and grey respectively. The template derived Und-P mannose, Mg^{2+} and GDP are coloured dark purple, yellow and gold respectively. (A). Ppm1 homology model with cofactor, donor and acceptor substrates from the template, in addition to the mutagenised *S. coelicolor* residues are highlighted. (B) Ribbon overlays of the template and model are displayed. The dashed lines represent proposed membrane boundaries.

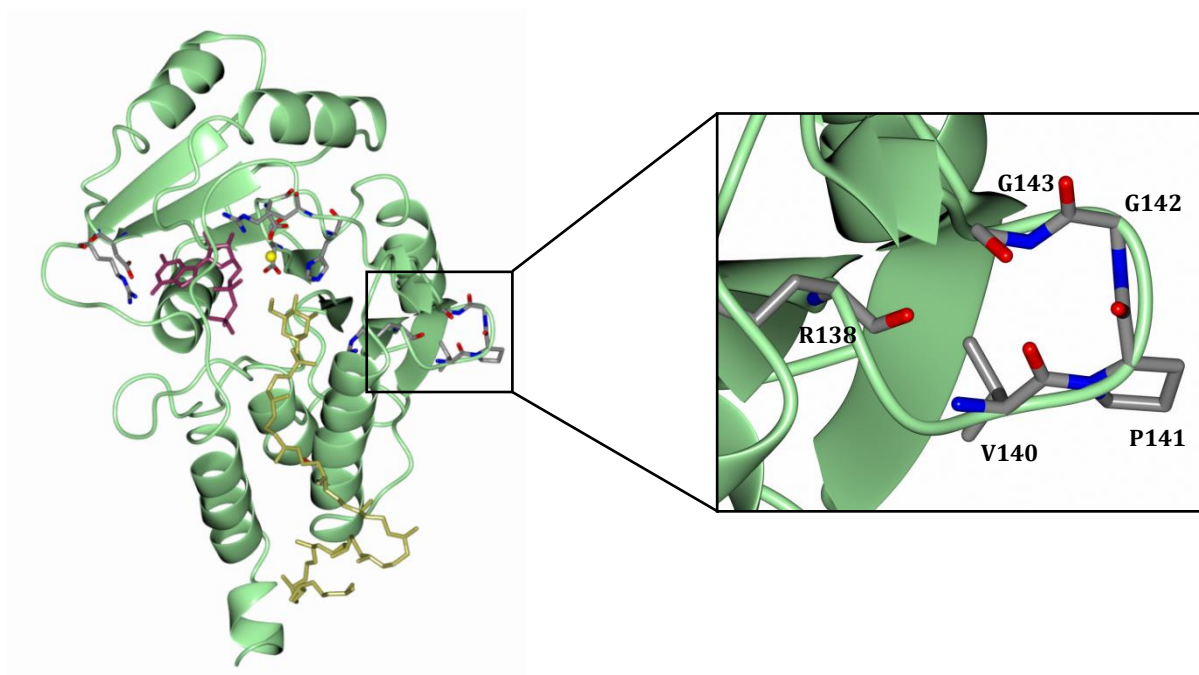


Figure 4.11: G143 is within a loop. Using Phyre2, the PDB structure of the archaeal *P. furiosus* DPMS (5MLZ) was used as a template to generate a homology model for *S. coelicolor* Ppm1 (residues 25-256 modelled). Residues targeted for mutation are highlighted as cylinders. The model is coloured green. The template derived Und-P mannose, Mg^{2+} and GDP are coloured dark purple, yellow and gold respectively. (A). Ppm1 homology model with cofactor, donor and acceptor substrates from the template, in addition to the mutagenised *S. coelicolor* residues are highlighted.

```

# Length: 243
# Identity:      97/243 (39.9%)
# Similarity:   144/243 (59.3%)
# Gaps:         22/243 ( 9.1%)
# Score: 378.5
#
#
#=====
Q8U4M3_PYRFU      5  VIIPTYNERENLEELFSRIDNALQGLNVEIVVDDDDSPDRTWEKAQELSS      54
   ||| ||| |. | | : : : : | : . | : . . . . : | . | : | | | . | : . | : | : :
Q9RKY2_STRCO     25  VIIPTYNEAENIKAIIVTRVREAVP--EAHVLVADQNSPDGTGKLADELAA      72

Q8U4M3_PYRFU     55  KYP-VKVIRRTKEKGLSSAVIRGFK---EASGDVFFVMDADLQHPPEVIP     100
   . . . | : | : . | : : : | | : . | : | : | | . . . . | : . | | | | . . | : | : |
Q9RKY2_STRCO     73  ADDHVQVMHRKGKEGLGAAYLAGFRWGLEHGYGVLIEMDADGSHQPEELP     122

Q8U4M3_PYRFU    101  KLIEAIKNGSDIAIGSRVYKGGKVENWPFYRKLISKGAIMVGRIALP-KI     149
   : | : . | : | | : : : | | | : | . | | : | . | | | . . | : | : | : | . . | | | . . :
Q9RKY2_STRCO    123  RLLTALK-GADLVLGSRWVPGGRVVNWPKSREIISRGGSMYSRIALDLPL     171

Q8U4M3_PYRFU    150  RDIKDPVSGFFALRKEVVEGVELNPIG-----FKI-LMEILIKGKYSKVV     193
   | | | . . | : . | . | : | : | : . . . . . | : : | . . . . | | . | |
Q9RKY2_STRCO    172  RDI---TGGYRAFRRRETLEGLGLEEVASQGYCFQVDLARRAIKAGY-HVW     217

Q8U4M3_PYRFU    194  EVPFTFGIRARGESKLGKKTIFEYLRHIYRLMKWEGEIDRIVK           236
   | | | . | | . . | : | : | : . . . . . | . | : | : . . | | . . | : | : |
Q9RKY2_STRCO    218  EVPIITFVERELGDSKMSRDILVEAL---WRVTTW-GVGERVVK           256

```

Figure 4.12: Strong conservation of the GT-2 domain in *S. coelicolor* Ppm1 and *P. furiosus* DPMS. EMBOSS Needle alignment of the *S. coelicolor* GT-2 domain (Uniprot entry: Q9RKY2_STRCO) with *P. furiosus* (Q8U4M3_PYRFU). The *S. coelicolor* residues targeted for mutation in this study are underlined in green.

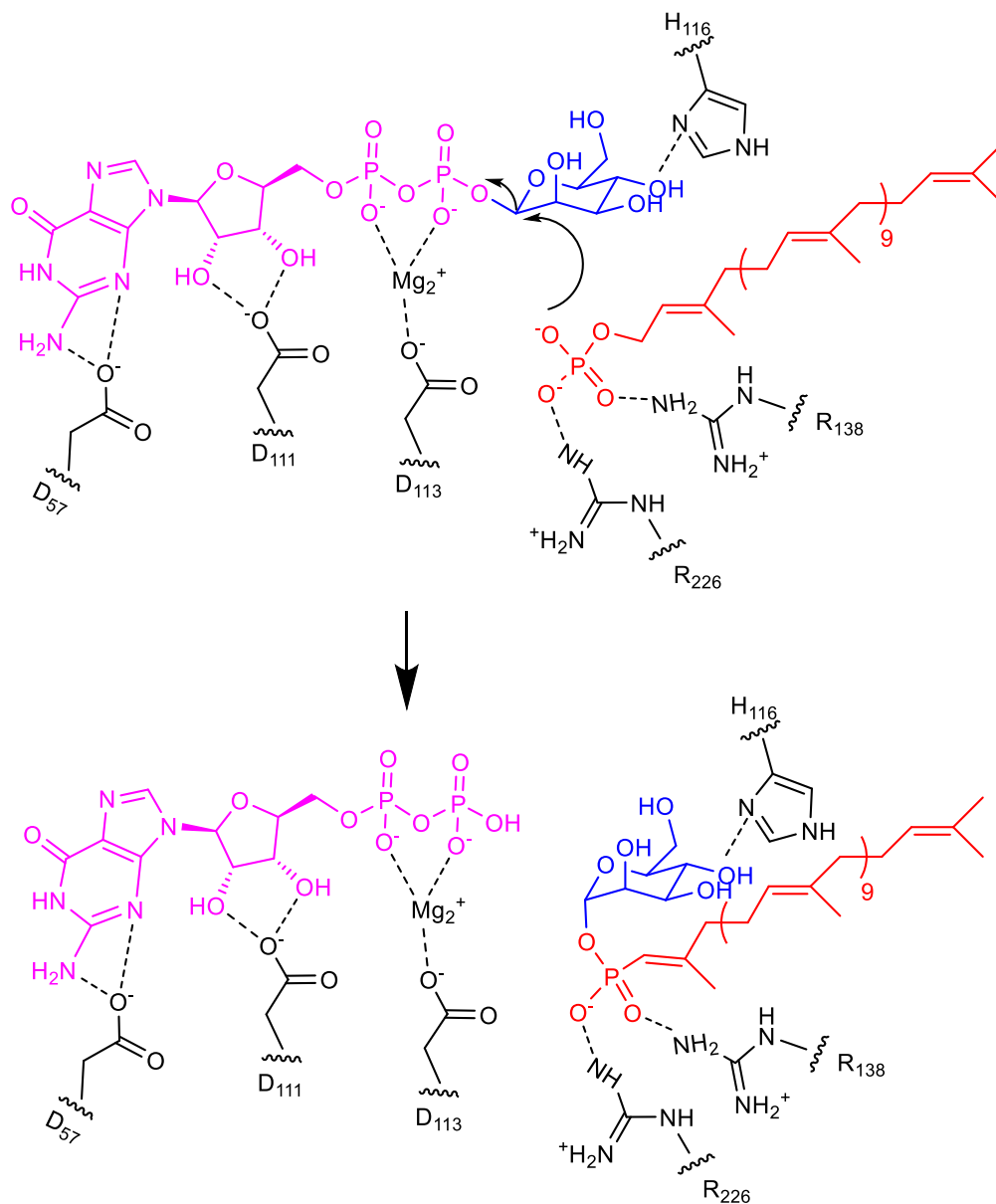


Figure 4.13: Proposed mechanism for Ppm1, an inverting glycosyl transferase that utilises a single step SN₂ mechanism. Nucleophilic attack by the Und-P phosphate oxygen on the C1 mannose carbon yields GDP and -P-Man. D113 coordinates the GDP-Man diphosphate groups via a metal cation. Residues D111 and D57 help to fix GDP in place by making contact with the ribose sugar and nucleoside guanosine respectively. Key side chains for positioning the Und-P phosphate group for mannose transfer include R138 and R228. residues/divalent cation, GDP, mannose and Und-P are coloured black, magenta, blue and red respectively.

4.4 Discussion

S. coelicolor ppm1 - strains DT1020, DT1029 and DT3017 were previously shown to have antibiotic hyper susceptibility phenotypes that were more extreme than that observed for the *pmt* - strains (DT1025 and DT2008) (Howlett *et al.*, 2018a; Wehmeier *et al.*, 2009). In addition, these strains had growth retarded phenotypes and resistance to Φ C31 Δ 25 infection (Howlett *et al.*, 2018a; Cowlshaw and Smith 2001; Cowlshaw and Smith 2002). These antibiotic hyper susceptibility phenotype observations suggested that both enzymes, are good targets for antimicrobials to be used in combination therapy with our existing arsenal of antibiotics. At the outset, only limited mutagenesis had been done on Ppm1/Dpm homologues with previous efforts focussed on the catalytically conserved DXD motif (Lairson *et al.*, 2008). Analysis of panels of mutants through *in vivo* molecular microbiology and *in vitro* biochemical assays has assigned roles for several critical residues. These assignments are consistent with the structure of Dpm synthase from *P. furiosus* (Gandini *et al.*, 2017) published mid-way through the work described in this Chapter which was carried out independently.

Our collaborator Pamela Dube at Warwick University made the following Ppm1 substitutions: D57A, R82A, D111A, D11A, H116D, R138A, G143V, S163L, R228A, in addition to a 42 residue C-terminal truncation (Δ 42) (Dube *et al.*, 2019). The alleles encoding these mutants were introduced into the *ppm1* - *S. coelicolor* strain DT3017. Antibiotic susceptibility testing showed that: Ppm1D111A, Ppm1D113A, Ppm1H116D, Ppm1R138A, Ppm1S163L and Ppm1R228A failed to complement DT3017. These strains therefore have an increased antibiotic susceptibility profile that matches the empty plasmid negative control for every antibiotic tested, in addition to growth retarded phenotypes and resistance to Φ C31 Δ 25 infection (observations also consistent with the empty plasmid negative control). Pamela Dube's biochemical data from the malachite green phosphate liberation assay showed the following *in vitro* normalised activities: Ppm1D111A (18 %), Ppm1D113A (4 %), Ppm1R138A (8 %), Ppm1R228 (7 %) and S163L (28 %), relative to the WT enzyme (Dube *et al.*, 2019). The mutants Ppm1 Δ 42 and Ppm1R82A successfully complemented DT3017 alleviating the antibiotic hypersusceptible phenotype, resensitising the bacteria to phage infection and restoring normal growth. The *in vitro* activities for Ppm1 Δ 42 and Ppm1R82A were 92 and 81 % respectively (Dube *et al.*, 2019). D57A showed sensitivity to phage infection and exhibited a healthy colony phenotype, however we observed significant increases in sensitivity to several cell wall targeting antibiotics, most notably, vancomycin. The sensitivity profile for D57A strains was intermediate between that observed for the WT complemented positive control and empty plasmid negative control. Strains containing G143V, like D57A, were sensitive to phage infection and had a large colony phenotype, however the antibiotic susceptibility profile was much closer to the empty plasmid

negative control. For Ppm1G143V and Ppm1D57A, the *in vitro* normalised activities were 42 and 36 % respectively, these intermediate reductions in activity are in general agreement with the partial complementation phenotypes observed *in vivo* for these mutants. In the study by Howlett (2018a), many of the antibiotics tested in this study were used to characterise *ppm1* - and *pmt* - strains. Where the amount of antibiotic added to the disc was the same in the two studies, the diameters of the zones of clearance were consistent, ranging from ~20-25 mm. This consistency between the studies, in addition to the good reproducibility (small SEM bars) gives confidence in the data obtained. The zone of clearance diameters for the non-complemented DT3017 strains are also comparable with the *S. coelicolor manB* - and *manC* - strains as expected. Indeed, it is known that strains depleted in enzyme activities used to generate polyprenol phosphate mannose (ManB, ManC and Ppm1) exhibited greater susceptibility to antibiotics than strains with depleted Pmt activity.

The residue corresponding to D57 of *S. coelicolor* Ppm1 was mutated to alanine in *Pyrococcus horikoshii* Ppm1 (D39A) (Urushibata *et al.*, 2008). The resulting mutant showed 2 % of the activity of the WT. Two other mutants of *P. horikoshii* Ppm1, D89A and D91A, (corresponding to *S. coelicolor* Ppm1 D111 and D113) showed 0.09 and 0.17 % activity of the WT enzyme respectively. The authors' conclusions were that this DXD motif was catalytic, a reasonable conclusion since the DXD motif is conserved in the GT-A family of glycosyl transferases (Lairson *et al.*, 2008). They also concluded that D39 plays an important role activity, but this residue may not participate directly in catalysis. This is to some extent supported by the homology model of Ppm1, from which we propose that D57 is remote from the DXD motif and would appear to make less critical interactions with the pyrimidine ring of the mannose donor GDP-Man. The intermediate or partial complementation phenotype (as discussed in Keenan *et al.*, 2019) in our *in vivo* assays strengthens the argument made by Urushibata and co-workers (2008) that while important for the enzymatic reaction, D57 is probably not a catalytic residue. When the structure of the *P. furiosus* Ppm1 was solved, Gandini *et al.*, (2017) also carried out SDM on the DXD motif. The activity of *P. furiosus* Ppm1 D89A and D91A mutants (*S. coelicolor* D111A and D113A) was ~25 % and ~50 % of WT levels respectively. The authors' hypothesised that the residual activity obtained (specifically for D91A) is due to Q93 and R202 rescuing some of the metal binding capacity of D91A. R202 but not Q93 is conserved in *S. coelicolor* Ppm1 (R226), where its substitution by alanine yielded a non-complementing mutant. Here we propose that, in accordance with the *P. furiosus* structure, the interaction of D113 with the anionic diphosphate group is mediated through a divalent metal cation. D111 in contrast directly interacts with the hydroxyl groups of the ribose sugar. The DXD motif therefore serves to fix the

GDP mannose firmly in place so that the C1 carbon of the mannose is correctly positioned for the reaction chemistry.

It is noteworthy that for *P. horikoshii* Ppm1, the DXD motif mutant activity was decreased to less than 1 % of that of the WT, while it was between ~25 % and 50 % respectively in the *P. furiosus* study (Urushibata *et al.*, 2008; Gandini *et al.*, 2017). This notably large discrepancy may be attributable to the different biochemical approaches taken by the authors. In the *P. furiosus* Ppm1 study a malachite green assay was used to monitor activity (Gandini *et al.*, 2017). In this assay, following the transfer of mannose to dolichol phosphate, the terminal phosphate (orthophosphate) is cleaved off GDP by a phosphatase and reacts with Malachite green and molybdate to create a complex that is detectable spectrophotometrically (Veldhoven *et al.*, 1987). In contrast, for the *P. horikoshii* Ppm1 study (Urushibata *et al.*, 2008), a radiometric assay method originally described by Orlean (1988) was used, whereby mannose is transferred from GDP-¹⁴C-mannose, to dolichol phosphate, with the Dol-P-¹⁴C-mannose product extracted and its radioactivity measured by scintillation counting. Analysis of data from Pi based assays like Malachite Green can be complicated by high background (caused by contamination by non-enzymatically produced Pi) and enzymatic hydrolysis of the substrate in assays conditions. Radiometric assays are arguably more sensitive, precise and have the advantage of directly monitoring mannose transfer. Based on this, in addition to the reductions being more consistent with the *in vitro* data obtained for the *S. coelicolor* DXD motif mutants (Dube *et al.*, 2019), the *P. horikoshii* Ppm1 study is probably more trustworthy (Urushibata *et al.*, 2008).

While the arginines corresponding to R138 and R226 in *S. coelicolor* Ppm1 (*P. furiosus* R117 and R202) were not substituted in the Gandini study, the close proximity of R226 to the DXD motif suggests a role in the enzymatic mechanism. This residue was proposed by Gandini *et al.*, (2017) to compensate for a DXD motif mutation, another possible role could be to assist R138 in orientating the nucleophilic phosphate head group of polyprenol phosphate. Correct orientation of this head group is needed to ensure the nucleophile is suitably positioned to attack the C1 carbon. This role was proposed for *P. furiosus* Ppm1 R117 rather than R202 (*S. coelicolor* R138 and R226). In our biochemical model, we propose that both R138 and R226 are involved in orientating the nucleophilic phosphate.

In human Dpm1, a G152V substitution was found in a human congenital disorder of glycosylation (CDG) patient (Yang *et al.*, 2013). The homologous residue in *S. coelicolor* Ppm1 (G143) was substituted to valine to mimic this mutation. In the homology model, G143 is part of a loop comprising V140 P141, G142 and G143. The glycine to valine substitution introduces a bulkier CH₂(CH₃)₂ side chain that is expected to alter the conformation of this loop, the resulting secondary structure change might then then destabilise the entire protein, or lead to an altered

conformation with reduced activity. Since this mutant only partially complements the DT3017 strain, the latter consequence appears more likely.

The remaining residues targeted and their substitutions were H116D and S163L. These substitutions reflect mutations previously identified in DT1020 and DT1029 respectively (Wehmeier *et al.*, 2009). The histidine in the homology model is positioned very close to the catalytic DXD motif. In active sites, histidines frequently serve as bases that deprotonate a nucleophile, the serine proteases being a notable example (Carter *et al.*, 1988). For GT-A catalysed reactions the phosphate head group of the acceptor does not require prior base activation, since it will already be deprotonated. This role of this conserved histidine has not been considered in the literature for any homologue. In the homology model, it is in hydrogen bonding distance of the C4 hydroxyl of the mannose (joined to polyprenol phosphate). It is therefore possible that H116 is able to stabilise both the donor substrate (pre catalysis) and the acceptor substrate (post catalysis). While not shown in the model, an alternate role could be to help orientate one of the aspartates within the DXD motif.

A role for S163 was not defined in this study. It is possible that mutation of S163 destabilise the protein. In the model, there are no polar residues within hydrogen bonding distance of the serine, indicating that destabilisation of the fold through loss of hydrogen bonding is unlikely. Another explanation is that this residue could be important for membrane localisation; the homologous residue in *P. furiosus* Dpm resides on an amphipathic helix that sits on top of the membrane, forming a boundary between the transmembrane and catalytic domains (Gandini *et al.*, 2017). It is therefore reasonable to propose a role in membrane localisation. The basis for membrane association of *S. coelicolor* Ppm1 remains unknown. Two mechanisms of membrane localisation have been identified in homologues, firstly *C. glutamicum* *M. tuberculosis* and *P. furiosus* Ppm1s comprise a single protein chain with separate catalytic and transmembrane membrane domains and secondly, *M. leprae*, Ppm1 comprises two separate proteins encoded by adjacent genes (Gandini *et al.*, 2017; Gibson *et al.*, 2003; Gurcha *et al.*, 2002). Since *S. coelicolor* Ppm1 does not possess a two domain architecture, an interacting partner remains the most likely explanation for membrane localisation. Further investigation is required to determine whether S163 (or another residue) is involved in this.

The motivation for substituting R82 and making a separate C-terminal truncation was based on a medical study of two siblings who carried mutant alleles of the *Dpm1* gene: 1) an R92A substitution and 2) a truncated C-terminus ($\Delta 47$) (Imbach *et al.*, 2000). The homologous *S. coelicolor* residue (R82) was substituted to alanine in our study and the allele surprisingly complemented DT3017. In the homology model, R82 is close to D57 and both residues would be expected to occupy the GDP-Man binding pocket. Imbach *et al.*, (2000), did not speculate on the

role of the arginine. The ability of the R82A mutant to fully complement DT3017 may be attributable to another nearby arginine or lysine (not conserved in human Dpm1) that can compensate for the loss of the residue.

Regarding the truncation mutant, the cause is premature translation termination at codon 213, leading to a loss of 47 residues from the C-terminus. Due to technical difficulties, a 42 rather than a 47 residue truncation of *S. coelicolor* Ppm1 was made by our collaborators. In *S. coelicolor* Ppm1, the C-terminal region is predicted to be disordered moreover, it is sparsely conserved across the prokaryotic and eukaryotic kingdoms. This truncated mutant nevertheless fully complemented DT3017. It is worth mentioning that the two children had both the R92A substitutions and the C Δ 47 truncation (Imbach *et al.*, 2000). Complementation studies (using *dpm1* - murine Thy1 deficient cells) to identify the impact of each mutation found that R82A presented a milder phenotype, while the truncation mutant had an extreme phenotype comparable with the empty plasmid negative control. Based on this, it could be that the active phenotype associated with *S. coelicolor* Ppm1 R82A can be attributed to a lack of sensitivity of the *in vivo* assays, which are unable to reveal an intermediate phenotype. This explanation is supported by our collaborator's biochemical data which show a 19 % reduction in activity. The oligomeric state of *S. coelicolor* Ppm1 is not known. It is understood that in *H. sapiens* DPM1 and DPM2 interact to form a complex in which DPM2 helps stabilise and correctly localise DPM1. It is known that the removal of the C-terminus in DPM1 inhibits this crucial oligomerisation. If *S. coelicolor* Ppm1 is monomeric (or the C-terminus is not involved in oligomerisation), this suggests an explanation of why the C-terminal truncation does not hinder the ability of the allele to complement DT3017. Another explanation is that the 42 residue truncation does not mimic the 47 residue truncation and that one or more of the intervening five residues is critical for Ppm1 activity, stability or localisation.

Chapter 5 - Identification of essential residues for *S. coelicolor* protein O-mannosyl transferase function

The *pmt* - strains: DT1025 and DT2008 were previously identified and isolated by Smith and co-workers. DT1025 was confirmed to have a premature stop codon in Pmt while DT2008 was not sequenced (Wehmeier *et al.*, 2009). Like the *ppm1* - strains mentioned in the previous chapter, Φ C31 phage is unable to form plaques with high efficiency on DT1025 and DT2008 strains, in contrast to the phage susceptible J1929 parent strain. Again, similarly to the *ppm1*- strains, DT1025 and DT2008 show retarded growth phenotypes and increased susceptibility to a number of cell wall/membrane targeting antibiotics compared to J1929 (Howlett *et al.*, 2018a). While *ppm1*- and *pmt* - colony phenotypes are broadly comparable, the *pmt* - strains are notably less susceptible to antibiotics than that obtained for the *ppm1* - strains, the reasons for this differential susceptibility remain poorly understood (Howlett *et al.*, 2018a).

In *S. cerevisiae*, PMTs are known to form dimeric complexes; a complex readily observed is Pmt1p-Pmt2p (Lommel and Strahl 2009). The human equivalent to PMTs are the POMT family, Pomt1-Pomt2 complexes have been well studied and are essential for mannosyl transferase activity (Akasaka-Manyu *et al.*, 2006; Lommel and Strahl 2009). Complex formation therefore appears to be critical for PMT O-linked mannosylation activity in yeast and humans, whereas there is a lack of evidence indicating that this is a prerequisite for PMT activity in prokaryotes such as the actinobacteria. The question remains, does *S. coelicolor* Pmt need to form homo or heterodimers in order to function? In the more closely related mycobacterial pathogens *M. tuberculosis* and *M. leprae*, the oligomerisation state of Pmt is also unknown (VanderVen *et al.*, 2005).

Mutagenesis of Pmt homologues from *S. cerevisiae* (Lommel *et al.*, 2011, Girrback *et al.*, 2000) and *M. tuberculosis* (VanderVen *et al.*, 2005), in addition to the homologue, ArnT from *C. metallidurans* (Petrou *et al.*, 2016), point to a number of residues that are likely to be important for function. Six residues mutated in these studies are either fully or partially conserved in *S. coelicolor*. It is not known whether all six of these residues will be critical for activity of *S. coelicolor* Pmt. Furthermore, many more residues in Pmts from across the prokaryotic and eukaryotic kingdoms are strongly conserved that are yet to be mutagenised.

The four objectives of this chapter were as follows:

1. Production of an *S. coelicolor pmt* rational mutagenesis library, guided by the literature and structural bioinformatics

2. Introduction of *S. coelicolor* mutant *pmt* alleles into *S. coelicolor* DT1025, DT2008 and J1929 strains, followed by spore preparation and strain harvesting
3. *In vivo* characterisation to probe essentiality of the targeted residues
4. Development of a robust mechanistic model for Pmt by combining *in vivo* data and structural bioinformatics with the literature

5.1 Pmt site directed mutagenesis

5.1.1 Identification of site directed mutagenesis targets

In order to probe amino acids essential for Pmt function, the Pmt sequence was aligned with homologues in prokaryotes (*S. griseus*, *M. smegmatis* and *M. tuberculosis*) and eukaryotes (*S. cerevisiae* and *H. sapiens*). The catalytic GT-2 domain is broadly conserved across the prokaryotic and eukaryotic kingdoms (Figure 5.1). Multiple conserved residues were identified, of which 27 were targeted and 23 changed to alanine: R82, D113, E114, V158, H159, P161, K164, R182, R201, R228, L231, L232, D233, K302, R338, P393, W400, H410, S421, W426, P503, R510, F564. Mutation of R100, Y156, Y356 and P569 to alanine was not achieved in spite of multiple attempts. The majority of these 27 residues were targeted on the basis of sequence conservation alone, with additional motivations to target seven residues (R100, D113, E114, H159, Y156, R182 and K302) as described below.

D113 and E114 constitute the conserved DE motif, a hallmark of GT-C fold glycosyl transferases (Lairson *et al.*, 2008). In *S. cerevisiae* Pmt1P, mutation of both homologous residues (D77, E78) led to notable reductions in *in vivo* glycosylation and complete elimination of *in vitro* mannosyl transferase activity (Lommel *et al.*, 2011). In another paper, mutations in the DE motif of *M. tuberculosis* (D55, E56) Pmt were carried out and *in vitro* mannosyl transferase activity was reduced, but not completely eliminated (VanderVen *et al.*, 2005). In an earlier study, R138 in *S. cerevisiae* Pmt1P (R182 in *S. coelicolor*) was shown to have an essential role in *in vitro* transferase activity (Girrbach *et al.*, 2000). Two other residues had been mutated: R64 (R100 in *S. coelicolor*) and L408, with both being essential for *in vitro* catalytic activity. R100 was not mutated and L408 is not conserved in prokaryotes. Finally, in *Cupriavidus metallidurans* ArnT, a lipid A glycosyl transferase, the mutation of D55, K85 and K203 (D113, H159 K302 in *S. coelicolor* respectively) eliminated *in vivo* function (Petrou *et al.*, 2016). Y82 (Y156 in *S. coelicolor*) was also shown to be essential for function but could not be mutated in this study.

<i>S. coelicolor</i> Pmt	-----GTGGYRDWAT-----KD	382
<i>S. griseus</i> Pmt	-----DKGYRNWAA-----TE	369
<i>M. smegmatis</i> Pmt	-----VNRY-----EV-----GR	308
<i>M. tuberculosis</i> Pmt	-----IDRH-----AV-----GQ	314
<i>S. cerevisiae</i> Pmt4	TNEEITTVTLEEGDGEIYPETLFAFQPLKKSDEGHVLSKKTVSFRLFHVDTSVALWTHND	490
<i>S. cerevisiae</i> Pmt2	TQWEVSGYGDN-VVGDNKDNWVIEIMDQRGDEDEPEKLHTLTTSFRIKNLEMGCYL-AQTG	496
<i>H. sapiens</i> Pomt2	KHYQVTGYGIN-GTGDSDNDFWRIEIVVNRKFGN---RIKVLRSRIRFIHLVTGCVL-GSSG	489
<i>S. coelicolor</i> Pmt	GANSSWSW-----LFPDWRSLWHYE-----	403
<i>S. griseus</i> Pmt	GKDSSWSW-----LFPDLRSLWHYE-----	390
<i>M. smegmatis</i> Pmt	SIGPDSIL-----PIPDALRSLWHYT-----	329
<i>M. tuberculosis</i> Pmt	AVGRNSVV-----PLPDAVRSLWHYT-----	335
<i>S. cerevisiae</i> Pmt4	ELLPDWGFQQQIEINGNKKVIDP--SNMNVVDEIVNLDVLRKVIYPKVVKPLPFLKKWIET	548
<i>S. cerevisiae</i> Pmt2	NSLPEWGFRRQQEVVCMKNPFKRDKRTWNIETHENER-LPPRPEDFQYPKTNFLKDFIHL	555
<i>H. sapiens</i> Pomt2	KVLPKWGWELVETCTPY-LKETLNSIWNVEDHINPK-LPNISLDVLQPS--FPEILLLES	545
<i>S. coelicolor</i> Pmt	-TQVLEFHTHLTS---PHTYQSNPWSWIVLGRPVSYFYESPASGSDGCPVDAGEKCARE	458
<i>S. griseus</i> Pmt	-NQVYDFHVGLTST---GHTYESNPWSWLVLRPVSFYFEEQ---TGCTQSSTGKCAAE	441
<i>M. smegmatis</i> Pmt	-HAAYRFHSNLTNADGNHHPWESKPWTWMSLRPVLAYIDNQDV--PGCG---AQSCVKA	383
<i>M. tuberculosis</i> Pmt	-AKAFHFHAGLTNSAGNYHPWESKPWTWMSLRPVLAYIDQQDV--AGCG---AQSCVKA	389
<i>S. cerevisiae</i> Pmt4	QKSMFEHNKLSSEH---PFASEPYSWPGSLSGVSFWT-----NGDEKKQ	590
<i>S. cerevisiae</i> Pmt2	NLAMMATNNALVPDPKFDYLASSAWQWPTLNVGLRLCG-----WGDDNPK	601
<i>H. sapiens</i> Pomt2	HMVMIRGNSGLKPKDNE---FTSKPWHWPINYQGLRFSG-----VNDTDFR	588
<i>S. coelicolor</i> Pmt	VLAGLGPLLWVGCFAIYLVLR-WL--F--RRDWR-----AGAIACGVA	498
<i>S. griseus</i> Pmt	VLAIGTPLLWNLACFALAYVVR-WF--F--RRDWR-----AGAIACGVV	481
<i>M. smegmatis</i> Pmt	VMLVGTAPAMWFIAPVVGWALLR-TV--V--RRDWR-----YGAVLVGYM	423
<i>M. tuberculosis</i> Pmt	EMLVGTAPAMWLVAVPVLAYAGWR-MF--V--RRDWR-----YAVVLVGYC	429
<i>S. cerevisiae</i> Pmt4	IYFIGNIIGWVQVIVLAVFVGIIVADLITRHRGYALNKM--TREKLYGPLMFFVSWC	648
<i>S. cerevisiae</i> Pmt2	YFLLGTPASTWASSVAVLAFMATVILLIRWQRQY-VDLRNPSPNWNVFLMGGFYPLLAWG	660
<i>H. sapiens</i> Pomt2	VYLLGNPVVWNLNLLSIALYLLSGSIIVAMQRGARLPAEVAAGLSQVLLRGGGQVLLGWT	648
<i>S. coelicolor</i> Pmt	AGYLPWFMYQERTIFLFYAVVFLPFLCLAVAMLLGAIIGRPGCT-----	542
<i>S. griseus</i> Pmt	AGWLPWFFYQERTIFLFYAVVFPFLCLAVTMLLGAIGPAAGTGARAEGLGLTTDDPTG-	540
<i>M. smegmatis</i> Pmt	AGFLPWAFADIDRQMYFFYATVMAPFLVLAIALILGDILYKPNQN-----	467
<i>M. tuberculosis</i> Pmt	AGWLPWFADIDRQMYFFYAATMAPFLVMGISLVLDGILYHPGQG-----	473
<i>S. cerevisiae</i> Pmt4	CHYFPFLMA-RQKFLHHYLPAPHLTACLFSGALWEVIFSDCKSLDLEK-----DEDISGA	702
<i>S. cerevisiae</i> Pmt2	LHYMPFVIMS-RVTVVHHYLPALYFALIIAYCFDA-----GLQKW-----SRSKCGR	707
<i>H. sapiens</i> Pomt2	LHYFPFLMG-RVLYFHYYFAMFLSSMLTGILWDLRLRLCAWGLASW-----PLA----	698
<i>S. coelicolor</i> Pmt	DTRRVAGA---TG---AGVLVLLIAWNFIYFWPLYTGTAIPM----EWRARMWLDTWV	591
<i>S. griseus</i> Pmt	ERRRTLGA---IA---VGLVLLIWNFIYFWPLYTGQIPE----DLWRDRMWLDTWV	589
<i>M. smegmatis</i> Pmt	PERRTLGL---LT---VCFYVALVITNFAMYPILTGLPISQ---TTWNLQIWLPSWR	516
<i>M. tuberculosis</i> Pmt	SERRTLGL---IV---VCCYVALVITNFALYLPVLTGLPISQ---QTWNLQIWLPSWR	522
<i>S. cerevisiae</i> Pmt4	SYERNPKVYVKPYTVFLVCSCAVAWFFVYFSPVYGDVSLSPSE---VVSREWFDIEL	758
<i>S. cerevisiae</i> Pmt2	I-MR---FV---LYAG-FMALVIG---CFWYFSPISFGMEGPS-----SNFRYLNWFSTWD	752
<i>H. sapiens</i> Pomt2	--R---GI---HVAG-ILSLLLTAYSFYLFHPLAYGMVGPLAQDPQSPMAGLRWLDSDW	749
<i>S. coelicolor</i> Pmt	-----	591
<i>S. griseus</i> Pmt	-----	589
<i>M. smegmatis</i> Pmt	-----	516
<i>M. tuberculosis</i> Pmt	-----	522
<i>S. cerevisiae</i> Pmt4	NFSK---	762
<i>S. cerevisiae</i> Pmt2	IADKQEA	759
<i>H. sapiens</i> Pomt2	F-----	750

Figure 5.1: The catalytic GT-2 domain is broadly conserved across the prokaryotic and eukaryotic kingdoms. Clustal Omega alignment of the *S. coelicolor* Pmt primary structure (Uniprot entry: Q9RKD3_STRCO) with *S. griseus* (A0A0D6UNW8_STRGR), *M. smegmatis* (PMT_MYCSE), *M. tuberculosis* (PMT_MYCTO), *S. cerevisiae* (PMT4_ & PMT2_ YEAST) and *H. sapiens* (POMT2_HUMAN). The *S. coelicolor* residues targeted for substitution to alanine are underlined in green.

5.1.2 Mutagenesis of targets

In order to make substitutions of the identified residues mentioned previously, initial efforts focussed on mutagenising the *pmt* allele and amplifying the recombinant plasmid. The *pmt* containing plasmid pDT10 was used as the template alongside the use of either back to back or partially overlapping primers to simultaneously introduce the mutation and amplify the entire plasmid in a single reaction. This approach often led to non-specific amplification products (data not shown). In cases where amplification was successful, the high proportion of impurities necessitated gel purification to obtain clean DNA appropriate for cloning. The low yield of desired full length plasmid product from the gel purifications was often insufficient for cloning. In other rare cases where a recombinant plasmid had been made and purified, sequencing revealed unwanted errors in the primer annealing regions.

Ultimately, amplification of the *pmt* allele via 2 PCR reactions proved successful:

- 1.) Forward flanking primer plus mutagenesis reverse primer
- 2.) Reverse flanking primer plus mutagenesis forward primer

Using 2 separate PCR reactions allowed for considerably shorter extension times, this reduced the non-specific primer binding considerably allowing higher yields of desired DNA fragments of the expected size to be purified by PCR clean up kits (Figure 5.2). The two inserts were subsequently joined together and cloned into pIJ10257 DNA sequencing and restriction digests confirmed correct mutagenesis and cloning of the *pmt* alleles encoding the following 23 changes: R82A, D113A, E114A, V158A, H159A, P161A, K164A, R182A, R201A, R228A, L231A, L232A, D233A, K302A, R338A, P393A, W400A, H410A, S421A, W426A, P503A, R510A, F564A.

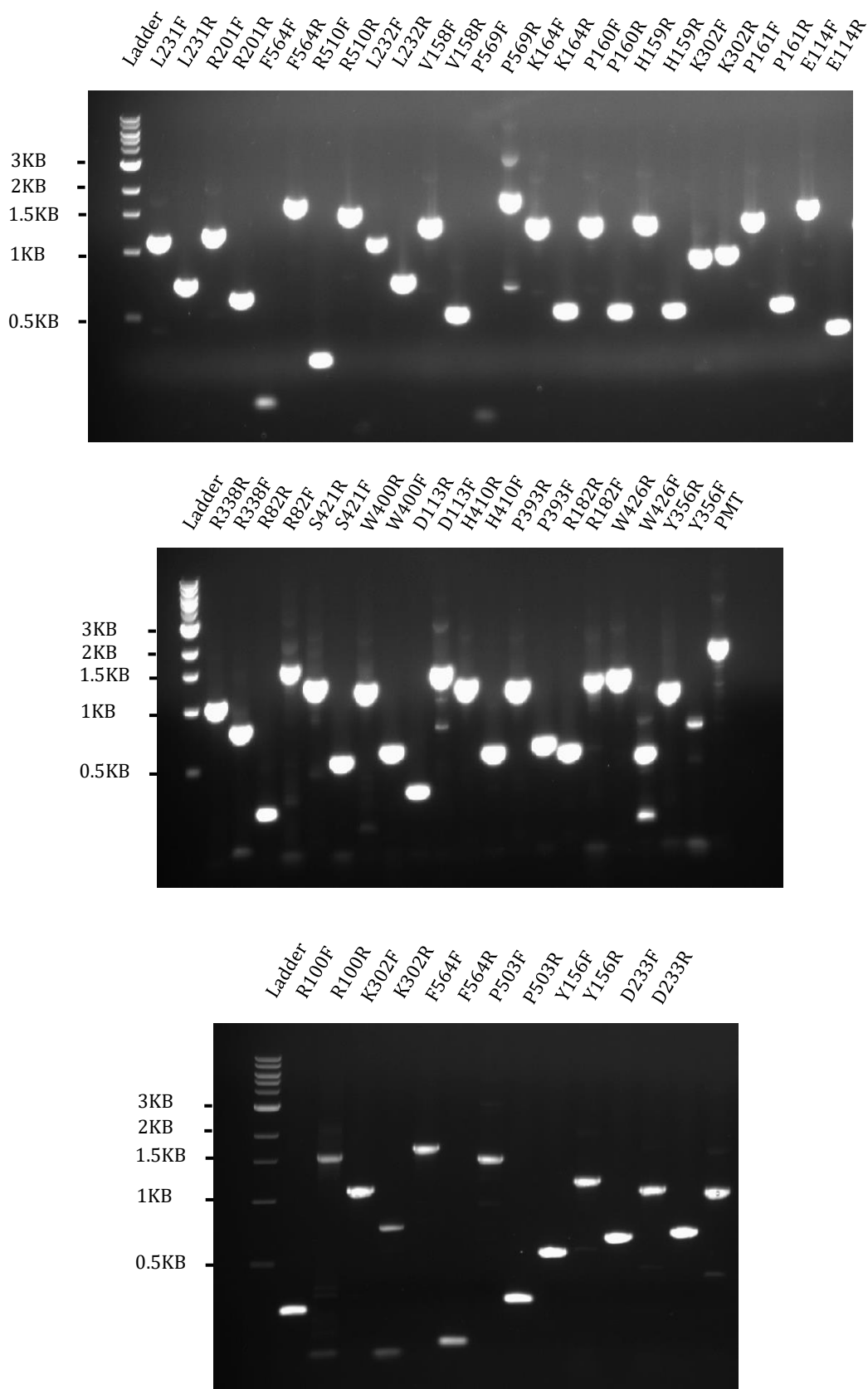


Figure 5.2: Introduction of the desired mutation by two separate PCR reactions gave high yields of correctly sized products. R100F refers to a PCR reaction using the forward mutagenesis primer, which would be used alongside the reverse flanking primer. The converse applies to R338R. The NEB 1 KB ladder is used for reference.

5.2 Pmt structural bioinformatics

5.2.1 Sequence analysis

S. coelicolor Pmt is predicted to have 11 transmembrane helices according to TMHMM (Transmembrane Helices; Hidden Markov Model) (Figure 5.3). The loop regions connecting these helices vary in size, with the predicted extracellular loops 1 and 7 being the largest with 82 and 94 residues respectively. The putative 11 transmembrane helices ranged in size from 17 to 22 residues with a mode of 22 residues.

In total 18 of the 23 residues substituted in this study are predicted to be located in extracellular loop domains. Seven residues (D113, E114, V158, H159, P161, K164 and R182) and five residues (P393, W400, H410, S421 and W426) are predicted to occupy loops 1 and 7 respectively. Another four residues (R228, L231, L232 and D233) are on the comparatively smaller loop 3, while residues K302 and R510 occupy loops 5 and 9 respectively. The hallmark DE motif is located within loop domain 1, as is universally observed in Pmt homologues across the prokaryotic and eukaryotic kingdoms. The active sites of Pmt family enzymes are mostly composed of extracellular residues and it is these regions that show the greatest sequence conservation.

Three of the substituted residues are predicted to be located on the cytoplasmic side of Pmt, with R82 in the N-terminal region and residues R201 and R338 located in loops 3 and 5 respectively. Finally, only two mutated residues are predicted to occupy the transmembrane spanning portion of Pmt, with residues P503 and F564 individually located on helices 9 and 11 respectively.

The N-terminal 82 residues preceding the first transmembrane helix of *S. coelicolor* Pmt encompass roughly 55 amino acids that are predicted to be highly disordered according to IUPred2A (≥ 0.5) (Figure 5.3). Subsequent moderate peaks in disorder tendency (< 0.5) are seen in the following regions: 135-156 (N-terminus), 259-282 (loop 1), 374-390 and 412-456 (loop 7) and 541-548 (loop 10).

ArnT is a GT-C fold glycosyl transferase from the bacterium *Cupriavidus metallidurans*, which catalyses aminoarabinose transfer to lipid A. This enzyme also has 11 transmembrane helices and the sequence of the extracellular loop domains (which constitute the globular domain in the GT-C family of enzymes) are strongly conserved between *S. coelicolor* Pmt and *C. metallidurans* ArnT (Figure 5.4). Alignment of the full *S. coelicolor* Pmt primary structure with *C. metallidurans* ArnT gave a sequence identity and similarity of 16.3 and 24.9 % respectively.

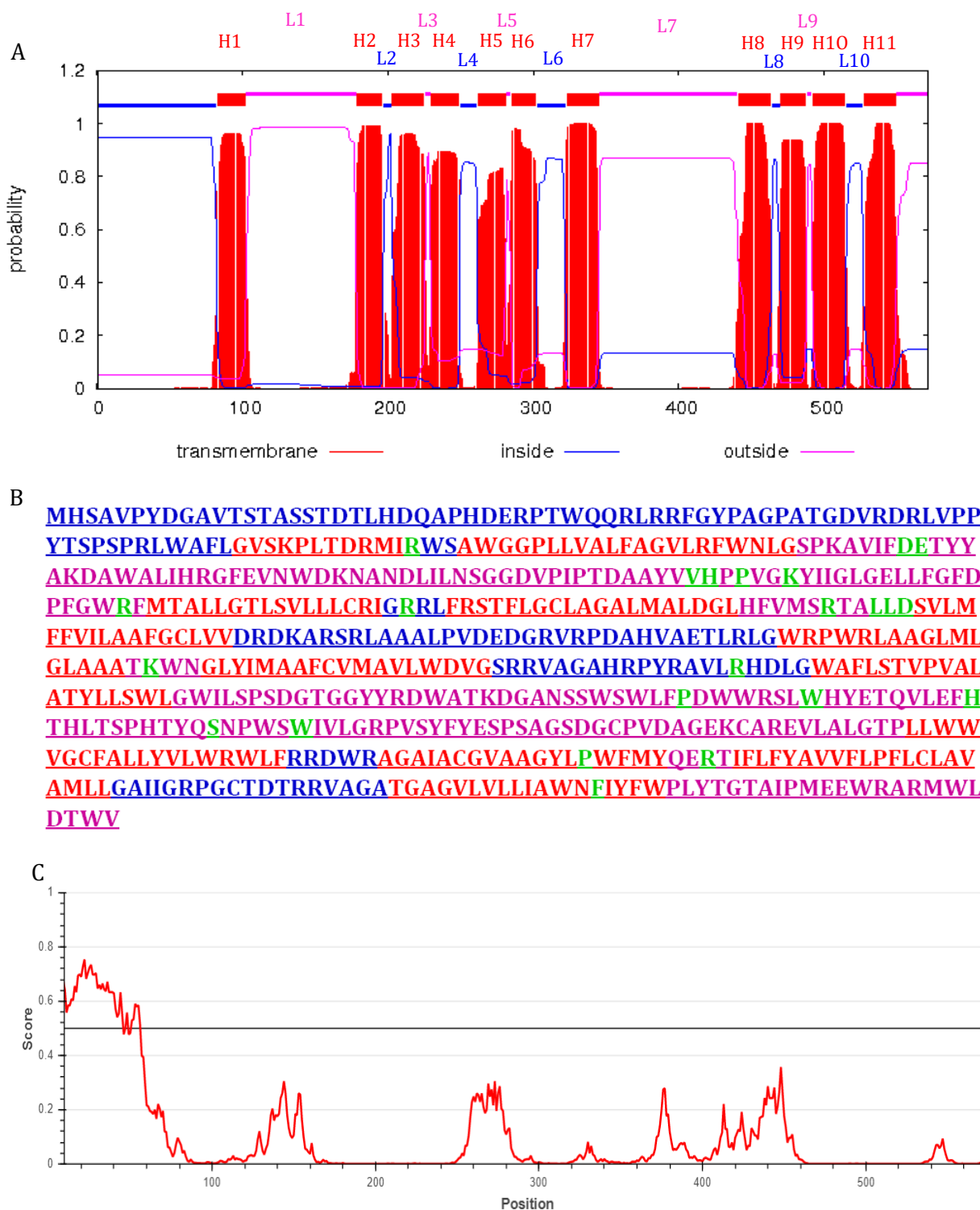


Figure 5.3: *S. coelicolor* Pmt has 11 predicted transmembrane helices and a disordered N-terminus. (A) TMHMM plot for *S. coelicolor* Pmt with regions predicted to be transmembrane helices, cytoplasmic portions and extracellular portions highlighted. H and L annotations refer to helix and loop respectively. (B) TMHMM results superimposed on to the *S. coelicolor* Pmt primary structure with conserved residues targeted for mutation highlighted in green. (C) IUPred2A plot shows the score of each residue in the protein from 0 to 1 (low to disorder respectively). A residue with a score of ≥ 0.5 is considered to have more disordered character.

```

# Length: 668
# Identity:    109/668 (16.3%)
# Similarity: 166/668 (24.9%)
# Gaps:       313/668 (46.9%)
# Score: 118.5
#
#
#=====
Q9RKD3_STRCO      1 MHSAPYDGA V T S T A S S T D T L H D Q A P H D E R P T W Q Q R L R R F G Y P A G P A T G D      50
Q1LLF9_CUPMC      1 -----
Q9RKD3_STRCO     51 VRDRLVPPYTSPSPRLWAF LGV-SKPLTDRMIRWS-AWGGPLLVALFAGV      98
Q1LLF9_CUPMC      1 -----MPQPTSQQRASVASSQSTQGA VGW SAATGWV VLFVAVALV      40
Q9RKD3_STRCO     99 LRFWNLGSPKAVIFDETY YAKDAWALIH RGF EVNWDKNANDLILNSGGDV     148
Q1LLF9_CUPMC     41 VWFVSLDMRHLVGPDEGRYA-----EISREMFA-----SGDW      73
Q9RKD3_STRCO    149 PIPTDA-AYVHPPVGVKI IGLGELLFGDFPGWR FMTALLG T LSV L L L C     197
Q1LLF9_CUPMC     74 TIRYNALKYFEKPPFHMWTVVGYELFGLGEWQARLAVALSGLLGIGVSM     123
Q9RKD3_STRCO    198 RIGRRLFRS-----TFLGCLAGALMALDGLHF---VMSRTALLDSVLMFF     239
Q1LLF9_CUPMC    124 MAARRWFGARAAAF TGLALLAAPMMSV-AAHFNTLDMTLAGVMSCVLAFM     172
Q9RKD3_STRCO    240 VLAAGCLVDRDKARSRLAAALPVDEDGRV RPD A HVAETLRLGWRPWRL     289
Q1LLF9_CUPMC    173 LMGQ-----HPDASVAAR-----RGMV      190
Q9RKD3_STRCO    290 AAGLMLGLAAATKWINGLY IMAAF CVMAVLW DVGSR RVAG AHRPYRAVLRH     339
Q1LLF9_CUPMC    191 ACWAAMGVAILTK--GLVGIALPGLV LVVYTLVTR-----      223
Q9RKD3_STRCO    340 DLGWAF LSTVPVALAT-----YLLS-----WLGW      363
Q1LLF9_CUPMC    224 --DWGLWRRLLHALGVV VMLVITVPWFYLVSVRNPEFPNFFF IHEHWQRY     271
Q9RKD3_STRCO    364 ILSPSDGTGGYYRDWATKDGANS SWSWLF PDWRS LWHYETQVLEFH THL     413
Q1LLF9_CUPMC    272 TSNIHRSRGSVFYFLPLVIGGFLPWAGIFPKLWTAM-----      307
Q9RKD3_STRCO    414 TSPHTYQSNPWSWIVLGRPVSYFYESP SAGSDGCPVDAGEK CAREVLALG     463
Q1LLF9_CUPMC    308 -----RAPVEGTQARFRPALMAG      325
Q9RKD3_STRCO    464 TPLLWVGCFA-----LLYVLRWLFRRDW---      488
Q1LLF9_CUPMC    326 ---IWAIAIFVFFSISRSLKPGYIVPVIPALGILAGVALDRLSPRSWGKQ     372
Q9RKD3_STRCO    489 ---RAGAIACGVA-----AGYLPWFMYQERTIFLFYAVVFLPFLCL     526
Q1LLF9_CUPMC    373 LIGMAIVAACGLLASPVVATLNANHIPNSFYRAYAVWAVAFVVM-LLGI     421
Q9RKD3_STRCO    527 AVAMLL---GAIIGRPGCTDRRVAGATGAGVLVLLIAWNFIYFWPLYTG     573
Q1LLF9_CUPMC    422 AVARLLLRGV-----      432

Q9RKD3_STRCO     574 TAIPMEWRARMWLDTW      591
Q1LLF9_CUPMC     433 -----      432

```

Figure 5.4: *S. coelicolor* Pmt and *C. metallidurans* ArnT have a sequence identity and similarity of 16.3 and 24.9 % respectively. The full length *S. coelicolor* Pmt primary structure was aligned with 432/600 to keep the lengths of the aligned sequences consistent.

5.2.2 Homology model analysis

The ArnT structure from *C. metallidurans* (PDB ID: 5ezmA) was used to generate a Phyre2 homology model of Pmt. 485 residues (82 %) were modelled at >90 % confidence using ArnT exclusively (figure 5.5). The excluded regions include residues 1-84 and 563-591, representing the N and C-termini respectively. These excluded regions included two mutated residues R82 and F564, which are consequently absent from the model.

Of the 11 predicted transmembrane helices, 8 appear to be modelled very well, with helix length in full agreement with the TMHMM plot (Figures 5.3 and 5.5). However, the modelling of helices 3, 7 and 10 partially agrees with the TMHMM plot and therefore may be unreliable. In the model, helix 3 is separated into 2 smaller helices, while for helices 7 and 10, roughly $\frac{1}{2}$ and $\frac{2}{3}$ of the residues were not modelled respectively. The helices: 1, 2, 4, 5, 6, 8, 9 and 11 did correspond well to the TMHMM plot and enabled membrane bilayer boundaries to be predicted.

The largest loops are 1 and 7, these can be easily seen between transmembrane helices 1 and 2 and 7 and 8 respectively. Both loops are comfortably above the defined membrane boundaries and sit on the periplasmic side of the membrane, as expected. The majority of residues targeted for substitution are predicted to occupy these loops (Figure 5.7). In the model, the residues: D113, E114, V158, H159, P161, K164 and R182 occupy a periplasmic facing loop that links transmembrane helices 1 and 2, as expected based on TMHMM. This region represents the hallmark loop 1 domain of GT-C fold glycosyl transferases. 5 residues are predicted to occupy the periplasmic loop domain 7: P393, W400, H410, S421 and W426. This is the second largest loop domain in the model and is clearly represented as being between transmembrane helices 7 and 8. While W400, H410 and S421 sit comfortably in the periplasmic loop as expected, P393 and W426 are shown to be just below the membrane boundaries. As expected, the smaller loop 3 is found between helices 3 and 4, with the residues: R228, L231, L232 and D233 shown above the membrane boundaries. The final periplasmic residues: K302 and R510 are also shown above the membrane boundaries and located in loops 5 and 9 respectively.

To summarise, of the 18 residues targeted for mutation that are predicted to occupy the periplasmic region, 16 (D113, E114, V158, H159, P161, K164, R182, R228, L231, L232, D233, K302, W400, H410, S421 and R510) are above the defined membrane boundaries, with each located in its expected loop domain. The TMHMM plot and model are therefore in agreement for these residues. Residues P393 and W426 were not identified in the periplasmic loop domain 7, it is however noteworthy that these residues occupy the periplasmic poles of the connecting transmembrane spanning helices 7 and 8 respectively.

For the cytoplasmic residues. R82 is not shown since the first 83 residues were not included in this model. The residue R338 is shown on the cytoplasmic pole of helix 5, while R201 is on the membrane boundary separating the cytoplasmic pole of helix 2 and loop 3. Considering the transmembrane helices, P503 is shown on helix 10 as expected. F564 is not included in this model due to exclusion of the final 27 residues.

To summarise, 18 of the 23 residues substituted in this study have a position in the model that is in full agreement with the TMHMM profile. 3 residues (R201, P393 and W426) are close to their expected location rather than distant while R82 and F564 were not modelled.



Figure 5.5: Phyre2 homology model of *S. coelicolor* Pmt has typical facets of GT-C fold glycosyl transferases. The model is based on the template ArnT (5F15) from *C. metallidurans*. 485 residues (82 %) were modelled at >90 % confidence. (A) Ribbon model coloured according to secondary structure. (B) Worm and tube model coloured according to rainbow format, going from blue (N-terminus) to red (C-terminus) with numbered transmembrane helices. Predicted membrane boundaries are represented as dashed lines.

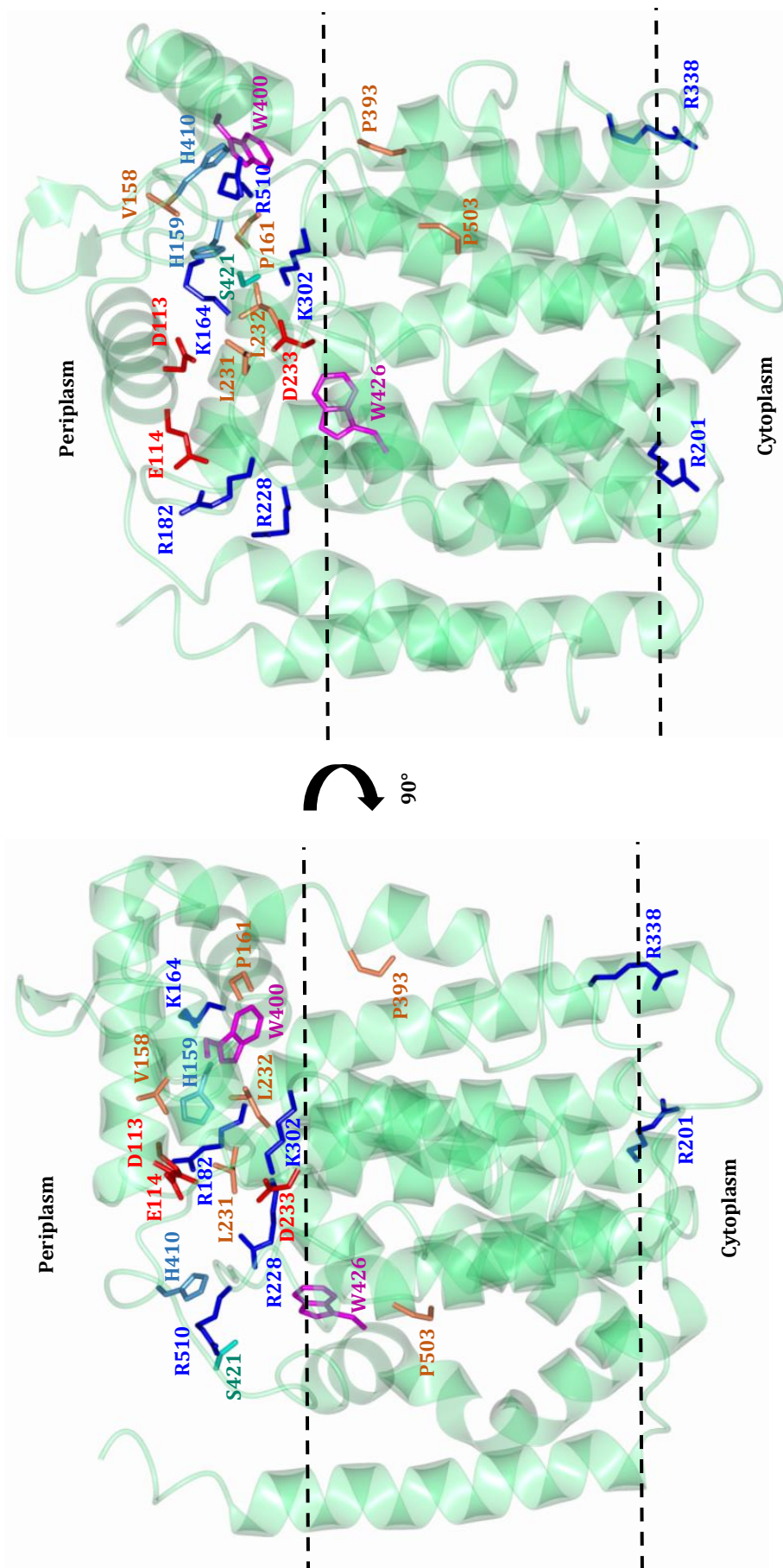


Figure 5.6: Pmt Phyre2 homology model exhibits typical facets of a GT-C fold glycosyl transferase. The model is based on the template ArnT (5F15), a GT-C fold glycosyl transferase from *C. metallidurans*. The model is shown as teal transparent ribbons. All residues targeted for mutation are represented as cylinders and coloured according to their type: hydrophobic (brown), aromatic (purple), nucleophilic (teal) amide (light blue), basic (dark blue) and acidic (red). Predicted membrane boundaries are represented as dashed lines.

5.3 *In vivo pmt* mutant characterisation

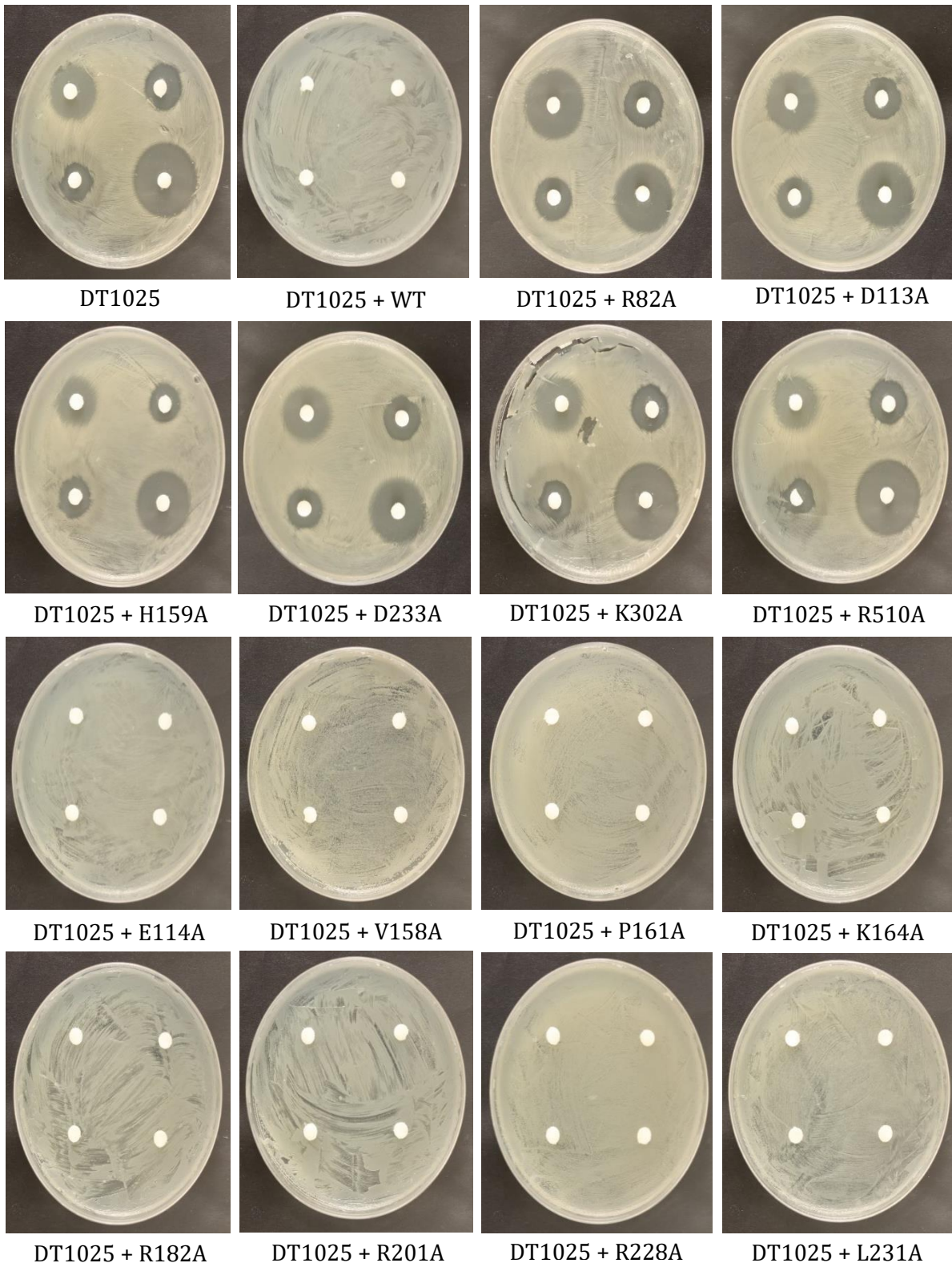
5.3.1 Identification of *pmt* mutants unable to alleviate the antibiotic susceptible phenotype of DT1025

Using the integrative vector pIJ10257, *S. coelicolor pmt* mutant alleles were stably introduced into the chromosome of the *pmt* - strain (DT1025) and the parent strain (J1929) and antibiotic disc diffusion assays carried out as described previously (Howlett *et al.*, 2018a). Six of the *pmt* mutant alleles tested failed to complement the *pmt* mutation in DT1025: These alleles encoded PmtR82A, PmtD113A, PmtH159A, PmtD233A, PmtK302A, PmtR510A (Figures 5.7 and 5.8). These strains showed significantly increased susceptibility to all cell wall and/or membrane targeting antibiotics tested, in addition to rifampicin and nitrofurantoin, when compared to the J1929 parent strain ($p < 0.05$).

DT1025 containing each of the six non-complementing *pmt* alleles had increased carbapenem (imipenem and meropenem) and vancomycin susceptibilities compared to J1929. The WT and 17 remaining mutant alleles were able to complement DT1025, alleviating the antibiotic susceptible phenotype (Figures 5.8 and 5.9). The antibiotic susceptibility for the complemented strains was consequently not significantly different to J1929 for any antibiotic tested ($p < 0.05$).

DT1025, the negative control strain (containing the plasmid only) and the non-complemented mutant strains interestingly did not exhibit significantly increased susceptibility to antibiotics inhibiting DNA replication and translation when compared to the J1929 parent strain ($p < 0.05$) (Figure 5.10), representing a clear contrast with the *ppm1* non-complemented mutants discussed in chapter 4. All 23 strains therefore exhibited comparable susceptibility, with the ability to complement therefore having no effect (Figures 5.10 and 5.11). In summary, the absence of active Pmt is only noted when antibiotics targeting the cell wall/membrane or transcription are used, indicating a clear mechanistic bias.

All mutant *pmt* alleles were additionally introduced into the J1929 parent strain. In these experiments, there was no significant difference in susceptibility to any antibiotic tested (Figures A8.3, A8.4, A8.5 and A8.6). This demonstrates that the expression of the non-complementing and complementing *pmt* mutants in the parent strain, failed to reduce or enhance the function of the WT enzyme respectively.



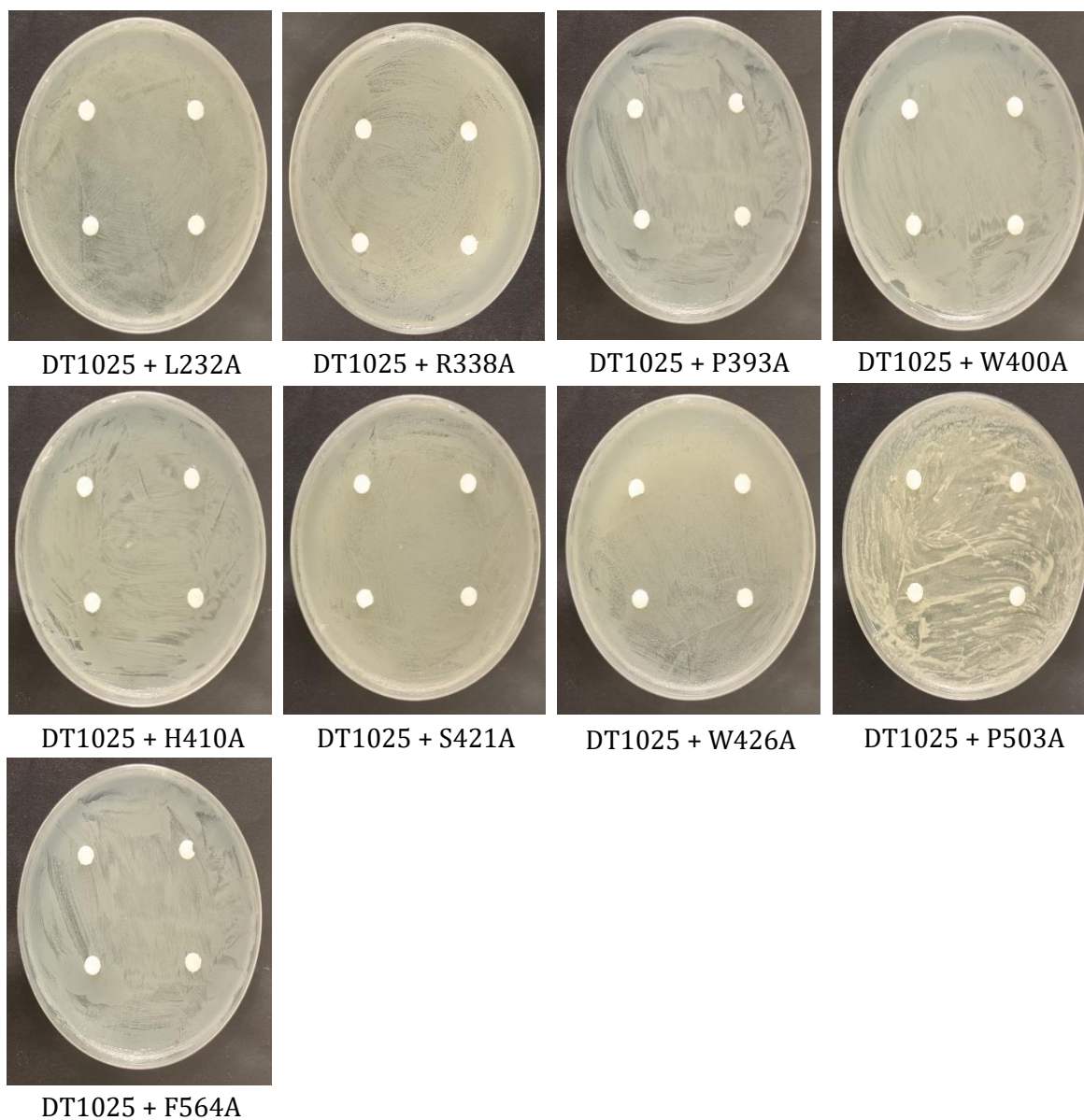


Figure 5.7: DT1025 strains that are not complemented with an active *pmt* allele exhibit increased susceptibility to antibiotic insult. *S. coelicolor* DT1025 spores were plated out on DN agar and 4 μ g of meropenem (top left), 40 μ g vancomycin (top right), 80 μ g ampicillin (bottom left) and 4 μ g imipenem (bottom right) were added to each disc. The plates were then incubated at 30 °C for 48 hours. Images are representative of 4 biological replicates.

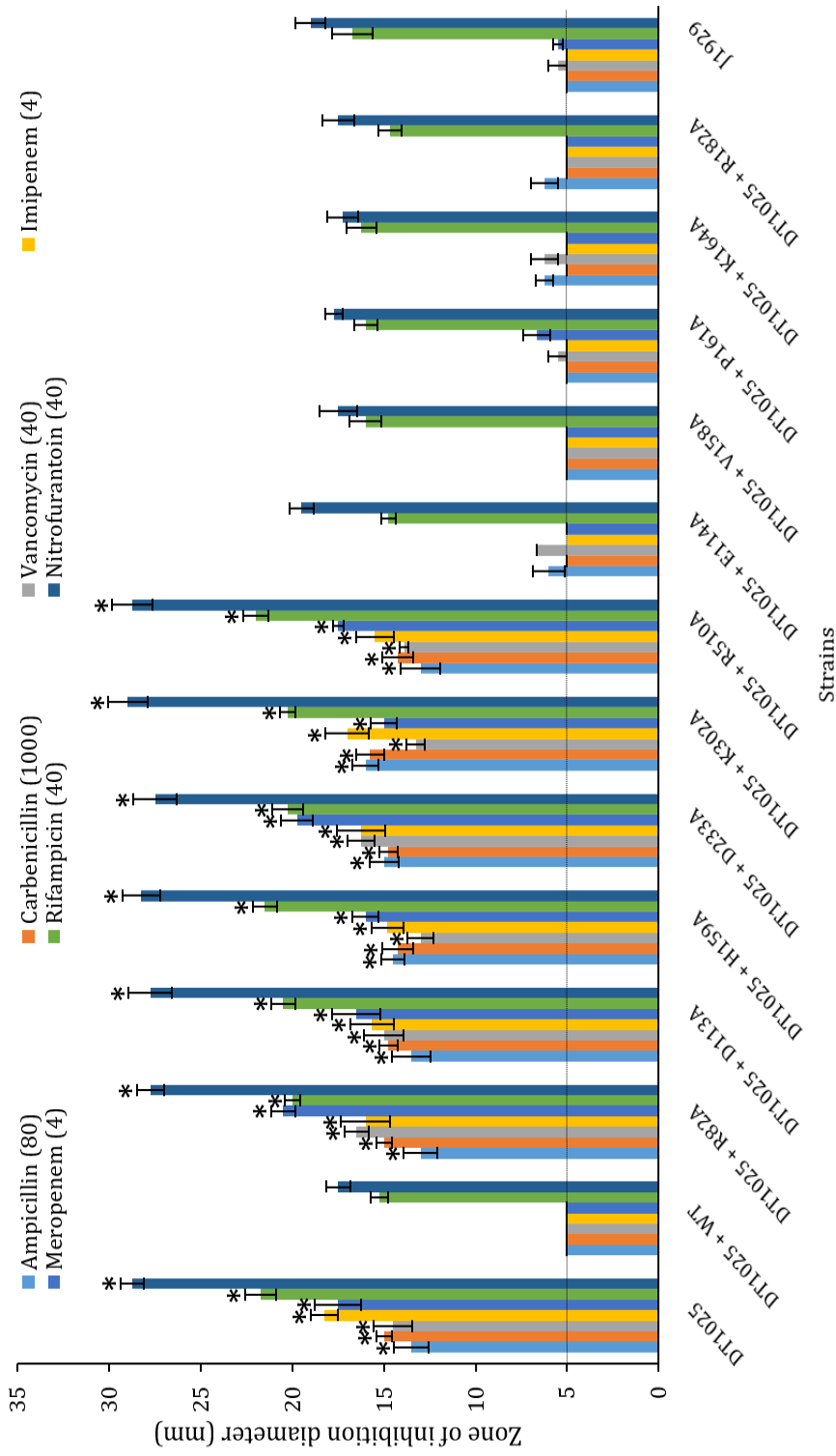


Figure 5.8: Non-complemented DT1025 strains show significant increases in sensitivity to cell wall/membrane targeting antibiotics, nitrofurantoin and rifampicin. Antibiotic sensitivity was quantified by measuring the zone of inhibition diameter for the DT1025 strains with WT *pmt* control, no *pmt* mutant and the *pmt* mutants. Strains were plated on DN agar and incubated at 30 °C for 48 hours. Shown are the averages of 4 biological replicates with SEM. The paper used to administer each antibiotic has a diameter of 5 mm and is shown as the dotted line threshold. The amount of antibiotic used in µg is shown in brackets in the legend.

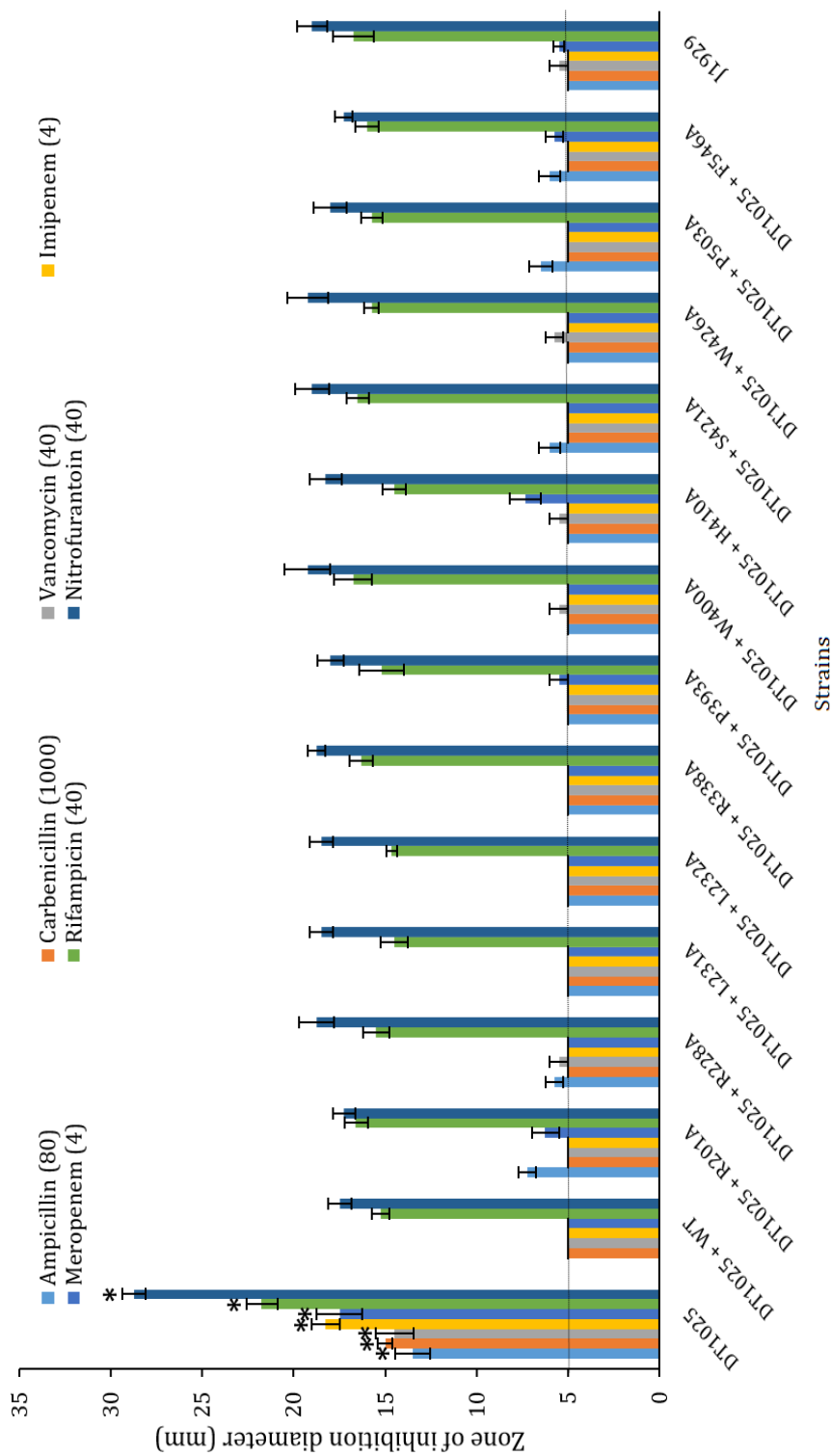


Figure 5.9: Complemented DT1025 strains show no significant increases in sensitivity to cell wall/membrane targeting antibiotics, nitrofurantoin and rifampicin. Antibiotic sensitivity was quantified by measuring the zone of inhibition diameter for the DT1025 strains with WT *pmt* control, no *pmt* control and the *pmt* mutants. Strains were plated on DN agar and incubated at 30 °C for 48 hours. Shown are the averages of 4 biological replicates with SEM. The paper used to administer each antibiotic has a diameter of 5 mm and is shown as the dotted line threshold. The amount of antibiotic used in µg is shown in brackets in the legend.

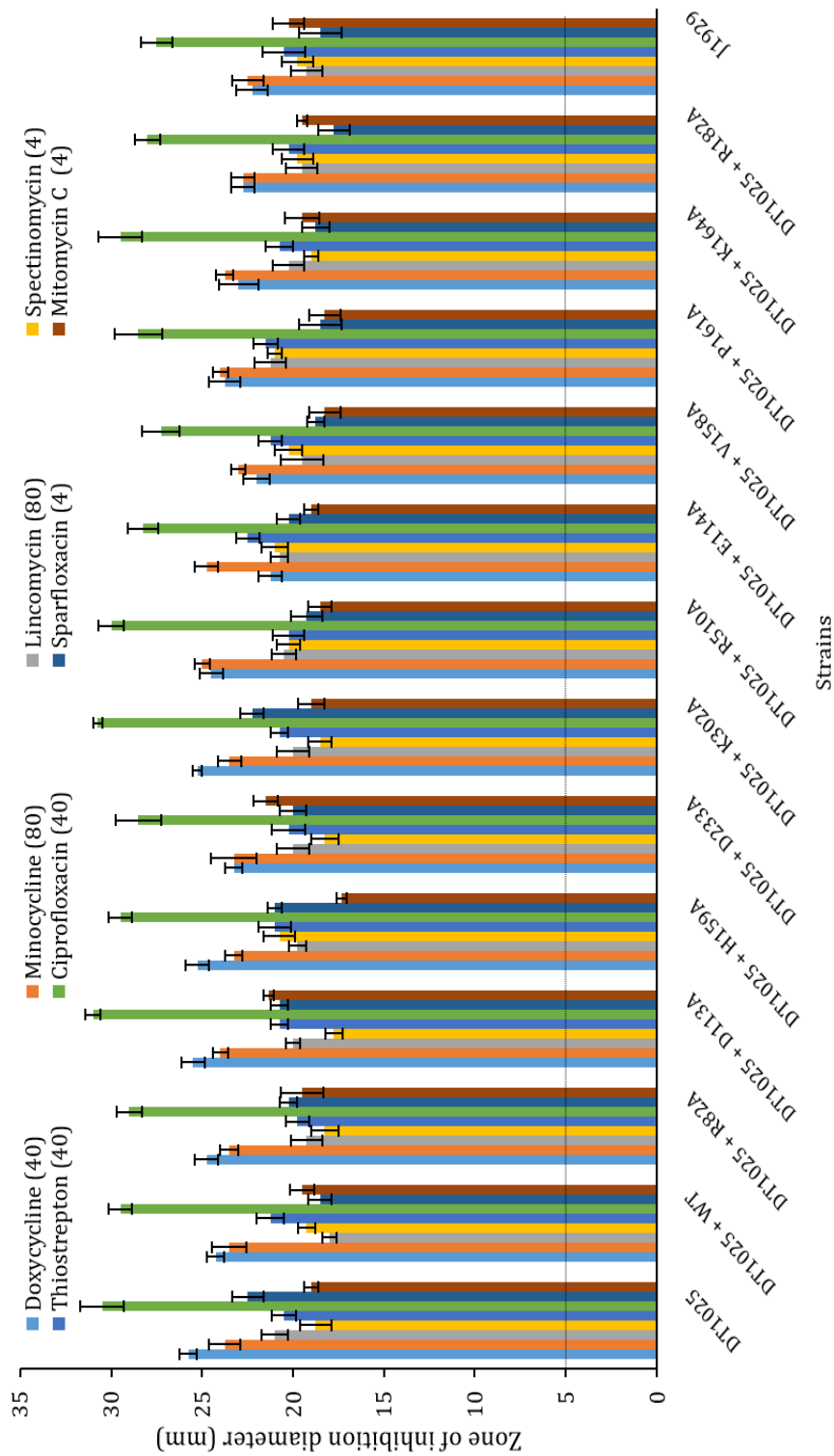


Figure 5.10: Complemented and non-complemented DT1025 strains show no significant increases in sensitivity to DNA replication and translation inhibitors. Antibiotic sensitivity was quantified by measuring the zone of inhibition diameter for the DT1025 strains with WT *pmt* control, no *pmt* control and the *pmt* mutants. Strains were plated on DN agar and incubated at 30 °C for 48 hours. Shown are the averages of 4 biological replicates with SEM. The paper used to administer each antibiotic has a diameter of 5 mm and is shown as the dotted line threshold. The amount of antibiotic used in µg is shown in brackets in the legend.

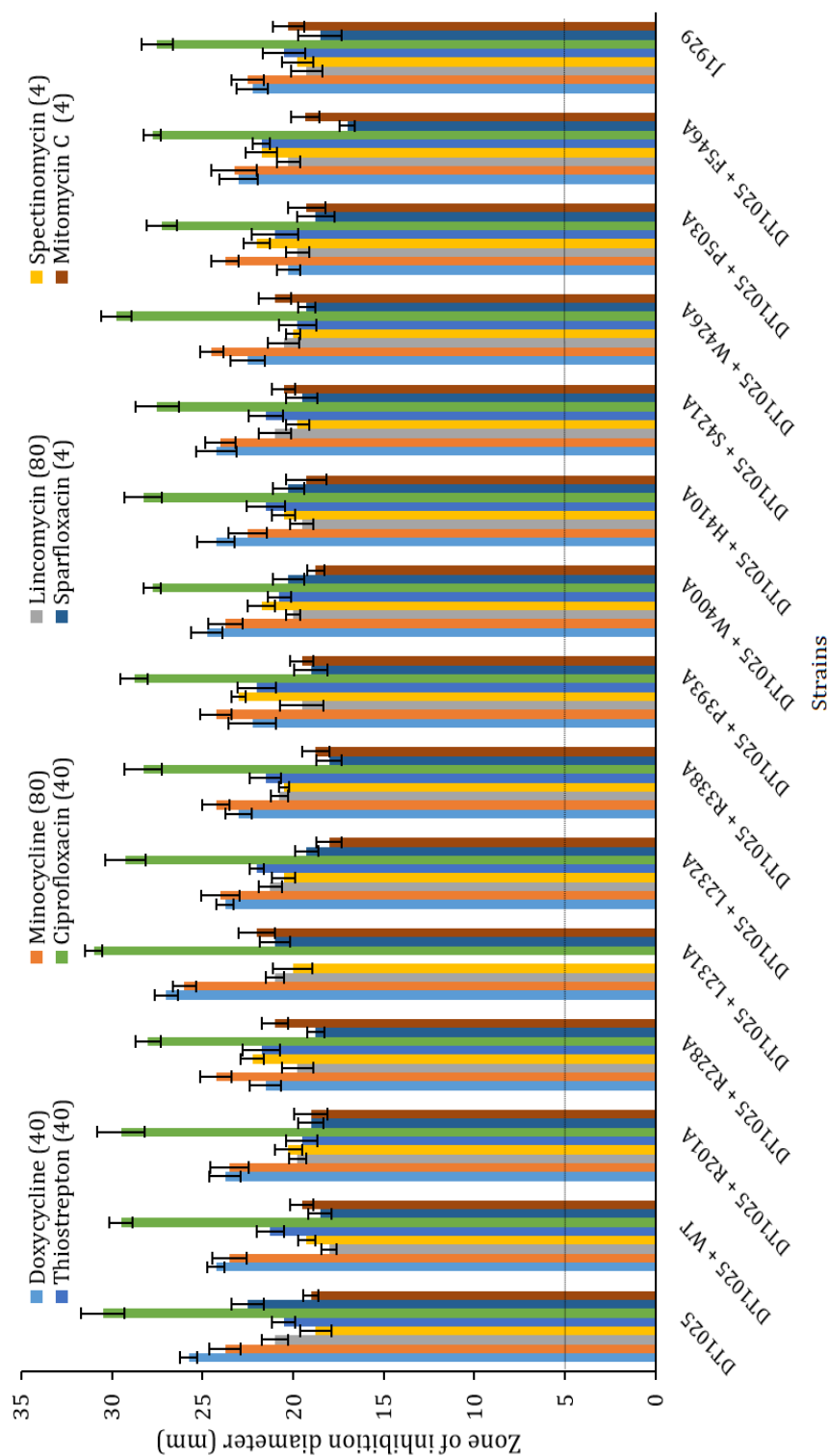


Figure 5.11: Complemented DT1025 strains show no significant increases in sensitivity to DNA replication and translation inhibitors. Antibiotic sensitivity was quantified by measuring the zone of inhibition diameter for the DT1025 strains with WT *pmt* control, no *pmt* control and the *pmt* mutants. Strains were plated on DN agar and incubated at 30 °C for 48 hours. Shown are the averages of 4 biological replicates with SEM. The paper used to administer each antibiotic has a diameter of 5 mm and is shown as the dotted line threshold. The amount of antibiotic used in μg is shown in brackets in the legend.

5.3.2 Complemented DT1025 are vulnerable to Φ C31 $c\Delta 25$ phage infection and exhibit increased growth rates

To further test the aforementioned strains, Φ C31 $c\Delta 25$ phage infection assays were performed (Figure 5.12 and Table 5.1). If integrity of the glycosylation cascade has been restored, the complemented strains should be vulnerable to infection by phage. As expected, the no gene negative control and the mutants that failed to alleviate the DT1025 antibiotic susceptible phenotype (R82A, D113, H159A, D233A, K302A and R510A) showed no evidence of infection within the phage dilution range tested. The WT positive control and the 17 complemented DT1025 strains that showed restored antibiotic susceptibility to that observed in the J1929 parent strain were vulnerable to phage infection, with countable plaques obtainable at a 10^{-6} phage stock dilution. The plaques obtained for the complemented strains were phenotypically comparable to the J1929 parent strain, typically large and clear. Clear plaques are a hallmark of infection by a lytic phage such as Φ C31 $c\Delta 25$ (Lomovskaya *et al.*, 1972). Introduction of the alleles in the J1929 parent strain had no effect on phage susceptibility (Table A8.3).

DT1025 possesses a small colony phenotype when grown on DN agar and SM agar, the strains complemented with WT and 17 complementing mutant alleles grew faster yielding large colonies consistent with J1929 (Figure 5.13). R82A, D113, H159A, D233A, K302A and R510A alleles failed to complement DT3017, as indicated by the small colony phenotype.

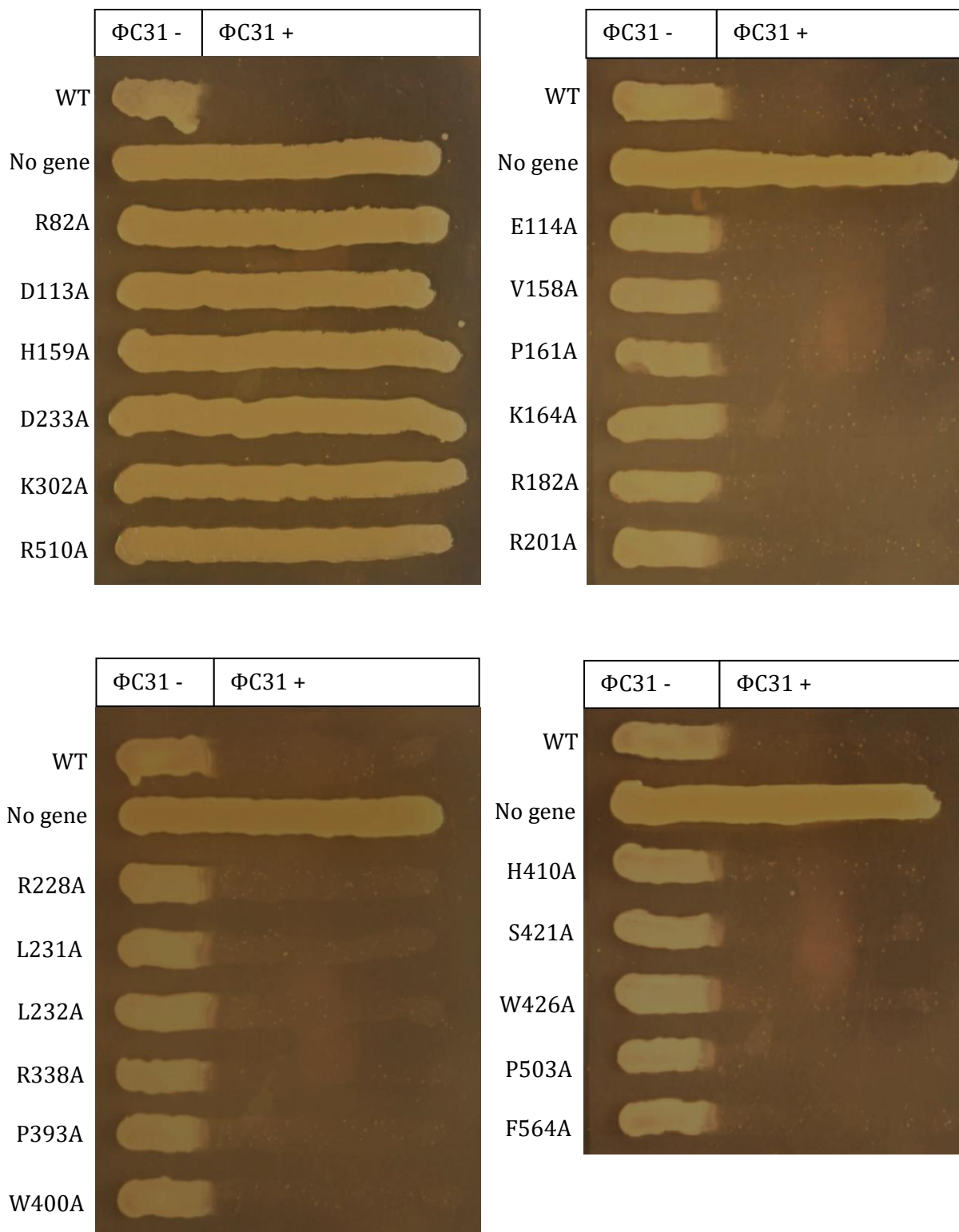
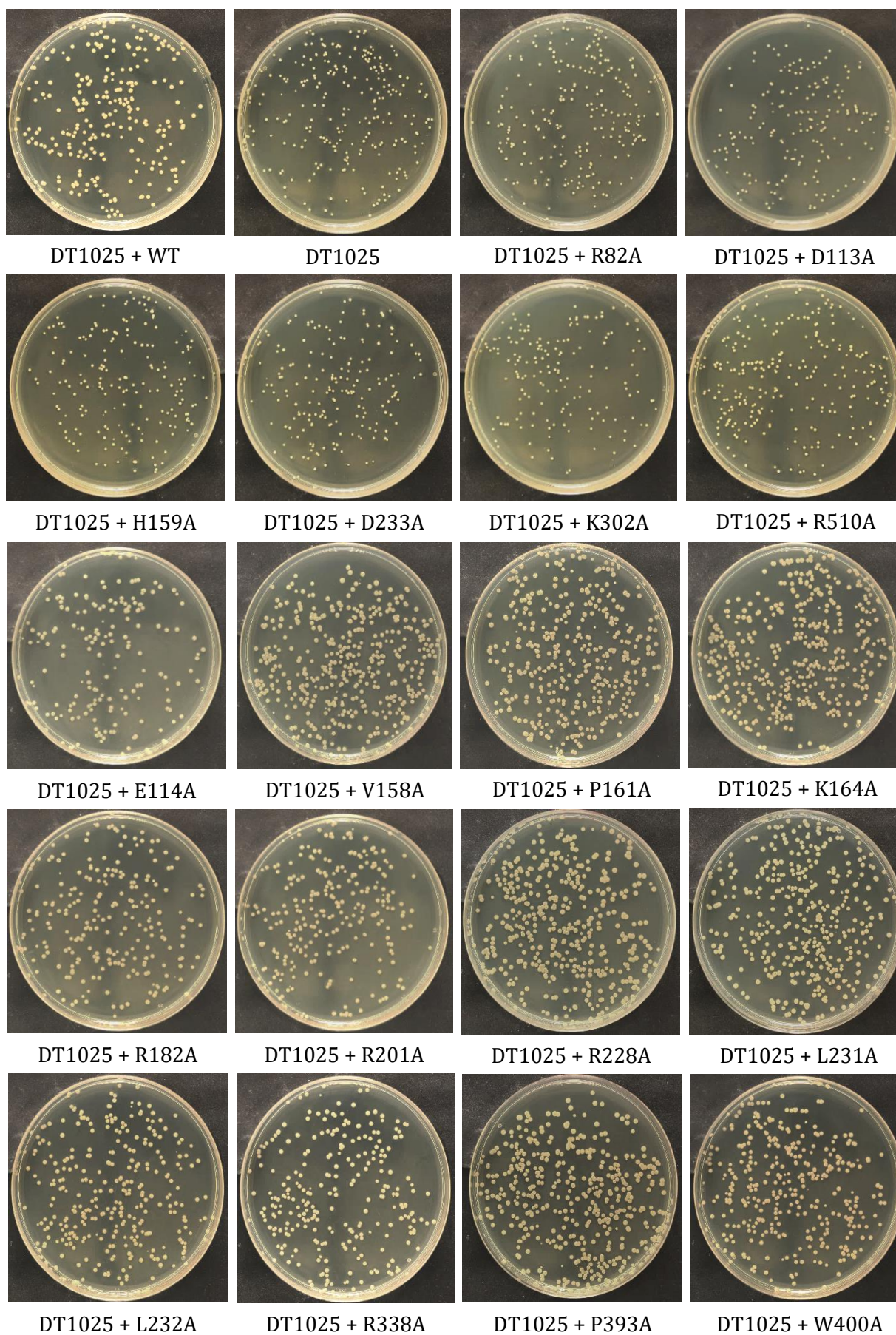


Figure 5.12: Complemented DT1025 strains are vulnerable to Φ C31 c Δ 25 phage infection. Phage were plated out on a portion of DN agar and then spores streaked from the phage absent region to the phage present region. Plates were incubated at 30 °C for 48 hours. Images are representative of 4 biological replicates.

Table 5.1: Complemented DT1025 strains are vulnerable to Φ C31 c Δ 25 phage infection.

Phage were plated out on DN agar and then SN agar containing spores was added to the top with the plates incubated at 30 °C for 18 hours. The average titre is shown \pm SEM from 4 biological replicates. 0.1 ml of a 10^{-6} phage stock dilution was used to obtain countable plaques for phage sensitive strains. Strains that showed no plaques at the lowest phage stock dilution tested (10^{-1}) are represented as having a PFU/ml $< 1 \times 10^2$.

Strain	Titre (PFU/ml)
DT1025	$< 1 \times 10^2$
DT1025 + WT	$(2.63 \pm 0.14) \times 10^8$
DT1025 + R82A	$< 1 \times 10^2$
DT1025 + D113A	$< 1 \times 10^2$
DT1025 + H159A	$< 1 \times 10^2$
DT1025 + D233A	$< 1 \times 10^2$
DT1025 + K302A	$< 1 \times 10^2$
DT1025 + R510A	$< 1 \times 10^2$
DT1025 + E114A	$(3.21 \pm 0.29) \times 10^8$
DT1025 + V158A	$(2.12 \pm 0.09) \times 10^8$
DT1025 + P161A	$(3.13 \pm 0.14) \times 10^8$
DT1025 + K164A	$(2.37 \pm 0.12) \times 10^8$
DT1025 + R182A	$(2.56 \pm 0.36) \times 10^8$
DT1025 + R201A	$(1.74 \pm 0.07) \times 10^8$
DT1025 + R228A	$(4.12 \pm 0.42) \times 10^8$
DT1025 + L231A	$(2.28 \pm 0.23) \times 10^8$
DT1025 + L232A	$(3.48 \pm 0.37) \times 10^8$
DT1025 + R338A	$(2.32 \pm 0.18) \times 10^8$
DT1025 + P393A	$(1.94 \pm 0.27) \times 10^8$
DT1025 + W400A	$(1.82 \pm 0.08) \times 10^8$
DT1025 + H410A	$(2.67 \pm 0.13) \times 10^8$
DT1025 + S421A	$(4.34 \pm 0.34) \times 10^8$
DT1025 + W426A	$(2.59 \pm 0.25) \times 10^8$
DT1025 + P503A	$(3.56 \pm 0.27) \times 10^8$
DT1025 + F564A	$(2.71 \pm 0.07) \times 10^8$



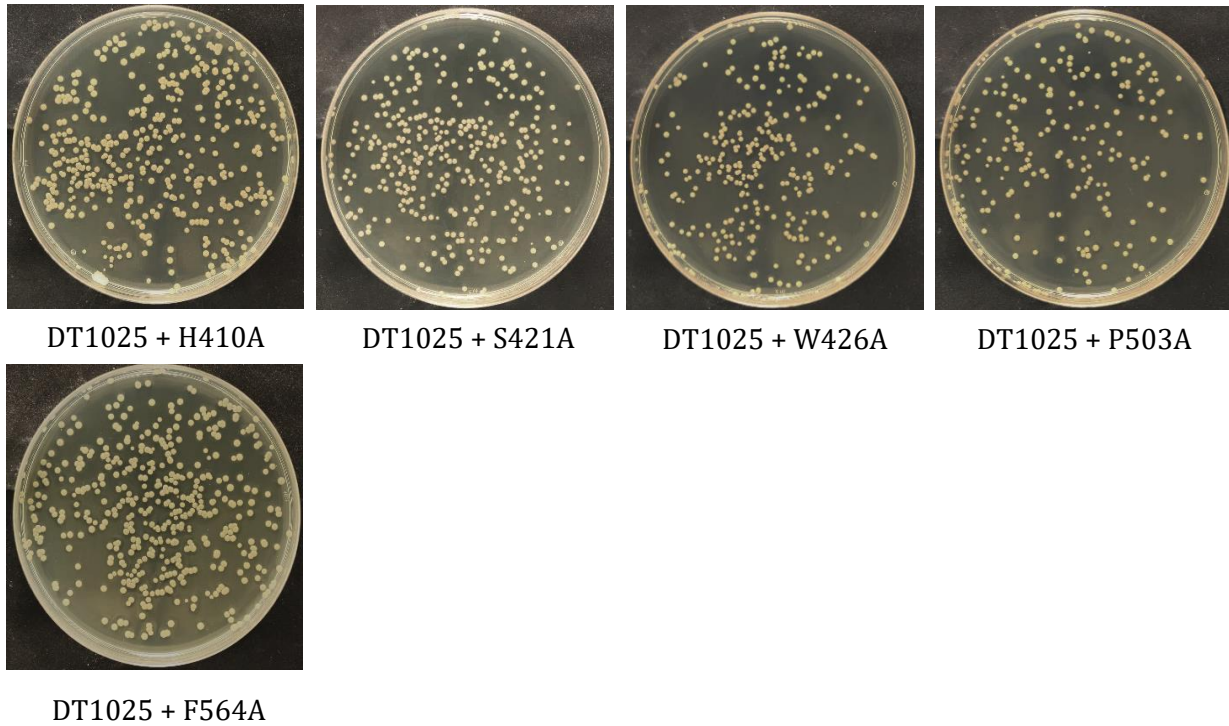


Figure 5.13: Non-complemented DT1025 strains show a small colony phenotype. Strains were grown on DN agar and incubated at 30 °C for 48 hours. Images are representative of 4 biological replicates.

5.3.3 Introduction of *pmt* mutants into DT2008

Only six of 23 mutant alleles complemented DT1025. Interestingly, alleles encoding PmtE114A and R182A were able to complement the *pmt* - mutation in DT1025. Residues homologous to these were noted to be important for activity in *S. cerevisiae* and *M. tuberculosis* Pmts (Lommel *et al.*, 2011; VanderVen *et al.*, 2005; Girrbach *et al.*, 2000). Based on this and the absence of intermediate antibiotic susceptibility profiles, the mutant alleles were introduced into another *pmt* - strain DT2008 and antibiotic disc diffusion assays carried out as described previously (Howlett *et al.*, 2018a). The antibiotic sensitivity profiles for the *pmt* - alleles in DT2008 strains were comparable with DT1025. The six mutant alleles that failed to complement DT1025, encoding Pmt: R82A, D113A, H159A, D233A, K302A and R510A, were also unable to complement DT2008. As observed previously, these strains showed significantly increased susceptibility to all cell wall and/or membrane targeting antibiotics tested, in addition to rifampicin and nitrofurantoin, when compared to the J1929 parent strain ($p < 0.05$) (Figure 5.14).

DT2008 strain containing the mutant *pmt* alleles were notably more susceptible to the cell wall and membrane inhibitors compared to J1929. The greatest susceptibility was to the carbapenems: imipenem and meropenem. As with DT1025, rifampicin also yielded the smallest increase in zone of inhibition for all six non-complemented strains compared to J1929. Rifampicin was therefore the least effective antibiotic for exploiting the antibiotic susceptibility phenotype. The WT and 17 remaining mutant alleles were able to complement DT2008, alleviating the antibiotic susceptible phenotype (figure 5.15), again all consistent with previous observations for DT1025. The antibiotic susceptibility of all complemented DT2008 strains was not significantly different to J1929 for any antibiotic tested ($p < 0.05$).

Neither the complemented or non-complemented DT2008 strains exhibited significantly increased susceptibility to antibiotics inhibiting DNA replication and translation when compared to the J1929 parent strain ($p < 0.05$), again mirroring the data previously obtained for DT1025 (Figures 5.16 and 5.17). The antibiotic susceptibility profiles of all 23 complemented and non-complemented strains in DT1025 and DT2008, was therefore comparable for all antibiotics tested, with only minor differences in antibiotic effectiveness ranking.

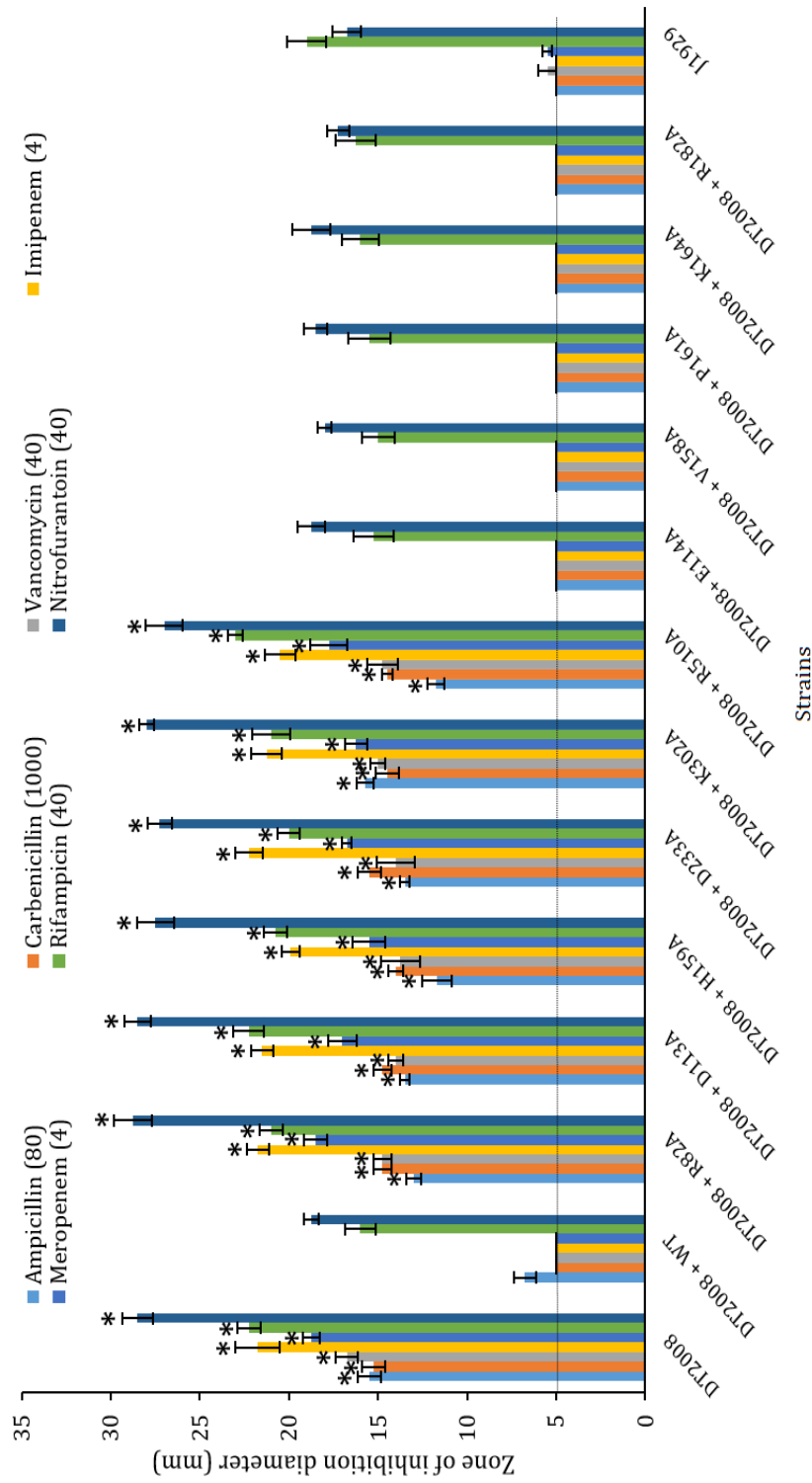


Figure 5.14: Non-complemented DT2008 strains show significant increases in sensitivity to cell wall/membrane targeting antibiotics, nitrofurantoin and rifampicin. Antibiotic sensitivity was quantified by measuring the zone of inhibition diameter for the DT2008 strains with WT *pmt* control, no *pmt* control and the *pmt* mutants. Strains were plated on DN agar and incubated at 30 °C for 48 hours. Shown are the averages of 4 biological replicates with SEM. The paper used to administer each antibiotic has a diameter of 5 mm and is shown as the dotted line threshold. The amount of antibiotic used in μg is shown in brackets in the legend.

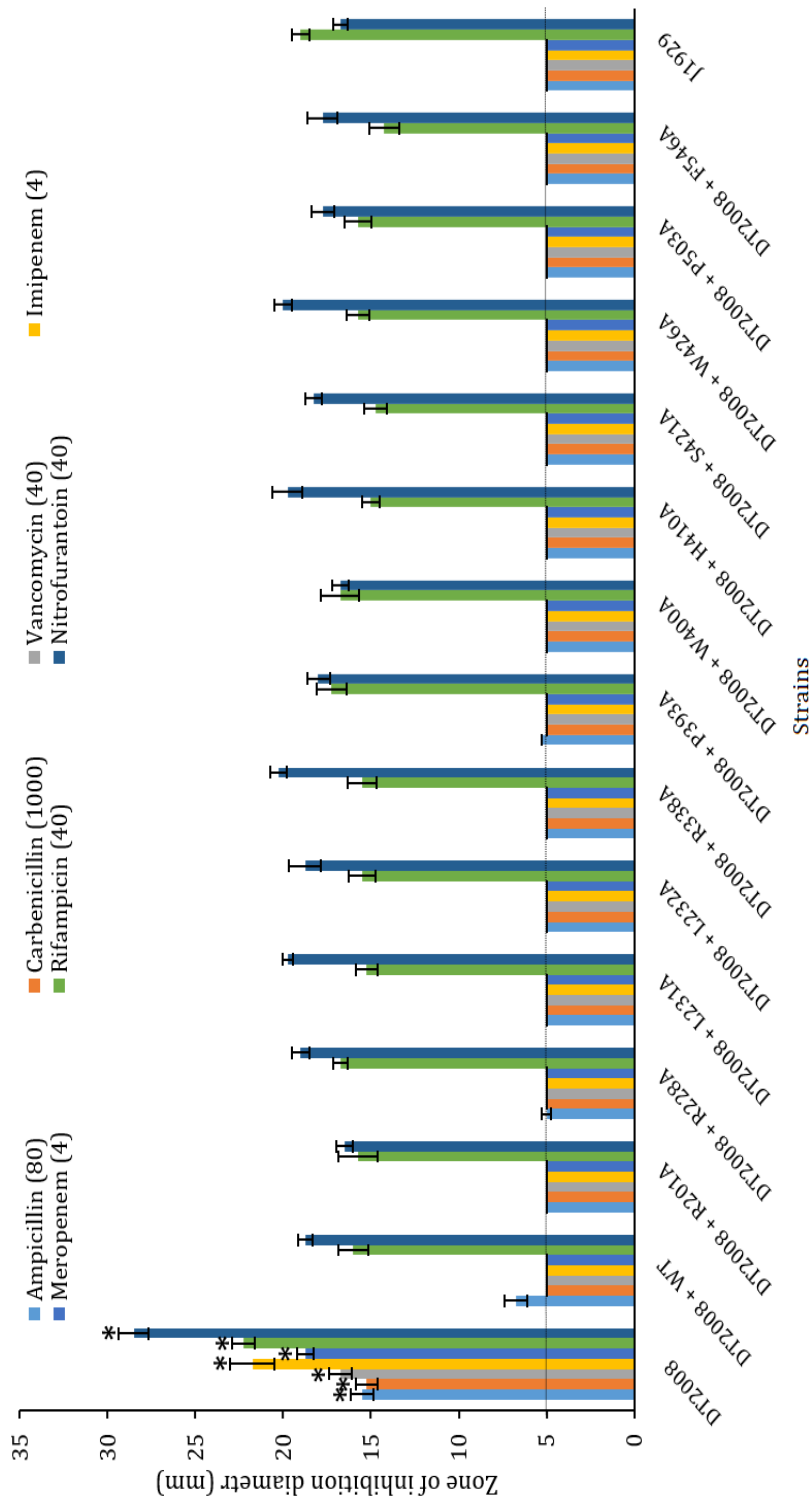


Figure 5.15: Complemented DT2008 strains show no significant increases in sensitivity to DNA replication and translation inhibitors. Antibiotic sensitivity was quantified by measuring the zone of inhibition diameter for the DT2008 strains with WT *pmt* control, no *pmt* control and the *pmt* mutants. Strains were plated on DN agar and incubated at 30 °C for 48 hours. Shown are the averages of 4 biological replicates with SEM. The paper used to administer each antibiotic has a diameter of 5 mm and is shown as the dotted line threshold. The amount of antibiotic used in μg is shown in brackets in the legend.

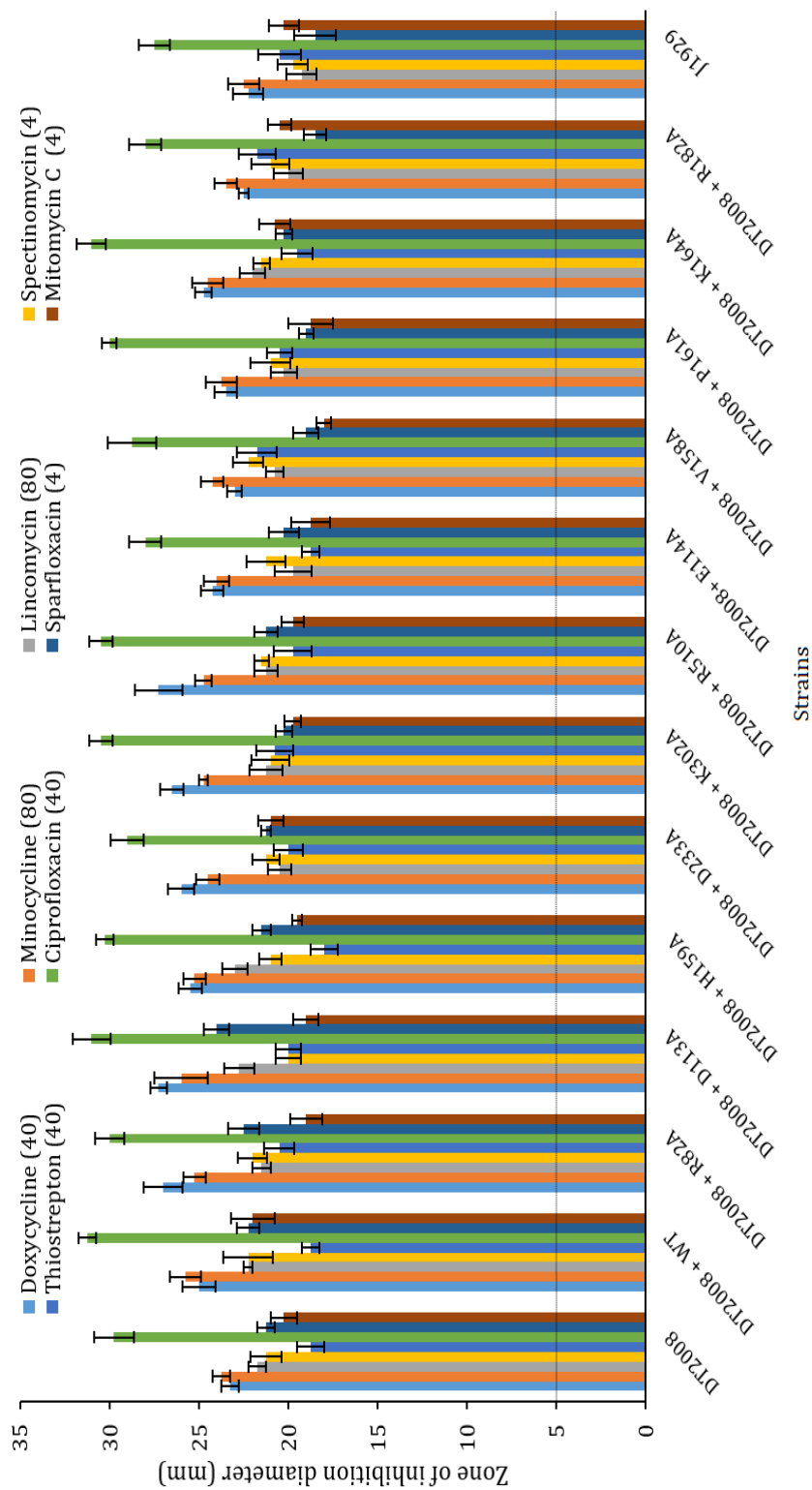


Figure 5.16: Complemented and non-complemented DT2008 strains show no significant increases in sensitivity to DNA replication and translation inhibitors. Antibiotic sensitivity was quantified by measuring the zone of inhibition diameter for the DT2008 strains with WT *pmt* control, no *pmt* control and the *pmt* mutants. Strains were plated on DN agar and incubated at 30 °C for 48 hours. Shown are the averages of 4 biological replicates with SEM. The paper used to administer each antibiotic has a diameter of 5 mm and is shown as the dotted line threshold. The amount of antibiotic used in µg is shown in brackets in the legend.

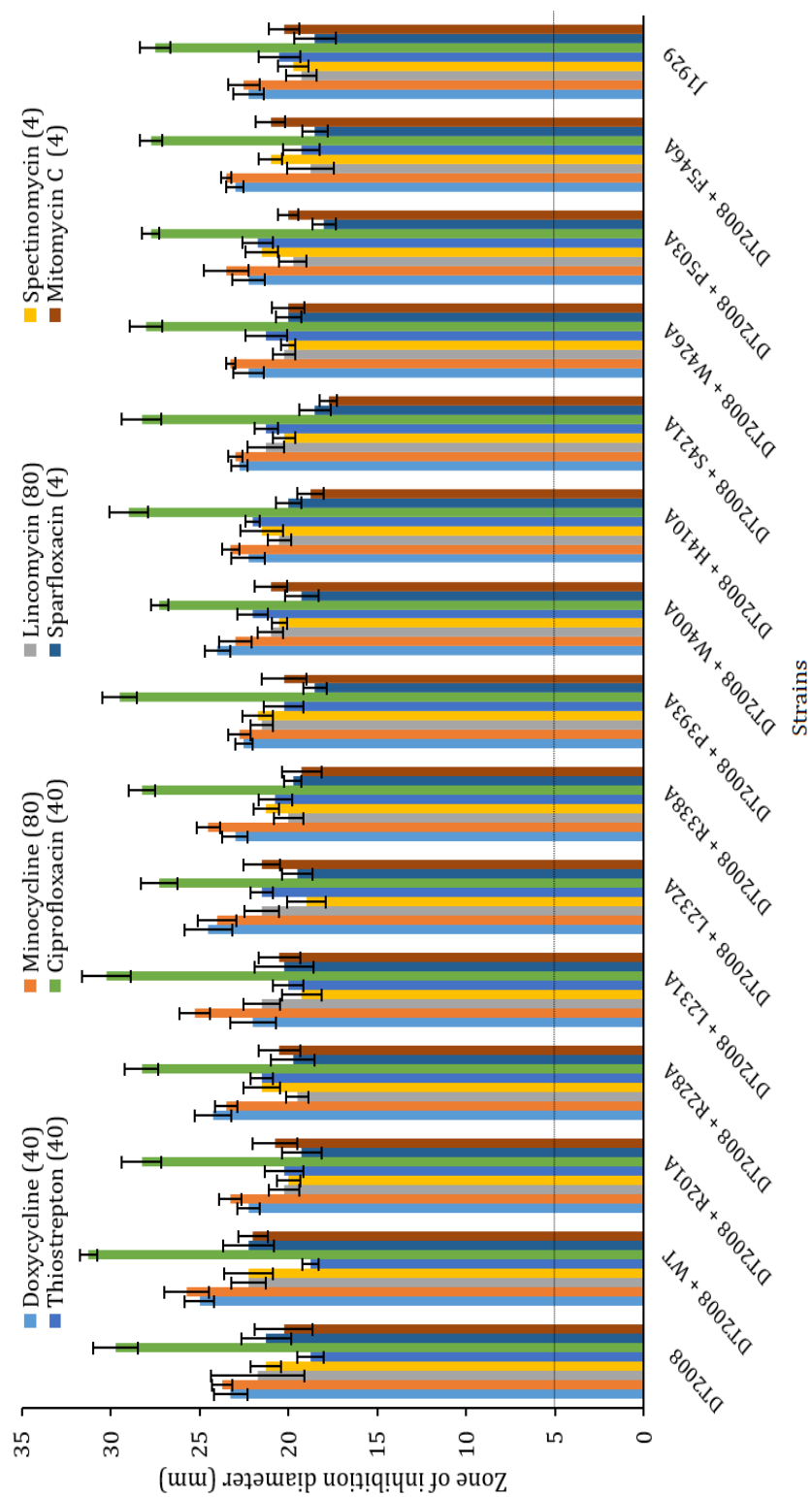


Figure 5.17: Complemented DT2008 strains show no significant increases in sensitivity to DNA replication and translation inhibitors. Antibiotic sensitivity was quantified by measuring the zone of inhibition diameter for the DT2008 strains with WT *pmt* control, no *pmt* control and the *pmt* mutants. Strains were plated on DN agar and incubated at 30 °C for 48 hours. Shown are the averages of 4 biological replicates with SEM. The paper used to administer each antibiotic has a diameter of 5 mm and is shown as the dotted line threshold. The amount of antibiotic used in μg is shown in brackets in the legend.

5.3.4 Complemented DT2008 are vulnerable to Φ C31 Δ 25 phage infection and exhibit increased growth rates

To further test the aforementioned strains, Φ C31 Δ 25 phage infection assays were performed (Figure 5.18 and table 5.2). If integrity of the glycosylation cascade has been restored, the complemented strains should be vulnerable to infection by phage.

As previously observed for DT1025, DT2008 containing the plasmid only (negative control) and the mutants that failed to complement the antibiotic susceptible phenotype (encoding *Pmt* R82A, D113, H159A, D233A, K302A and R510A) showed no evidence of infection within the phage dilution range tested. The DT1025 strains complemented with the WT positive control and the 17 mutants that restored the antibiotic susceptibility observed in the J1929 parent strain were vulnerable to phage infection, with countable plaques obtainable at a 10^{-6} phage stock dilution. The phage titres obtained for the complemented strains were in the same order of magnitude as those previously obtained for DT1025, with the plaques again large and clear.

The DT1025 strains complemented with WT and 17 complementing mutant alleles grew faster yielding large colonies consistent with J1929. *Pmt* alleles encoding R82A, D113, H159A, D233A, K302A and R510A that failed to complement DT2008 grew with the small colony phenotype resembling that for DT1025 and DT2008.

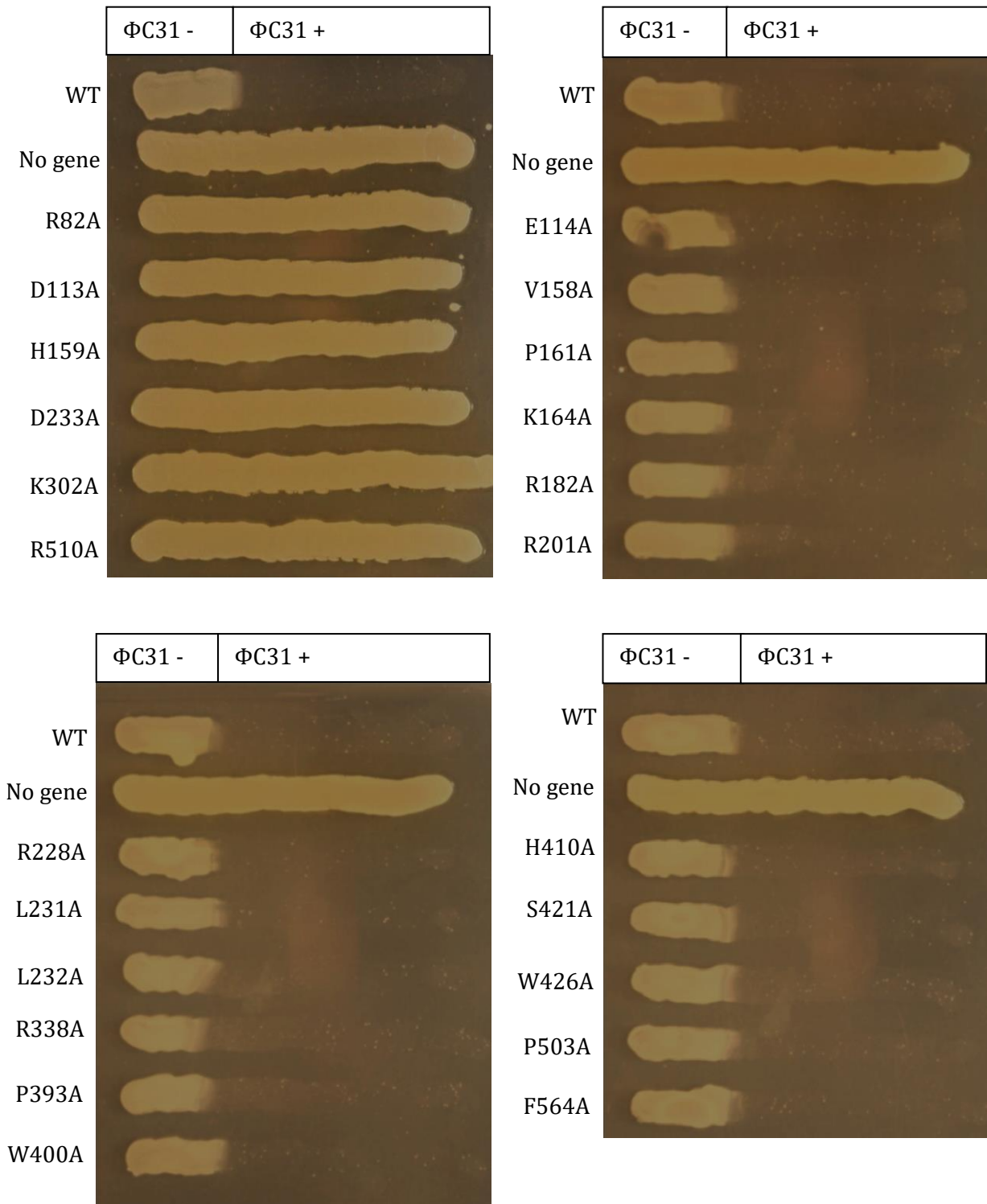


Figure 5.18: Complemented DT2008 strains are vulnerable to Φ C31 $c\Delta 25$ phage infection. Phage were plated out on a portion of DN agar and then spores streaked from the phage absent region to the phage present region. Plates were incubated at 30 °C for 48 hours.

Table 5.2: Complemented DT2008 strains are vulnerable to Φ C31 c Δ 25 phage infection.

Phage were plated out on DN agar and then SN agar containing spores was added to the top with the plates incubated at 30 °C for 18 hours. The average titre is shown \pm SEM from 4 biological replicates. 0.1 ml of a 10^{-6} phage stock dilution was used to obtain countable plaques for phage sensitive strains. Strains that showed no plaques at the lowest phage stock dilution tested (10^{-1}) are represented as having a PFU/ml $< 1 \times 10^2$.

Strain	Titre (PFU/ml)
DT2008	$< 1 \times 10^2$
DT2008 + WT	$(1.81 \pm 0.23) \times 10^8$
DT2008 + R82A	$< 1 \times 10^2$
DT2008 + D113A	$< 1 \times 10^2$
DT2008 + H159A	$< 1 \times 10^2$
DT2008 + D233A	$< 1 \times 10^2$
DT2008 + K302A	$< 1 \times 10^2$
DT2008 + R510A	$< 1 \times 10^2$
DT2008 + E114A	$(2.13 \pm 0.12) \times 10^8$
DT2008 + V158A	$(2.83 \pm 0.24) \times 10^8$
DT2008 + P161A	$(2.84 \pm 0.29) \times 10^8$
DT2008 + K164A	$(2.94 \pm 0.07) \times 10^8$
DT2008 + R182A	$(2.73 \pm 0.16) \times 10^8$
DT2008 + R201A	$(1.73 \pm 0.34) \times 10^8$
DT2008 + R228A	$(3.02 \pm 0.12) \times 10^8$
DT2008 + L231A	$(1.78 \pm 0.64) \times 10^8$
DT2008 + L232A	$(2.56 \pm 0.11) \times 10^8$
DT2008 + R338A	$(1.84 \pm 0.38) \times 10^8$
DT2008 + P393A	$(2.62 \pm 0.43) \times 10^8$
DT2008 + W400A	$(2.69 \pm 0.09) \times 10^8$
DT2008 + H410A	$(1.95 \pm 0.34) \times 10^8$
DT2008 + S421A	$(2.23 \pm 0.08) \times 10^8$
DT2008 + W426A	$(2.66 \pm 0.20) \times 10^8$
DT2008 + P503A	$(2.31 \pm 0.39) \times 10^8$
DT2008 + F564A	$(3.21 \pm 0.42) \times 10^8$

5.4 Pmt mechanistic model

Five of the six alleles that failed to complement the *pmt*⁻ strains DT1025 and DT2008 encoded changes in residues that are putatively located in the periplasmic loop domains and are in close proximity to each other in the *in silico* model of Pmt (Figure 5.19). The side chains of D113, D233, K302 and H159 are predicted to point towards each other, in what is likely to be the active site, since D113 is part of the catalytic DE motif of GT-C fold glycosyl transferases. Interestingly, the R510 side chain is predicted to be pointing away from this region. When the undecaprenyl phosphate substrate derived from the *C. metallidurans* ArnT template is docked into the *S. coelicolor* Pmt model, the phosphate head group sits comfortably between D113, D233, K302 and H159 (Figure 5.19).

It is necessary to assign direct roles to these residues (Figure 5.20). In the *S. coelicolor* Pmt model K302 is pointing towards D233, K302 may therefore form a salt bridge interaction to help position D233. Divalent cations have been shown to be important for function in multiple GT-C fold enzymes. D233 will be positioned to coordinate the divalent cation, a likely role for the cation is to help orientate the glycosidic bond linking polyprenol phosphate to mannose. Assuming the negative charge of D223 is involved in a salt bridge interaction with K302, only the negative charge on D113 would be available to act as the nucleophile. This nucleophile will deprotonate a hydroxyl on the acceptor serine or threonine, yielding a more powerful nucleophile that will attack the anomeric carbon on the mannose. Since the corresponding residue of H159 in *C. metallidurans* is involved in positioning the donor phosphate, it is possible it has the same function in *S. coelicolor*. This is further supported by the close proximity of H159 to the undecaprenyl phosphate docked into the model. The side chain of R510 is orientated away from the predicted active site in the model, making it difficult to assign a role. It could be involved in forming a salt bridge interaction with another critical acidic residue, an alternate role could be to interact with the main chain of the acceptor serine or threonine residue.

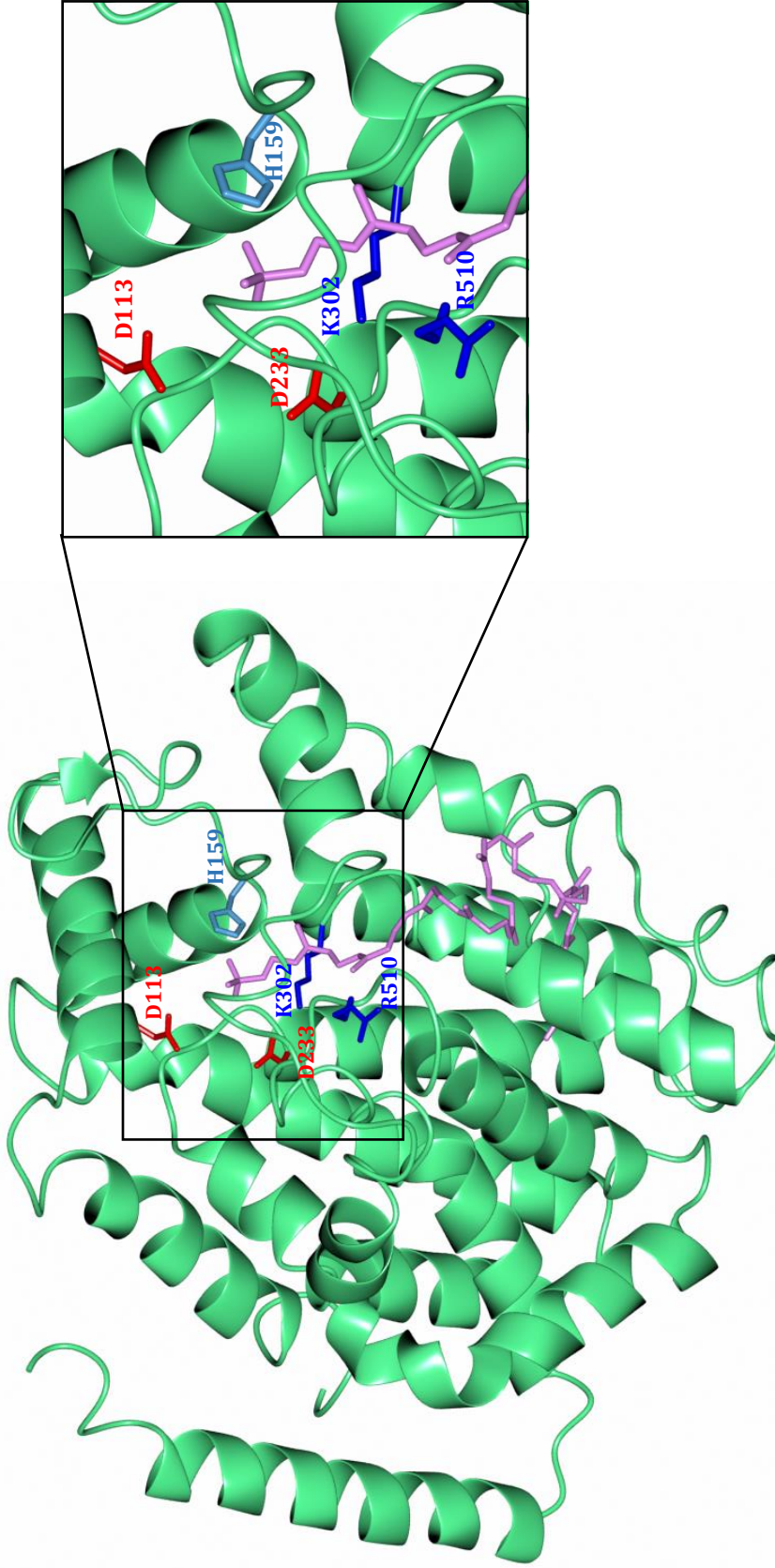


Figure 5.19: *S. coelicolor* Pmt homology model exhibits typical facets of GT-A fold glycosyl transferase. The model is based on the template ArnT (5F15), a GT-C fold glycosyl transferase from *C. metallidurans*. All residues targeted for mutation are represented as cylinders and coloured according to their type: amide (light blue), basic (dark blue) and acidic (red). The template derived undecaprenyl phosphate mannose is coloured pink.

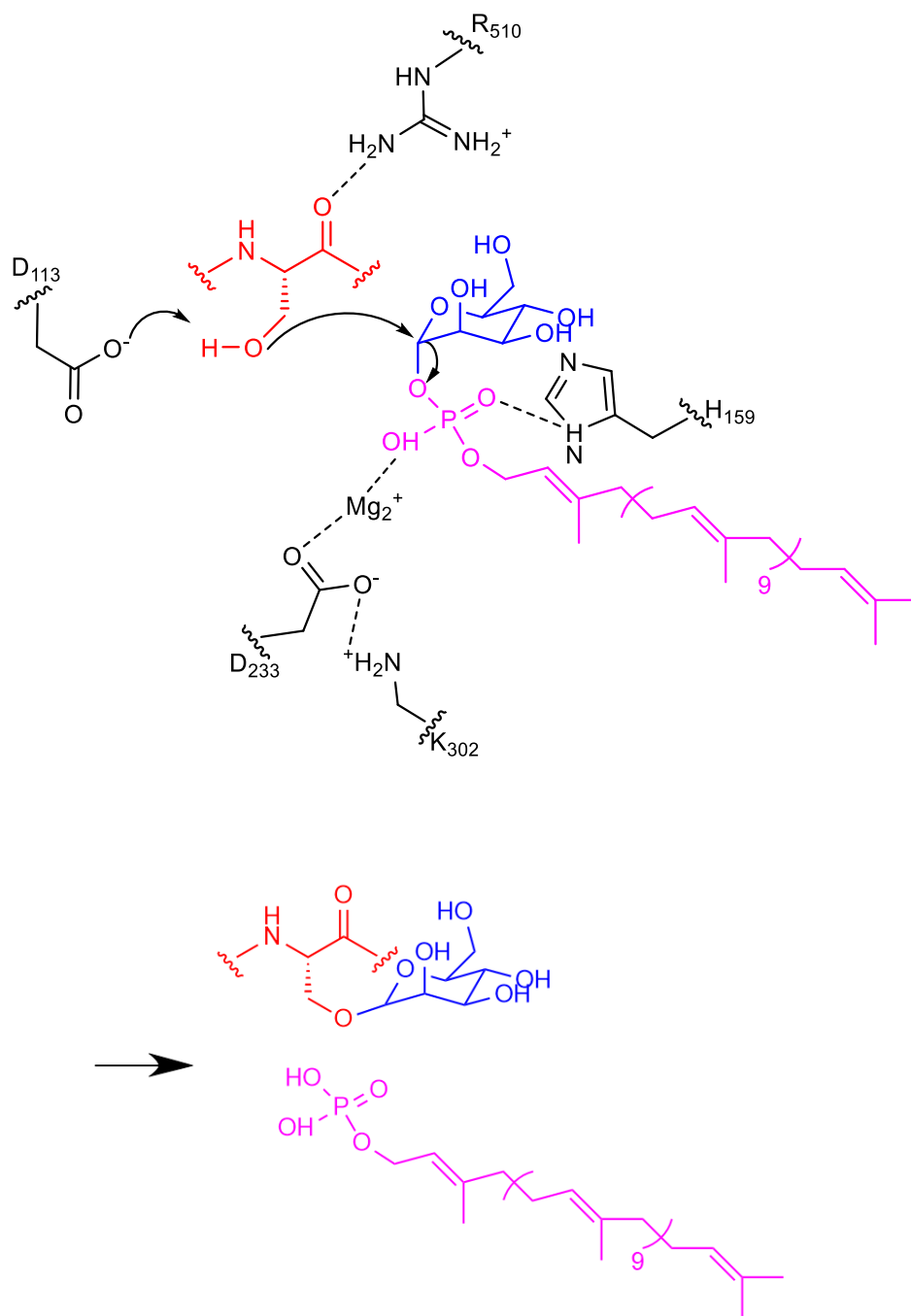


Figure 5.20: Proposed mechanism for Pmt, an inverting glycosyl transferase that utilises a single step SN₂ mechanism. Nucleophilic attack by an acceptor serine or threonine yields mannosylated protein and liberated polyprenol phosphate. D233 both coordinate the phosphate group of the donor via a divalent metal cation. D113 activates a serine or threonine hydroxyl for nucleophilic attack of the C1 mannose, while D233 is fixed in position with K302 through a salt bridge. H116 helps position the phosphate while R510 interacts with the main chain of the serine or threonine residue. Amino acids/divalent cation, polyprenol phosphate, mannose and protein are coloured black, magenta, blue and red respectively.

5.5 Discussion

5.5.1 Overview of key findings

In the study conducted by Howlett *et al.*, (2018a) both the *S. coelicolor pmt* - strains DT1025 and DT2008 had mildly increased susceptibilities to β -lactams and vancomycin. These increases in susceptibility were not as extreme as those obtained for *ppm1* -, *manB* - or *manC* - strains, however the growth retarded phenotypes and Φ C31 Δ 25 phage resistance phenotypes were consistent across all strains (Howlett *et al.*, 2018b; Wehmeier *et al.*, 2009; Cowlshaw and Smith 2001; Cowlshaw and Smith 2002). Based on the severity of the *ppm1* - phenotype (for antibiotic susceptibility), it was considered a more appealing target for novel antimicrobials to be used in conjunction with the existing arsenal of antibiotics. Following the Ppm1 mutant analysis described in Chapter 4, the next logical step was to carry out a site directed mutagenesis study of Pmt. The majority of published mutagenesis data in the literature concerns the catalytically conserved DE motif, a hallmark of the GT-C family of glycosyl transferases (Lairson *et al.*, 2008). In this study six critical residues for Pmt function were identified, the majority of these have not been previously mutagenised in a protein O-mannosyl transferase. Roles for these critical residues have been defined and several have been further supported by the recently published structures of GT-C fold glycosyl transferases including *C. metallidurans* ArnT (PDB: 5F15) and the *S. cerevisiae* Pmt1-Pmt2 complex (PDB: 6P25) (Petrou *et al.*, 2016; Bai *et al.*, 2019). The structure of the *S. cerevisiae* Pmt1-Pmt2 complex represents a significant breakthrough in our understanding of glycosyl transferases. Its structure was published following the conclusion of the work described in this Chapter.

Using literature searches and sequence alignments, 23 residues of interest were identified and substituted to alanine. The alleles were introduced into the *pmt* - *S. coelicolor* strains DT1025 and DT2008. Antibiotic susceptibility testing showed that alleles encoding PmtR82A, PmtD113A, PmtH159A, PmtD233A, PmtK302A and PmtR510A failed to complement both *pmt* - strains. The strains therefore had increased antibiotic susceptibility to β -lactams and vancomycin, in addition to growth retarded phenotypes and resistance to Φ C31 Δ 25 infection. These observations for the non-complemented DT1025 and DT2008 strains were consistent with the published literature (Howlett *et al.*, 2018a; Wehmeier *et al.*, 2009; Cowlshaw and Smith 2001; Cowlshaw and Smith 2002). Furthermore, the Ppm1 mutants (D57A and G143V) exhibited intermediate antibiotic hyper susceptibility, indicative of partial complementation, more recently this phenomenon was documented in a recent glycoproteomics study (Keenan *et al.*, 2019). No such partial complementation phenotypes were obtained in this Pmt studies presented here; DT1025 and DT2008 strains were either fully complemented and had

antibiotic/phage susceptibilities, in addition to colony phenotypes that resembled the J1929 strain, or were not complemented and retained the null mutant phenotypes.

Many of the antibiotics tested in this study were previously used by Howlett *et al.*, (2018a) to characterise *ppm1* - and *pmt* - strains. The reported mildly increased susceptibilities of *pmt* - strains to β -lactam antibiotics and vancomycin (in comparison to greatly increased susceptibility in *ppm1* - strains) was also observed in this study for the six mutants that failed to complement. Where the amount of antibiotic used in this study was consistent with that used by Howlett *et al.*, (2018a), the magnitude of increase in sensitivity was comparable. The consistency in antibiotic sensitivities of non-complemented and complemented *pmt* - strains in this study to the values reported in previous studies (Howlett *et al.*, 2018a; Keenan *et al.*, 2019) gives greater confidence in the robustness of the antibiotic hyper susceptibility assay, and indicates that the phenotypes are unlikely to be either under or overestimated. As expected, the mildly increased susceptibilities to antibiotics for the non-complemented *pmt* - strains was also lower than those reported for *ppm1* - *manB* - and *manC* - strains (Howlett *et al.*, 2018a; Howlett *et al.*, 2018b). Statistically significant increases in sensitivity to cell wall inhibitors was routinely observed for the non-complemented strains (relative to J1929), this combined with minimal variation (shown by consistently small SEM error bars) gave greater confidence in the data obtained.

Interestingly, the non-complemented DT1025 and DT2008 strains did not exhibit significantly increased susceptibility to antibiotics targeting DNA replication or translation (relative to J1929). This contrasts with the mildly increased susceptibilities of non-complemented DT3017 strains to these antibiotics, as discussed in Chapter 4. Nevertheless, significant increases in sensitivity to cell wall targeting antibiotics has been routinely observed for *ppm1* - and *pmt* - strains and this requires further discussion. A possible explanation for the elevated susceptibility to antibiotics targeting the cell wall, is provided by the recent in-depth characterisation of the *S. coelicolor* membrane glycoproteome (Keenan *et al.*, 2019). Using glycoproteome enrichment by lectin affinity chromatography followed by mass spectrometry, 95 glycopeptides were characterised from 38 glycoproteins (37 of which were newly identified). At least seven of the 38 glycoproteins have predicted roles in cell wall biosynthesis. SCO4847 (D-Ala-D-Ala carboxypeptidase) and SCO4934 (L,D transpeptidase) were each characterised in detail and *S. coelicolor* knock out mutants for both genes (*S. coelicolor* TK006 and TK008 respectively) were made. There was no change in colony morphology or phage susceptibility, the latter observation is interesting as it indicated that neither SCO4847 or SCO4934 acts as the ϕ C31 receptor. Of greater relevance to this work, the strains show increased susceptibility to β -lactams. It is therefore reasonable to assume that increased

susceptibility to antibiotics that exploit the cell wall, is due to impaired mannosylation of crucial proteins involved in cell wall synthesis and integrity. The likely result of this would be increased susceptibility to antibiotics that exploit the cell wall as their target. As expected the six non-complemented DT1025 strains had higher susceptibilities to imipenem, meropenem and ampicillin than the TK006 and TK008 strains reported in the Keenan *et al.*, study (2019), while having comparable zones of clearance to the control DT1025 strain. The disc diffusion assays also showed that TK006 and TK008 could be partially complemented by the reintroduction of WT copies of SCO4847 and SCO4934 respectively.

Another interesting phenomenon is that unlike for the Ppm1 mutant study presented here, no evidence of reversion was obtained for DT1025 and DT2008 strains carrying the six non-functional alleles. This contrasts with the Ppm1 study where the *S. coelicolor* spore growth protocol had to be shortened, in order to minimise the emergence of revertent colonies which eventually outgrew the non-revertent colonies that retained the critical substitution. Reversion of *ppm1* and *pmt* alleles to the WT gene has been discussed in a study of vancomycin resistance in *S. coelicolor* (Read *et al.*, 2019). In the case of DT2008, the mutation that confers the null mutant phenotype remains unknown and sequencing attempts to elucidate the source of the phenotype during this study were ultimately unsuccessful. Consequently, it is difficult to speculate on the presence or absence of a template based DNA repair mechanism. The mutation that confers the null mutant phenotype of DT1025 is however known and is due to a premature stop codon insertion at residue position 390. In the case of the *ppm1* - strain DT3017, it was understood that the native locus allele could act as a template to repair the introduced mutation, resulting in reversion back to the J1929 parent strain phenotype. The only instance of this not being observed was when the introduced allele had the same mutation as the allele at the native site (E218V). Assuming a similar repair mechanism is in operation for DT1025, it would be expected that five of the six non complementing *pmt* alleles introduced into DT1025 (R82A, D113A, H159A, D233A and K302A) would revert back to the WT gene, since all WT codons preceding codon 390 exist in the native locus *pmt* allele. Consequently, only R510A would be expected to not be susceptible to reversion by this mechanism. The same integrase containing plasmid pIJ10257 was used to introduce the *ppm1* and *pmt* mutant alleles therefore the location of the integrated allele is also the same. Sequencing of the PCR amplified integrated alleles was routinely carried out to verify the presence of the expected substitution and ensure reversion had not taken place.

5.5.2 Defining the roles of the DE motif and the divalent metal

The structure of *C. metallidurans* aminoarabinose transferase (ArnT) published half way through the work presented here was used to help define roles for the six critical residues identified (PmtR82, PmtD113, PmtH159, PmtD233 and PmtK302). Even though ArnT uses a lipid (lipid A) rather than protein as the glycosyl acceptor, it was used as the template to develop a homology model of *S. coelicolor* Pmt due to its high sequence identity and similarity with Pmt.

An obvious mutagenesis target was the DE motif, a hallmark of the GT-C fold glycosyl transferases (Lairson *et al.*, 2008). In this study, both DE residues were individually substituted to alanine in *S. coelicolor* Pmt. The E114A mutant fully complemented the *pmt*- strains DT1025 and DT2008 but the D113A mutant did not. As previously mentioned, the majority of residue substitutions reported in the literature concern this motif and therefore requires a thorough discussion. In a recent paper, the DE motif in *S. cerevisiae* was targeted for mutation and interestingly, when D77 and E78 were substituted to alanine individually there were negligible differences in *in vivo* glycosylation, indicating that other Pmt complexes could be compensating (Lommel *et al.*, 2011). Indeed, the existence of eukaryotic Pmt complexes in the literature is well documented (Lommel *et al.*, 2011). *In vitro* glycosylation was hampered when E78 was substituted to alanine with more modest effects observed for D77 however, when both residues were substituted together, *in vivo* glycosylation was notably reduced (though not eliminated) and *in vitro* there was no detectable mannosyl transferase activity (Lommel *et al.*, 2011). It was also noted that DE motif substitutions did not prevent or reduce Pmt1p-Pmt2p heteromeric complex formation. These results can be compared with data on single residue substitution mutants in the DE motif of *M. tuberculosis* Pmt (VanderVen *et al.*, 2005). Here, the DE-AE substitution decreased activity to a much greater extent than DE-DA and interestingly, the DE-AA substitution failed to completely abolish catalytic activity in contrast to the findings for *S. cerevisiae* pmt1p (Lommel *et al.*, 2011; VanderVen *et al.*, 2005). Nevertheless, both studies point to the importance of the DE motif in catalysis. In another important paper, E78 in *S. cerevisiae* Pmt1p was substituted with alanine and catalytic activity was dramatically reduced *in vitro*, indicating an essential role in transferase activity (Girrbach *et al.*, 2000). The results obtained here support the idea that the aspartate in the DE motif likely has a critical role in catalysis, while the glutamate is not critical (VanderVen *et al.*, 2005). It is not clear why the DE motif glutamate appears to have a more critical role than the aspartate for *S. cerevisiae* Pmt activity. Another possible explanation for the ability of E114A to complement both DT1025 and DT2008, is simply a consequence of the antibiotic susceptibility phenotype being less severe than that obtained for *ppm1*⁻, *manB*⁻, and *manC*⁻ (Howlett *et al.*, 2018a; Howlett *et al.*, 2018b). Due to

this less severe increase, it may be that the antibiotic sensitivity assay is not sensitive enough to detect a partial complementation phenotype, which would presumably arise from a partially active mutant as described *in vitro* by VanderVen *et al.*, (2005) and *in vivo* by Keenan *et al.*, (2019). *C. metallidurans* D57 (*S. coelicolor* D113) was mutated in the study and a polymyxin B growth assay was used to monitor the *in vivo* consequences of mutation, a lack of lipid A glycosylation due to substitution of a critical residue would correlate with susceptibility to polymyxin. While the glutamate in the DE motif was not targeted for substitution, activity was eliminated following substitution of the aspartate by alanine (or even the conservative substitution to glutamate), indicating that strict conservation is necessary to maintain function. In the ArnT structure the aspartate is involved in coordinating the acceptor phosphate of lipid A. Based on this observation, we have hypothesised that D113 interacts with and activates the nucleophilic hydroxyl group of a serine or threonine on the acceptor protein, for attack on the C1 carbon of the mannose of the polyprenol phosphate mannose donor.

Since a divalent metal cation is known to be important for activity in Pmt family enzymes from yeast and the prokaryotes, we propose that the divalent cation also has an important role in *S. coelicolor* Pmt catalysis, where it will be retained within the active site. This contrasts with *C. metallidurans* where the divalent metal cation is released from the active site to make the lipid A cavity accessible for donor substrate binding. Clues to the role of the divalent cation in *S. coelicolor* Pmt are provided by other structures. In the recently published structure of the *Campylobacter lari* oligosaccharyltransferase PglB (Napiorkowska *et al.*, 2018) which carries out N-glycosylation, it was suggested that the divalent metal ion stabilises the pyrophosphate leaving group of the donor substrate. The divalent metal cation in Pmt could perform the same function and stabilise the phosphate head group of polyprenol phosphate before and after mannose transfer. D113 may therefore have an additional role in coordinating the metal ion so it remains in position to interact with the donor phosphate, though we have not defined this role in our mechanistic model.

Interestingly, in ArnT H267 (*S. coelicolor* H410), H265 (H408) and E85 (not conserved in *S. coelicolor*) are each critical for activity and important for coordinating a divalent cation (Zn^{2+}), which fixes a loop in position and consequently opens up the binding cavity for the donor substrate (Petrou *et al.*, 2016). H410 was mutated in our study but fully complemented both DT1025 and DT2008 without issue. The position of H410 in the *S. coelicolor* Pmt model is consistent with a role in divalent cation binding. The failure of this substitution to adversely impact Pmt activity could simply be due to one or more nearby residues compensating for the loss of H410.

S. coelicolor D113 (as part of the DE motif) was previously considered to constitute the acceptor binding site and would specifically activate the hydroxyl of a serine or threonine. The homologous residue in *S. cerevisiae* Pmt1 (D77) is proposed to function in the same way, based on its close proximity to the nucleophilic threonine on the peptide acceptor. Interestingly, in the Pmt1-Pmt2 structure, E78 (in the DE motif) forms a salt bridge with R138, this interaction is thought to direct D77 towards the acceptor residue. R138 is not conserved in *S. coelicolor* Pmt suggesting either that another nearby arginine forms a salt bridge with E114, or based on the activity of E114A mutants in vivo, there is an alternate mechanism by which D113 is orientated towards the acceptor serine/threonine in *S. coelicolor* Pmt that does not involve the DE motif glutamate. While the structure of *S. cerevisiae* Pmt1-Pmt2 has not clarified the role of the glutamate in the DE motif, it has supported the hypothesis that the aspartate plays a critical role in activating a serine/threonine nucleophile in the *S. coelicolor* Pmt catalysed reaction.

5.5.3 Defining the roles of H159, D233, K302 and R510

As well as D55 (D113), another aspartate (D158) in the *C. metallidurans* ArnT was critical for coordinating the phosphate head group of lipid A. This aspartate is not however conserved in *S. coelicolor* Pmt. In this study D233 in *S. coelicolor* Pmt residue was shown to play an important role. According to the homology model, D233 may well perform in *S. coelicolor* Pmt, the same role as D158 in *C. metallidurans* Pmt. Therefore, D233 may directly (or indirectly via the divalent cation) fix the phosphate in place so the bond between mannose and the phosphate in appropriate position for attack by a nucleophilic serine or threonine on the acceptor protein.

The *C. metallidurans* ArnT structure was also used to help define a role for K302. The corresponding residue in ArnT forms a salt bridge with D158 and likely has a role in helping to delocalise the charge on the aspartate (Petrou *et al.*, 2016). In our mechanistic model we suggest *S. coelicolor* K302 forms a salt bridge with D233, based on its position in the homology model.

It has proved difficult to propose a role for R510 in *S. coelicolor* Pmt based on the homology model, since it points away from the active site. Arginine (R58) in ArnT plays a similar role to K203 in *C. metallidurans* ArnT in charge delocalisation, however this residue is not conserved (Petrou *et al.*, 2016). Alternatively, the homology model of *S. coelicolor* Pmt may be misleading and instead of pointing away from active site, R510 may point inwards to contribute to the reaction chemistry.

The critical *S. coelicolor* Pmt residue H159 corresponds to K85 in *C. metallidurans* ArnT. When this residue is substituted to alanine, activity is completely eliminated (Petrou *et al.*, 2016). K85 is well positioned in ArnT to interact with the phosphate group of undecaprenyl phosphate.

Based on this observation, we propose a role for H116 in binding the phosphate of polyprenol phosphate in *S. coelicolor* Pmt.

Finally, R82 was identified as a critical residue in this study. There is no data concerning mutation of homologous residues in GT-C family enzymes. Out the six critical residues identified in this study, R82 alone is not located in the periplasmic globular domain. Instead it is located on the cytosolic face of the membrane. It may be involved in binding polyprenol phosphate mannose or flipping the donor substrate across the membrane, although this is purely speculative.

For *C. metallidurans* ArnT, a number of mutations were made to explore the role of hydrophobic residues that line the undecaprenyl amino arabinose binding pocket. None of these substitutions affected ArnT activity and the residues are not conserved in bacterial Pmts. In our study we substituted multiple hydrophobic residues conserved across Pmts in the prokaryotic/eukaryotic kingdoms including W400, L231, P393 to alanine. Based on the docking of the template derived undecaprenyl phosphate onto the *S. coelicolor* Pmt model, these residues are suitably positioned to engage in hydrophobic contacts with the donor. None of the substitutions yielded a non-complementing allele. This is not necessarily surprising, since multiple residues would be expected to form hydrophobic contacts with the isoprenoid chain of polyprenol phosphate. Consequently, multiple mutations would presumably have to be made simultaneously for deleterious effects on donor binding to be observed.

In the Girrbaach study (2000) several additional *S. cerevisiae* Pmt1p residues were substituted to alanine including R64, R138 and L408. All three residues were shown to be essential for activity. Furthermore, R138 was also shown to be essential for Pmt1p-Pmt2p dimerisation. *S. coelicolor* Pmt R182 (*S. cerevisiae* Pmt1p R138) was substituted to alanine in the present study and the mutant was active and complemented both DT1025 and DT2008. In the *S. coelicolor* Pmt homology model, R182 forms a putative salt bridge to E114 indicating that as in *S. cerevisiae* Pmt1 (REF), an ionic interaction may play a critical role in orientating the DE motif in *S. coelicolor* Pmt. However, the activity of the R182A mutant indicates that either this interaction does not take place, or is not important for activity of the enzyme.

5.5.4 Building an improved homology model for *S. coelicolor* Pmt

Recently and following the completion of this work, the first structure of a Pmt complex was published (Bai *et al.*, 2019). The *S. cerevisiae* Pmt1-Pmt2 complex was therefore used as a template to build a new model of *S. coelicolor* Pmt (Figure 5.21). It was hoped that by using a new template a more reliable model could be built allowing a more complete interpretation of the mutagenesis data. The new homology model consisted of 547 residues (92 %) modelled *at*

>90% confidence, compared with 477 residues (80 %) modelled at >90 % confidence for the previous model.

In the previous model, 8 of 11 predicted transmembrane helices corresponded to the TMHMM predictions, helices 3, 7 and 10 however deviated from the plot. The modelling of helix 3 is separated into two smaller helices, while for helices 7 and 10, roughly $\frac{1}{2}$ and $\frac{2}{3}$ of the residues were not modelled respectively. Interestingly, in the new model, helix 3 is again split into two smaller helices (3a and 3b), this helix 3 topology is seen in the structures of both *C. metallidurans* ArnT and *S. cerevisiae* Pmt1-Pmt2 and could be a hallmark of GT-C fold glycosyl transferases. Importantly, in the new model all residues predicted to constitute helices 7 and 10 are fully modelled. The resulting longer helices cover a greater portion of the predicted transmembrane space. Furthermore, helix 8 is orientated parallel to the other membrane spanning helices.

When considering the positions of residues substituted in the present work, the previous homology model had a number of shortfalls. In total 18 out of 23 residues were modelled, with positions that were in full agreement with the TMHMM plot. Of the remaining five residues, three (R201, P393 and W426) were modelled but their positions deviated from the TMHMM plot, while large stretches of the N and C termini, which included the residues R82 and F564 respectively, were not modelled at all. In the new model R82 and F564 have been modelled and their positions are in agreement with the TMHMM profile. In the new model, the positions of residues R201, P393 and W426 are consistent with the TMHMM profile. In the previous model P393 and W426 occupied the periplasmic poles of the connecting transmembrane spanning helices 7 and 8 respectively, while in the new model both residues occupy periplasmic loop domain 7. Finally, in the previous model, R201 was located on the membrane boundary separating the cytoplasmic pole of helix 2 and loop 3. R201 in the later model is in loop 3.

A clear difference between the old and new models is that in the latter, R510 is clearly orientated towards critical residues in the predicted active site. When considering the Pmt1-Pmt2 complex, R649 (*S. coelicolor* R510), it is orientated towards the phosphate of the donor substrate and can therefore be assumed to be a dolichol phosphate mannose binding residue. Based on the orientation of R510 in the new homology model and the known interaction of the homologous R649 with the donor substrate, we can revise the role of R510, the biochemical model has now been amended (Figures 5.22, 5.23) to reflect the more likely interaction of R510 with the polyprenol phosphate mannose donor, rather than the peptide mannose acceptor.

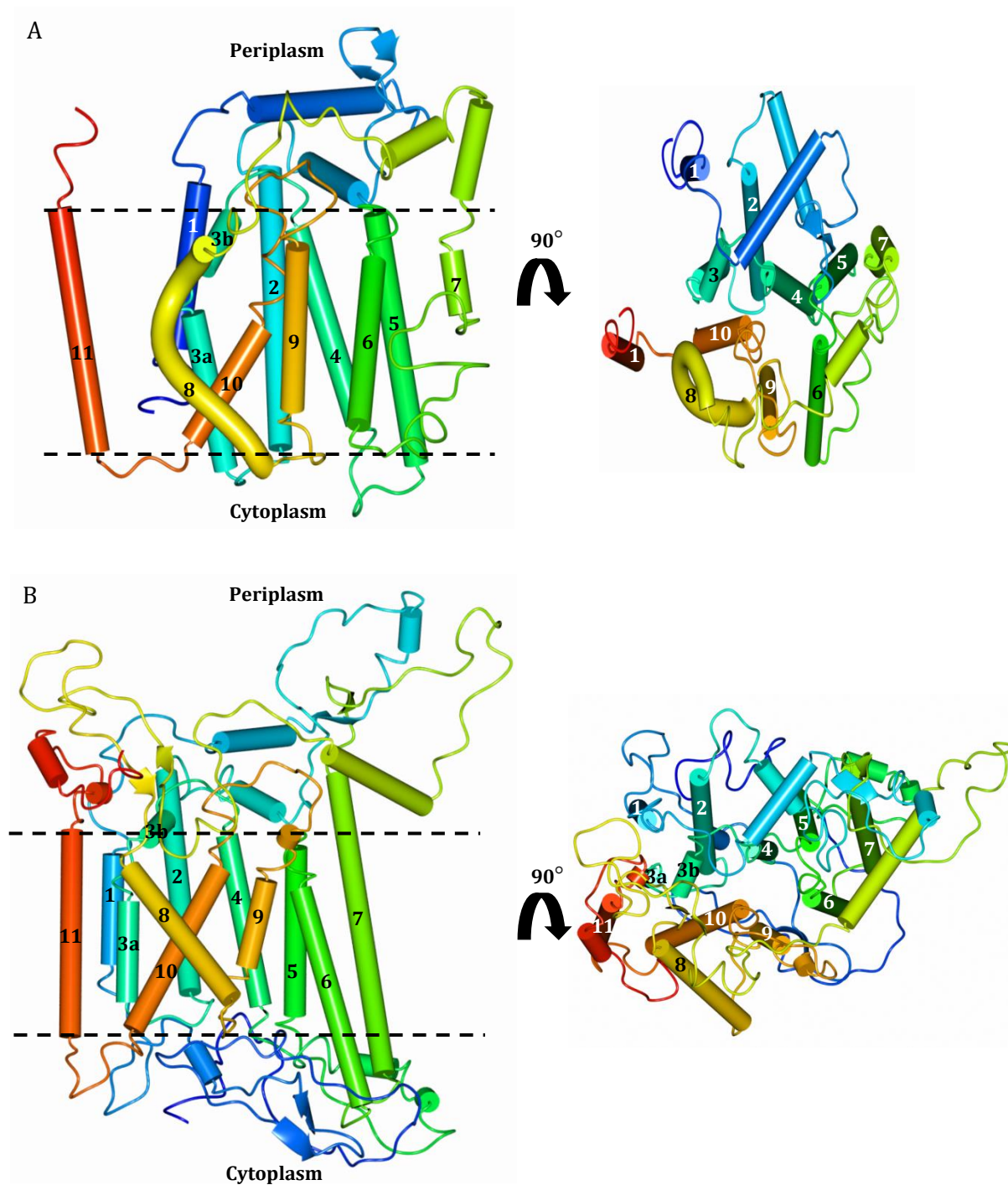
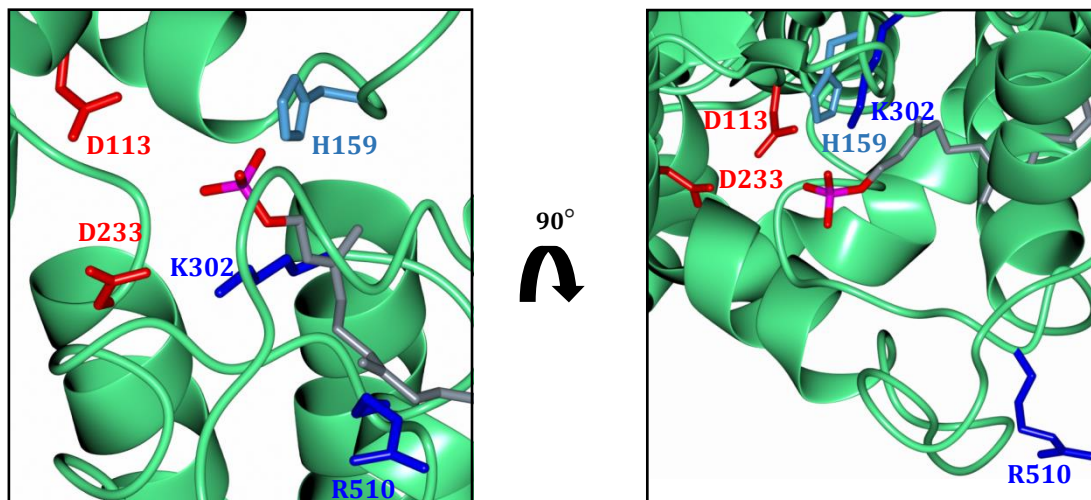


Figure 5.21: Phyre2 homology models of *S. coelicolor* Pmt have typical facets of GT-C fold glycosyl transferases. (A) Homology model of *S. coelicolor* Pmt based on the template ArnT (5F15) from *C. metallidurans*. 477 residues (80 %) were modelled at >90 % confidence (B) Homology model of *S. coelicolor* Pmt based on the template Pmt1-Pmt2 (6P25) from *S. cerevisiae*. 547 residues (92 %) were modelled at >90 % confidence. Worm and tube model coloured according to rainbow format, going from blue (N-terminus) to red (C-terminus) with numbered transmembrane helices. Predicted membrane boundaries are represented as dashed lines.

A



B

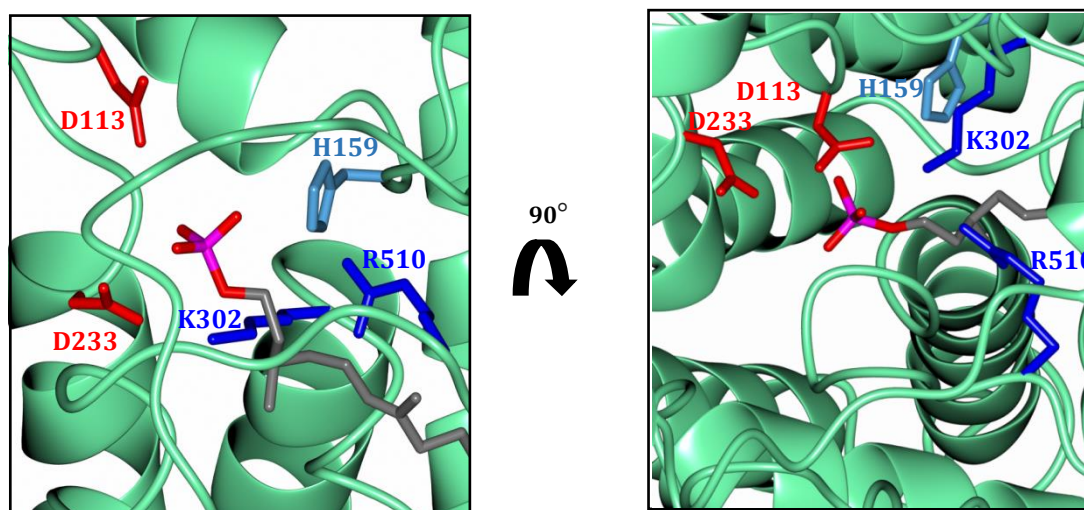


Figure 5.22: *S. coelicolor* Pmt homology model exhibits typical facets of GT-C fold glycosyl transferase. (A) Homology model of *S. coelicolor* Pmt based on the template ArnT (5F15) from *C. metallidurans*. (B) Homology model of *S. coelicolor* Pmt based on the template Pmt1-Pmt2 (6P25) from *S. cerevisiae*. All residues targeted for mutation are represented as cylinders and coloured according to their type: amide (light blue), basic (dark blue) and acidic (red). The template derived dolichol phosphate is coloured grey.

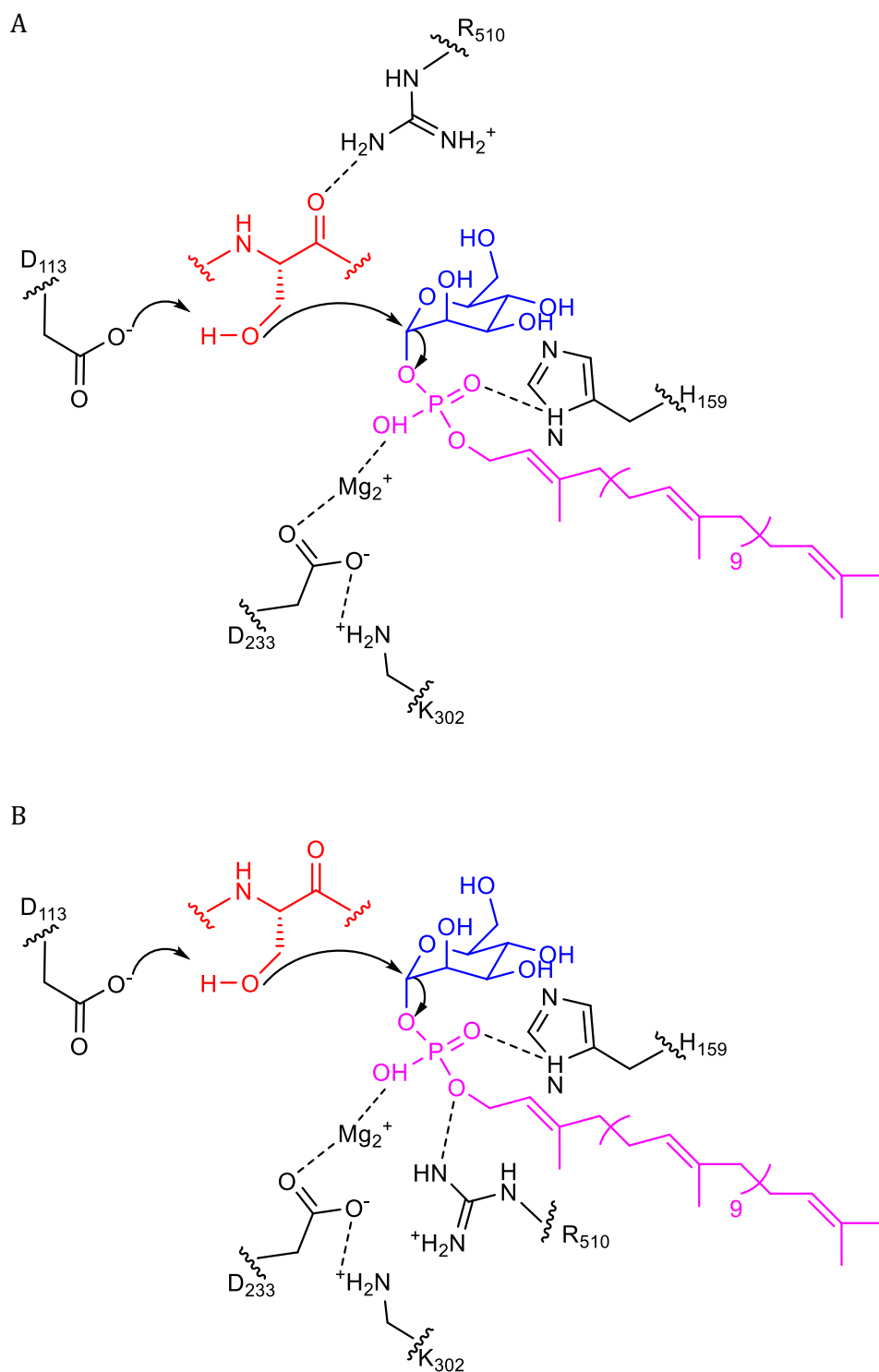


Figure 5.23: Proposed mechanism of Pmt action, an inverting glycosyl transferase that utilises a single step SN2 mechanism. (A) Initial model: R510 binds the mannose acceptor peptide (B) Alternate model: R510 binds the mannose donor polyprenol phosphate mannose

Chapter 6 – Pmt localisation studies and mutant library expansion

In the previous chapter, six *pmt* alleles were identified encoding PmtR82A, PmtD113A, PmtH159A, PmtD233A, PmtK302A and PmtR510A that failed to complement the *pmt* - strains DT1025 and DT2008. To better understand the role of these critical residues, further characterisation was necessary. Since Pmt is an integral membrane protein, it was thought that some of the critical residues identified could have a role in targeting the protein to the membrane. Tagging the six mutants would therefore provide the opportunity to do western blotting to check for the presence of Pmt in purified membrane fractions.

In addition, making conservative and semi-conservative mutations in the aforementioned six residues would enable an understanding of whether strict conservation was necessary to preserve function. These six residues are very tightly conserved across the prokaryotic and eukaryotic kingdoms, strongly indicating that even subtle changes in physicochemical properties would not be well accommodated.

The aim of this chapter was to probe Pmt mutant localisation and expand the mutant library, with the following objectives:

1. Add Strep II tags to either the N or C-termini of mutant Pmt and use Western blotting to determine the presence and abundance of Pmt variants in purified membrane fractions
2. Make a small library of conservative and semi-conservative Pmt substitutions to ascertain if these critical residues need to be strictly conserved to maintain function

6.1 Western blotting to probe enzyme localisation

Six mutant alleles encoding PmtR82A, PmtD113A, PmtH159A, PmtD233A, PmtK302A and PmtR510A were identified in Chapter 5 that failed to complement the *pmt* - strains DT1025 and DT2008. With the exception of D113 (which has been substituted in multiple Pmt homologues), the roles of these critical residues were not well understood. Western blotting presented an opportunity to determine whether the mutant enzymes encoded by these non-complementing alleles, were present or absent from the membrane. Absence would suggest the targeted residue was directly involved in membrane localisation, or was critical for the maintenance of stability or correct protein folding.

PCR was used to add the eight residue Strep II tag (WSHPQFEK) to either the N or C-terminus of the six non-complementing *pmt* mutant alleles. Upon addition of the tag, the alleles were cloned into the integrative plasmid pIJ10257 using Infusion. Following conjugal transfer of recombinant plasmids via *E. coli* ET12567 (pUZ8002), mutant alleles were introduced into the chromosomes of the *pmt* - strains DT1025 and DT2008 by conjugation and spores of exconjugants were harvested. Phage susceptibility testing was first carried out and as expected, Φ C31 Δ 25 was unable to plaque on DT1025 (Table 6.1) and DT2008 (Table A8.5) strains containing each of the six non-complementing alleles. Strains that had received the wild type (WT) allele with either an N or C-terminal Strep II tag were susceptible to infection, with the phage titres within the same order of magnitude as their non-tagged counterparts. This confirmed that the presence and position of the Strep II tag does not interfere with the ability of a *pmt* allele to complement either minus strain.

The strains were then grown in liquid culture, the cells were lysed and membrane fractions obtained. Following separation of proteins by SDS-PAGE, transfer to a PVDF membrane and subsequent wash steps, an anti-Strep II tag antibody was used to probe for the presence of Pmt in the membrane fractions by Western blotting. No signal corresponding to the six inactive Pmt variants was obtained in soluble or membrane fractions in DT1025 (Figure 6.1) and DT2008 (Figure A8.6). The WT positive control alone yielded a signal at (~55 kDa), this compares with the theoretical molecular weight (MW) of (~66 kDa) for Strep II tagged Pmt. This discrepancy while unexpected, was reproducible. The empty plasmid (pIJ10257) negative control possessed no signal, strongly indicating that the signal obtained from the positive control was the Strep II tagged Pmt.

Table 6.1: Presence of the Strep Tag II on either termini does not affect the ability of *pmt* alleles to complement DT1025. Φ C31 $c\Delta 25$ phage were plated out on DN agar and then SN agar containing spores was added to the top with the plates incubated at 30 °C for 18 hours. The average titre is shown \pm SEM from 4 biological replicates. 0.1 ml of a 10^{-6} phage stock dilution was used to obtain countable plaques for phage sensitive strains. Strains that showed no plaques at the lowest phage stock dilution tested (10^{-1}) are represented as having a PFU/ml $< 1 \times 10^2$.

Strain	C-terminal Strep Tag II Titre (PFU/ml)	N-terminal Strep Tag II Titre (PFU/ml)
DT1025	$< 1 \times 10^2$	$< 1 \times 10^2$
DT1025 + WT	$(3.47 \pm 0.37) \times 10^8$	$(2.03 \pm 0.19) \times 10^8$
DT1025 + R82A	$< 1 \times 10^2$	$< 1 \times 10^2$
DT1025 + D113A	$< 1 \times 10^2$	$< 1 \times 10^2$
DT1025 + H159A	$< 1 \times 10^2$	$< 1 \times 10^2$
DT1025 + D233A	$< 1 \times 10^2$	$< 1 \times 10^2$
DT1025 + K302A	$< 1 \times 10^2$	$< 1 \times 10^2$
DT1025 + R510A	$< 1 \times 10^2$	$< 1 \times 10^2$

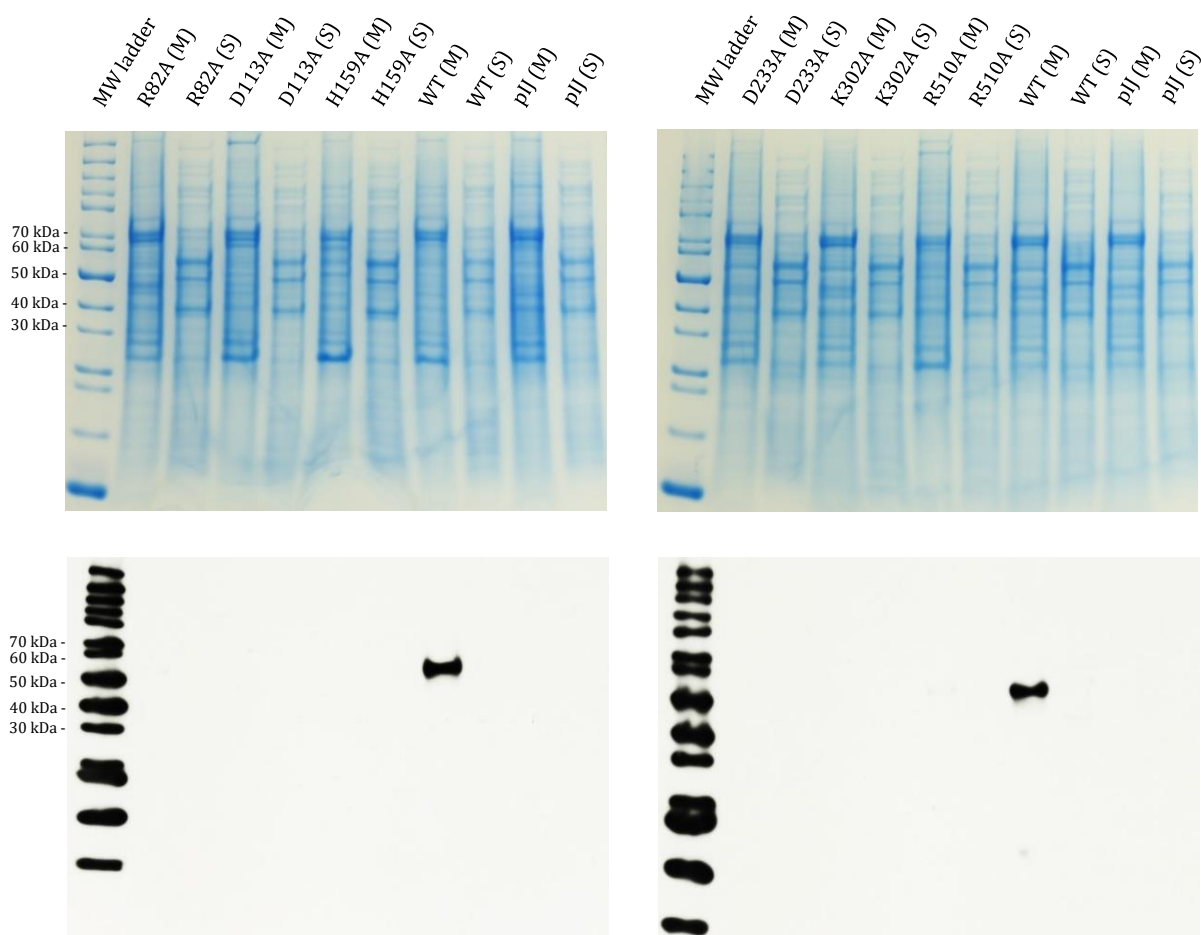


Figure 6.1: C-terminal Strep II tagged non-complementing Pmt variants are absent in DT1025 membrane fractions. Membrane and soluble fraction samples were first loaded onto a 12 % SDS-PAGE gel which was run and stained to ensure protein concentrations of samples were consistent. After transfer of proteins from an SDS-PAGE gel to a PVDF membrane and subsequent wash steps, the membrane was incubated with Strep Tag II Antibody HRP Conjugate, substrate added and X-ray film developed. pIJ refers to the empty pIJ10257 control and WT to the *pmt* WT complemented strain control.

Fractions taken at the three steps preceding the final 100,000 x g spin in the differential centrifugation protocol (i. Sonication, ii. 5,000 x g spin and iii. 15,000 x g spin) failed to yield any detectable signal by Western blotting (data not shown). To investigate further, genomic DNA from the DT1025 strains was purified and *pmt* at the integration and native loci (including 100 bp up and downstream) were amplified by PCR. Sequencing the PCR products showed no unexpected changes in the DNA sequence that could explain the lack of signal for the six mutants (data not shown). The absence of detectable signal in the membrane fractions for the non-complementing alleles indicates an activity localisation relationship, whereby only functional Pmt will correctly localise to the membrane.

The absence of signal corresponding to any of the six Pmt variants in purified membrane fractions was unexpected, however the positive and negative controls consistently yielded signal presence and absence respectively. The decision was subsequently made to add Strep II tags to mutant alleles that were previously shown to complement DT1025 and DT2008. In this case, it would be expected that signal comparable in both intensity and position to the WT, would be observed in purified membrane fractions isolated from strains expressing a functional Strep II tagged Pmt. Of the 17 candidates available, six alleles were chosen encoding: PmtP160A, PmtK164A, PmtR228A, PmtL231A, PmtR335A and PmtS421A. As with the non-complementing alleles, Strep II tags were added using PCR and Infusion cloning. In the interest of time, the Strep II tag was only added to the C-terminus, since it was already known that the position of the tag had no effect on *in vivo* activity of the WT. The C-terminus was chosen since this is predicted to face the periplasm, while the N-terminus is predicted to be intracellular. The recombinant plasmids were introduced into DT1025 (Table 6.2) and DT2008 (Table A8.5) via pIJ10257. Phage susceptibility testing showed that all strains were vulnerable to phage infection. The titres were in the same order of magnitude as their non-tagged counterparts as in chapter 5, in addition to the positive control. Again, the position of the tag was of no consequence.

Membrane fractions were purified as described above. Signal corresponding to active Pmt variants (tagged at either termini) were indeed present in the membrane fractions and absent from the soluble fractions in DT1025 (Figure 6.2) and DT2008 (Figure A8.7). The signal obtained in the western blot is at the same MW as the WT positive control, roughly half way between the 50 and 60 kDa reference bands. It is noteworthy that for the WT positive control and active variants, a protein band corresponding to this signal could not be clearly identified in the SDS-PAGE, indicating that the *ermE** promoter, while constitutive, does not drive clearly visible, over expression of the integrated *pmt* gene, which is expected.

A selection of strains individually expressing 4 active and 4 inactive Pmt variants were chosen to demonstrate that mutant Pmt localisation (or lack of) could be identified on the same blot

(figure 6.3). As before, active mutants could be detected in membrane fractions while inactive mutants could not.

From the data obtained, there is clearly a strict activity localisation relationship. It was hoped that at least a few of the variants encoded by these non-complementing alleles would be present in the membrane fractions. This would have then allowed biochemical characterisation by, for example, incubating the membranes with peptide glycosylation substrates and monitoring the outcome of glycosylation using mass spectrometry or thin layer chromatography. The absence of all six inactive variants in membrane fractions however prevented sensible progression to biochemical characterisation. While active Pmt variants were indeed present in purified membrane fractions, there would be little merit in the biochemical characterisation of these active enzymes, since their activity would not be expected to significantly deviate from that of the WT.

Table 6.2: Presence of the Strep Tag II on either termini does not affect the ability of *pmt* alleles to complement DT1025. Φ C31 $c\Delta 25$ phage were plated out on DN agar and then SN agar containing spores was added to the top with the plates incubated at 30 °C for 18 hours. The average titre is shown \pm SEM from 4 biological replicates. 0.1 ml of a 10^{-6} phage stock dilution was used to obtain countable plaques for phage sensitive strains. Strains that showed no plaques at the lowest phage stock dilution tested (10^{-1}) are represented as having a PFU/ml $< 1 \times 10^2$.

Strain	C-terminal Strep Tag II Titre (PFU/ml)	N-terminal Strep Tag II Titre (PFU/ml)
DT1025	$< 1 \times 10^2$	$< 1 \times 10^2$
DT1025 + WT	$(3.47 \pm 0.37) \times 10^8$	$(2.03 \pm 0.19) \times 10^8$
DT1025 + P160A	$(2.52 \pm 0.32) \times 10^8$	$(2.50 \pm 0.26) \times 10^8$
DT1025 + K164A	$(2.79 \pm 0.19) \times 10^8$	$(4.05 \pm 0.23) \times 10^8$
DT1025 + R228A	$(2.18 \pm 0.13) \times 10^8$	$(3.10 \pm 0.25) \times 10^8$
DT1025 + L231A	$(3.20 \pm 0.23) \times 10^8$	$(2.43 \pm 0.17) \times 10^8$
DT1025 + R335A	$(4.10 \pm 0.23) \times 10^8$	$(2.71 \pm 0.76) \times 10^8$
DT1025 + S421A	$(2.68 \pm 0.18) \times 10^8$	$(2.35 \pm 0.31) \times 10^8$

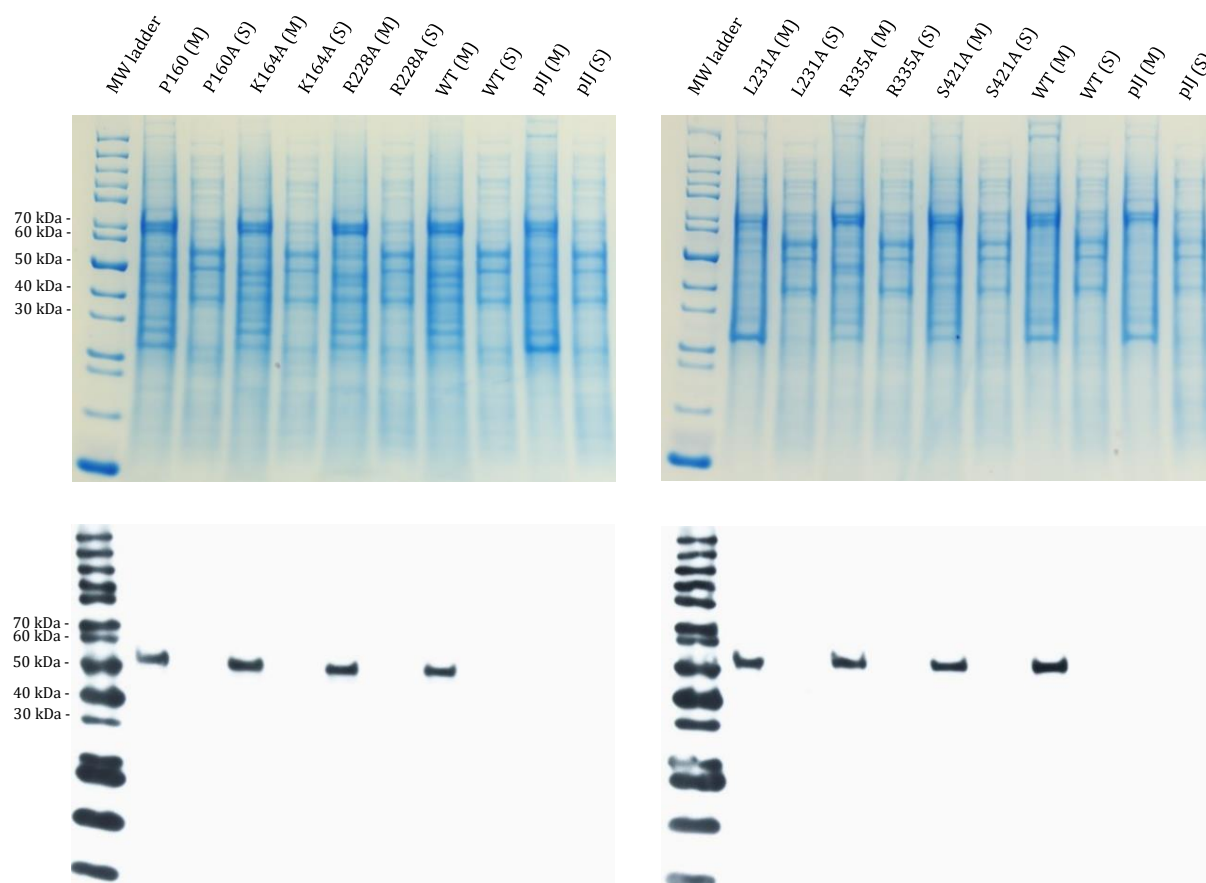


Figure 6.2: C-terminal Strep II tagged complementing Pmt variants are present in DT1025 membrane fractions. Membrane and soluble fraction samples were first loaded onto a 12 % SDS-PAGE gel which was run and stained to ensure protein concentrations of samples were consistent. After transfer of proteins from an SDS-PAGE gel to a PVDF membrane and subsequent wash steps, the membrane was incubated with Strep Tag II Antibody HRP Conjugate, substrate added and X-ray film developed. pIJ refers to the empty pIJ10257 control and WT to the *pmt* WT complemented strain control.

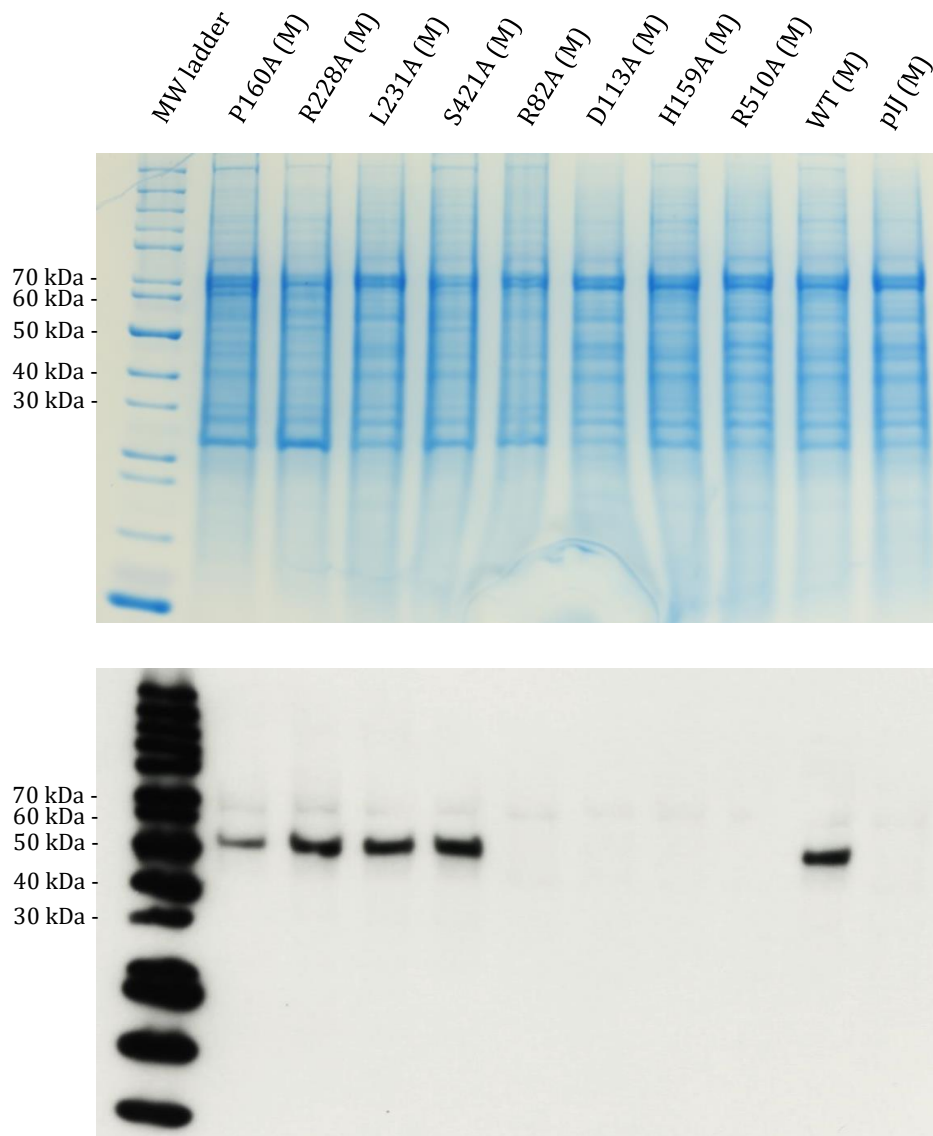


Figure 6.3: C-terminal Strep II tagged complementing and non-complementing variants were present and absent respectively in DT1025 membrane fractions. Membrane fraction samples were first loaded onto a 12 % SDS-PAGE gel which was run and stained to ensure protein concentrations of samples were consistent. After transfer of proteins from an SDS-PAGE gel to a PVDF membrane and subsequent wash steps, the membrane was incubated with Strep Tag II Antibody HRP Conjugate, substrate added and X-ray film developed. pIJ refers to the empty pIJ10257 control and WT to the *pmt* WT complemented strain control.

6.2 Expansion of the *pmt* mutant library

All mutations hitherto described were simple substitutions to alanine. The previous western blotting data showed that for these alanine substitutions, variants encoded by complementing and non-complementing alleles were present and absent from the membrane respectively. The next step was to create a smaller library of conservative and semi-conservative mutations. With this library, the goal was to identify a strain with an intermediate phenotype. With such a phenotype, the variant would still localise to the membrane fractions, however the activity would be diminished compared to the WT, which would then justify further biochemical characterisation.

All six critical residues were subject to both conservative and semi-conservative substitutions. In addition D113 (due to it being well characterised in the literature) was subject to additional non-conservative mutations for comparison. To summarise, R82 was mutated to lysine and histidine, H159 to lysine and asparagine, D233 to glutamate and asparagine, K332 to histidine and arginine, R510 to histidine and lysine and finally D113 was mutated to glutamate, leucine, asparagine, proline, arginine serine and tyrosine. As previously described, these mutant alleles were all cloned into pIJ10257.

In the interest of time, the alleles were introduced into one *pmt* - strain (DT1025). Since there had previously not been any difference in phenotypes obtained between complemented and non-complemented DT1025 and DT2008 strains. DT1025 was chosen since the mutation that confers the minus phenotype is known, enabling sequencing of the native locus as necessary. The mutant alleles were introduced into DT1025 as described previously. Since these mutations were novel, they were first tested by phage infection assays (Table 6.3). For the phage assays, three out of the 17 strains had received complementing alleles encoding PmtR82K, PmtD113N and D233E and were therefore susceptible to infection by phage, with a comparable order of magnitude to the WT. The remaining 14 alleles failed to complement DT1025. Regarding the three active mutants, D233E and R82K were conservative substitutions while D113N was semi-conservative. Admittedly, the failure of the conservative D113E substitution to complement, in comparison to the success of the semi conservative D113N, was unexpected.

Table 6.3: The majority of conservative and semi conservative substitutions yielded *pmt* alleles that were unable to complement DT1025. Φ C31 c Δ 25 phage were plated out on DN agar and then SN agar containing spores was added to the top with the plates incubated at 30 °C for 18 hours. The average titre is shown \pm SEM from 4 biological replicates. 0.1 ml of a 10^{-6} phage stock dilution was used to obtain countable plaques for phage sensitive strains. Strains that showed no plaques at the lowest phage stock dilution tested (10^{-1}) are represented as having a PFU/ml $< 1 \times 10^2$.

Strain	Titre (PFU/ml)
DT1025	$< 1 \times 10^2$
DT1025 + WT	$(2.20 \pm 0.69) \times 10^8$
DT1025 + R82H	$< 1 \times 10^2$
DT1025 + R82K	$(2.46 \pm 0.77) \times 10^8$
DT1025 + D113E	$< 1 \times 10^2$
DT1025 + D113L	$< 1 \times 10^2$
DT1025 + D113N	$(1.47 \pm 0.82) \times 10^8$
DT1025 + D113P	$< 1 \times 10^2$
DT1025 + D113R	$< 1 \times 10^2$
DT1025 + D113S	$< 1 \times 10^2$
DT1025 + D113Y	$< 1 \times 10^2$
DT1025 + H159K	$< 1 \times 10^2$
DT1025 + H159N	$< 1 \times 10^2$
DT1025 + D233E	$(1.94 \pm 1.14) \times 10^8$
DT1025 + D233N	$< 1 \times 10^2$
DT1025 + K332H	$< 1 \times 10^2$
DT1025 + K332R	$< 1 \times 10^2$
DT1025 + R510H	$< 1 \times 10^2$
DT1025 + R510K	$< 1 \times 10^2$

Antibiotic susceptibility tests were then carried out to see if an intermediate phenotype could be obtained (Figure 6.4). A limited selection of antibiotics was chosen: ampicillin, vancomycin, imipenem and meropenem. The selection was based on these antibiotics giving the biggest difference in zone of clearance diameter between complemented and non-complemented strains. In previous assays, DT1025 expressing one of three previously identified active mutants (R82K, D113N, D233E) showed no increased sensitivity to the antibiotics (at the concentrations tested) compared to the WT complemented strain. The remaining 14 non-complemented strains had notably increased susceptibility, comparable to the empty plasmid negative control, with zone of inhibition diameters ≥ 15 mm. The most effective antibiotic for exploiting the antibiotic susceptibility phenotype was imipenem, with zones of clearance diameters ≥ 20 mm. Similarly to the data obtained in chapter 5 for the alanine mutants, there were no intermediate phenotypes, all strains resembled either the positive or negative control.

While no evidence of an intermediate phenotype was obtained in the antibiotic and phage assays, it was necessary to confirm this with western blotting. As before, the strains were grown in liquid culture, the cells lysed and membrane fractions purified. When Strep II tag recognising antibodies were added to the membrane fractions, signal at the expected MW was observed only for membrane fractions from strains complemented with alleles encoding PmtR82K, PmtD113N and PmtD233E (Figure 6.5). This is consistent with previous data which showed a positive correlation between active mutants and presence in the membrane. The membrane fractions from remaining non-complemented strains showed no comparable signal. Not one conservative or semi-conservative substitution gave the desired intermediate phenotype. As with the alanine mutants described previously, Western blotting of samples from stages preceding the 100,000 x g spin (i. sonication, ii. 5,000 x g spin and iii. 15,000 x g spin) , gave comparable western blotting results. Furthermore, sequencing analysis confirmed no unexpected changes in *pmt* alleles at the integration or native loci. Expansion of the mutant library to include conservative and semi-conservative substitutions therefore failed to break the strict activity localisation relationship. This strengthened the hypothesis that activity and membrane localisation of Pmt are closely linked.

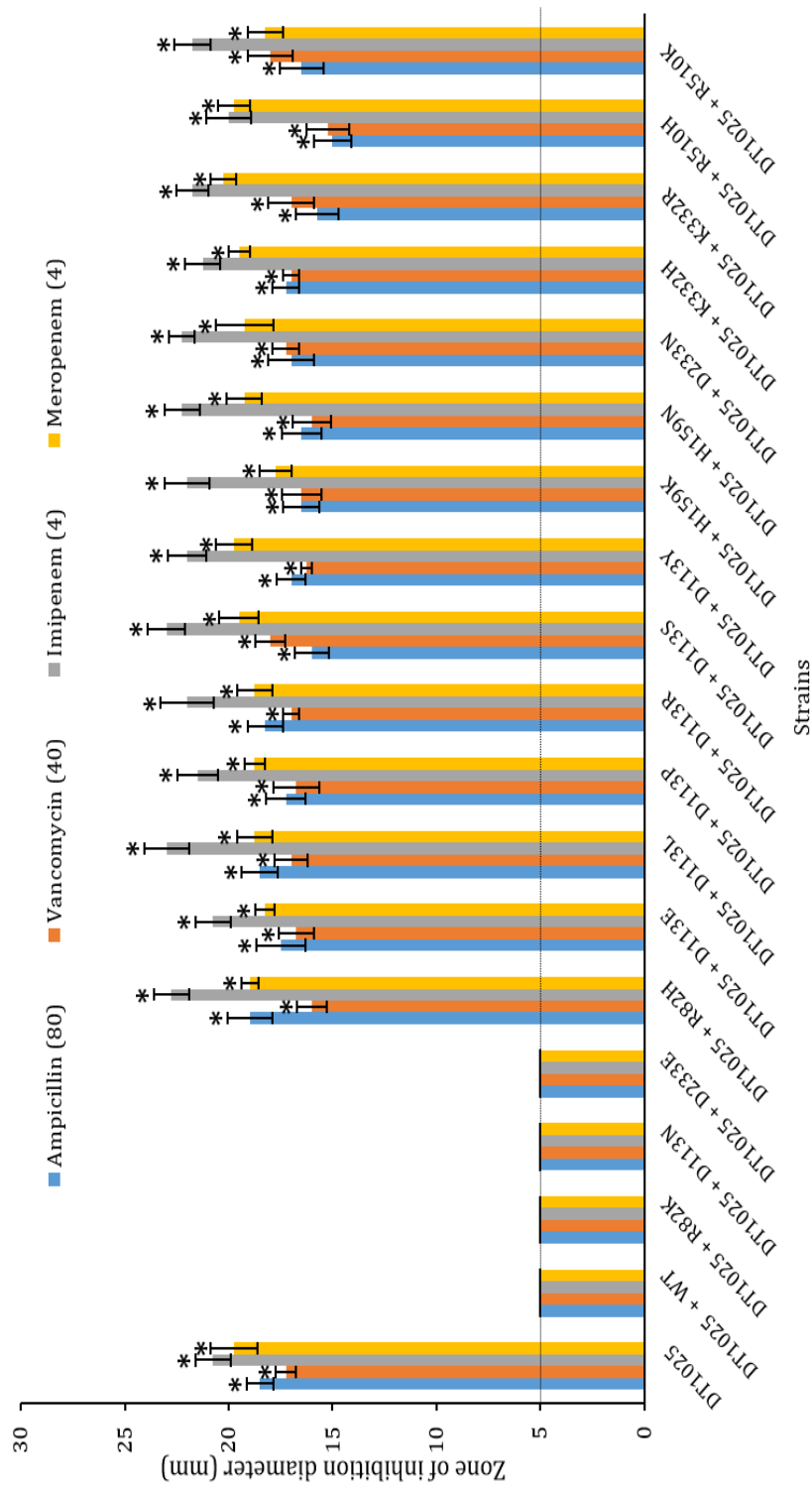


Figure 6.4: Successfully complemented DT1025 strains do not show hypersensitivity to antibiotics targeting the bacterial cell wall and/or membrane. Antibiotic hypersensitivity was quantified by measuring the zone of inhibition diameter for *pmt* mutants. Strains were plated on DN agar and incubated at 30 °C for 48 hours. Shown are the averages of 4 biological replicates with SEM. The paper used to administer each antibiotic has a diameter of 5 mm and is shown as the dotted line threshold. The amount of antibiotic used in μg is shown in brackets in the legend.

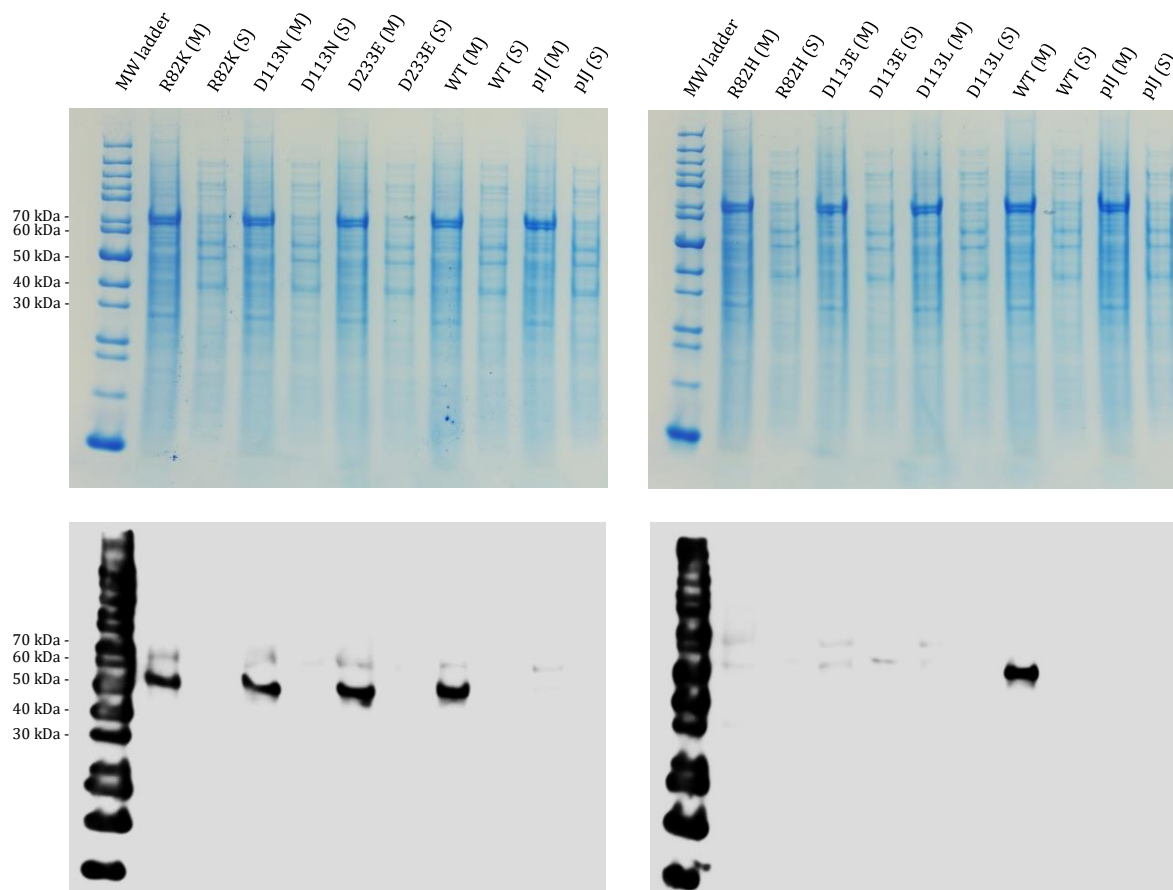


Figure 6.5a: C-terminal Strep II tagged non-complementing Pmt variants are absent in DT1025 membrane fractions. Membrane and soluble fraction samples were first loaded onto a 12 % SDS-PAGE gel which was run and stained to ensure protein concentrations of samples were consistent. After transfer of proteins from an SDS-PAGE gel to a PVDF membrane and subsequent wash steps, the membrane was incubated with Strep Tag II Antibody HRP Conjugate, substrate added and X-ray film developed. pIJ refers to the empty pIJ10257 control and WT to the *pmt* WT complemented strain control.

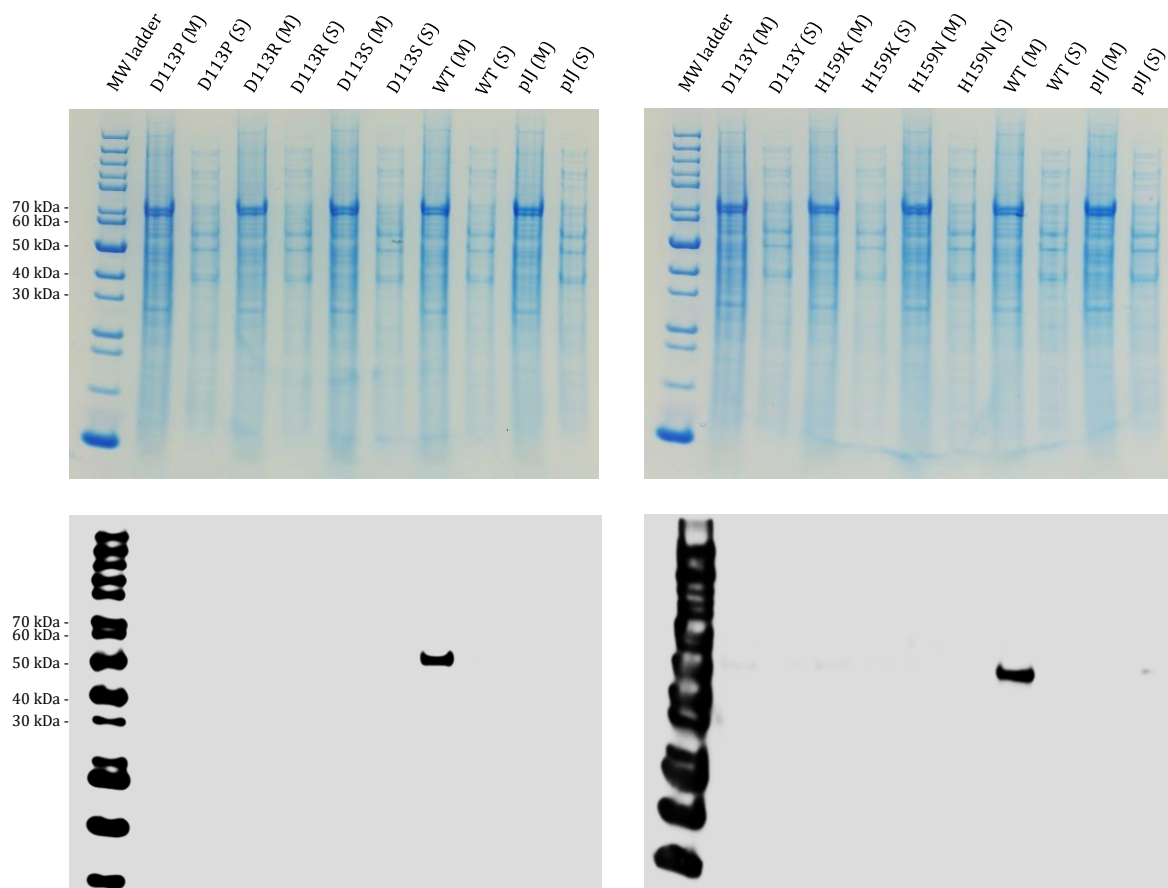


Figure 6.5b: C-terminal Strep II tagged non-complementing Pmt variants are absent in DT1025 membrane fractions. Membrane and soluble fraction samples were first loaded onto a 12 % SDS-PAGE gel which was run and stained to ensure protein concentrations of samples were consistent. After transfer of proteins from an SDS-PAGE gel to a PVDF membrane and subsequent wash steps, the membrane was incubated with Strep Tag II Antibody HRP Conjugate, substrate added and X-ray film developed. pIJ refers to the empty pIJ10257 control and WT to the *pmt* WT complemented strain control.

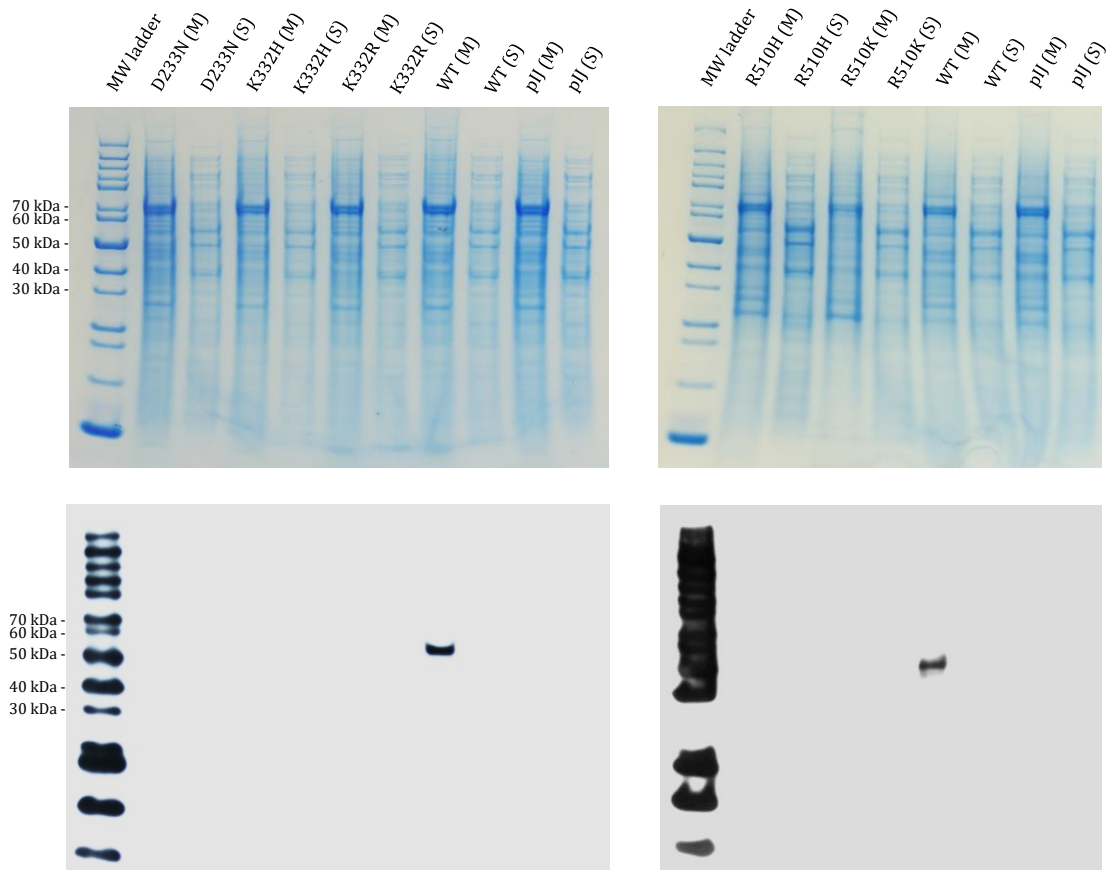


Figure 6.5c: C-terminal Strep II tagged non-complementing *Pmt* variants are absent in DT1025 membrane fractions. Membrane and soluble fraction samples were first loaded onto a 12 % SDS-PAGE gel which was run and stained to ensure protein concentrations of samples were consistent. After transfer of proteins from an SDS-PAGE gel to a PVDF membrane and subsequent wash steps, the membrane was incubated with Strep Tag II Antibody HRP Conjugate, substrate added and X-ray film developed. pIJ refers to the empty pIJ10257 control and WT to the *pmt* WT complemented strain control.

6.3 Discussion

In chapter 5, six critical residues for Pmt function were identified: PmtR82, PmtD113, PmtH159, PmtD233, PmtK302 and PmtR510. Substitution of these residues to alanine yielded mutant alleles that failed to complement the *S. coelicolor pmt* - strains (DT1025 and DT2008). The strains therefore had increased antibiotic susceptibility to β -lactams and vancomycin, in addition to growth retarded phenotypes and resistance to Φ C31 Δ 25 infection. These observations for the non-complemented DT1025 and DT2008 were consistent with previously published literature (Howlett *et al.*, 2018a; Wehmeier *et al.*, 2009; Cowlshaw and Smith 2001; Cowlshaw and Smith 2002).

The next step was to ascertain why these six residues were critical for function. Strep II tags were added to these non-complementing mutants and they were introduced into DT1025 and DT2008. Following purification of membrane fractions from these strains, western blotting analysis showed a lack of signal at the expected MW, in contrast the WT positive control alone yielded a clear signal at ~55 kDa, admittedly lower than the theoretical MW of (~66 kDa) for Strep II tagged Pmt. Encouragingly, no signal was detected for the empty plasmid (pIJ10257) negative control. Strep II tags were later added to a set of active variants: PmtP160A, PmtK164A, PmtR228A, PmtL231A, PmtR335A and PmtS421A. Signal was detected in the membrane fractions for all six of these variants and as before, the signal was again lower (55 kDa). It should be stressed that when preparing the protein samples for SDS PAGE, instead of a standard 10 minute boiling step at 80 °C following β -mercaptoethanol addition, the protein samples were left in a 30 °C water bath for one hour (H). A boiling step was avoided to stop the proteins aggregating and consequently failing to enter the gel correctly (Sagne *et al.*, 1996; Lee *et al.*, 2005). It is possible that the 30 °C incubation, combined with the addition of SDS and β -mercaptoethanol was not sufficient to fully denature the protein. In this case mobility would likely not be proportional to the MW.

A possible explanation for the lack of signal in the membrane fractions of the non-complementing mutants is that substitution of these critical residues yielded aggregation prone, aberrantly folded proteins. These proteins may be subject to clearance by the cell. Prokaryotes possess cellular molecular machinery to combat misfolding and aggregation termed the proteostasis network (Becker *et al.*, 2016). Aggregation prone Pmt that cannot be refolded by chaperones, would be degraded by intracellular proteases. In eukaryotes and archaea proteasomes mediate intracellular protein degradation. While only certain orders of bacteria have proteasomes, a greater dependency on proteases is therefore observed in prokaryotes, FtsH is a particularly interesting protease as it has substrates which are misfolded membrane proteins (Becker *et al.*, 2016). Bacterial proteasomes were first studied in actinobacteria such as

M. tuberculosis and *S. coelicolor* (Nagy *et al.*, 1998; Lin *et al.*, 2016). Aggregation can be driven by non-physiologically relevant levels of protein expression. We used integrase containing plasmids (pIJ10257) in this study to stably introduce the Strep II tagged alleles into the host genome with expression of the *pmt* genes under the control of the constitutive *ermE** promoter. If a variant protein has a propensity for aggregation due to changes to its 3D conformation arising from a single residue substitution, this could be exacerbated by high levels of expression which could overwhelm the proteostasis network. Rather than the chaperones refolding the aggregation prone proteins, the latter are instead degraded by proteases to prevent a potentially toxic build-up of aggregates.

It should be pointed out that no evidence of overexpression of the *pmt* alleles was seen in SDS-PAGE. Other constitutive promoters drive higher levels of expression in *S. coelicolor* such as *PSCO5768*, which increases the expression of GFP threefold compared to *ermE** (Li *et al.*, 2015). In contrast *PSCO4508* yields two-fold lower levels of expression. It is unlikely that the *ermE** promoter is driving non-physiologically relevant levels of expression since this would presumably lead to an observable fitness cost in the complemented strains. The phenotype therefore would be expected to have deviated from that of the *S. coelicolor* J1929 parent strain. Results in Chapter 5 however showed full consistency between the phenotypes of the complemented strains and the J1929 parent strain. Furthermore, reproducible signal at the same MW was consistently obtained for all complemented strains. Based on these observations, it is unlikely that placing the gene under the control of a different promoter would have yielded a different result.

Assuming these proteins are stable but not targeted to the membrane, their presence in either the soluble fraction or one of the earlier steps in the differential centrifugation protocol would be expected. No such signals were observed. The lack of signal immediately post sonication is particularly important, as it indicates that the factors contributing to the lack of Pmt signal are acting pre lysis, the most plausible explanation likely being protease mediated degradation.

Genomic DNA from the non-complemented DT1025 strains was purified and *pmt* at the integration and native loci (including 100 bp up and downstream) were amplified by PCR. Of specific interest was the *ermE** promoter region, since mutations in the region that prevent expression would explain the absence of signal however, no such mutations were observed. There were also no deviations in the DNA sequences of the ORF and termination region.

More conservative substitutions of PmtR82, PmtD113, PmtH159, PmtD233, PmtK302 and PmtR510 were introduced in an effort to obtain mutants that had diminished *in vivo* activity, as shown by a partial complementation phenotype, but that would still be localised to the

membrane (Keenan *et al.*, 2019). The majority of conservative and semi-conservative substitutions yielded non-complementing alleles. For three critical residues (H159, K332 and R510) strict conservation was crucial and no substitutions were tolerated.

Three substitutions yielded active mutants D233E and R510K and D113N. Interestingly when D113 was substituted to glutamate the mutant failed to complement. In chapter 5, we hypothesised that D113 activates the serine or threonine to attack the mannose C1 carbon. It is therefore possible that the addition of an extra CH₂ group is sufficient to cause an unfavourable steric clash with the acceptor serine or threonine. Asparagine however is isosteric with aspartate but it is a much weaker nucleophile. Asparagine's ability to compensate for the loss of aspartate indicates that the asparagine would need to first be activated to act as a nucleophile. Known mechanisms of asparagine activation (that have been documented in N-linked glycosylation) include acid base catalysed activation and twisted amide activation (Lizak *et al.*, 2013). Interestingly, the same conservative and semi-conservative substitutions to glutamate and asparagine respectively were introduced into *C. metallidurans* ArnT and in both cases resulted in non-functional enzyme (Petrou *et al.*, 2016). It is important here to highlight that in *C. metallidurans* ArnT, the DE motif aspartate is coordinating the nucleophilic phosphate head group of the lipid A acceptor substrate, rather than activating a serine or threonine hydroxyl in the case of *S. coelicolor* Pmt.

Since D233E in our model is proposed to bind the phosphate of polyprenol phosphate mannose via a divalent metal cation, it would appear that the slight lengthening of the side chain has not interfered with its ability to do so. Another explanation is that the aspartate directly binds the phosphate and lengthening the side chain does not result in unfavourable steric clashes.

The R510K substitution being tolerated is not so surprising since R510 is predicted to be on a cytoplasmic loop, rather than within the periplasmic active site. However, this conservative substitution being accommodated does not help us understand why this residue is critical for *in vivo* activity.

The majority of the conservative and semi-conservation substitutions introduced into the expanded mutant library failed to complement DT1025 and none uncoupled the strict activity localisation relationship. The hypothesis that activity and localisation are linked has been strengthened and further supported by extensive troubleshooting. The molecular basis of this rather fascinating activity-localisation relationship remains unknown.

Chapter 7 – Overall conclusions and future perspectives

In this work a combination of complementation assays and structural bioinformatics has been used to identify residues critical for the *in vivo* activity two *S. coelicolor* enzymes Ppm1 and Pmt. Furthermore, the *in vivo* data obtained for the Ppm1 mutants is supported by biochemical data provided by a collaborator.

Analysis of these results in the context of the wider literature, has allowed roles to be defined/proposed for (i) eight of the nine critical Ppm1 residues identified, and (ii) five of the six critical Pmt residues identified. For both enzymes, the positions of these critical residues in the homology models indicates the majority have a role in either 1) participating directly in the catalytic reaction and/or binding either the donor or acceptor substrate. In this way, we have defined multiple critical active site residues. Identifying and/or developing inhibitors to target these enzymes, especially Ppm1 is an important future priority. To exploit an enzyme as an anti-microbial-target requires knowledge of both structure and function. Research described in this thesis has focussed heavily on functional studies and while we have identified multiple critical amino acids, the structures of these enzymes unfortunately remain elusive.

Since expression and purification conditions have already been established for Ppm1, future efforts should focus on obtaining a high resolution 3D structure to corroborate the inferences drawn from the mechanistic studies which underpin our biochemical model. Critically, the availability of a 3D structure will enable screening of fragment libraries and the identification of promising fragments, which could later be combined to generate a tight binding inhibitor. In theory fragment screening could be carried out in the absence of a structure. However assembling the fragments into the tighter binding inhibitor and then improving the affinity and efficacy of any resulting lead is much more likely to be successful if guided by structure (Murray and Rees 2009). As a result, future efforts should continue to focus on obtaining suitably diffracting crystals for high resolution structure determination.

Chapter 8 – Appendix

8.2 Chapter 4 appendix

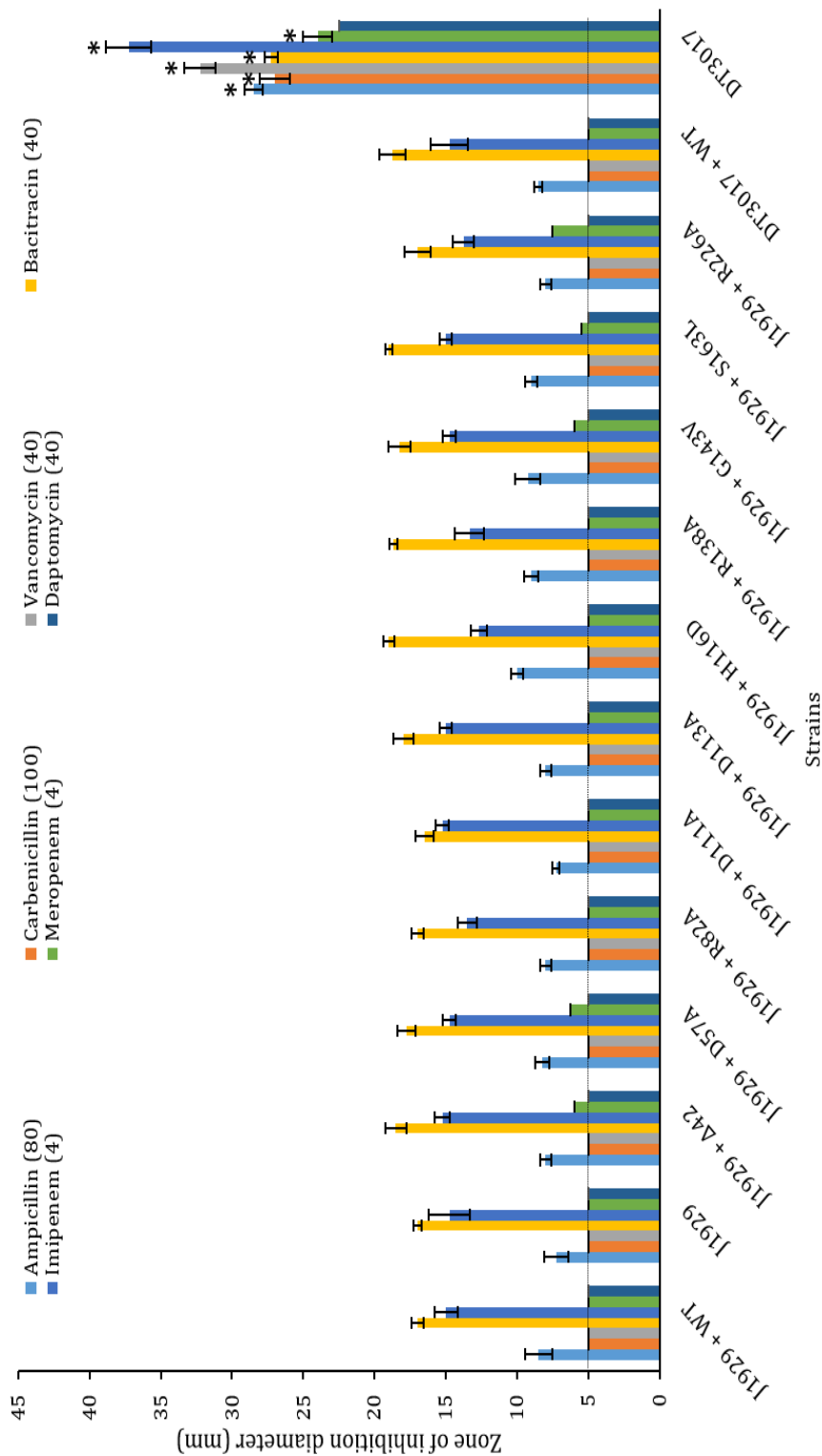


Figure A8.1: Introduced *ppm1* alleles have no effect on the antibiotic sensitivity profile of the J1929 parent strain. Sensitivity to antibiotics targeting the cell wall and/or membrane was quantified by measuring the zone of inhibition diameter for the WT *ppm1* control, no gene control and the *ppm1* mutants. Data for DT3017 complemented with the WT *ppm1* and no gene controls are also provided. Strains were plated on DN agar and incubated at 30 °C for 48 hours. Shown are the averages of 4 replicates with SEM. The paper used to administer each antibiotic has a diameter of 5 mm and is shown as the dotted line threshold. The amount of antibiotic used in µg is shown in brackets in the legend

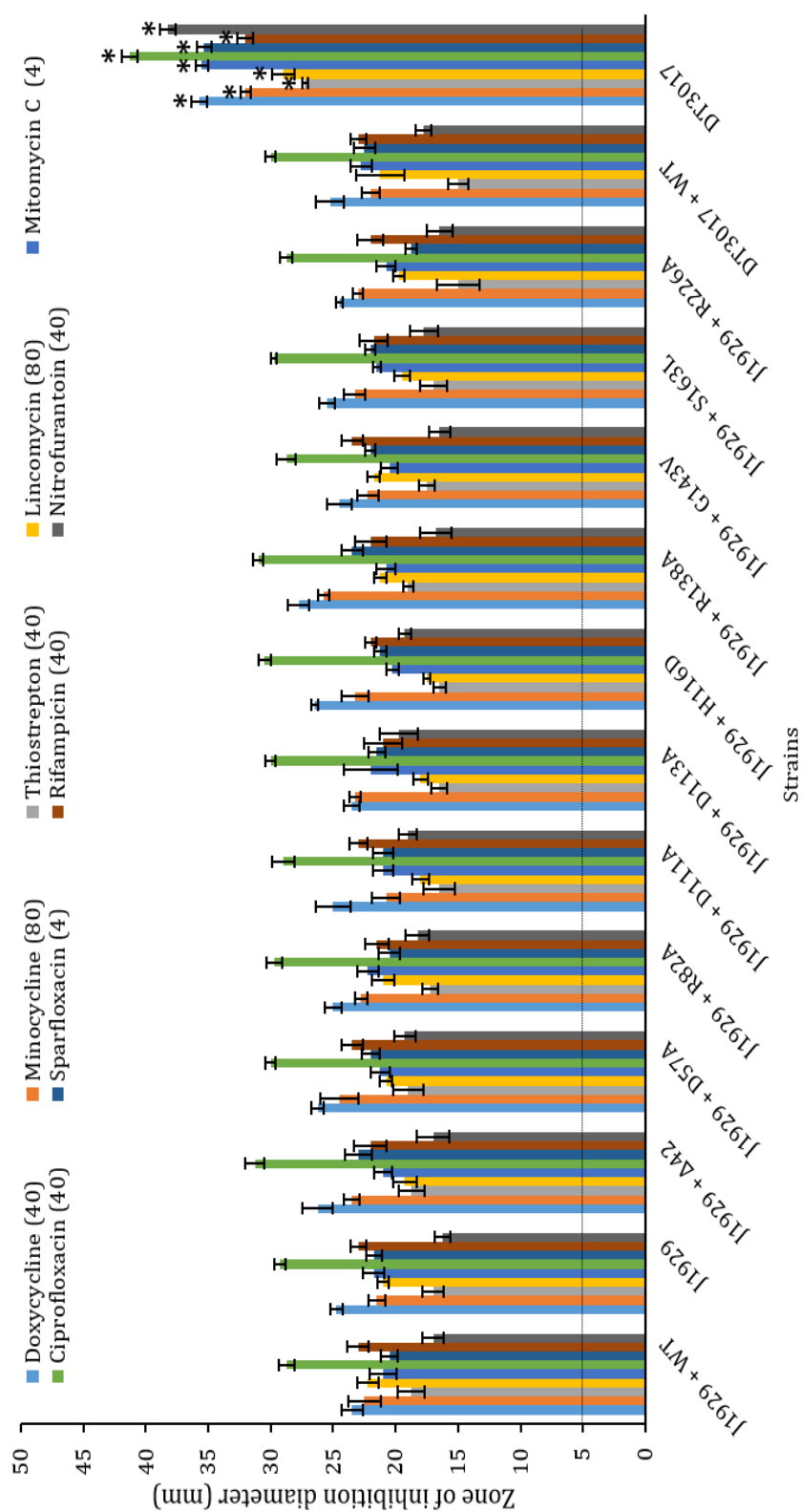


Figure A8.2: Introduced *ppm1* alleles have no effect on the antibiotic sensitivity profile of the J1929 parent strain. Sensitivity to antibiotics targeting DNA replication, transcription and translation (B) was quantified by measuring the zone of inhibition diameter for the WT *ppm1* control, no gene control and the *ppm1* mutants. Data for DT3017 complemented with the WT *ppm1* and no gene controls are also provided. Strains were plated on DN agar and incubated at 30 °C for 48 hours. Shown are the averages of 4 replicates with SEM. The paper used to administer each antibiotic has a diameter of 5 mm and is shown as the dotted line threshold. The amount antibiotic used in µg is shown in brackets in the legend

Table A8.1: Introduction of mutant alleles into J1929 had no effect on Φ C31 phage infection titres. Phage were plated out on DN agar and then SN agar containing spores was added to the top with the plates incubated at 30 °C for 18 hours. The average titre is shown \pm SEM from 4 biological replicates. 0.1 ml of a 10^{-6} phage stock dilution was used to obtain countable plaques for phage sensitive strains. Strains that showed no plaques at the lowest phage stock dilution tested (10^{-1}) are represented as having a PFU/ml $< 1 \times 10^2$.

Strain	Titre (PFU/ml)
J1929 + WT	$(1.75 \pm 0.09) \times 10^8$
J1929	$(1.30 \pm 0.09) \times 10^8$
J1929 + Δ 42	$(1.47 \pm 0.13) \times 10^8$
J1929 + D57A	$(2.05 \pm 0.10) \times 10^8$
J1929 + R82A	$(2.53 \pm 0.19) \times 10^8$
J1929 + D111A	$(2.65 \pm 0.06) \times 10^8$
J1929 + D113A	$(2.77 \pm 0.13) \times 10^8$
J1929 + H116D	$(1.50 \pm 0.04) \times 10^8$
J1929 + R138A	$(1.10 \pm 0.13) \times 10^8$
J1929 + G143V	$(1.41 \pm 0.41) \times 10^8$
J1929 + S163L	$(2.08 \pm 0.08) \times 10^8$
J1929 + R226A	$(2.05 \pm 0.19) \times 10^8$

8.3 Chapter 5 appendix

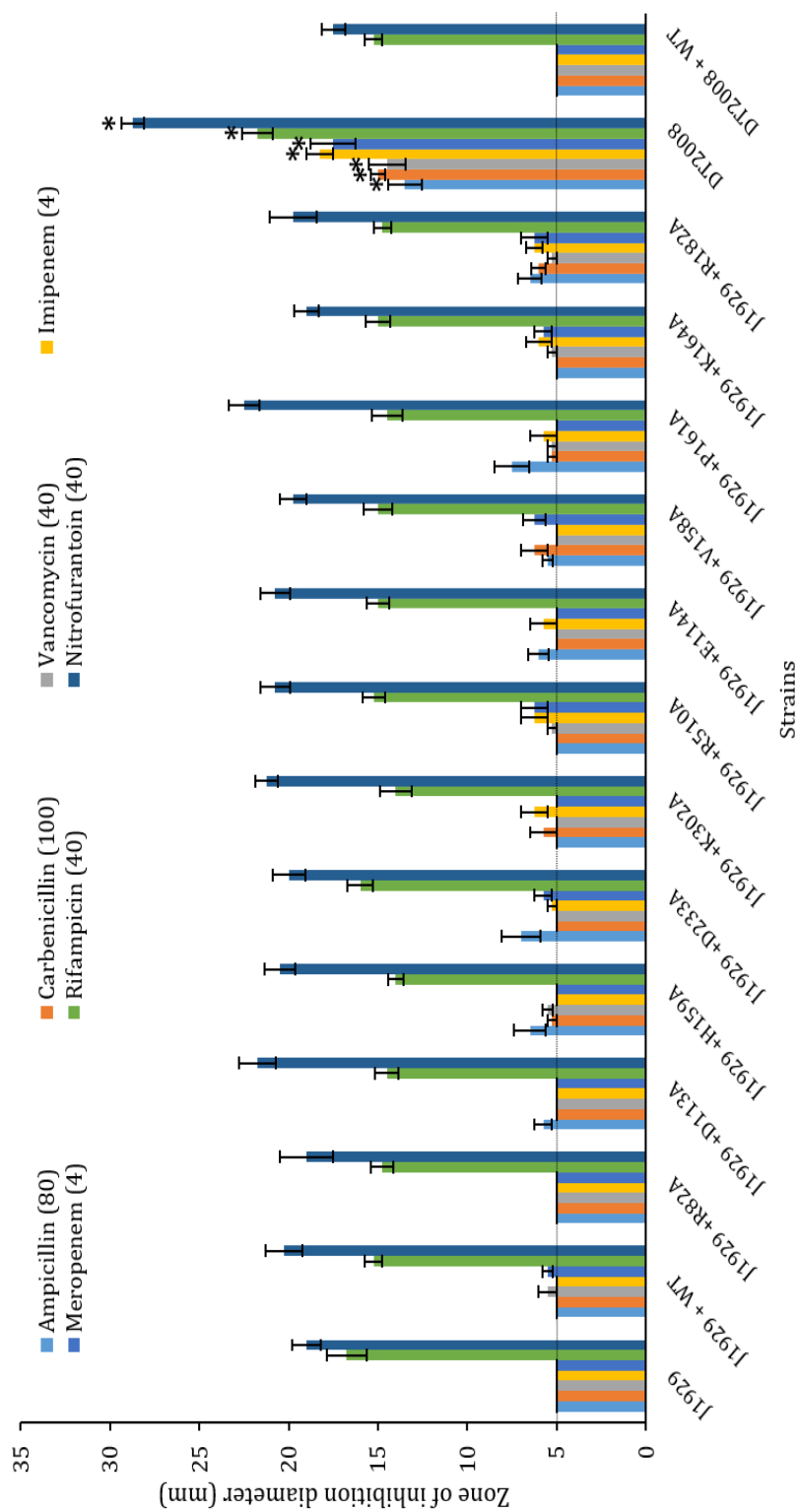


Figure A8.3: Introduced *pmt* alleles have no effect on the antibiotic sensitivity profile of the J1929 parent strain. Antibiotic sensitivity was quantified by measuring the zone of inhibition diameter for the DT2008 strains with WT *pmt* control, no *pmt* control and the *pmt* mutants. Strains were plated on DN agar and incubated at 30 °C for 48 hours. Shown are the averages of 4 biological replicates with SEM. The paper used to administer each antibiotic has a diameter of 5 mm and is shown as the dotted line threshold. The amount of antibiotic used in µg is shown in brackets in the legend.

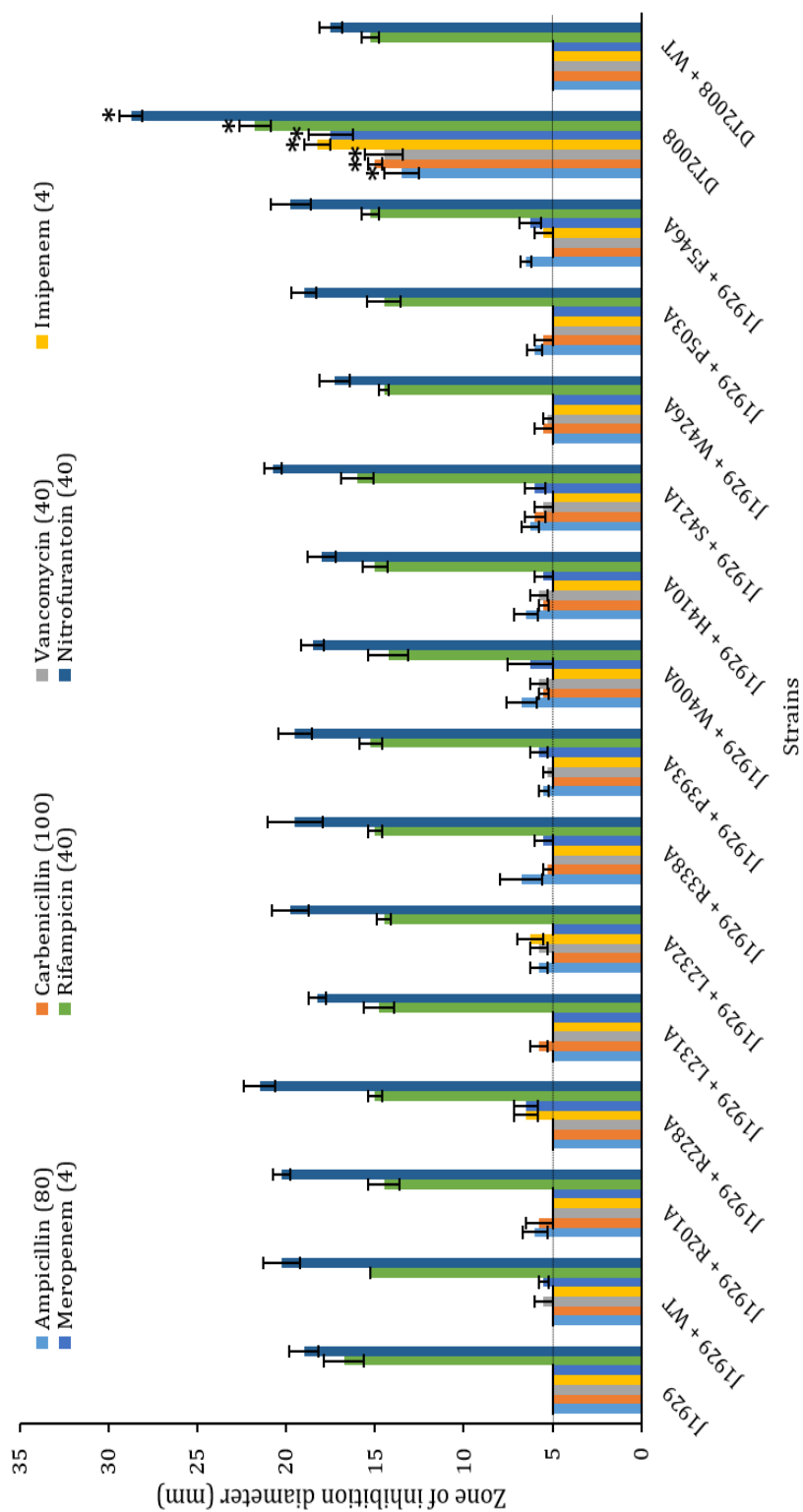


Figure A8.4: Introduced *pmt* alleles have no effect on the antibiotic sensitivity profile of the J1929 parent strain.

Antibiotic sensitivity was quantified by measuring the zone of inhibition diameter for the DT2008 strains with WT *pmt* control, no *pmt* control and the *pmt* mutants. Strains were plated on DN agar and incubated at 30 °C for 48 hours. Shown are the averages of 4 biological replicates with SEM. The paper used to administer each antibiotic has a diameter of 5 mm and is shown as the dotted line threshold. The amount of antibiotic used in μg is shown in brackets in the legend.

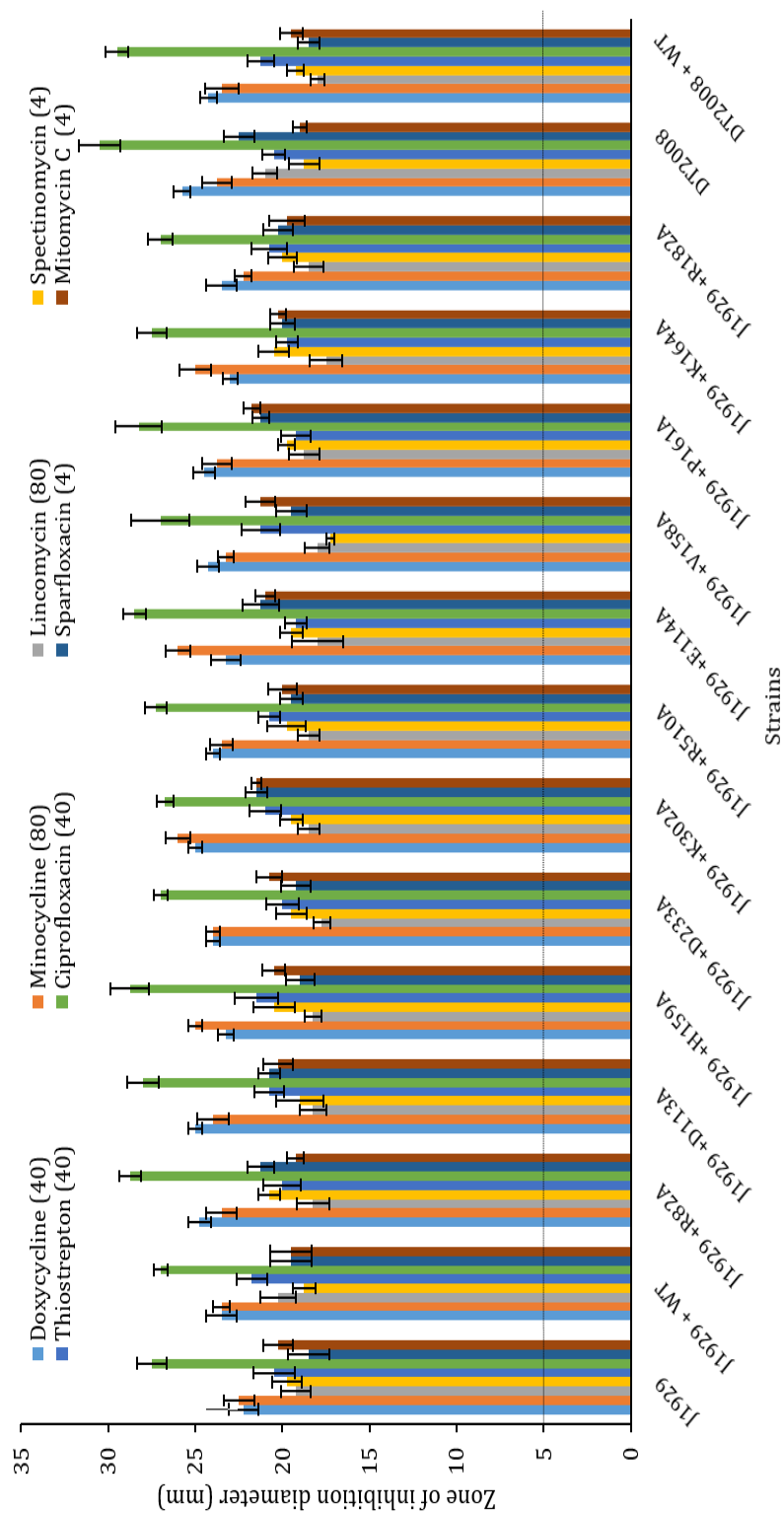


Figure A8.5: Introduced *pmt* alleles have no effect on the antibiotic sensitivity profile of the J1929 parent strain.

Antibiotic sensitivity was quantified by measuring the zone of inhibition diameter for the DT2008 strains with WT *pmt* control, no *pmt* control and the *pmt* mutants. Strains were plated on DN agar and incubated at 30 °C for 48 hours. Shown are the averages of 4 biological replicates with SEM. The paper used to administer each antibiotic has a diameter of 5 mm and is shown as the dotted line threshold. The amount of antibiotic used in μg is shown in brackets in the

Legend

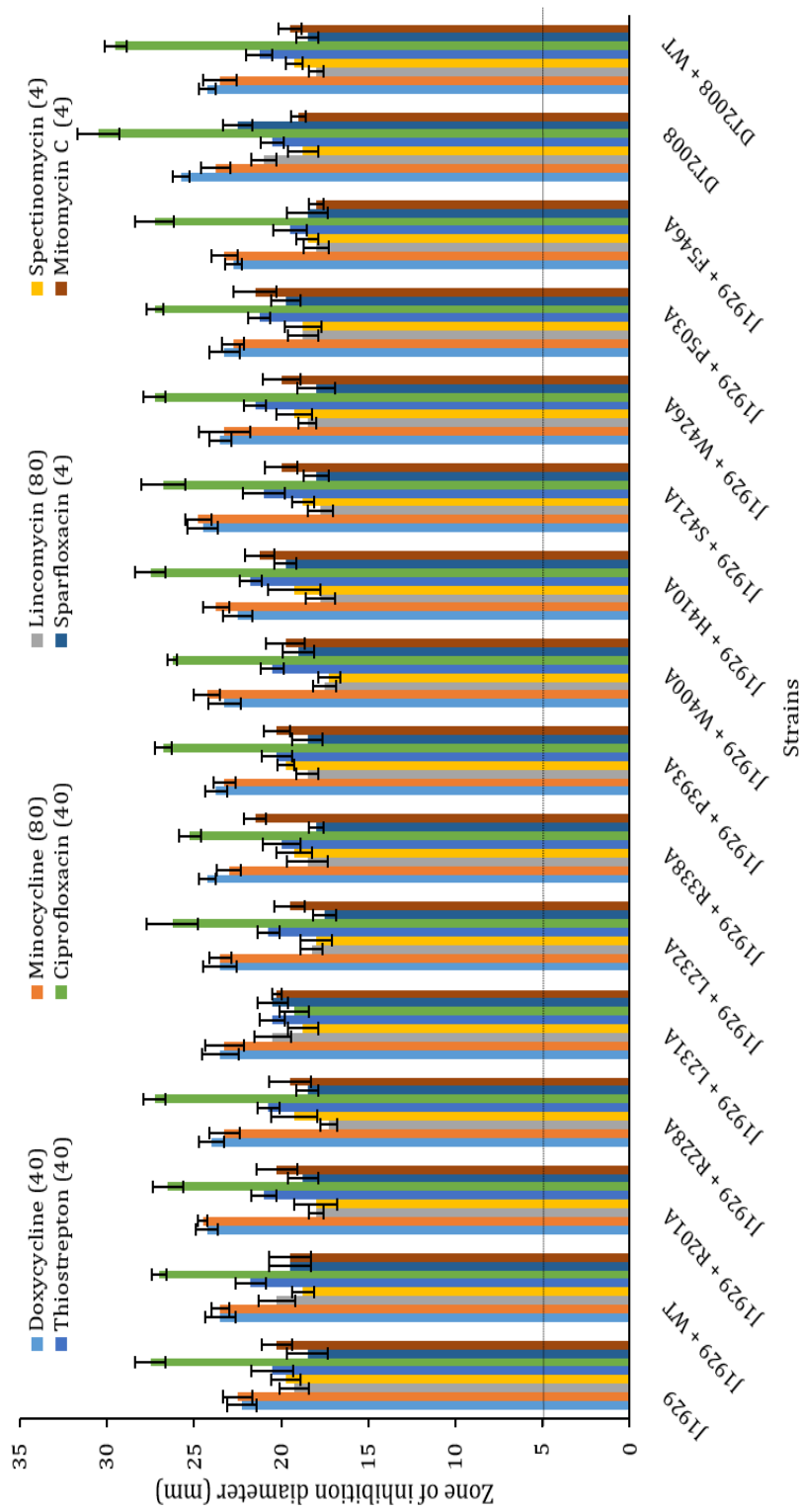


Figure A8.6: Introduced *pmt* alleles have no effect on the antibiotic sensitivity profile of the J1929 parent strain. Antibiotic sensitivity was quantified by measuring the zone of inhibition diameter for the DT2008 strains with WT *pmt* control, no *pmt* control and the *pmt* mutants. Strains were plated on DN agar and incubated at 30 °C for 48 hours. Shown are the averages of 4 biological replicates with SEM. The paper used to administer each antibiotic has a diameter of 5 mm and is shown as the dotted line threshold. The amount of antibiotic used in μg is shown in brackets in the legend.

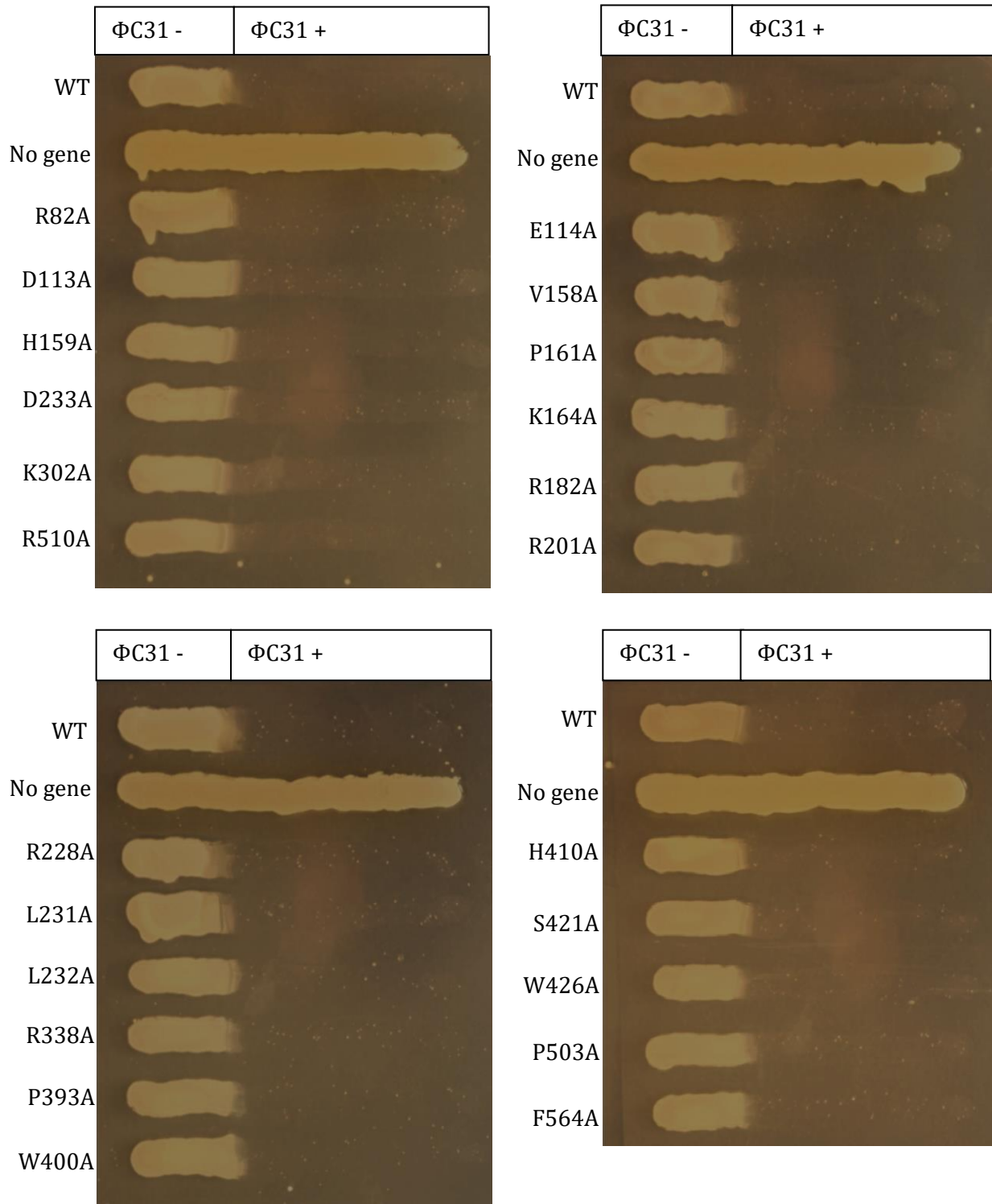


Figure A8.7: All J1929 strains are vulnerable to Φ C31 $c\Delta 25$ phage infection. Phage were plated out on a portion of DN agar and then spores streaked from the phage absent region to the phage present region. Plates were incubated at 30 °C for 48 hours.

Table A8.2: Introduced *pmt* alleles have no effect on the phage sensitivity J1929 parent strain. Φ C31 $c\Delta 25$ Phage were plated out on DN agar and then SN agar containing spores was added to the top with the plates incubated at 30 °C for 18 hours. The average titre is shown \pm SEM from 4 biological replicates. 0.1 ml of a 10^{-6} phage stock dilution was used to obtain countable plaques.

Strain	Titre (PFU/ml)
J1929	$(3.17 \pm 0.23) \times 10^8$
J1929 + WT	$(3.47 \pm 0.37) \times 10^8$
J1929 + R82A	$(3.40 \pm 0.36) \times 10^8$
J1929 + D113A	$(2.43 \pm 0.22) \times 10^8$
J1929 + H159A	$(3.90 \pm 0.30) \times 10^8$
J1929 + D233A	$(3.15 \pm 0.34) \times 10^8$
J1929 + K302A	$(2.92 \pm 0.49) \times 10^8$
J1929 + R510A	$(2.30 \pm 0.20) \times 10^8$
J1929 + E114A	$(1.85 \pm 0.17) \times 10^8$
J1929 + V158A	$(3.25 \pm 0.27) \times 10^8$
J1929 + P161A	$(2.42 \pm 0.18) \times 10^8$
J1929 + K164A	$(3.50 \pm 0.25) \times 10^8$
J1929 + R182A	$(3.00 \pm 0.37) \times 10^8$
J1929 + R201A	$(4.45 \pm 0.28) \times 10^8$
J1929 + R228A	$(3.10 \pm 0.29) \times 10^8$
J1929 + L231A	$(3.25 \pm 0.41) \times 10^8$
J1929 + L232A	$(4.05 \pm 0.21) \times 10^8$
J1929 + R335A	$(2.40 \pm 0.19) \times 10^8$
J1929 + P393A	$(3.70 \pm 0.25) \times 10^8$
J1929 + W400A	$(3.65 \pm 0.13) \times 10^8$
J1929 + H410A	$(0.22 \pm 0.12) \times 10^8$
J1929 + S421A	$(3.95 \pm 0.26) \times 10^8$
J1929 + W426A	$(2.98 \pm 0.22) \times 10^8$
J1929 + P503A	$(4.56 \pm 0.24) \times 10^8$
J1929 + F564A	$(2.60 \pm 0.19) \times 10^8$

8.4 Chapter 6 appendix

Table A8.3: Presence of the Strep Tag II on either termini does not affect the ability of *pmt* alleles to complement DT2008. Φ C31 Δ 25 phage were plated out on DN agar and then SN agar containing spores was added to the top with the plates incubated at 30 °C for 18 hours. The average titre is shown \pm SEM from 4 biological replicates. 0.1 ml of a 10^{-6} phage stock dilution was used to obtain countable plaques for phage sensitive strains. Strains that showed no plaques at the lowest phage stock dilution tested (10^{-1}) are represented as having a PFU/ml $< 1 \times 10^2$.

Strain	C-terminal Strep Tag II Titre (PFU/ml)	N-terminal Strep Tag II Titre (PFU/ml)
DT2008	$< 1 \times 10^2$	$< 1 \times 10^2$
DT2008 + WT	$(2.68 \pm 0.18) \times 10^8$	$(2.20 \pm 0.69) \times 10^8$
DT2008 + R82A	$< 1 \times 10^2$	$< 1 \times 10^2$
DT2008 + D113A	$< 1 \times 10^2$	$< 1 \times 10^2$
DT2008 + H159A	$< 1 \times 10^2$	$< 1 \times 10^2$
DT2008 + D233A	$< 1 \times 10^2$	$< 1 \times 10^2$
DT2008 + K302A	$< 1 \times 10^2$	$< 1 \times 10^2$
DT2008 + R510A	$< 1 \times 10^2$	$< 1 \times 10^2$
DT2008 + P160A	$(2.70 \pm 0.25) \times 10^8$	$(2.53 \pm 0.27) \times 10^8$
DT2008 + K164A	$(2.16 \pm 0.17) \times 10^8$	$(2.16 \pm 0.14) \times 10^8$
DT2008 + R228A	$(3.05 \pm 0.20) \times 10^8$	$(3.10 \pm 0.25) \times 10^8$
DT2008 + L231A	$(2.58 \pm 0.23) \times 10^8$	$(3.40 \pm 0.21) \times 10^8$
DT2008 + R335A	$(3.35 \pm 0.37) \times 10^8$	$(2.70 \pm 0.23) \times 10^8$
DT2008 + S421A	$(3.64 \pm 0.32) \times 10^8$	$(3.20 \pm 0.18) \times 10^8$

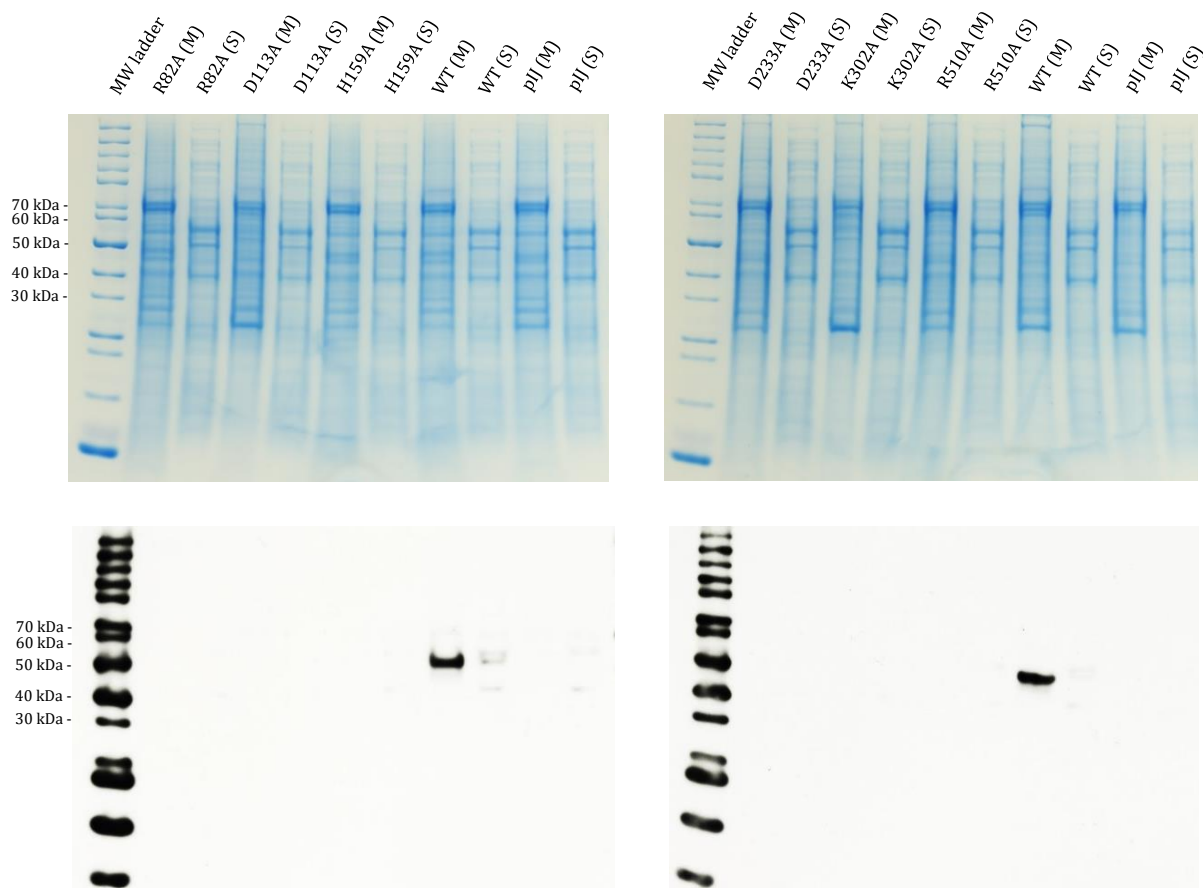


Figure A8.8: C-terminal Strep II tagged non-complementing Pmt mutants are absent in DT2008 membrane fractions. Membrane and soluble fraction samples were first loaded onto a 12 % SDS-PAGE gel which was run and stained to ensure protein concentrations of samples were consistent. After transfer of proteins from an SDS-PAGE gel to a PVDF membrane and subsequent wash steps, the membrane was incubated with Strep Tag II Antibody HRP Conjugate, substrate added and X-ray film developed. pIJ refers to the empty pIJ10257 control and WT to the Pmt WT complemented strain control.

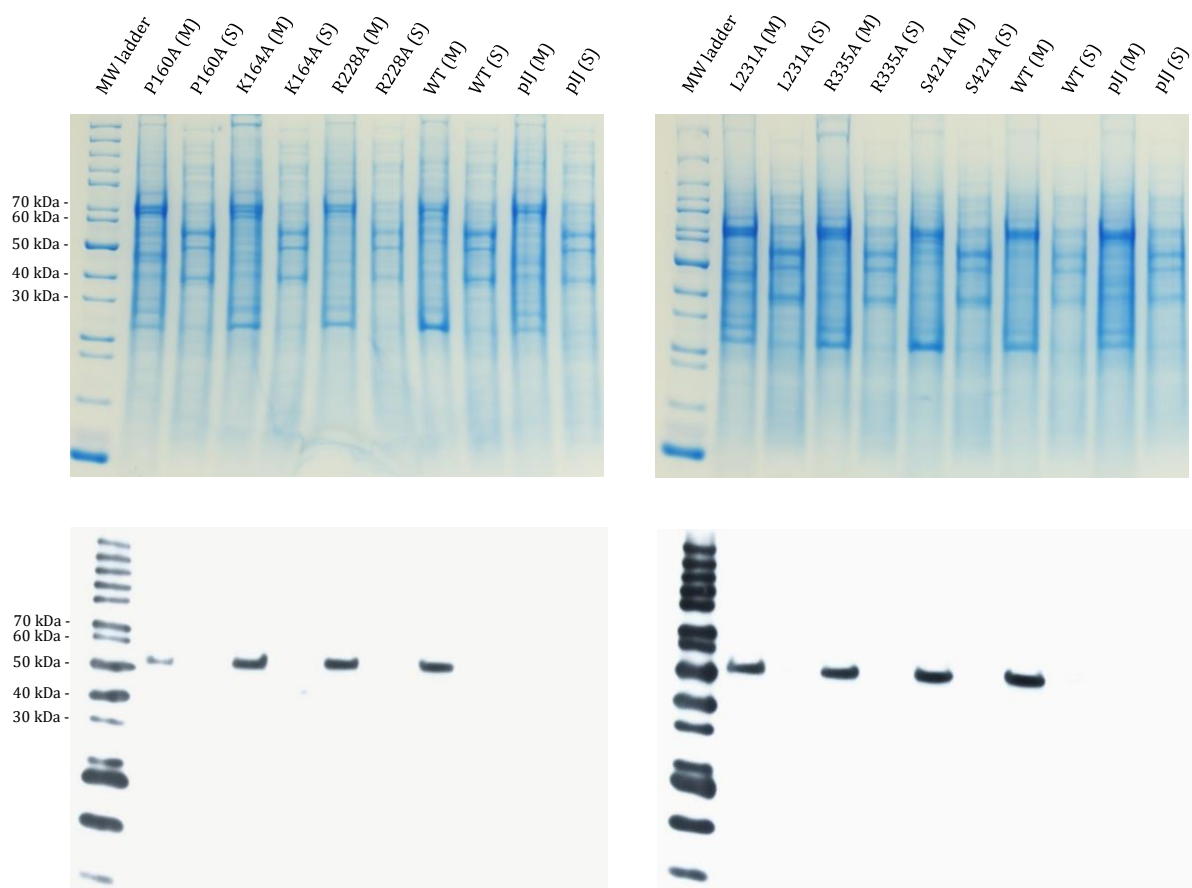


Figure A8.9: C-terminal Strep II tagged complementing Pmt mutants are present in DT2008 membrane fractions. Membrane and soluble fraction samples were first loaded onto a 12 % SDS-PAGE gel which was run and stained to ensure protein concentrations of samples were consistent. After transfer of proteins from an SDS-PAGE gel to a PVDF membrane and subsequent wash steps, the membrane was incubated with Strep Tag II Antibody HRP Conjugate, substrate added and X-ray film developed. pIJ refers to the empty pIJ10257 control and WT to the Pmt WT complemented strain control.

References

- Akasaka-Manyá K, Manyá H, Nakajima A, Kawakita M, Endo T (2006). Physical and functional association of human protein O-mannosyltransferases 1 and 2. *J Biol Chem.* 281, 19339-19345.
- Angert ER (2005). Alternatives to binary fission in bacteria. *Nat Rev Microbiol.* 2005 3, 214-224.
- Bai L, Kovach A, You Q, Kenny A, Li H (2019). Structure of the eukaryotic protein O-mannosyltransferase Pmt1-Pmt2 complex. *Nat Struct Mol Biol.* 26, 704-711.
- Baulard AR, Gurcha SS, Engohang-Ndong J, Gouffi K, Locht C, Besra GS (2003). *In vivo* interaction between the polyprenol phosphate mannan synthase Ppm1 and the integral membrane protein Ppm2 from *Mycobacterium smegmatis* revealed by a bacterial two-hybrid system. *J Biol Chem.* 278, 2242-2248.
- Becker SH, Darwin KH (2016). Bacterial Proteasomes: Mechanistic and Functional Insights. *Microbiol Mol Biol Rev.* 81, 1.
- Bentley SD, Chater KF, Cerdeño-Tárraga AM, Challis GL, Thomson NR, James KD, Harris DE, Quail MA, Kieser H, Harper D *et al.*, (2002). Complete genome sequence of the model actinomycete *Streptomyces coelicolor* A3 (2). *Nature.* 417, 141-147.
- Bibb M (1996). The regulation of antibiotic production in *Streptomyces coelicolor* A3 (2). *Microbiology.* 142, 1335-1344.
- Bedford DJ, Laity C, Buttner MJ (1995). Two genes involved in the phase-variable phi C31 resistance mechanism of *Streptomyces coelicolor* A3(2). *J Bacteriol.* 177, 4681-4689.
- Bortolin RC, Gasparotto J, Vargas AR, da Silva Morrone M, Kunzler A, Henkin BS, Chaves PR, Roncato S, Gelain DP, Moreira JCF (2017). Effects of Freeze-Thaw and Storage on Enzymatic Activities, Protein Oxidative Damage, and Immunocontent of the Blood, Liver, and Brain of Rats. *Biopreserv Biobank.* 15, 182-190.
- Buurman ET, Westwater C, Hube B, Brown AJ, Odds FC, Gow NA (1998). Molecular analysis of CaMnt1p, a mannosyl transferase important for adhesion and virulence of *Candida albicans*. *Proc Natl Acad Sci U S A.* 95, 7670-7675.
- Carter P, Wells JA (1988). Dissecting the catalytic triad of a serine protease. *Nature.* 332, 564-568.
- Carvalho SB, Botelho HM, Leal SS, Cardoso I, Fritz G, Gomes CM (2013). Intrinsically Disordered and Aggregation Prone Regions Underlie β -Aggregation in S100 Proteins. *PLoS One.* 8, e76629.

- Charlop-Powers Z, Owen JG, Reddy BV, Ternei MA, Guimarães DO, de Frias UA, Pupo MT, Seepe P, Feng Z, Brady SF (2015). Global biogeographic sampling of bacterial secondary metabolism. *Elife*. 19,4.
- Chen FK, Wang K, Stewart J, Belas R (2006). Induction of multiple prophages from a marine bacterium: a genomic approach. *Appl. Environ. Microbiol.* 72, 4995-5001.
- Chinenova TA, Mkrtumian NM, Lomovskaya ND (1982). Genetic characteristics of a new phage resistance trait in *Streptomyces coelicolor* A3(2). *Genetika*. 18, 1945-1952.
- Choulet F, Gallois A, Aigle B, Mangenot S, Gerbaud C, Truong C, Francou F, Borges F, Fourrier C, Guérineau M, Decaris B, Barbe V *et al.*, (2006). Intraspecific variability of the terminal inverted repeats of the linear chromosome of *Streptomyces ambofaciens*. *J Bacteriol.* 188, 6599-6610.
- Clark-Curtiss JE, Jacobs WR, Docherty MA, Ritchie LR, Curtiss R 3rd. (1985). Molecular analysis of DNA and construction of genomic libraries of *Mycobacterium leprae*. *J Bacteriol.* 161, 1093-102.
- Cole ST, Brosch R, Parkhill J, Garnier T, Churcher C, Harris D, Gordon SV, Eiglmeier K, Gas S, Barry CE, Tekaia F *et al.*, (1998). Deciphering the biology of *Mycobacterium tuberculosis* from the complete genome sequence. *Nature*. 393, 537-544.
- Colussi PA, Taron CH, Mack J, Orlean P (1997). Human and *Saccharomyces cerevisiae* dolichyl phosphate mannose synthases represent two classes of the enzymes, but both function in *Schizosaccharomyces pombe*. *Proc Natl Acad Sci. USA*. 94, 7873-7878.
- Córdova-Dávalos LE, Espitia C, González-Cerón G, Arreguín-Espinosa R, Soberón-Chávez G, Servín-González L (2014). Lipoprotein N-acyl transferase (Lnt1) is dispensable for protein O-mannosylation by *Streptomyces coelicolor*. *FEMS Microbiol Lett.* 350, 72-82.
- Cowlshaw DA, Smith MCM (2001). Glycosylation of a *Streptomyces coelicolor* A3(2) cell envelope protein is required for infection by bacteriophage fC31. *Mol Microbiol.* 41, 601-610.
- Cowlshaw DA, Smith MCM (2002). A gene encoding a homologue of dolichol phosphate-b-d-mannose synthase is required for infection of *Streptomyces coelicolor* A3(2) by Phage fC31. *J Bacteriol.* 184, 6081-6083.
- Dobos KM, Swiderek K, Khoo KH, Brennan PJ, Belisle JT (1995). Evidence for glycosylation sites on the 45-kilodalton glycoprotein of *Mycobacterium tuberculosis*. *Infect Immun.* 63, 2846-2853.
- Dube PB, Holman NDM, Wilkinson AJ, Smith MCM, Tosin M (2019) – Paper in preparation.
- Espitia C, Mancilla R (1989). Identification, isolation and partial characterization of *Mycobacterium tuberculosis* glycoprotein antigens. *Clin Exp Immunol.* 77, 378-383.

- Fleming A (1945). Penicillin. Nobel Lecture, 84-93.
- Fogg PCM, Younger E, Fernando BD, Khaleel T, Stark WM, Smith MCM (2018). Recombination directionality factor gp3 binds ϕ C31 integrase via the zinc domain, potentially affecting the trajectory of the coiled-coil motif. *Nucleic Acids Res.* 46, 1308-1320.
- Gandini R, Reichenbach T, Tan TC, Divne C (2017). Structural basis for dolichylphosphate mannose biosynthesis. *Nat Commun.* 8, 120.
- Gentsch M, Tanner W (1996). The PMT gene family: Protein O-glycosylation in *Saccharomyces cerevisiae* is vital. *Embo J.* 15, 5752-5759.
- Gibson KJ, Eggeling L, Maughan WN, Krumbach K, Gurcha SS, Nigou J, et al., (2003). Disruption of Cg-Ppm1, a polyprenyl monophosphomannose synthase, and the generation of lipoglycan-less mutants in *Corynebacterium glutamicum*. *J Biol Chem.* 278, 40842-40850.
- Girrbach V, Zeller T, Priesmeier M, Strahl-Bolsinger S (2000). Structure-function analysis of the dolichyl phosphate-mannose: protein O-mannosyltransferase ScPmt1p. *J Biol Chem.* 275, 19288-19296.
- Godfrey C, Clement E, Mein R, Brockington M, Smith J, Talim B, Straub V, Robb S, Quinlivan R, Feng L *et al.*, (2007). Refining genotype phenotype correlations in muscular dystrophies with defective glycosylation of dystroglycan. *Brain.* 130, 2725-2735.
- González-Cerón G, Miranda-Olivares OJ, Servín-González L (2009). Characterization of the methyl-specific restriction system of *Streptomyces coelicolor* A3 (2) and of the role played by laterally acquired nucleases. *FEMS Microbiol Lett.* 301, 35-43.
- Gregory RB (1988). The Influence of Glycerol on Hydrogen Isotope Exchange in Lysozyme. *Biopolymers* 27, 1699-1709.
- Gurcha SS, Baulard AR, Kremer L, Loch C, Moody DB, Muhlecker W, Costello CE, Crick DC, Brennan PJ, Besra GS (2002). Ppm1, a novel polyprenol monophosphomannose synthase from *Mycobacterium tuberculosis*. *Biochem J.* 365, 441-450.
- Haines N, Seabrooke S, Stewart BA (2007). Dystroglycan and protein Omannosyltransferases 1 and 2 are required to maintain integrity of *Drosophila* larval muscles. *Mol Biol Cell.* 18, 4721-4730.
- Hanahan D (1983). Studies on transformation of *Escherichia coli* with plasmids. *J Mol Biol.* 166, 557-80.
- Harty C, Strahl S, Romisch K (2001). O-Mannosylation protects mutant alphafactor precursor from endoplasmic reticulum-associated degradation. *Mol Biol Cell.* 12, 1093-1101.

- Haselbeck A, Tanner W (1983). O-glycosylation in *Saccharomyces cerevisiae* is initiated at the endoplasmic reticulum. *FEBS Lett.* 158, 335–338.
- Hong P, Koza S, Bouvier ESP (2012). Size-Exclusion Chromatography for the Analysis of Protein Biotherapeutics and their Aggregates. *J Liq Chromatogr Relat Technol.* 35, 2923–2950.
- Horn C, Namane A, Pescher P, Rivière M, Romain F, Puzo G, Bâzu O, Marchal G (1999). Decreased capacity of recombinant 45/47-kDa molecules (Apa) of *Mycobacterium tuberculosis* to stimulate T lymphocyte responses related to changes in their mannosylation pattern. *J Biol Chem.* 274, 32023-32030.
- Howlett R, Anttonen K, Read N, Smith MCM (2018a). Disruption of the GDP-mannose synthesis pathway in *Streptomyces coelicolor* results in antibiotic hyper-susceptible phenotypes. *Microbiology.* 164, 614-624.
- Howlett R, Read N, Varghese A, Kershaw C, Hancock Y, Smith MCM (2018b). *Streptomyces coelicolor* strains lacking polyprenol phosphate mannose synthase and protein O-mannosyl transferase are hyper-susceptible to multiple antibiotics. *Microbiology.* 164, 369-382.
- Ichimiya T, Manya H, Ohmae Y, Yoshida H, Takahashi K, Ueda R, Endo T, Nishihara S. (2004). The twisted abdomen phenotype of *Drosophila* POMT1 and POMT2 mutants coincides with their heterophilic protein Omannosyltransferase activity. *J Biol Chem.* 279, 42638–42647.
- Imbach T, Schenk B, Schollen E, Burda P, Stutz A, Grunewald S, Bailie NM, King MD, Jaeken J, Matthijs G, Berger EG, Aebi M, Hennet T (2000). Deficiency of dolichol-phosphate-mannose synthase-1 causes congenital disorder of glycosylation type Ie. *J Clin Invest.* 105, 233-239.
- Jordan S, Hutchings MI, Mascher T (2008). Cell envelope stress response in Gram-positive bacteria. *FEMS Microbiol Rev.* 32, 107-146.
- Jurado LA, Coloma A, Cruces J (1999). Identification of a human homolog of the *Drosophila* rotated abdomen gene (POMT1) encoding a putative protein O-mannosyltransferase, and assignment to human chromosome 9q34.1. *Genomics.* 58, 171-180.
- Keenan T, Dowle A, Bates R, Smith MCM (2019). Characterization of the *Streptomyces coelicolor* glycoproteome reveals glycoproteins important for cell wall biogenesis. 10, e01092-19.
- Kelley LA, Mezulis S, Yates CM, Wass MN, Sternberg MJ (2015). The Phyre2 web portal for protein modeling, prediction and analysis. *Nat Protoc.* 10, 845-858.
- Kieser T, Bibb MJ, Buttner MJ, Chater KF, Hopwood DA (2000). *Practical Streptomyces Genetics*. Norwich: The John Innes Foundation.

- Kim HJ, Brennan PJ, Heaslip D, Udey MC, Modlin RL, Belisle JT (2015). Carbohydrate-dependent binding of langerin to SodC, a cell wall glycoprotein of *Mycobacterium leprae*. *J Bacteriol.* 197, 615-25.
- Kobler L, Schwertfirm G, Schmieger H, Bolotin A, Sladkova I (1991). Construction and transduction of a shuttle vector bearing the cos site of Streptomyces phage phi C31 and determination of its cohesive ends. *FEMS Microbiol Lett.* 62, 347-53.
- Kornfeld R, Kornfeld S (1985). Assembly of asparagine-linked oligosaccharides. *Annu Rev Biochem.* 54, 631-64.
- Kuhstoss S, Richardson MA, Rao RN (1991). Plasmid cloning vectors that integrate site-specifically in Streptomyces spp. *Gene.* 97, 143-146.
- Lairson LL, Henrissat B, Davies GJ, Withers SG (2008). Glycosyltransferases: structures, functions, and mechanisms. *Annu Rev Biochem.* 77, 521-555.
- Lee YN, Chen LK, Ma HC, Yang HH, Li HP, Lo SY (2005). Thermal aggregation of SARS-CoV membrane protein. *J Virol Methods.* 129, 152-61.
- Lefeber DJ, Schönberger J, Morava E, Guillard M, Huyben KM, Verrijp K, Grafako O *et al.*, (2009). Deficiency of Dol-P-Man synthase subunit DPM3 bridges the congenital disorders of glycosylation with the dystroglycanopathies. *Am J Hum Genet.* 85, 76-86.
- Li S, Wang J, Li X, Yin S, Wang W, Yang K (2015). Genome-wide identification and evaluation of constitutive promoters in streptomycetes. *Microb Cell Fact.* 14,172.
- Li Z, Deguchi T, Yasuda M, Kawamura T, Kanematsu E, Nishino Y, Ishihara S, Kawada Y. (1998). Alteration in the GyrA subunit of DNA gyrase and the ParC subunit of DNA topoisomerase IV in quinolone-resistant clinical isolates of *Staphylococcus epidermidis*. *Antimicrob. Agents Chemother.* 42, 3293-3295.
- Lin G, Hu G, Tsu C, Kunes YZ, Li H, Dick L, Parsons T, Li P, Chen Z, Zwickl P, Weich N, Nathan C (2006). *Mycobacterium tuberculosis* prcBA genes encode a gated proteasome with broad oligopeptide specificity. *Mol Microbiol.* 59, 1405-1416.
- Liu CF, Tonini L, Malaga W, Beau M, Stella A, Bouyssié D, Jackson MC, Nigou J, Puzo G, Guilhot C, Burlet-Schiltz O, Rivière M (2013). Bacterial protein-O-mannosylating enzyme is crucial for virulence of *Mycobacterium tuberculosis*. *Proc Natl Acad Sci U S A.* 110, 6560-6565.
- Lizak C, Gerber S, Michaud G, Schubert M, Fan YY, Bucher M, Darbre T, Aebi M, Reymond JL, Locher KP (2013). Unexpected reactivity and mechanism of carboxamide activation in bacterial N-linked protein glycosylation. *Nat Commun.* 4, 2627.
- Lombard V, Golaconda Ramulu H, Drula E, Coutinho PM, Henrissat B (2014). The Carbohydrate-active enzymes database (CAZy) in 2013. *Nucleic Acids Res* 42. D490-D495.

- Lommel M, Strahl S (2009). Protein O-mannosylation: conserved from bacteria to humans. *Glycobiology*. 19, 816-828.
- Lommel M, Schott A, Jank T, Hofmann V, Strahl S (2011). A conserved acidic motif is crucial for enzymatic activity of protein O-mannosyltransferases. *J Biol Chem*. 286, 39768-39775.
- Lomovskaya ND, Mkrtumian NM, Gostimskaya NL, Danilenko VN (1972). Characterization of Temperate Actinophage ϕ C31 Isolated from *Streptomyces coelicolor* A3(2). *J Virology*. 9, 258-262.
- Lomovskaya ND, Chater KF, Mkrtumian NM (1980). Genetics and molecular biology of *Streptomyces* bacteriophages. *Microbiol Rev*. 44, 206-229.
- Loria R, Kers J, Joshi M (2006). Evolution of plant pathogenicity in *Streptomyces*. *Annu Rev Phytopathol*. 44, 469-487.
- Lussier M, Sdicu AM, Bussey H (1999). The KTR and MNN1 mannosyltransferase families of *Saccharomyces cerevisiae*. *Biochim Biophys Acta*. 1426, 323-334.
- MacNeil DJ (1988) Characterization of a unique methyl-specific restriction system in *Streptomyces avermitilis*. *J. Bacteriol*. 170, 5607-5612.
- Manya H, Chiba A, Yoshida A, Wang X, Chiba Y, Jigami Y, Margolis RU, Endo T (2004). Demonstration of mammalian protein O-mannosyltransferase activity: Coexpression of POMT1 and POMT2 required for enzymatic activity. *Proc Natl Acad Sci USA*. 101, 500-505.
- Macfarlane RG (1984). *Alexander Fleming: The Man and the Myth*. Harvard University Press.
- McNicholas S, Potterton E, Wilson KS, Noble ME (2011). Presenting your structures: the CCP4mg molecular-graphics software. *Acta Cryst.*, D67, 386-394
- Mescher MF, Strominger JL (1976). Purification and characterization of a prokaryotic glycoprotein from the cell envelope of *Halobacterium salinarium*. *J Biol Chem*. 251, 2005-2014.
- Michell SL, Whelan AO, Wheeler PR, Panico M, Easton RL, Etienne AT, Haslam SM, Dell A, Morris HR, Reason AJ, Herrmann JL, Young DB, Hewinson RG (2003). The MPB83 antigen from *Mycobacterium bovis* contains O-linked mannose and (1-->3)-mannobiose moieties. *J Biol Chem*. 278, 16423-16432.
- Milde-Langosch K, Karn T, Schmidt M, Eulenburg C, Oliveira-Ferrer L, Wirtz RM, Schumacher U, Witzel I, Schütze D, Müller V (2014). Prognostic relevance of glycosylation-associated genes in breast cancer. *Breast Cancer Res Treat*. 145, 295-305.

- Mishra R, Bhat R, Seckler R (2007). Chemical chaperone mediated protein folding: Stabilization of P22 tail spike folding intermediates by glycerol. *Biol Chem.* 388, 797–804.
- Morita YS, Sena CB, Waller RF, Kurokawa K, Sernee MF, Nakatani F, Haites RE, Billman-Jacobe H, McConville MJ, Maeda Y, Kinoshita T (2006). PimE is a polyprenol-phosphate-mannose-dependent mannosyltransferase that transfers the fifth mannose of phosphatidylinositol mannoside in mycobacteria. *J Biol Chem.* 281, 25143-25155.
- Mouyna I, Kniemeyer O, Jank T, Loussert C, Mellado E, Aimanianda V, et al., (2010). Members of protein O-mannosyltransferase family in *Aspergillus fumigatus* differentially affect growth, morphogenesis and viability. *Molecular Microbiol.* 76, 1205–1221.
- Murray CW, Rees DC (2009). The rise of fragment-based drug discovery. *Nat Chem.* 1, 187-192.
- Nagy I, Tamura T, Vanderleyden J, Baumeister W, De Mot R (1998). The 20S proteasome of *Streptomyces coelicolor*. *J Bacteriol.* 180, 5448-5453.
- Nakatsukasa K, Okada S, Umebayashi K, Fukuda R, Nishikawa S, Endo T (2004). Roles of O-mannosylation of aberrant proteins in reduction of the load for endoplasmic reticulum chaperones in yeast. *J Biol Chem.* 279, 49762–49772.
- Napiórkowska M, Boilevin J, Darbre T, Reymond JL, Locher KP (2018). Structure of bacterial oligosaccharyltransferase PglB bound to a reactive LLO and an inhibitory peptide. *Sci Rep.* 8, 16297.
- O'Neil (2014) Review on antimicrobial resistance: Tackling a crisis for the health and wealth of nations.
- Olsen JV, Macek B, Lange O, Makarov A, Horning S, Mann M (2007). Higher-energy C-trap dissociation for peptide modification analysis. *Nat Methods.* 4, 709-712.
- Olson GM, Fox DS, Wang P, Alspaugh JA, Buchanan KL (2007). Role of protein O-mannosyltransferase Pmt4 in the morphogenesis and virulence of *Cryptococcus neoformans*. *Eukaryot Cell.* 6, 222–234.
- Omura S, Ikeda H, Ishikawa J, Hanamoto A, Takahashi C, Shinose M, Takahashi Y, Horikawa H, Nakazawa H, Osonoe T, Kikuchi H, Shiba T, Sakaki Y, Hattori M (2001). Genome sequence of an industrial microorganism *Streptomyces avermitilis*: deducing the ability of producing secondary metabolites. *Proc Natl Acad Sci U S A.* 98, 12215-12220.
- Orlean PC, Albright C, Robbins PW (1988). Cloning and sequencing of the yeast gene for dolichol phosphate mannose synthase, an essential protein. *J Biol Chem.* 263, 17499-17507.

- Orlean P (1990). Dolichol phosphate mannose synthase is required *in vivo* for glycosyl phosphatidylinositol membrane anchoring, O mannosylation, and N glycosylation of protein in *Saccharomyces cerevisiae*. *Mol Cell Biol.* 10, 5796-5805.
- Petrou VI, Herrera CM, Schultz KM, Clarke OB, Vendome J, Tomasek D, Banerjee S, Rajashankar KR, Belcher Dufresne M, Kloss B, Kloppmann E, Rost B, Klug CS, Trent MS *et al.*, (2016). Structures of aminoarabinose transferase ArnT suggest a molecular basis for lipid A glycosylation. *Science.* 351, 608-612.
- Prieu A, Almagor A, Yedgar S, Gavish B (1996). Glycerol decreases the volume and compressibility of protein interior. *Biochemistry.* 35, 2061-2066.
- Prill SK, Klinkert B, Timpel C, Gale CA, Schröppel K, Ernst JF (2005). PMT family of *Candida albicans*: five protein mannosyltransferase isoforms affect growth, morphogenesis and antifungal resistance. *Mol Microbiol.* 55, 546-60.
- Ragas A, Roussel L, Puzo G, Rivière M (2007). The Mycobacterium tuberculosis cell-surface glycoprotein apa as a potential adhesin to colonize target cells via the innate immune system pulmonary C-type lectin surfactant protein A. *J Biol Chem.* 282, 5133-5142.
- Rana AK, Singh A, Gurcha SS, Cox LR, Bhatt A, Besra GS (2012). Ppm1-encoded polyprenyl monophosphomannose synthase activity is essential for lipoglycan synthesis and survival in *mycobacteria*. *PLoS One.* 7, e48211.
- Read N, Howlett R, Smith MCM (2019). An operon encoding enzymes for synthesis of a putative extracellular carbohydrate attenuates acquired vancomycin resistance in *Streptomyces coelicolor*. *Microbiology.* 165, 208-223.
- Rice P, Longden I, Bleasby A (2000). EMBOSS: the European Molecular Biology Open Software Suite. *Trends Genet.* 16, 276-277.
- Romero PA, Lussier M, Veronneau S, Sdicu AM, Herscovics A, Bussey H (1999). Mnt2p and Mnt3p of *Saccharomyces cerevisiae* are members of the Mnn1p family of alpha-1,3 mannosyltransferases responsible for adding the terminal mannose residues of O-linked oligosaccharides. *Glycobiology.* 9, 1045-1051.
- Sagne C, Isambert MF, Henry JP and Gasnier B (1996). SDS-resistant aggregation of membrane proteins: application to the purification of the vesicular monoamine transporter. *Biochem J.* 316, 825-831.
- Sandbrook JEF, Maniatis T (1989). "Molecular cloning : a laboratory manual" in Cold Spring Harbor Lab. Press, Plainview, NY.
- Sartain MJ, Belisle JT (2009). N-Terminal clustering of the O-glycosylation sites in the *Mycobacterium tuberculosis* lipoprotein SodC. *Glycobiology.* 19, 38-51.

- Schlimpert S, Flärdh K, Buttner J (2016). Fluorescence Time-lapse Imaging of the Complete *S. venezuelae* Life Cycle Using a Microfluidic Device. *J Vis Exp.* 28, 53863.
- Shambaugh GE (1966). History of sulphonamides. *Arch Otolaryngol.* 83, 1– 2.
- Shematek EM, Braatz JA, Cabib E (1980). Biosynthesis of the yeast cell wall. I. Preparation and properties of beta-(1 leads to 3)glucan synthetase. *J Biol Chem.* 255, 888-894.
- Sievers F, Wilm A, Dineen D, Gibson TJ, Karplus K, Li W, Lopez R, McWilliam H, Remmert M, Söding J, Thompson JD, Higgins DG (2011). Fast, scalable generation of high-quality protein multiple sequence alignments using Clustal Omega. *Mol Syst Biol.* 11, 539.
- Smith MC, Burns RN, Wilson SE, Gregory MA (1999). The complete genome sequence of the *Streptomyces* temperate phage straight phiC31: evolutionary relationships to other viruses. *Nucleic Acids Res.* 27, 2145–2155.
- Smith CL, Powell KR (2000). Review of the sulfonamides and trimethoprim. *Pediatr Rev.* 21, 368-71.
- Smith GT, Sweredoski MJ, Hess S (2014). O-linked glycosylation sites profiling in *Mycobacterium tuberculosis* culture filtrate proteins. *J Proteomics.* 97, 296-306.
- Stetsenko A, Guskov A (2017). An Overview of the Top Ten Detergents Used for Membrane Protein Crystallization. *Crystals.* 7,19.
- Stevens VL (1995). Biosynthesis of glycosylphosphatidylinositol membrane anchors. *Biochem J.* 310, 361-370.
- Strahl-Bolsinger S, Tanner W (1991). Protein O-glycosylation in *Saccharomyces cerevisiae*. Purification and characterization of the dolichyl-phosphate-D-mannose-protein O-D-mannosyltransferase. *Eur J Biochem.* 196, 185-190.
- Strahl-Bolsinger S, Gentsch M, and Tanner W (1999). Protein O mannosylation. *Biochim Biophys Acta.* 1426, 297–307.
- Sumby P, Smith MC (2003). Phase variation in the phage growth limitation system of *Streptomyces coelicolor* A3(2). *J Bacteriol.* 185, 4558-4563.
- Taniguchi K, Kobayashi K, Saito K, Yamanouchi H, Ohnuma A, Hayashi YK, *et al.*, (2003). Worldwide distribution and broader clinical spectrum of muscle–eye–brain disease. *Hum Mol Genet.* 12, 527-534.
- Takahashi S, Sasaki T, Manya H, Chiba Y, Yoshida A, Mizuno M, Ishida H, Ito F, Inazu T, Kotani N *et al.* (2001). A new beta-1,2-Nacetylglucosaminyltransferase that may play a role in the biosynthesis of mammalian O-mannosyl glycans. *Glycobiology.* 11, 37-45.

- Travers KJ, Patil CK, Wodicka L, Lockhart DJ, Weissman JS, Walter P (2000). Functional and genomic analyses reveal an essential coordination between the unfolded protein response and ER-associated degradation. *Cell*. 101, 249–258.
- Trujillo ME, Goodfellow M (2003). Numerical phenetic classification of clinically significant aerobic sporoactinomycetes and related organisms. *Antonie Van Leeuwenhoek*. 84, 39-68.
- Urushibata Y, Ebisu S, Matsui I (2008). A thermostable dolichol phosphoryl mannose synthase responsible for glycoconjugate synthesis of the hyperthermophilic archaeon *Pyrococcus horikoshii*. *Extremophiles*. 12, 665-676.
- Vagenende V, Yap MG, Trout BL (2009). Mechanisms of protein stabilization and prevention of protein aggregation by glycerol. *Biochemistry*. 48, 11084-11096.
- Van Reeuwijk J, Janssen M, Van Den Elzen C, Beltran-Valero de Bernabe D, Sabatelli P, Merlini L, Boon M, Scheffer H, Brockington M, Muntoni F *et al.*, (2005). POMT2 mutations cause alpha-dystroglycan hypoglycosylation and Walker-Warburg syndrome. *J Med Genet*. 42, 907–912.
- Van Reeuwijk J, Maugendre S, Van Den Elzen C, Verrips A, Bertini E, Muntoni F, Merlini L, Scheffer H, Brunner HG, Guicheney P *et al.*, (2006). The expanding phenotype of POMT1 mutations: From Walker-Warburg syndrome to congenital muscular dystrophy, microcephaly, and mental retardation. *Hum Mutat*. 27, 453–459.
- VanderVen BC, Harder JD, Crick DC, Belisle JT (2005). Export-mediated assembly of mycobacterial glycoproteins parallels eukaryotic pathways. *Science*. 309, 941-943.
- Van Veldhoven PP, Mannaerts GP (1987). Inorganic and organic phosphate measurements in the nanomolar range. *Anal Biochem*. 161, 45-48.
- Ventura M, Canchaya C, Tauch A, Chandra G, Fitzgerald GF, Chater KF, van Sinderen D (2007). Genomics of *Actinobacteria*: tracing the evolutionary history of an ancient phylum. *Microbiol Mol Biol Rev*. 71, 495-548.
- Waksman SA, Schatz A, Reynolds DM (1946). Production of antibiotic substances by actinomycetes. *Ann N Y Acad Sci*. 48, 73–85.
- Wehmeier S, Varghese AS, Gurucha SS, Tissot B, Panico M, Hitchen P, Morris HR, Besra GS, Dell A, Smith MC (2009). Glycosylation of the phosphate binding protein, PstS, in *Streptomyces coelicolor* by a pathway that resembles protein O-mannosylation in eukaryotes. *Mol Microbiol*. 71, 421-433.
- Willer T, Prados B, Falcón-Pérez JM, Renner-Müller I, Przemeck GK, Lommel M, Coloma A, Valero MC, de Angelis MH, Tanner W *et al.*, (2004). Targeted disruption of the Walker-Warburg syndrome gene *Pomt1* in mouse results in embryonic lethality. *Proc Natl Acad Sci U S A*. 101, 14126-14131.

- Willer T, Brandl M, Sipiczki M, Strahl S (2005). Protein O-mannosylation is crucial for cell wall integrity, septation and viability in fission yeast. *Mol Microbiol.* 57, 156–170.
- Xiang H, Chan D, Bates R (2015). Minimization of Freeze/Thaw-Induced Protein Aggregation and Optimization of a Drug Substance Formulation Matrix. *BioPharm International.* 28, 30–37.
- Xing J, W. Forsee T, Lamani E, Maltsev SD, Leonid L. Danilov LL, Shibaev VN, Schutzbach JS, Cheung HC, and Jedrzejewski MJ (2000). Investigations of the active site of *Saccharomyces cerevisiae* dolichyl-phosphate-mannose synthase using fluorescent labeled dolichyl-phosphate derivatives. *Biochemistry.* 39, 7886-7894.
- Yang AC, Ng BG, Moore SA, Rush J, Waechter CJ, Raymond KM, Willer T, Campbell KP, Freeze HH, Mehta L (2013). Congenital disorder of glycosylation due to DPM1 mutations presenting with dystroglycanopathy-type congenital muscular dystrophy. *Mol Genet Metab.* 110, 345-351.
- Zhang T, Faraggi E, Li Z, Zhou Y (2013). Intrinsically semi-disordered state and its role in induced folding and protein aggregation. *Cell Biochem Biophys.* 67, 1193-1205.

Abbreviations and acronyms

AI: Autoinduction

CGD: Congenital disorder glycosylation

DDM: n-Dodecyl β -D-maltoside

Dp: Dolichol phosphate

Dpm: Dolichol phosphate mannose

DN: Difco nutrient

DNB: Difco nutrient broth

DNA: Difco nutrient agar

ER: Endoplasmic reticulum

FPLC: Fast Protein Liquid Chromatography

FT: Flow through

GDP: Guanosine diphosphate

GT: Glycosyl transferase

HPLC: High Performance Liquid Chromatography

HRP: Horseradish peroxidase

H: Hour

IPTG: Isopropyl- β -D-thiogalactoside

kDa: Kilodalton

LB: Luria Burtani

MSA: Mannitol soya flour agar

Man: Mannose

mAU: Milli-absorbance units)

Min: Minute

MSA: Mannitol soya flour agar

MW: Molecular weight

ORF: Open reading frame

PCR: Polymerase chain reaction

PDB: Protein data bank

PFU: Plaque forming units

Pi: Inorganic phosphate

PMT: Protein mannosyl transferase

POMT: Protein O-mannosyl transferase

Pp: Polyprenol phosphate

Ppm: Polyprenol phosphate mannose

PVDF: Polyvinylidene difluoride

S: Second

SDS PAGE: Sodium dodecyl sulfate polyacrylamide gel electrophoresis

SEC-MALLS: Size exclusion chromatography multiple angle laser light scattering

SEM: Standard error of the mean

SN: Soft nutrient

TMHMM: Transmembrane Helices; Hidden Markov Model

Und-P: Undecaprenyl phosphate

WT: Wild type